Photoluminescence Properties of Silicon Nanocrystallites

by

Arun A. Seraphin

B.A. Political Science
B.E. Engineering Science
State University of New York at Stony Brook, 1991

Submitted to the Department of Materials Science and Engineering
in partial fulfillment of the requirements for the degree of

Doctor of Philosophy in Electronic Materials

at the
Massachusetts Institute of Technology

June 1996

Signature of Author: _____
Department of Materials Science and Engineering
May 3, 1996

Certified by: _____
Kirk D. Kolenbrander
Associate Professor of Electronic Materials
Thesis Supervisor

Accepted by: _____
Michael F. Rubner
TDK Professor of Materials Science and Engineering
Chair, Departmental Committee on Graduate Students

Photoluminescence Properties of Silicon Nanocrystallites

by

Arun A. Seraphin

Submitted to the Department of Materials Science and Engineering
on May 3, 1996 in Partial Fulfillment of the Requirements
for the Degree of Doctor of Philosophy in Electronic Materials

ABSTRACT

A great deal of attention focuses on the visible light emitting properties of silicon nanostructures because of their potential use in optoelectronic applications. The origin of the emitted light and the role that the particle sizes and surfaces play in the emission mechanism are still under considerable debate. To study these questions, thin films of Si nanocrystallites have been deposited using a novel pulsed laser ablation supersonic expansion source. The films consist of a polydisperse collection of crystalline Si particles embedded in a native oxide matrix which efficiently emits visible light under ultraviolet photoexcitation. The films have been treated using a number of post-deposition processing steps, including hydrofluoric acid and nitric acid etches and oxidation furnace treatments, in order to control the sizes and surfaces of the Si particles. The films have been characterized using photoluminescence emission spectroscopy and x-ray photoelectron spectroscopy to correlate the sizes and surface properties to the luminescence behavior. Additionally, the non-linear optical response of the films has been studied using degenerate four-wave mixing spectroscopy.

Particle size determines the emission energy of the films through the quantum confinement of photoexcited carriers. Nanostructure size has been controlled through the use of acid etch/oxide regrowth cycles. This has resulted in a consistent blueshift of the emission energy, as is predicted by theories of quantum confinement in semiconductor nanostructures. Both the photoluminescence temperature and pump power dependence are consistent with emission due to a recombination of quantum confined carriers.

Optical properties are also strongly influenced by the extent of surface passivation, which controls the density of nonradiative recombination centers. Neither unpassivated, gas phase nanoparticles nor as-deposited unpassivated thin films show visible luminescence behavior, while films processed to passivate their surfaces show efficient visible emission. Surface passivation also improves the nonlinear optical response of the films. Hydrogen, oxygen, and iodine have been used to passivate the nanostructure surfaces. While the emission intensity scales with the extent of surface passivation, the emission energy is independent of the specific chemical nature of the passivating species and is only determined by particle size.

Thesis Supervisor: Kirk D. Kolenbrander
Title: Associate Professor of Electronic Materials

Table of Contents

List of Figures

Acknowledgments

I have decided that this should be a list of things to remember about graduate school, in case I someday want to look back to my time at MIT. I'm pretty sure I don't like MIT as an institution, or the attitudes it seems to encourage, or the way it treats its people. I'm sure the reason I was able to stay and even enjoy my time there had everything to do with the people I got to meet and work with, and almost nothing to do with the "great science" or "excellence" for which MIT is famous. I am grateful for these people, and I guess I thank MIT for bringing them together in such a unique environment.

First, I would like to thank my thesis advisor, Professor Kirk Kolenbrander. I was told more than once that there was only one professor I could have possibly worked for here, and I was lucky enough to find him. Professor Kolenbrander has taught me a lot, not just about science and research, but also about being a good person and father and teacher. We have often disagreed about my choices throughout this process, but I always felt grateful that he supported me whenever I really needed it. I consider him a mentor, role model, and friend, and will never forget his patience despite all the things I have put him through.

I did some science while at MIT, and it was fun and challenging, and I learned more than I could have ever imagined. I express my sincere gratitude to the people who helped me accomplish what's in this thesis. Special thanks go to my thesis committee: Professors Thompson, Chiang, and Kimerling for their insights and feedback on the work. The technical assistance of Francisco Aranda, Das Chowdhury, and Jurgen Michel is very much appreciated.

By far the people who taught me the most were the various members of the Kolenbrander research group. I will always be grateful for the chance to work with and befriend my fellow students: Leon Chiu, Tracey Burr, Eric Werwa, Shih-Tung Ngiam, Shuba Balasubramanian, and Danielle Russell. This was and is a great bunch of people, who always seemed to give me more then I ever gave back in return. It was always very light and a lot of fun to be in the lab, and we sometimes even managed to get some good science done on the side. Of everything about grad school, I will miss the group most of all. For the record, here is an honor roll of all the other folks who served time in 13-5044: Bobby Korn, Stacy Holander, Teresa Lau, Jen Brady, Cade Murray, Jen McMurray, Devin MacKenzie, Jeanette

Ryan, Chuxin Zhou, Bob Martinez, Yoli Leung, Julie Ngau, Andrea Santoro, Anna Lena Thilderkvist, and Jimmie Walker. I can't fail to mention Morgan Kennedy, Ed Mellinger, and Peter Heron (whose antics were the stuff of legend), for their periodic counseling sessions and understanding.

Without a doubt, my time at MIT would have been unbearable without an assortment of people and events that kept me functioning, like baby-sitting and dinners in Natick; going to Fenway with Naveen; lunch at 11:30 and coffee at 3 with Doug, Erika, Erin, and Hal; and John Matz trying to help me get big. I am thankful for roommates (Hiten, Jen, Patrick, Mohammed, and Amir); TV folks (Tara Macpherson, CCTV, and Rob at the Center); stir-fried chicken and a soda at the trucks; weddings; Nat's CD player and Allison Engine; the Walt Disney Company™; poker at Peter's; 13-4009B; Mike Dauenheimer and the art of conventions; the secret garden; the Draper crowd at the Muddy; sneaking out to see movies; and my buddies at Fresco's. And of course Howard, Robin, Jackie, Fred, and Gary.

I will always remember the great people who were a part of my life during this time. Thanks for everything to: Heather, Annie, Mike, Kate, Brett, Cherie, Ann and Locksee, Laura, Jim, Jay, Ali, Jeff, Kumiko, Rita, as well as to all the other cool people who took time out of their busy MIT lives to stop and chat in the hall, or get a reference, or join the slack train. They made MIT and my time in Boston more "human".

I am grateful for the encouragement of my family, especially Vinod and Mary Anne, whose home was a great escape from graduate school. I particularly thank my parents, who always heard about the worst of MIT through my miserable phone calls home. Their unfailing support and understanding enabled me get through. Finally, I would like to thank my nieces and nephews (Ivy, Peter, Audrey, and Stephen), who I bragged about nonstop, and whose happy faces in pictures on my office wall could always cheer me up, no matter how bad MIT was being to me. I dedicate this work to you, for all the joy you have brought into my life.

5/21/96

1. Introduction

1.1 Thesis Outline

This thesis is divided into four parts. Chapter 1 provides some motivation for the study of silicon nanocrystallites, reviews the basic issues and fundamental physics relevant to the field, and defines the questions that will be addressed in this work. Chapter 2 describes the experimental techniques used in the synthesis and characterization of the films, as well as a brief description of the structural properties of the as deposited films used in the optical experimentation. Chapter 3 focuses on the processing and optical characterization of the films and descriptions of the physical phenomena that the observed behaviors imply. Chapter 4 summarizes the work by drawing conclusions as to the origins and potential usefulness of the observed properties, as well as proposing some avenues for future research.

1.2 Motivation: Silicon photonics and optoelectronics

The continual push for higher speed and lower cost telecommunications and information processing have led to attempts to engineer new devices that can fulfill demanding technical specifications and exploit new potential market opportunities. In particular, the fields of optoelectronics, using electronics to manipulate optical signals, and photonics, using light to control optical signals, may provide the foundation on which these new technologies can be built. The development of optoelectronic devices, such as lasers, detectors, and light emitting diodes, and photonic devices, such as directional couplers and all-optical switches, have been spurred by the need to improve the speed and quality of information flow, while reducing device dimensions and manufacturing costs. Silicon based devices and materials are a clear step in these directions, for they can fulfill many of the strict materials engineering and performance requirements presented by the potential opportunities in photonics and optoelectronics, in a well established commercial technology.

One of the many opportunities in photonic devices revolves around the ability to switch information flow. The progression of information switching technology from the mechanical switching of the telegraph to the electronic switching of signals in fiber optic networks has increased transmission rates roughly 2 billion times. However, new demands for global voice, video, and data transmission will require further improvements in transmission rates and switching speed, which can be provided by the development of all-optical switching technology.

A typical optoelectronic switch in use today is shown in Figure 1-1. This 8x8 crossbar switch consists of an array of 8 photodetectors linked through an electronic switch circuit to an array of 8 light emitting diodes (LEDs).[1] The optoelectronic devices at either end of this package are coupled to fiber optic cables which transmit information signals in the form of light. The optical signals are converted to electronic pulses in the detectors and passed to the switch circuit, where they are logically processed. The electronic signal is then sent to an appropriate LED and finally reconverted into an optical signal for transmission on the downstream fiber. This switching system is slowed down by the two required conversions between photons and electrons as signal carriers, as well as the limitation that a typical electronic switch can only handle one incoming and outgoing signal at a time.

In contrast, a photonic switch could improve on the speed of this type of system. The proposed system shown in Figure 1-2 would use a pump beam to gate the flow of a signal beam by exploiting an optical nonlinearity in a switch placed in the waveguiding material. The high switching speed of such a system would be based on the extremely fast nonlinearities in the switch material, in this case semiconductor nanocrystallites, and the removal of the previously required step of conversions to slower electronic signals. In addition, by tuning the resonance frequency of this nonlinearity it would be possible to utilize signals on a number of wavelengths at the same time, assuming efficient transmission through the waveguides. Finally, this passive system requires no external power supply, and by eliminating electronics, eliminates problems of electrical noise and crosstalk.

The production of a photonic device such as this switch awaits the development of nonlinear optical materials which meet the requirements of such a system. The materials should show strong and fast optical nonlinearities for efficient switching. They should be

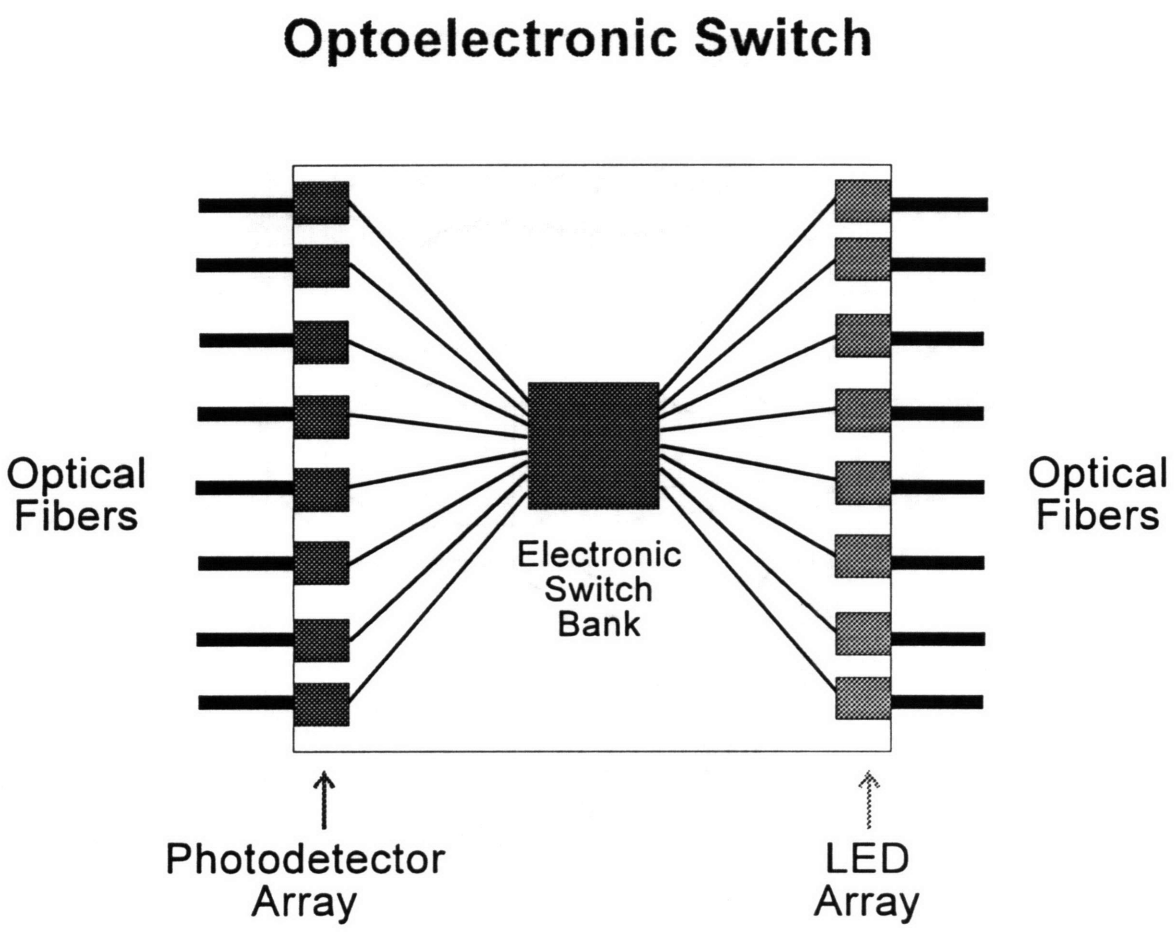

Figure 1-1 Schematic of an optoelectronic 8 x 8 crossbar switch. (From Ref. 1)

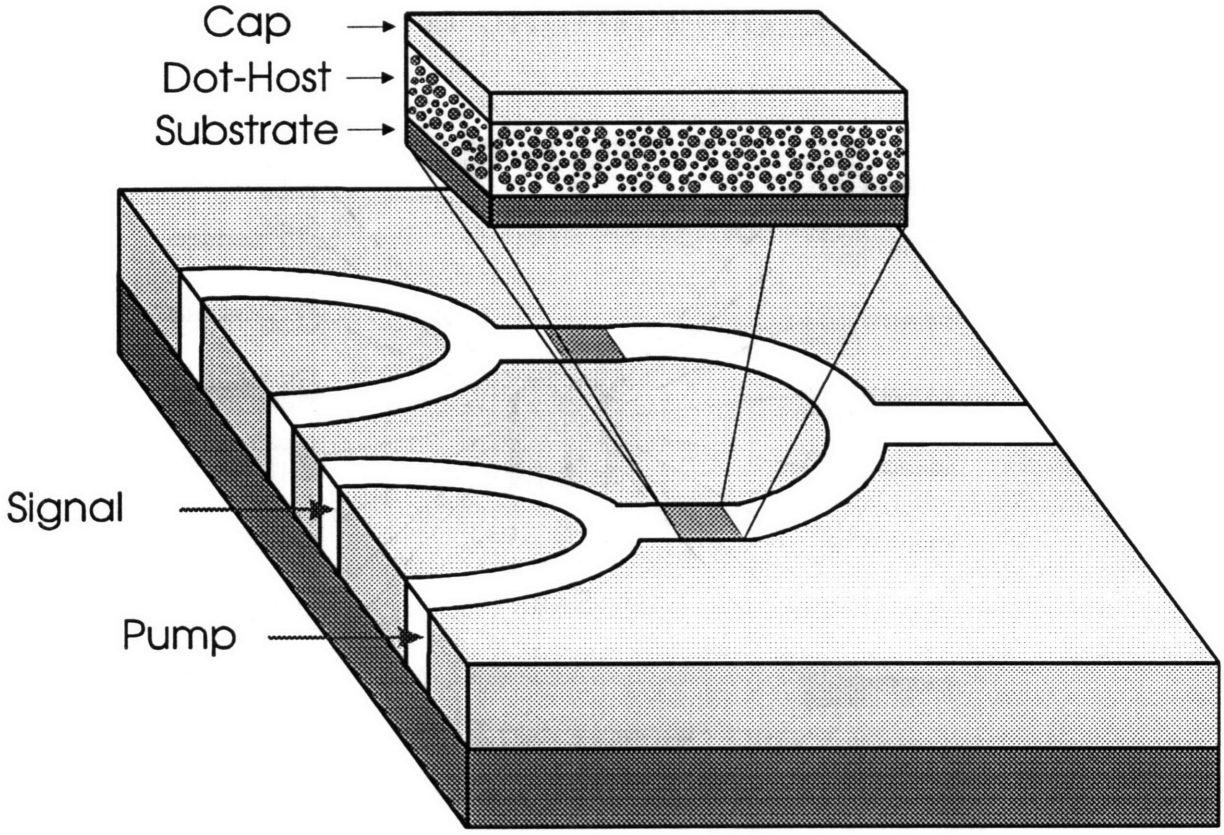

Figure 1-2 Schematic of proposed photonic switch using semiconductor nanocrystallites as active switch material.

reliable and defect free when produced. Finally, the materials should be easily integrable with existing growth and processing techniques and device architectures, to ensure successful wide scale commercialization and profitable deployment of the technology.

Opportunities in optoelectronic devices revolve around similar themes. There is a constant drive for miniaturization of computer technology, producing exponential growth of device densities in integrated circuitry, and creating new device fabrication and materials processing challenges. As the power of microprocessors increases alongside this miniaturization, the requirements for electrical connections on smaller scales is leading to an electronic bottleneck on the chip and board level. A rule of thumb for partitions of large computer systems is Rent's rule which states that the number of input/output connections for a system of chips containing N logic elements is $N^{2/3}$.[2] For a chip system using 100,000 logic elements, this requires 2100 pinouts. This large number creates spatial problems that can be eased by moving from electronic signals to optical signals. A typical optical pinout requires over 50 times less space than an equivalent electrical bonding pad, providing freedom for design of device architecture and allowing for further miniaturization.[3] However, the production of these optical circuit elements requires the development of optoelectronic technology that is compatible with existing microelectronic technology on this scale. Additionally, a great savings in cost and time can be achieved by moving from systems which utilize many different materials to integrated systems based on one material. For example, the optoelectronic switch in Figure 1-1 can have silicon photodetectors and electronics with present technology, but cannot use silicon LEDs. There would be a great savings in production time and cost if such a switch could be made using all silicon-based technology.

Again, the production of these new optoelectronic devices requires the development of new materials first. The materials must as always be easily grown and processed reliably to device specifications. The development of optoelectronic materials for display applications demands production of tunable, visible, and efficient light emitters. Emitters for fiber optic transmission must be compatible with fiber optic technology, for example, taking advantage of the dispersion minimum at a wavelength of 1.54 microns in silica fibers. The new materials also need to be compatible with future miniaturization needs, as well as easily integrable into existing electronics and device manufacturing regimens for commercial success.

1.3 Materials Choices I: Silicon

Given the opportunities and requirements in areas of photonic and optoelectronic applications, one clear choice of material is silicon. As the basis of the entire microelectronics industry, silicon is the focus of billions of dollars of investment and decades worth of technical expertise on the growth and processing of electronics grade materials and the design and performance of devices. New technologies based on silicon can tap into these advantages to outstrip competitors.

Silicon is an elemental semiconductor of with an energy band gap of 1.12 eV, and can be easily doped using a variety of impurities to alter its conductivity over many orders of magnitude. Control of the impurity type can change the nature of the dominant conduction processes from conduction by negative charge carriers (electrons) to conduction by positive charge carriers (holes). Adjusting the doping levels down to concentrations of one part per million can drastically change the overall conductivity of the material. This control of the electronic properties of silicon makes it an ideal system for use in device technologies.

The major advantage of silicon over other potential photonic and optoelectronic materials is in growth and processing knowledge and costs. Crystalline silicon can be produced today regularly with impurity and defect levels of less than one part in ten billion. It was the development of this level of defect control in bulk silicon that made possible the implementation of the device concepts that stemmed from the invention of the transistor by Shockley, Bardeen, and Bratton in 1947. Silicon processing has developed so that its costs are much less than its typical semiconductor rivals for both wafers and devices.

Silicon processing technology has developed alongside the growth of the microelectronics industry. Today, silicon can easily be grown in bulk form from the melt and in thin films using a variety of vapor phase techniques. Silicon growth can neglect the often difficult problems of maintaining stoichiometry that are faced during the synthesis of compound semiconductor materials. Silicon has a native oxide (SiO_2), which can be easily grown and etched using a variety of techniques that have already been scaled up to commercial industrial projects. Silicon dioxide's electronic properties make it ideal as an

insulator and as a surface passivation agent. It also has a very low density of interface states in bulk systems, which would reduce emission and carrier transport efficiency by acting as electronic traps.

Considering all of the advantages of silicon based electronics, it would seem logical to develop matching photonic and optoelectronic applications from the material as well. However, traditional bulk silicon is for the most part a poor optical material. This behavior results from the fundamental properties of bulk silicon. Silicon is an indirect gap semiconductor (Figure 1-3)[4] and as such is a very poor light emitter. In most semiconducting materials, radiative emission occurs when a charge carrier relaxes to a lower energy band and gives off its energy in the form of a photon. An indirect gap material has its conduction band minimum and valence band maximum at different values of charge carrier momentum (**k**). These extrema are the location of the highest carrier densities and the highest transition probabilities. This means that an electron making the smallest energy transition between the bands requires a change in momentum as well as energy. This can only occur through the emission or absorption of a phonon.

In a direct gap semiconductor the electron and hole are already at the same momentum. Therefore, while a direct gap material only requires a hole and electron for recombination to occur, an indirect gap material also requires the simultaneous presence of a phonon. This three body event is less likely to occur, and as such the recombination efficiency drops -- making the indirect gap material a less efficient light emitter than the direct gap material. Thus, today's semiconductor light emitters and lasers generally must be made from materials which have direct band gap (such as GaAs) or at least have a modified indirect gap, for example, properly doped indirect gap semiconductors -- whose defect-related energy states modify the transition probabilities.

In silicon, the inefficiency of these radiative transitions strongly limits the material's emission capabilities and nonlinear optical response. Along with this is the fact that silicon's

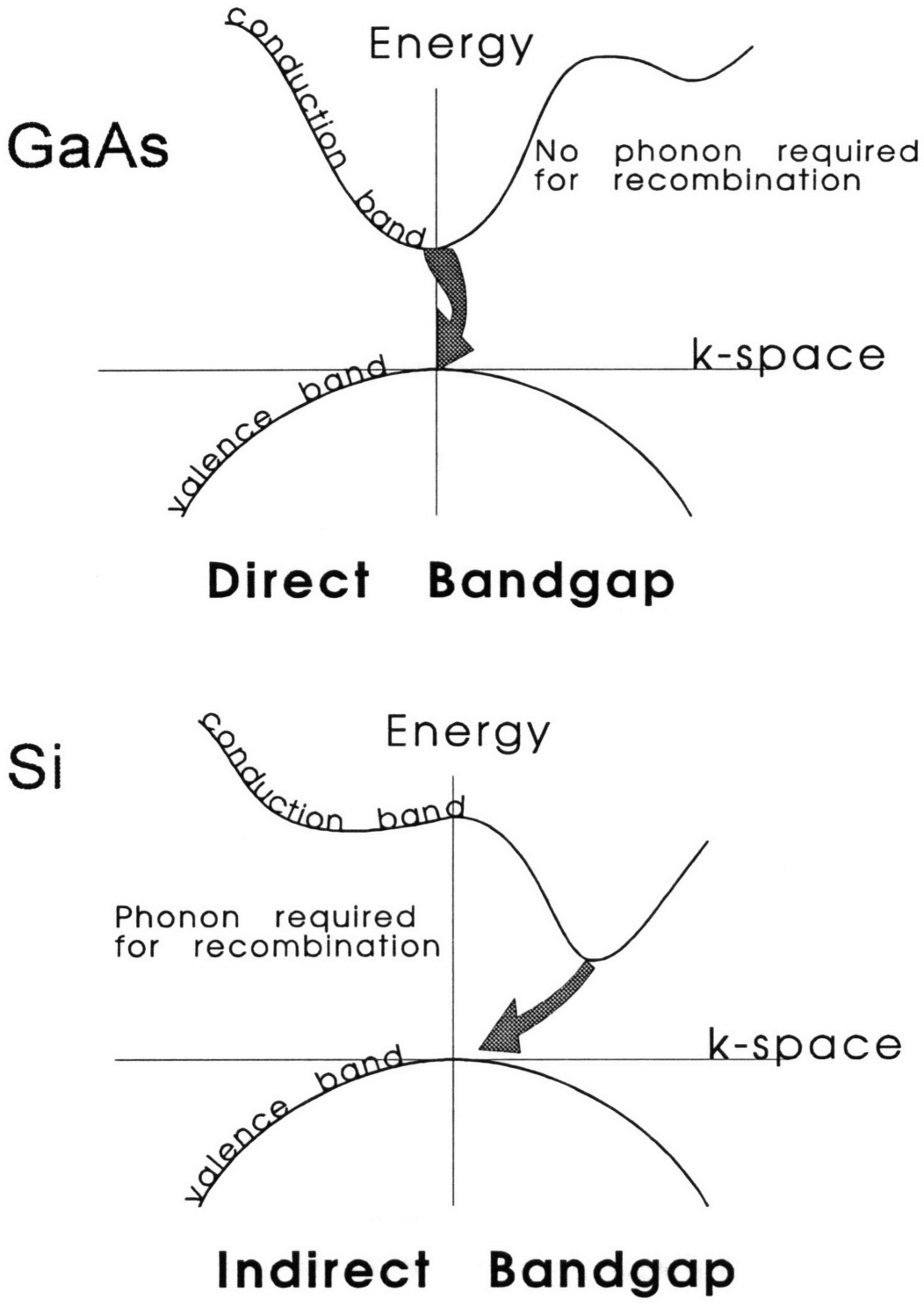

Figure 1-3 Schematic comparison of direct and indirect semiconductor band structures. (From Ref. 4)

band gap lies at 1.12 eV. From the relation,

$$\lambda = \frac{hc}{E}$$

where λ is the wavelength of emitted light, h is Planck's constant, c is the speed of light in a vacuum, and E is the energy of the transition, this energy can be converted to a wavelength of light. For silicon, this is an emission at 1100 nm, in the infrared portion of the photonic spectrum. This makes bulk silicon useless for visible display and emitter applications. Therefore, in order to exploit the processing advantages of silicon in any optoelectronic or photonic devices, it first becomes necessary to overcome its optical limitations.

1.4 Materials Choices II: Light Emitting Silicon

A number of methods have been proposed and attempted to overcome the natural optical limitations of silicon.[5] In order to promote light emission, or luminescence, in silicon materials it is necessary to increase the overlap of the electron and hole wavefunctions in the system, to encourage radiative recombination. This overlap can be increased in silicon systems in a number of ways.

1.4.1 Impurities

Impurities introduced into a crystalline silicon lattice result in a modification of the silicon energy band structure by the introduction of midgap defect states. These states can act to change the energy of possible transitions as well as increasing the likelihood for those transitions to occur. This results from the relaxed **k** (carrier momentum wave vector) selection rules that occur for transitions that are localized around the impurities. From the Heisenberg Principle, the uncertainty in a carrier's position and momentum are controlled by the relation,

$$\Delta k \cdot \Delta x \geq h$$

where Δk is carrier momentum, Δx is the carrier position, and h is Planck's constant. At an impurity site, the carrier's position is very well defined, implying that its momentum has no specific value, and thereby allowing transitions previously forbidden by carrier momentum

selection rules. The two more common impurity luminescence centers in silicon are isoelectronic traps and rare earth elements.

Isoelectronic traps are states caused by the introduction of impurities in silicon which are isovalent with silicon in the lattice.[6] Common examples of this are sulfur doped Si and complexes of four lithium atoms replacing a Si vacancy. The luminescence properties of these materials vary greatly by the type of impurity atom, but in general the emission lies in the infrared part of the spectrum; has a quantum efficiency of only a few percent at very low temperatures and even smaller at room temperature; and has long radiative transition lifetimes, meaning that competing, faster nonradiative transitions can severely limit the radiative efficiency.

Rare earth doped silicon materials have been studied because they show considerable promise for applications as emitters coupled to existing fiber optic systems.[7] In erbium (Er) doped silicon, the luminescence transition is between two levels of the Er^{3+} 4f manifold of states. This transition is forbidden in bulk Er, but the presence of the crystal field of the Si lattice removes this barrier to emission. This emission sits at 1.54 μm, putting it near the dispersion minimum for silica optical fibers. Erbium doped silicon materials treated with oxygen have been shown to exhibit strong low temperature photoluminescence and electroluminescence. However, work is still being done to increase the concentration of Er emission centers in the silicon lattice, and to better understand the specific mechanism for recombination.

1.4.2 Si based alloys

Alloys of silicon and germanium (Ge) have been shown to emit in the near infrared at low temperatures. In these systems, the band structure of silicon is engineered through the alloying process, or through the growth of $Si/Si_{1-x}Ge_x$ superlattices. These materials are believed to have a pseudo-direct gap, and as a result enhanced transition probabilities.[8] Alloying leads to exciton localization away from nonradiative recombination sites and an increase in emission efficiency.[9] However, a number of issues still must be resolved, including the role of defects, such as dislocations, in limiting radiative efficiencies, and the role of strain in the band structure modification.

1.4.3 Amorphous silicon

Amorphous silicon light emitters show different behavior from bulk silicon due to the effects of alloying and structural disorder on the silicon band structure. Typically, hydrogenated amorphous silicon (a-Si:H) contains 5-10 atomic percent hydrogen. The hydrogen serves to tie up dangling bonds in the amorphous network and to expand the band gap of the alloy. Disorder in the material alters the band structure such that ideas of E-**k** dispersion relations and momentum selection rules lose their meaning. However, the material still has a density of allowed energy levels, in bands separated by a gap of 1.6-1.8 eV, as measured by optical absorption.[10] Disorder in the lattice perturbs the electronic states of carriers such that the band edges are broadened into Urbach tails. These tails fall away exponentially from the traditional band edges. The band edge itself is termed the mobility edge; it separates delocalized carriers in the conduction band from localized carriers in the band tail. The localization of carriers increases deeper in the tails, towards the center of the band gap.

Emission intensity from hydrogenated bulk amorphous silicon has been shown to increase with hydrogen content.[11] Photoluminescence in a-Si:H ranges from 0.93-1.5 eV, and blueshifts with increasing hydrogen content. The higher energy emissions are believed to originate from shallow states in the band tails, while the lower energy emissions are the result of recombination between deeper lying, more localized carriers. Fluorinated amorphous silicon has shown very similar optical behavior to a-Si:H.[12] Here, the fluorine passivates dangling bonds in the amorphous network and blueshifts the absorption tail.

Both hydrogenated and nonhydrogenated amorphous silicon (a-Si) have been used to create superlattices that show optical properties reflecting the quantum confinement of carriers. Superlattices of a-Si:H/a-SiN_x:H have shown increasing optical gap and radiative efficiency with decreasing layers thickness.[13] Superlattices of a-Si/SiO_2 have shown blueshifted emission with decreasing layer thickness.[14] Both of these systems demonstrate significant promise in display applications.

1.4.4 Polysilanes and Polymers

Highly disordered alloys (SiH_x) and silicon based polymers, such as siloxene ($Si_6O_3H_6$) and polysilane $(SiH_2)_n$, have also been shown to emit strongly in the visible and ultraviolet parts of the spectrum.[15] These materials do not show the good electrical transport properties that are necessary for the development of useful electroluminescent devices, nor do they have the structural reliability of crystalline silicon based materials. Moreover, they are far enough removed from traditional silicon materials to lose most of the growth and processing benefits that would prompt one to work in silicon in the first place.

1.4.5 Quantum Confined Silicon Structures

Another approach to improving the emission efficiency of silicon materials, and moving the energy gap and therefore emission wavelength from the infrared to the visible, is to use quantum confined structures.[16] In these materials, such as quantum wells, porous silicon, and silicon nanocrystallites, bulk silicon band structures are modified through reduction of the volume of space available for electron and hole wavefunctions, and exploiting the resulting increased wavefunction overlap. Porous and nanocrystalline materials and their controversial emission properties will be described in section 1.7.

1.5 Quantum Confinement Effects in Semiconductors

Development of useful silicon based optoelectronic and photonic devices hinges on overcoming the inherent limitations of the bulk silicon band structure, namely its indirect nature and energy gap which lies in the infrared. These limitations can be overcome through quantum confinement of carriers within crystalline structures grown on a nanometer scale.

A simple notion of the development of the band structure of semiconductor materials can be gained from applying the concepts of quantum mechanics and the Pauli exclusion principle to a system of electrons interacting in an periodic potential of a crystalline lattice.[17] The density of allowable energy states for the charge carriers of a material is given by

$$g(E) = \frac{dN}{dE}$$

where N is the number of allowed states at energy level E. The density of states is a function of the size and dimensionality of the system. It is the ability to exploit this reduced dimensionality that motivates the study of quantum-confined materials.

A bulk or traditional, three dimensional system has a density of energy states given by

$$g(E) = \frac{(2m)^{3/2}}{2\pi^2\hbar^3} E^{1/2}$$

where m is the mass of an electron and E is the energy of a carrier.

This continuous range of allowable states begins to change with reduced dimensionality, as shown in Figure 1-4. Confining a system in one dimension, that is, making one dimension small on the scale of the carrier wavefunctions, produces a two dimensional material or quantum well. For a system with well thickness d, the system has a density of states given by,

$$g(E) = \frac{m}{\pi\hbar^2 d}$$

This leads to a step function defined at each allowed energy level of the system. Confining the system again in another dimension produces a one dimensional material or quantum wire, whose density of states is shown in Figure 1-4c, and can be expressed as

$$g(E) = \frac{\left(\frac{1}{d_1 d_2}\right)\left(\frac{m^{1/2}}{\sqrt{2}\pi\hbar}\right)}{E^{1/2}}$$

where d_1 and d_2 are the confined dimensions of the wire. Finally, confining a material in three dimensions results in a quantum box or quantum dot, whose density of states is shown in Figure 1-4d, and is given by

$$g(E) = \delta(E)$$

The allowed energy levels are discrete and well separated, and the density of states is a series of delta functions. The discrete nature of the density of states makes the quantum dot system very similar to a molecular system in that the bands of allowed energies characteristic of a solid semiconductor have been totally lost.

This discrete density of states modifies a semiconductor's optical properties so that even in a material like silicon, photonic applications become possible. First, quantum confined

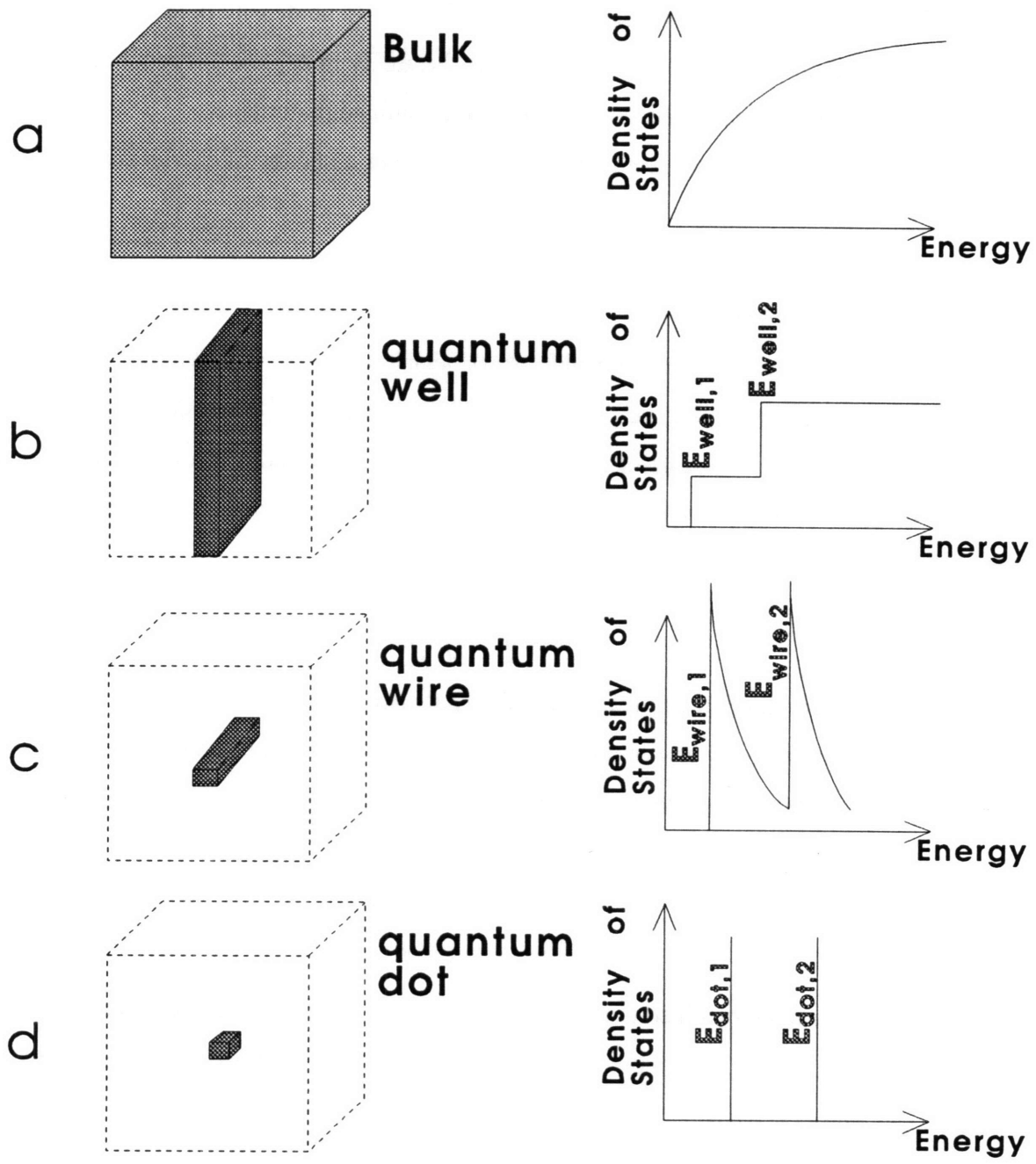

Figure 1-4 Density of states as a function of increasing dimesional confinement.

silicon can become a stronger absorber of light. This stems from the fact that in these discrete systems, all concepts of indirect versus direct band gaps are no longer applicable. Also, the discrete nature of the states means that all of the oscillator strength of the material is focused to transitions that match the levels.[18] The quantum confined silicon then can become a strong absorber at exceedingly narrow resonant linewidths. Sharpening of absorption lines relative to bulk behavior has been demonstrated in quantum dots synthesized from II-VI semiconductors, such as cadmium selenide (CdSe).[19]

Second, the levels themselves have a finite capacity depending on the size of the system, so that only a limited number of carriers can fit into each. This enables the possibility of saturating the levels by filling them completely with excited carriers. Then absorption of energy by the system into those levels becomes impossible, and the material becomes transparent at that excitation energy (or wavelength of light). This saturable absorption is the basis of the photonic switch shown in Figure 1-2. The pump beam is used to saturate the energy levels of the quantum dots in the switch, so that they become transparent to the signal beam, and the signal passes through. When the pump beam is turned off the quantum dots in the switch can absorb the signal beam, and the signal is not transmitted, as shown in Figure 1-5.

Quantum confinement effects also result in properties that can make silicon useful in optoelectronic display applications. As is the case for the energy levels of a simple particle-in-a-box system, as the size of the system becomes smaller, the energy difference between the levels becomes larger. For semiconductor quantum dots, which are often modeled as being spherical, this results in a proportionality between the particle radius and its energy gap. The energy of the fundamental electronic transition in a spherical quantum dot has been described with the relation

$$E(r) = E_g + \frac{\hbar}{2r^2}\left(\frac{1}{m_e} + \frac{1}{m_h}\right) - \frac{1.8e^2}{\varepsilon\, r}$$

where m_e and m_h are the effective masses of electrons and holes, r is the particle radius, and the third term represents a Coulombic attraction regulated by the dielectric constant (ε) of the system.[20] For decreasing r (smaller clusters), this term can become negligible and the energy gap varies inversely as the square of the particle radius.

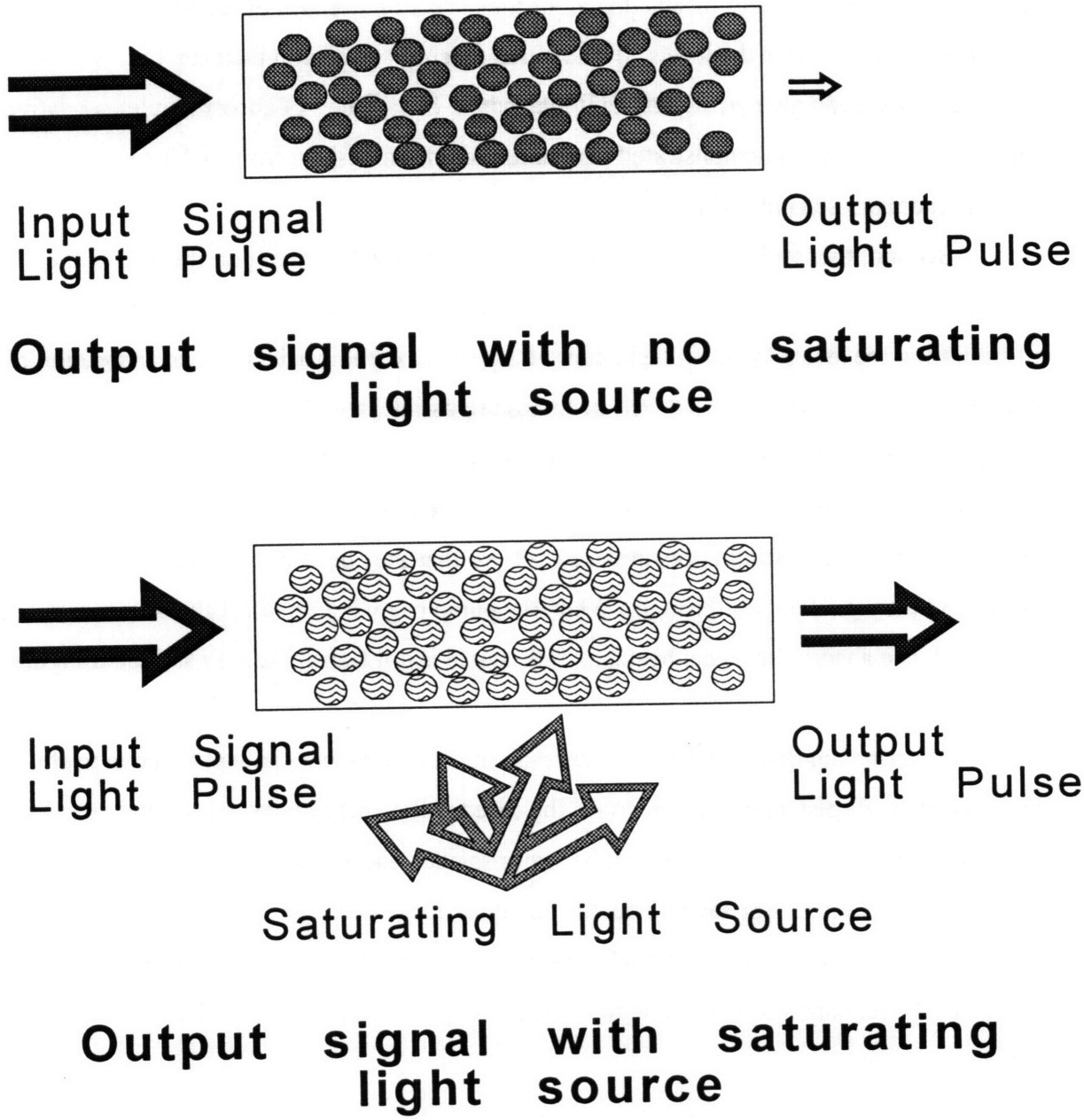

Figure 1-5 Schematic of saturable absorption behavior in the nonlinear optical switch based on semiconductor nanocrystallites. The pump beam is used to saturate the absorption of t nanocrystallites to make it transparent to the signal beam.

The control of energy gap, and therefore radiative emission energy, by particle size opens up the possibility of creating tunable emitters. From the relationship between energy and wavelength, it can be seen that larger particles would emit at lower energies or longer wavelengths, while smaller particles would emit at higher energies or shorter wavelengths. In silicon systems, quantum confinement effects have been predicted to shift the energy gap of the bulk material from 1.12 eV to values between 1.5 and 6 eV, lying in the visible and ultraviolet parts of the spectrum.[21] The result of one theoretical calculation for silicon nanostructures is shown in Figure 1-6.[22]

The effects of quantum confinement are not seen in semiconductor systems until the particle sizes are reduced to the nanometer scale. Roughly, quantum confinement effects are expected to be seen in nanostructures when the crystallite size approximates the size of the Bohr exciton radius for the given material. This radius is given by

$$r = \frac{4\pi\hbar^2\varepsilon}{e^2 m_r}$$

where m_r is the reduced mass of the electron and hole pair and e is the charge on a carrier. In silicon, this radius has been calculated as 4.3 nm.[23] Germanium, with a smaller band gap and a larger dielectric constant, has a bigger radius, calculated as 11.5 nm.[23] As particle diameter reaches this small size, the electron and hole wavefunctions that make up an exciton are compressed closer together than in bulk systems. This "confinement" of the wavefunctions results in the energy gap increase and enhanced overlaps that are responsible for efficient visible light emission predicted from silicon nanostructures.

The quantum confinement of carriers within quantum dots or semiconductor nanocrystallites is predicted to improve the emission efficiency. Similar to the case described above for impurities in silicon, the small structures and their surfaces disrupt the symmetry of the crystalline lattice, resulting in a breakdown of the momentum selection rules in these systems. As size decreases the wavefunction overlap between electrons and holes increases, and makes radiative transitions more likely for structurally perfect nanocrystallites. This leads to the efficient emission that is required for silicon based light emitting applications.

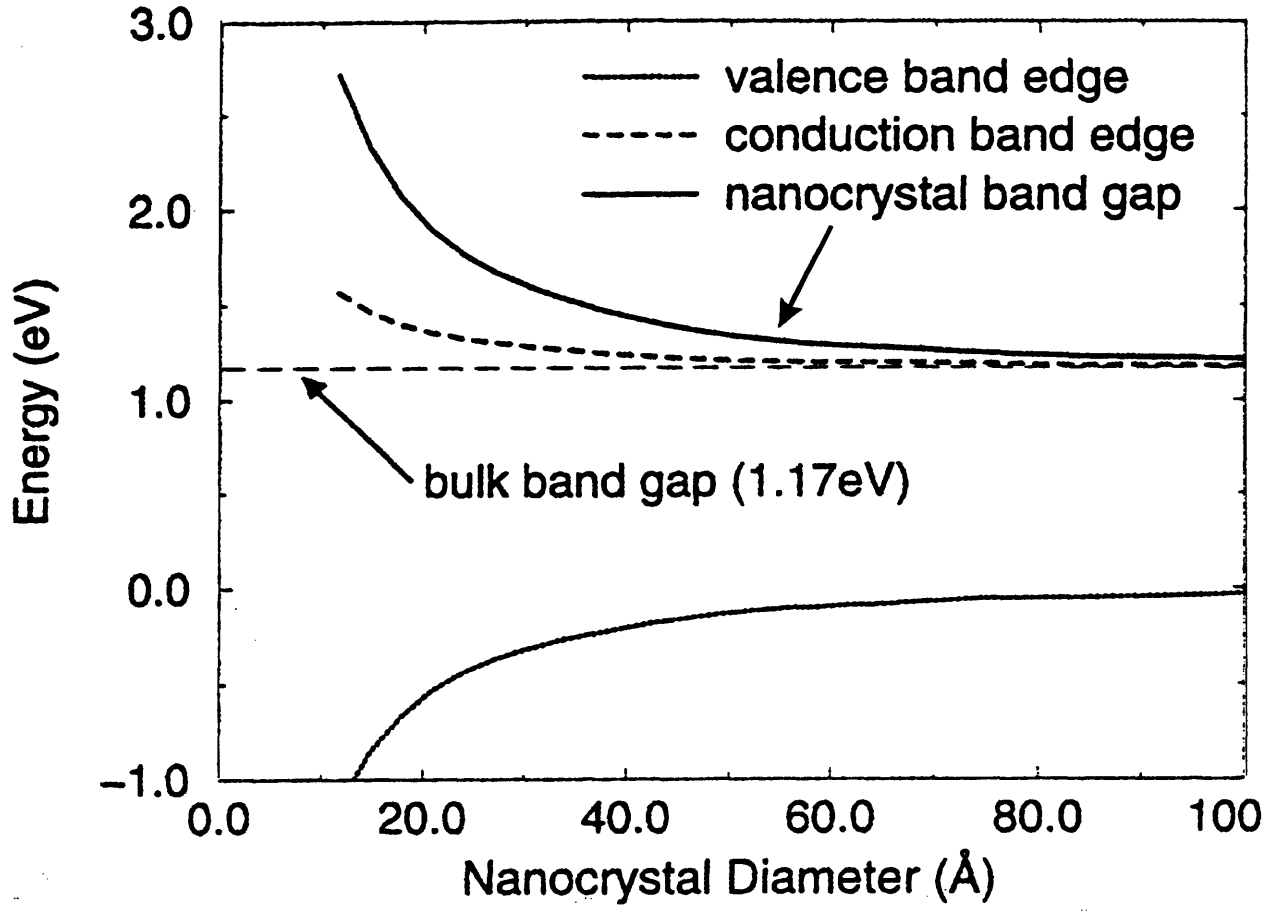

Figure 1-6 Theoretical calculation of energies of band edges and band gap in nanocrystalline silicon. 0 K band gap of bulk silicon is shown for comparison. (From Ref. 94)

1.6 Semiconductor Nanostructures

1.6.1 Cadmium Selenide

Significant progress has been made in the chemical synthesis and characterization of quantum dots made from cadmium selenide. Murray has developed a technique involving the size selective precipitation of crystallites formed by the pyrolysis of organometallic reagents injected into a coordinating solvent. By controlling the growth temperature it is possible to control the size distribution of the crystallites. Since the absorption properties of the crystallites will be a function of the size polydispersity, it is possible to monitor the size range during synthesis, and continuously adjust the reaction temperature to control the distribution. This distribution can be further narrowed by the size selective precipitation and subsequent removal of particles through the addition of solvents. Dots have been produced in narrow size ranges from ~1.2 to 11.5 nm.[19] The dots are produced well passivated with organic capping groups, and the technique has been extended to work in cadmium telluride (CdTe) and cadmium sulfide (CdS).

Quantum dot samples of CdSe have been shown to be extremely monodisperse to a level of <5%. As such they show the very clear optical features that would be expected from the narrow resonances developed in the discrete density of states of such a material. Figure 1-7 shows how the absorption edge of these materials can be controlled by shifting the sizes of the particles, as is predicted by quantum confinement theory.

Cadmium selenide quantum dots have also been used to develop efficient light emitting devices and as part of luminescent semiconductor heterostructures. In all cases, the nanocrystallites show very efficient and tunable luminescence as would be expected for a quantum confined direct gap material. Emission has also been demonstrated from CdSe nanocrystals embedded in zinc selenide[24] (ZnSe) and zinc sulfide[25] (ZnS). Chemical synthesis of II-VI semiconductors such as these show much promise in developing efficient light emitters, but the commercial viability of large scale production of these materials is still an important question that remains unanswered.

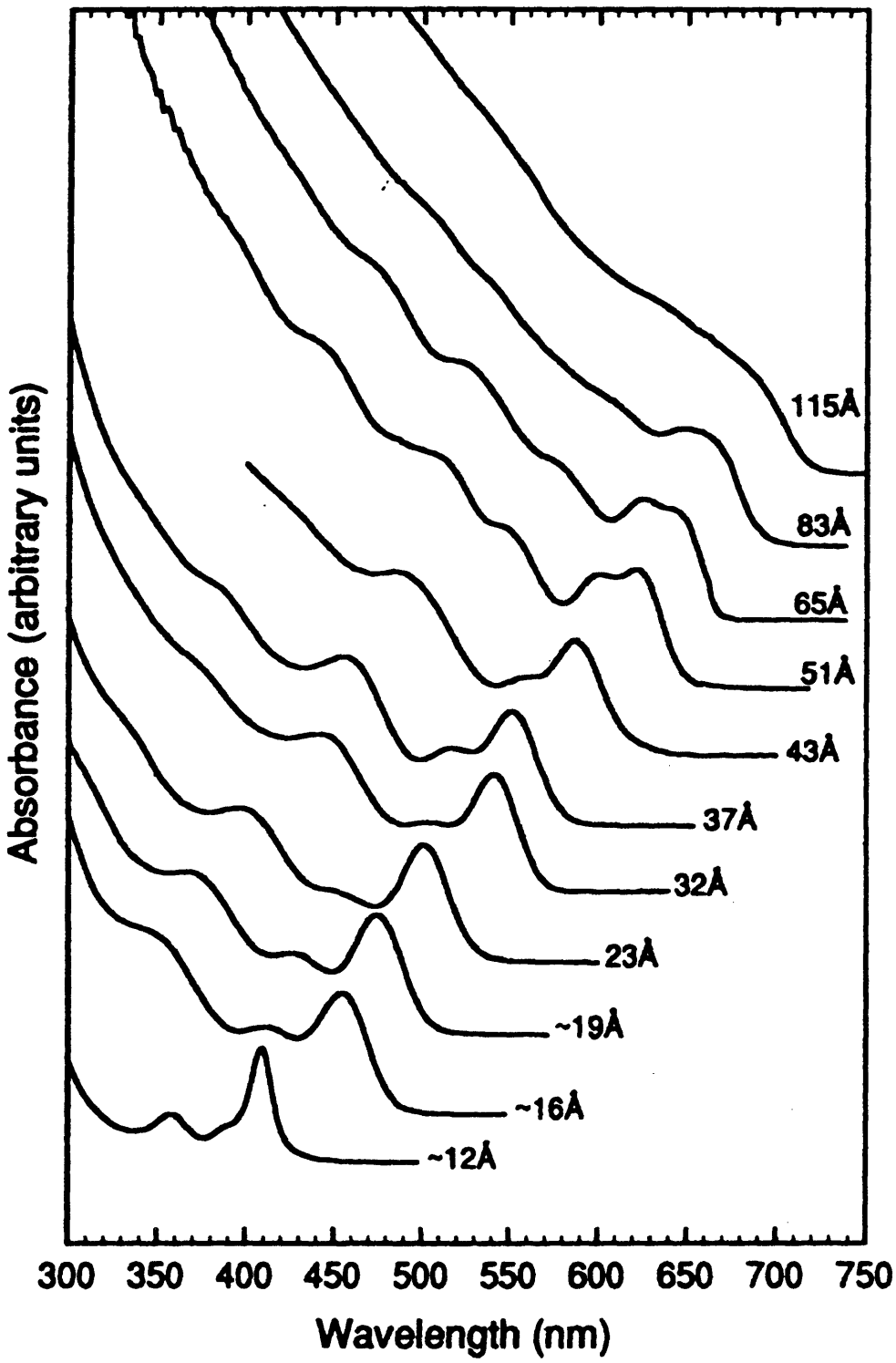

Figure 1-7 Shift in room temperature optical absorption with changing size in CdSe nanocrystallites dispersed in hexane. (From Ref. 19)

1.6.2 Germanium

A number of groups have produced nanocrystallites from germanium. These have been synthesized through a variety of techniques, including pulsed laser ablation supersonic expansion,[26] ion implantation[27] or dc magnetron sputtering[28] of Ge into SiO_2 matrices with subsequent annealing to nucleate nanocrystallites, cluster beam evaporation,[29] and chemical synthesis.[30] These systems have been shown to have a significant size distribution of nanocrystalline material.

Like silicon, nanocrystalline germanium is expected to show quantum size effects, including an energy gap expansion and a conversion towards a direct gap. Since the exciton radius in germanium is larger than that of silicon, these effects are likely to be seen in larger particles. Luminescence from these materials has been reported by a number of groups.[31,32] This luminescence has often appeared in the blue region of the visible spectrum.[33] This is also the region where emission from the oxide host matrix for these materials would lie, and it has not been clearly shown as of yet that the emission centers are actually germanium. No group has shown a clear correlation between absorption or emission behavior and size reductions as produced by post deposition processing steps. The systems in general do not show strong luminescence, most likely due to the difficulty of creating an efficient surface passivation layer. The importance of this passivation layer will be discussed in section 1.10.

1.6.3 Other Materials Systems

Semiconductor nanostructures have also been produced in other materials. This includes gallium arsenide (GaAs) crystallites produced by spark ablation,[34] porous gallium phosphide (GaP) produced by electrochemical anodization,[35] SiGe quantum dot materials fabricated by electron beam lithography and reactive ion etching,[36] and copper chloride (CuCl) and copper bromide (CuBr) nanocrystals grown in porous glass matrices,[37] to name a few. This experimental work has been complemented by a significant amount theoretical analysis of the electronic structure and optical properties of semiconductor nanocrystallites.[23]

In general, these materials have been shown to exhibit optical properties reflecting the quantum confinement of excited charge carriers within the nanostructures. There does not seem to be as much controversy about the origins of the new optical effects in direct gap

semiconductor nanostructures as there is in the indirect band gap materials -- germanium and silicon. All of this work in semiconductor systems also points to the important roles that both the sizes and surfaces of the particles play in determining the optical behavior.

1.7 Silicon Nanostructures

When attempting to develop new optoelectronic and photonic applications, it becomes clear that one would like to take advantage of the processing and growth advantages of silicon and the optical enhancements provided by quantum confinement. This has led to a considerable amount of work in the area of nanocrystalline silicon and porous silicon to characterize the visible light emission behavior both experimentally and theoretically.[38] In addition, a number of attempts have been made to fabricate light emitting devices from these materials, and to understand their electroluminescence and electrical characteristics. Research leading to a better understanding of these materials and their unique optical behaviors will be a first step in the development of silicon based visible LEDs and lasers.[39]

1.7.1 Silicon Nanostructure Synthesis

1.7.1.1 *Porous Silicon Formation*

Porous silicon is usually synthesized by the anodic etching of crystalline silicon wafers using an electrochemical cell containing dilute hydrofluoric acid (HF).[40] A typical apparatus for the production of porous silicon is shown in Figure 1-8. Although the mechanism of porous silicon formation is still unclear, a number of models for the process have been proposed.[41] In general, the bulk silicon wafer begins to dissolve under anodic bias through the removal of Si atoms upon reaction with HF and holes, as given by the reaction

$$Si + 4HF + (4\text{-}n)h^+ \rightarrow SiF_4 + 4H^+ + ne^-$$

where h^+ represents holes and e^- represents electrons. Holes are required for this reaction to occur, so commonly p^+ doped wafers are used to make porous silicon. However, low p-doped or n-type silicon can be used as well, either at lower formation efficiencies, or by using external sources, such as illumination, to generate the holes needed for the reaction. Typical

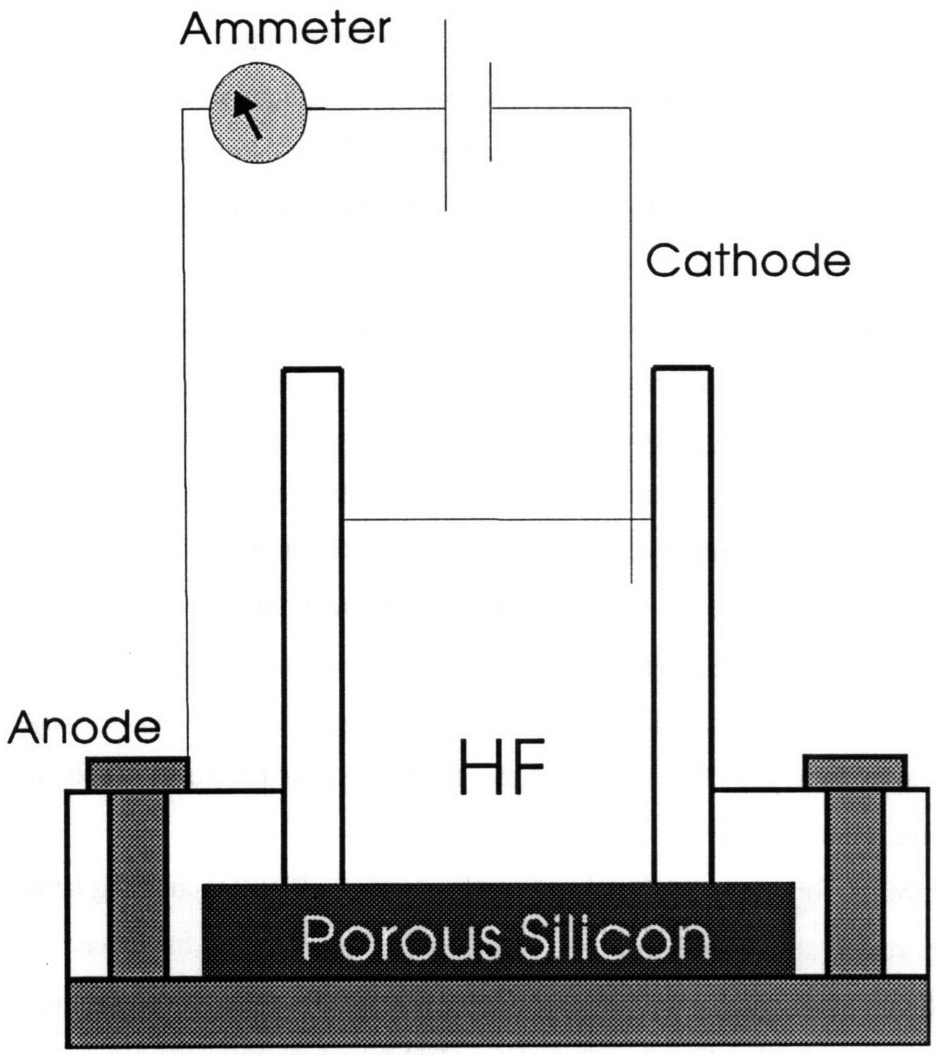

Figure 1-8 Apparatus used for the anodic etching of silicon wafers to form porous silicon.

current densities for the formation process are in the 1-30 mA/cm^2 range, in a variety of electrolytes. Groups have reported success in producing porous silicon in 25% HF,[15] HF:Ethanol,[42] HF:Ammonium Fluoride,[43] and HF:Methanol:Water.[44] Porous silicon has also been formed using a stain etch of HF/HNO_3 without any applied voltage,[45] as is described in section 1.9.2.1.

The selective dissolution of the bulk crystal into a porous material has been proposed to be the result of the presence or absence of positive charge carriers at the surface of the wafer being etched. As the etching process continues, some areas of the wafer will become constricted in size. One model proposes that these constrictions become areas of larger energy gaps through quantum confinement, and therefore exclude hole currents.[46] The holes then travel to the unetched regions alongside the constrictions and continue the etching process, resulting in an ever magnifying preferential etching, and leading to the development of long constricted wires of leftover silicon. Another model suggests that a space charge layer exists at the surface of the wafer. Tunneling of holes to the bases of the pores is enhanced, and the etching rate is increased at these areas.[47]

The result of the formation process is a complex sponge of interconnecting layers of silicon nanostructures, as shown in Figure 1-9. The freshly prepared films have been characterized as being hydrogen passivated, as can be expected from the HF present in the solution. Study by transmission electron microscopy (TEM) and scanning electron microscopy (SEM) has revealed that layers can range in thickness up to hundreds of microns, and consist of crystalline silicon regions intermixed with open pores.[48] Measured pore sizes can vary from ~100 nm in macroporous material, to <2 nm in mesoporous material. The remaining silicon regions have been described as amorphous,[49] or crystalline quantum wires or dots, some in the size range (< 5 nm) where quantum confinement effects can be expected.[50]

There is a wide range of conflicting data being produced in the porous and nanocrystalline silicon literature. One of the difficulties in this system is the size distribution of silicon nanocrystallites that exists in every porous silicon sample. Nanostructures range from nearly atomic silicon up to pieces that can be considered bulk silicon. The convolution of the size dependent optical and electronic properties of all of these particles makes characterization of the systems very difficult. Another difficulty arises from the great variation in formation

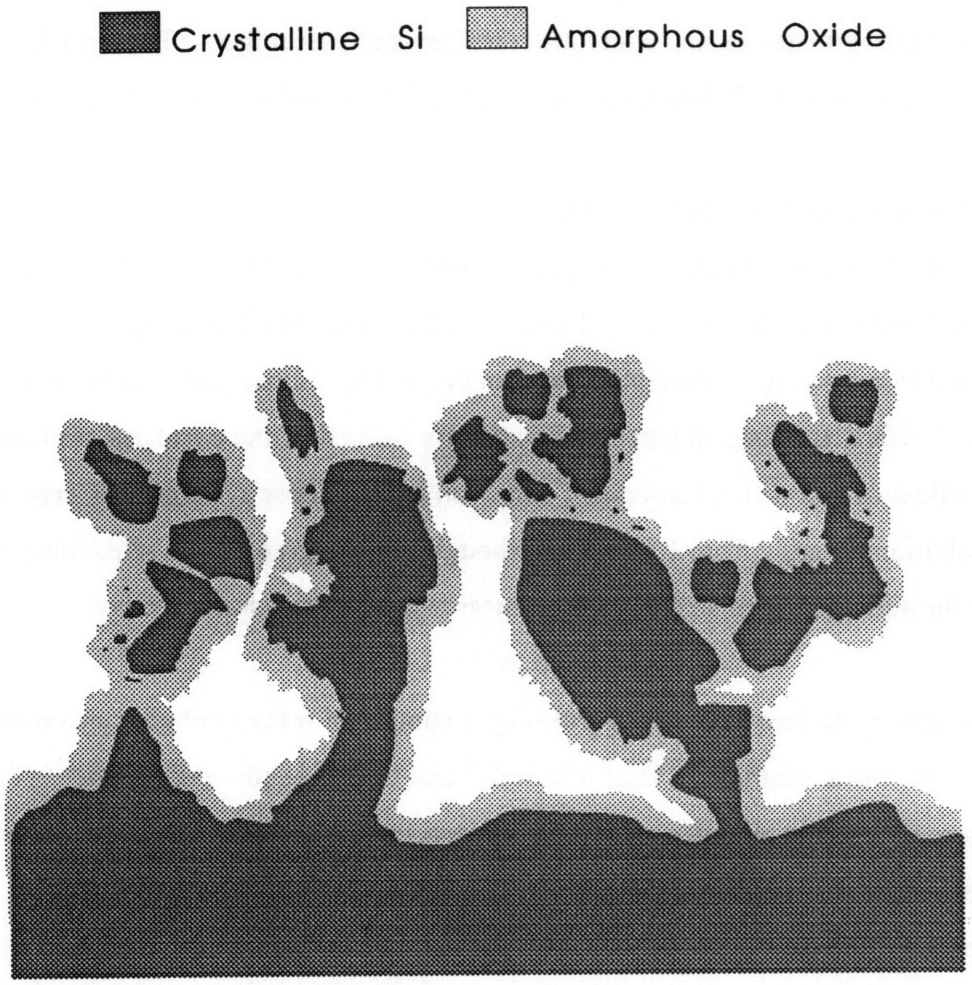

Figure 1-9 Schematic of proposed structure of porous silicon. Porous silicon contains nanoscale wire and nanocrystallite regions, as well as amorphous silicon and oxide.

conditions and resulting materials and microstructure between researchers. These variations are very likely to result in very different electrical and optical behaviors for the final materials.

1.7.1.2 *Nanocrystalline Silicon Formation*

A number of groups are also working to produce silicon nanostructures by other methods. AT&T researchers have produced luminescent colloids of oxide capped nanocrystalline silicon by a high temperature aerosol process and subsequent bubbling through ethylene glycol.[51] Here, oxidized silicon nanocrystals are formed by the pyrolysis of disilane in a high pressure flow of He, with a subsequent oxidation in O_2. These systems also have a large size distribution, roughly from 1.5 to 4 nm, though some degree of size selection has been achieved through the use of size exclusion chromatography and size selective precipitation.

Silicon nanocrystallites have been formed by a number of other methods, including spark ablation,[52] chemical synthesis,[53] laser ablation,[54] and laser breakdown of silane.[55] These processes in general result in an oxide passivated nanocrystalline surface. Each also produces nanocrystallites with a very large size distribution that shows a relatively efficient visible photoluminescence response.

The nanocrystalline and porous silicon are similar in that they both consist of a size distributed set of silicon structures. In both cases, many of these structures are on a nanometer scale, and as such can be expected to feel the effects of quantum confinement. However, many nanocrystalline and porous silicon systems are very different in their structure and therefore in expected properties. First, the passivation of most as prepared nanocrystallite systems is oxygen, while that of as prepared porous silicon is hydrogen. Second, porous silicon starting material is almost always doped, while the starting materials in most nanocrystalline silicon systems is not. Considering a doping level of 10^{16} atoms/cm^3, and nanocrystallites of 1000 atoms that emit light, this implies that 1 in 10^3 crystallites would contain a dopant atom. This crystallite would then have an entirely different electronic structure than ones that are undoped, and as such would be expected to show very different behavior. Nanocrystalline materials generally sit in thin films on a substrate made from some other material. This differs from porous silicon, whose thicker films are usually intimately

connected to a bulk silicon wafer. There may also be structural differences, since nanocrystalline silicon is built up from atomic silicon, while porous silicon is broken down from the bulk and so may retain some of the crystallinity of that system. These differences between the two materials should not be neglected when trying to compare the properties of the two systems.

1.7.2 Light Emission From Silicon Nanostructures

Efficient, visible photoluminescence and electroluminescence behavior has been observed in both porous and nanocrystalline silicon materials.[56] The visible emission has been centered around two major bands: a blue band lying between 2.5 and 2.8 electron volts (eV), and a red band lying at 1.2-2.2 eV. The key properties of these bands is summarized in Figure 1-10.[38] A typical red band photoluminescence spectrum is shown in Figure 1-11.[57] The emissions measured have varied considerably in intensity, lifetime, and temperature dependence, especially as a function of materials processing. As a result, the luminescence mechanism for these materials is still under considerable debate. Much evidence exists to support and refute each of the proposed models, but still no clear and final consensus has been reached in the research community.

The luminescence behavior in nanostructured silicon has been described using five major models:

1. Emission from amorphous silicon regions in the materials,
2. Emission from silicon based polymers existing on the surface of the materials,
3. Emission through defects in the oxide layer or at the silicon/oxide interface,
4. Emission through surface states in an expanded nanocrystalline silicon energy gap,
5. Emission from a bulk-like recombination of quantum confined excited carriers in the crystalline nanostructures.

1.7.2.1 *Amorphous silicon*

Evidence for emission occurring from amorphous regions in the porous silicon network stems from structural studies that show evidence of amorphous material in the system.[43] The nonexponential decay of the red band luminescence in porous silicon is very

Energy Range (eV)	Key Properties
Visible or Red Band (1.2 - 2.2)	• Sensitive to porosity in most cases • Sensitive to surface treatments • Energy, intensity, and decay time are temperature dependent • Multiexponential temporal decay • Dominant band in freshly prepared materials
Blue Band (2.5-2.8)	• Weak dependence on porosity • Fast decay time • Strong in high temperature oxidized material • Correlated to presence of oxide
IR Band (0.8-1.3)	• Weak dependence on porosity • Weak intensity compared to visible band • Sensitive to surface treatments

Figure 1-10 Key properties of observed emission bands from porous silicon. These are the characteristics typically reported in the literature. (From Ref. 38)

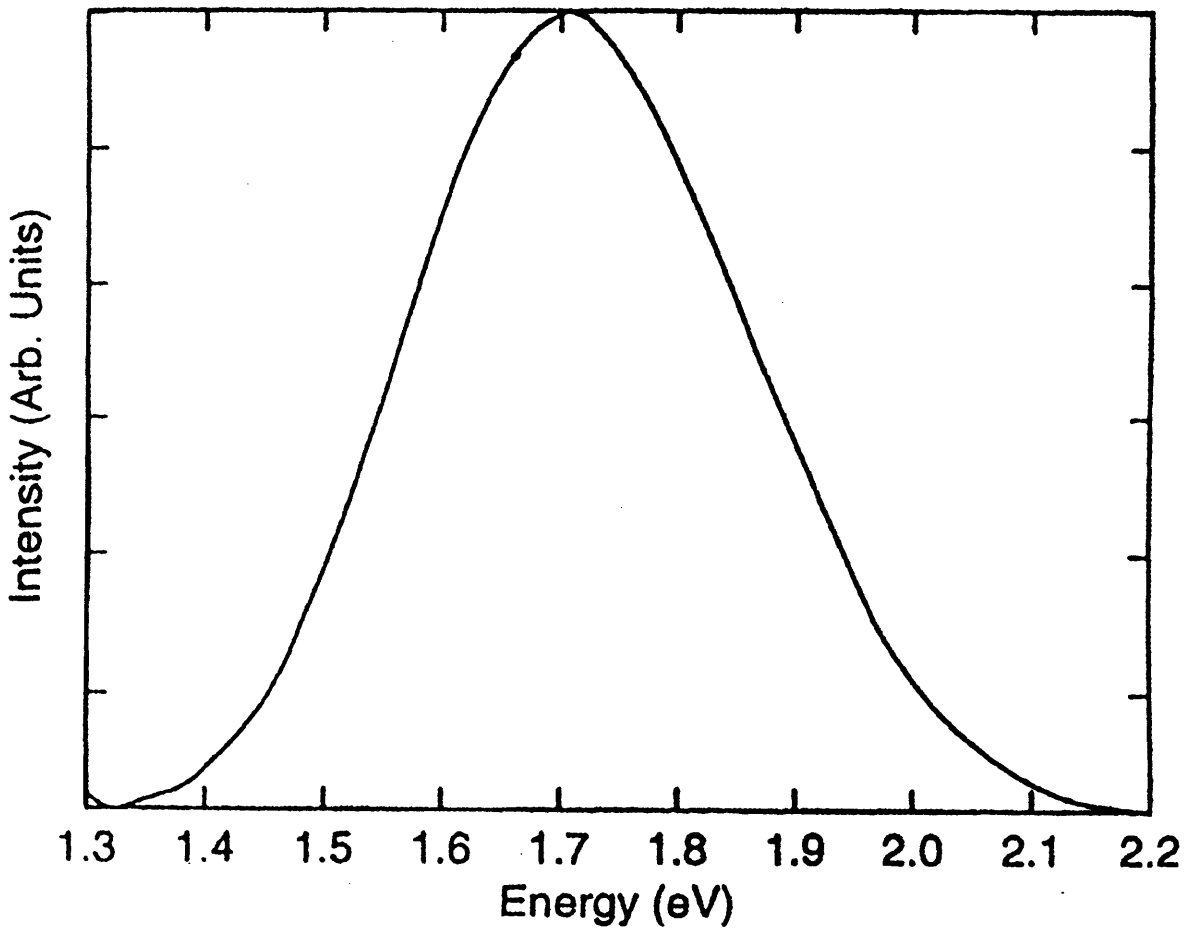

Figure 1-11 Typical red band photoluminescence spectrum from porous silicon. (From Ref. 57)

similar to that of amorphous silicon, where the emission involves trapped carriers.[58] The photoluminescence excitation behavior of porous silicon increases exponentially above the energy level of the luminescence peak.[59] This Urbach tail of states in the energy gap has also been identified in amorphous silicon. Recently, quantum confined structures of nonhydrogenated amorphous Si in superlattices has been shown to emit visible light, which could be shifted in energy through control of well width.[14] However, EXAFS (extended x-ray-absorption fine structure) studies have shown that the luminescent material has some form of crystallinity.[60] Heat treatments of porous silicon at high enough temperatures to drive off hydrogen from the amorphous matter have also failed to destroy the luminescence behavior,[61] indicating that hydrogenated amorphous silicon is not likely to be the luminescent center.

1.7.2.2 *Siloxene and related materials*

Polysilane and silicon based polymers have long be known to emit visible light under excitation. These materials are proposed to be created at the surface of the porous silicon during the etching and subsequent aging process, when there is plentiful hydrogen and oxygen around to form the complex molecular structures.[62] In general, these materials are believed to consist of chains or rings of Si interconnected by oxygen, or silicon layers with both hydrogen and hydroxide terminations. The optical properties of these materials are very similar to those observed in porous silicon, and the visible emission can also be tuned by chemical modification of the emitting species. Porous silicon samples which have been dipped in hydrofluoric acid to strip off their oxide layers, and then oxidized again to shrink their crystalline cores, should have been expected to show blueshifts of emission wavelength with decreasing particle size. This behavior is not always seen, and in fact, on occasion these treatments lead to a redshifting of the luminescence behavior according to some researchers.[15] These results, combined with the appearance of silicon-hydride peaks in infrared spectra of porous silicon, lend weight to the theory that the hydrogen content and the polysilane/SiH_x or siloxene[63] present determine the emission behavior, and that the particle size only controls the surface area and therefore how much area is available for "surface scum". Once again, other data exists to contradict these results and conclusions. The EXAFS data mentioned above points to a crystalline origin of the luminescent material. NEXAFS (near-edge x-ray absorption fine

structure) data from the same group shows that no oxygen is necessary to produce visible emission from the materials.[64] Also, the ability to heat treat porous silicon and drive off hydrogen from the samples without destroying the luminescence behavior cast doubts on this emission model.[42]

1.7.2.3 *Oxide Defects*

The oxide layer at the surface of porous and nanocrystalline silicon has also been proposed as the origin of the blue band emission behavior. The high energy, blue emission appears to grow in intensity with extended oxidation of the silicon nanostructures, and correlates with increases in the intensity of Si-O related infrared absorption signal.[44,65] This is not unexpected, as silicon dioxide is known to show visible luminescence.[66] In addition, the nanosecond luminescence lifetimes measured in this band and its insensitivity to oxidation steps designed to reduce average crystallite size point to an oxide surface related luminescence behavior.[67] However, other evidence is used to show that the blue band emission actually occurs from quantum confined recombination of carriers in the silicon crystalline cores. For example, the fast lifetimes for the blue band are argued to be indicative of direct recombination in nanocrystalline silicon, as opposed to slower recombination by carriers which are generated in the crystalline cores and then move into oxide interface states.[68] This proposed band structure is depicted in Figure 1-12.

The red band luminescence has also been explained as being related to the oxide interface states and related defects. Theoretical calculations have shown that an O-terminated Si sheet, similar to the surface of nanocrystalline silicon, would show direct gap behavior at 1.7 eV.[69] The nonexponential radiative decay of the red band luminescence[70] indicates that the emission might occur via carriers tunneling into localized surface states. The emission spectrum of the red behavior appears to redshift on a microsecond timescale, as more carriers move from the blue emitting cores into the red emitting oxide interface states. Electron spin resonance (ESR) studies indicate the presence of active oxygen-centric defects which correlate with photoluminescence intensity, pictured in Figure 1-13.[71] These non-bridging oxygen hole centers (NBOHCs) are known to emit visibly in the red part of the visible spectrum, and have been seen to shift in emission energy in the presence of hydrogen.[72]

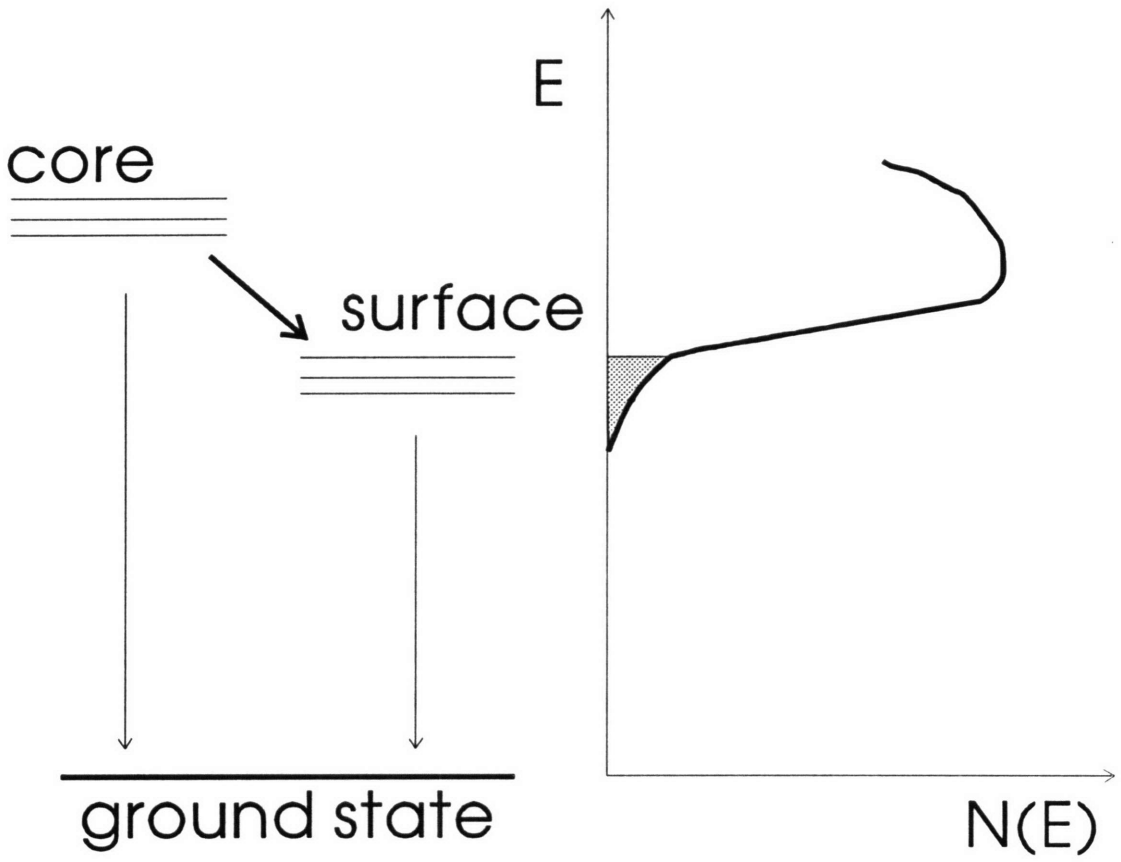

Figure 1-12 Kanemitsu model of density of states in oxidized silicon nanocrystallites. There are two luminescent centers, the core and surface states. The density of states falls of exponentially from the level of the core states. Higher energy transitions represent core state recombination, while lower energy transitions are coupled to localized surface states. (From Ref. 68)

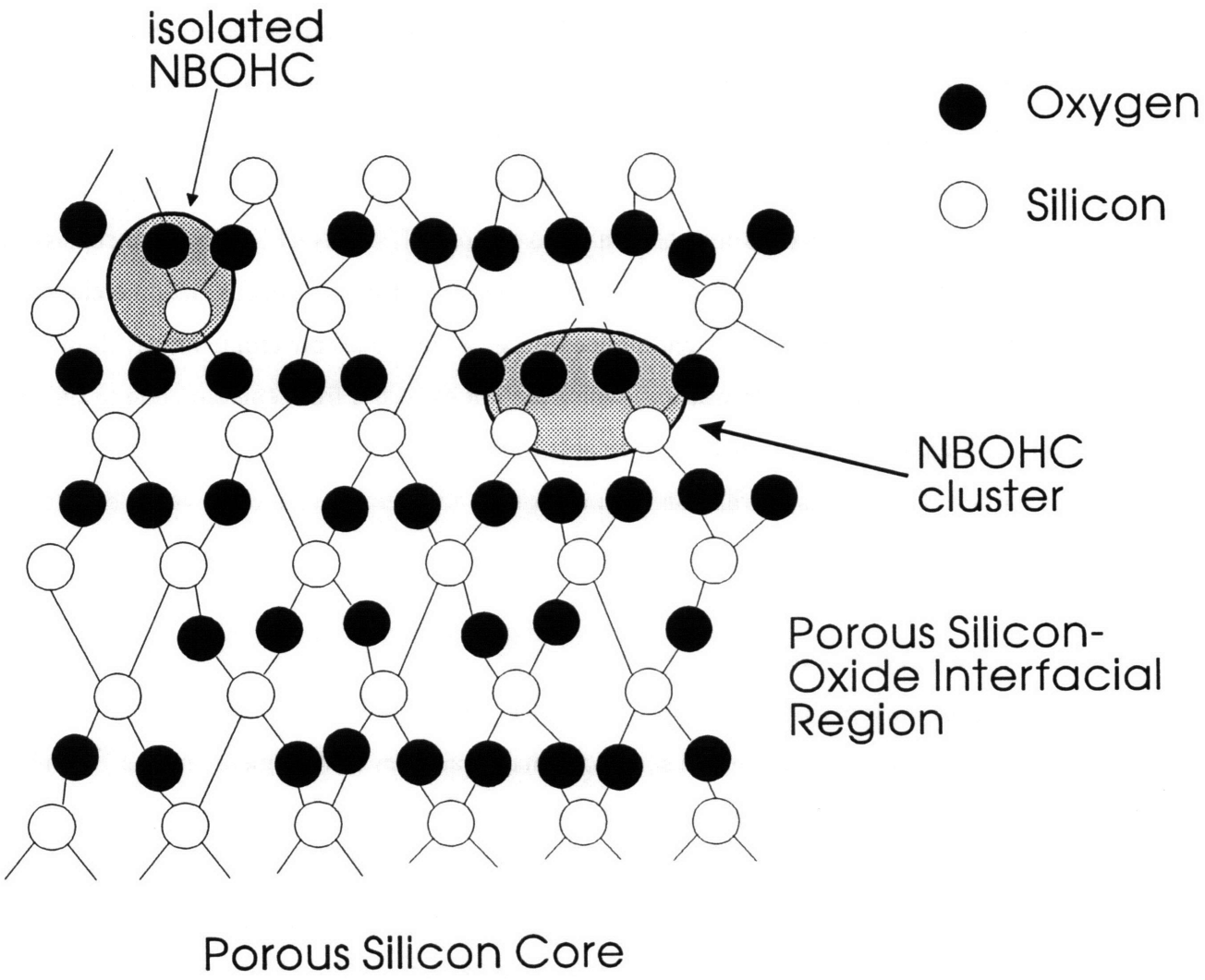

Figure 1-13 Model of non-bridging oxygen hole centers (NBOHCs) at disordered porous silicon-oxide interface. Center consists of a trapped hole on a $Si\text{-}O^{\bullet}$ complex in the interfacial region. (From Ref. 71)

Other evidence points against the likelihood that the red luminescence is due to oxide states. Porous silicon after formation is predominantly hydrogen passivated, as a result of being formed in HF. These as prepared samples consistently exhibit very strong red-orange emission behavior. As mentioned above, EXAFS studies have confirmed that oxygen is not required for visible emission from silicon nanostructures. The NBOHC theory is inconsistent with the fact that its emission does not cover the range of observed porous silicon emissions, and that characterization via resonant luminescence excitation at low temperatures shows the presence of phonon assisted transitions, which are not expected from emission due to oxide defects.[73] Finally, many groups have been able to shift the emission energy through shifts in mean particle size.[74] This correlation will not exist in a system controlled by oxide defect states.

1.7.2.4 *Surface States*

One of the more popular proposed mechanisms of luminescence from porous and nanocrystalline silicon is the surface state or "Smart Quantum Confinement" model.[75] This theory holds that the strong emission is the result of recombination events that occur via surface states in the energy gap of the quantum confined crystalline silicon cores. The theory can be considered an outgrowth of normal quantum confinement considerations, since it still postulates that transition energies will be controlled by particle size. However, the energy states in the gap that control luminescence are controlled by the surface bonding of the silicon particles.[76] In this system, the blue emission band reflects excitonic emission from the core of crystallites, while lower energy emissions arise from the surface states. A schematic of this model is depicted in Figure 1-14. In many ways this model also embraces the ideas of the oxide interface models described above, since it involves recombination through surface or interface states. However, these states are intrinsic to the semiconductor nanocrystallite system and are not extrinsic features like defects in the oxide.

Strong evidence supporting this model comes from the repeated ability of many groups to shift the luminescence behavior of porous silicon through a variety of processing steps, including heat treatments to effuse surface hydrogen,[77] and dips in a variety of chemical species.[78] A clear indication of the trends for hydrogen and oxygen passivated porous silicon

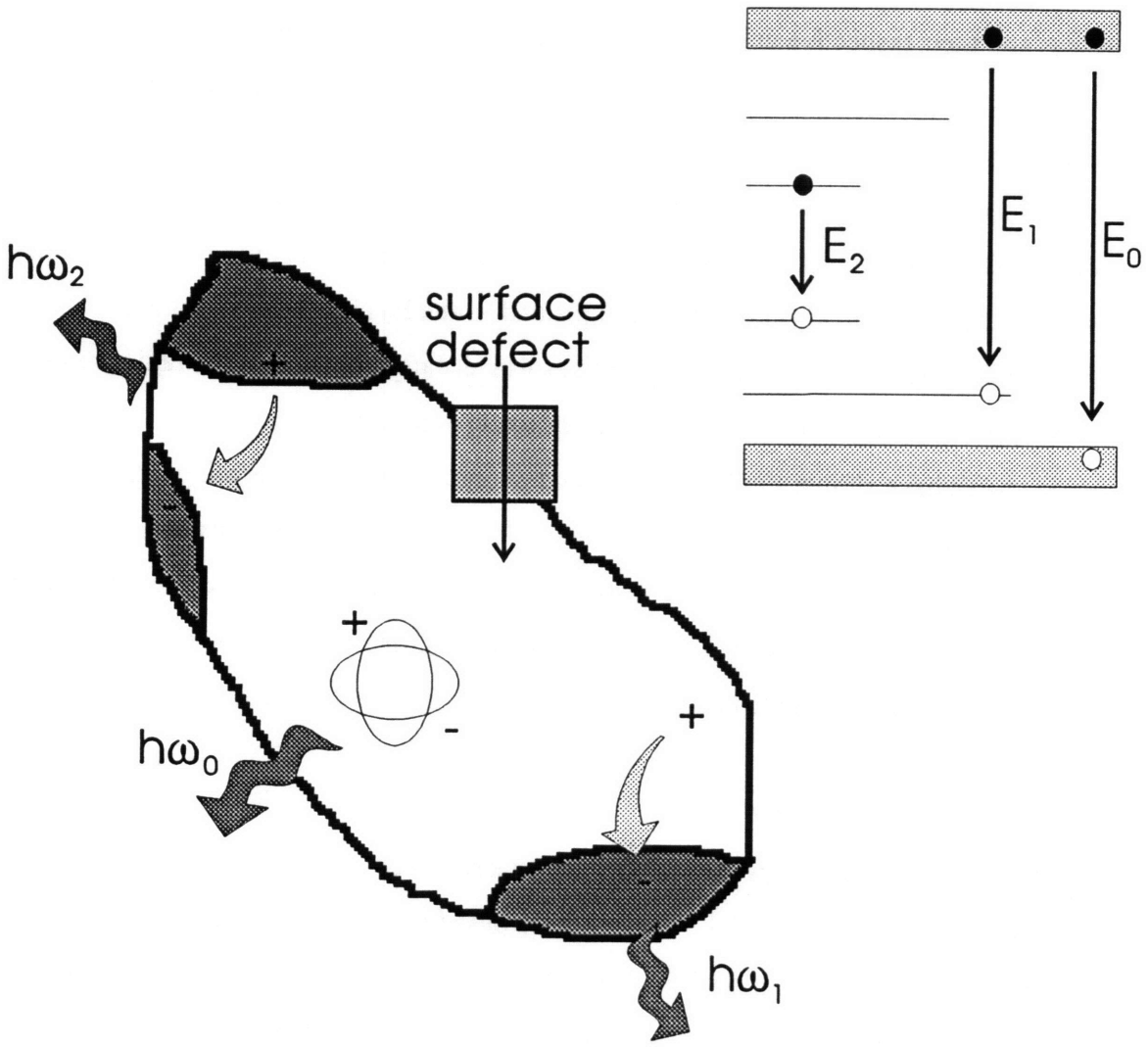

Figure 1-14 Koch surface state model of porous silicon luminescence. E_0 transitions represent excitonic recombination in core of crystallite. E_1 transitions represent recombination coupled to one localized surface state. E_2 emissions are low energy transitions are between two localized surface states. Surface defects act as nonradiative recombination centers. (From Ref. 75)

surfaces and their respective emission energies is reproduced in Figure 1-15.[79] In addition, the decay of the red luminescence has been found to be nonexponential, as would be expected from free or excitonic recombination of carriers.[80]

Since the smart quantum confinement model embraces the quantum confinement and oxide interface approaches, it is difficult to provide clear evidence refuting it. All correlations between size and emission energy can be explained as the E_0 transitions in Figure 1-14. Any redshifts in luminescence point strongly to the surface states controlling the radiative behavior. However, photoluminescence measurements of oxide and hydride passivated silicon nanostructures have shown similar lifetimes and phonon structure, indicating that the surface passivating species is not controlling the emission behavior.[74] Correlations between the increase in the ratio of silicon oxide to crystalline silicon concentration and the increase in blue luminescence[81] also present difficulties for this model, as this band has been ascribed to recombination in the crystallite cores and not through surfaces or interfaces.

1.7.2.5 *Quantum Confinement*

The simplest model for the visible light emission from silicon nanostructures is the pure quantum confinement model. This model is based entirely on the quantum confinement of carriers as described in section 1.5. Theoretical calculations have been made to predict the optical properties of quantum wires and nanocrystallites, such as the one shown in Figure 1-6. These models predict a great sensitivity of emission energy on nanocrystallite size, as well as a more direct-like transition in these materials. Evidence supporting this model comes from the body of work correlating nanocrystallite size with the luminescence emission energy, for example as shown in Figure 1-16.[60] Size distributions in these systems have been controlled in a number of ways, including size selective precipitation,[82] and repeated etching and/or oxidation steps,[83] and have shown a blueshift in emission wavelength with decreasing size. TEM and SEM characterization points to the existence of particles which are of the size range to exhibit quantum confinement effects in their behavior.[48] Shifts in the absorption edge of porous silicon films have been correlated correctly to porosity (and therefore crystallite size) in the films.[84] Finally, fine structure in the low temperature luminescence spectra of porous silicon point to a bulk silicon-like phonon assisted transition occurring at the crystalline cores

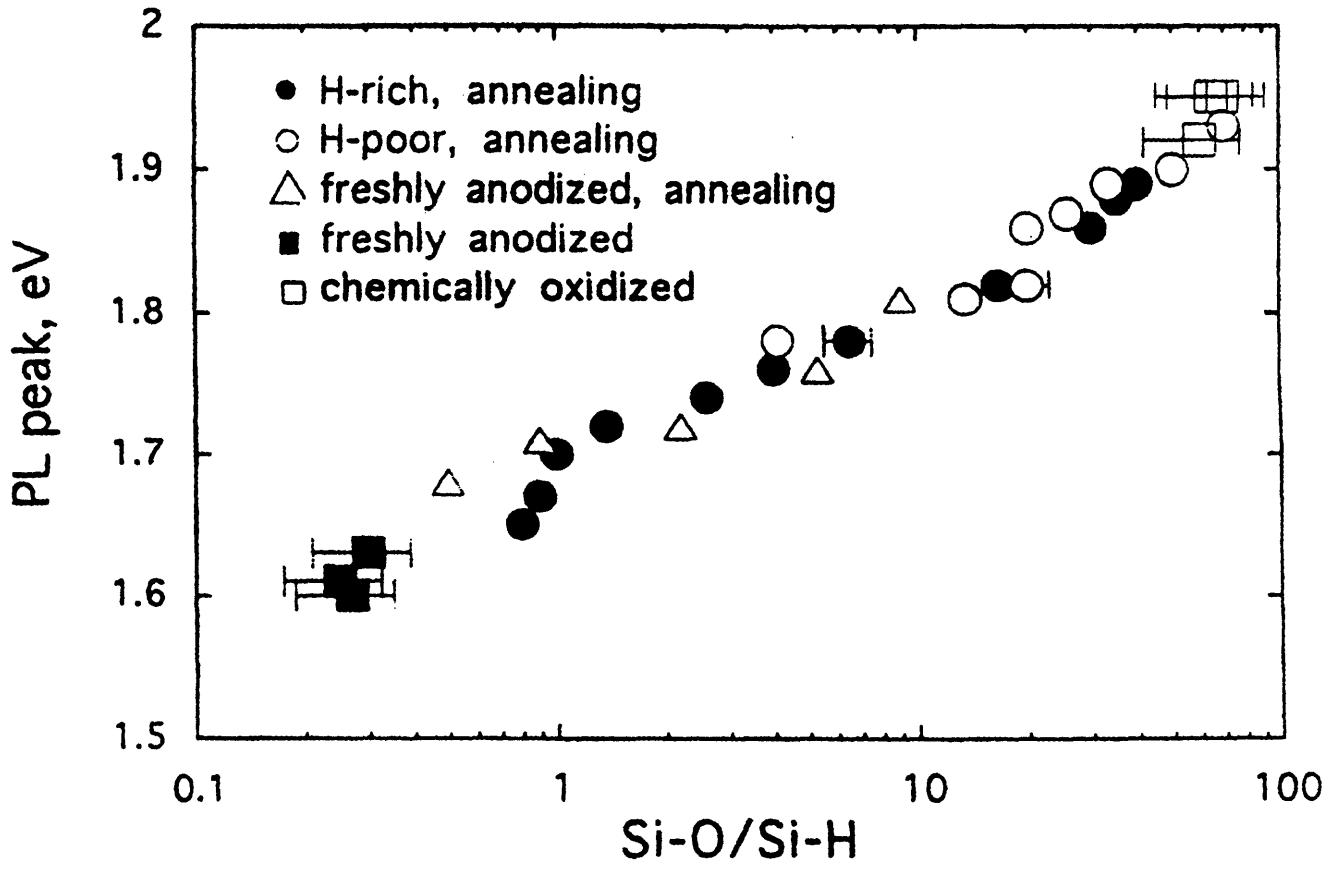

Figure 1-15 Correlation of PL peak energy from porous silicon with Si-O/Si-H bond ratio as measured by FTIR. (From Ref. 79)

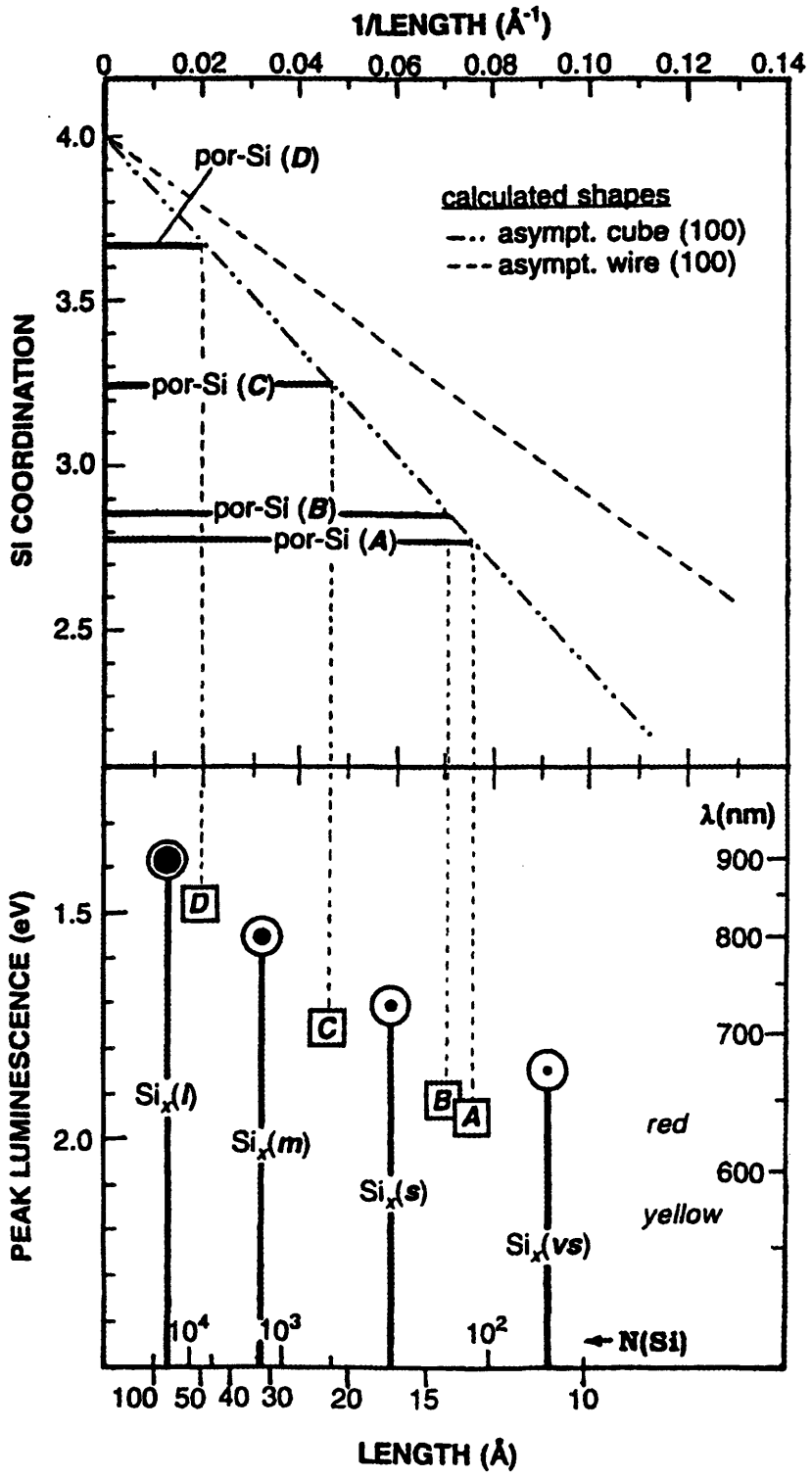

Figure 1-16 Correlation between emission energy and size as measured by PL, TEM, NEXAFS, and EXAFS for oxidized silicon nanocrystallites produced by disilane pyrolysis and porous silicon. Also shown are theoretical calculations for size as a function of silicon coordination in nanostructures. (From Ref. 60)

of the nanostructures rather than in any different chemical species that would be present at the particle surfaces.[73,74]

Though the quantum confinement model is the simplest model to explain the emission behavior, it is also the simplest model to contradict. Any evidence of red shifting of luminescence through treatments that should reduce particle size are difficult to explain away,[42] without resorting to complications such as the size distribution of emitting species, and the relative efficiencies of the various sizes. The nonexponential decay from the red band luminescence points to a more complicated luminescence behavior. Finally, the anomalous temperature dependence behaviors seen by many groups are difficult to justify using this simple model.[85]

Currently, there is much debate surrounding the luminescence mechanism from these silicon nanostructures. This is understandable considering the volumes of contradictory research that are being produced. At this point, most workers in the field have been grouped into one of three camps, supporting emission models based on NBOHCs, surface states, or simple quantum confinement. Evidence exists both supporting and contradicting each of the emission models. It appears that a great deal of future work will be necessary to clarify all the problems and questions that still exist in this system.

1.7.3 Structure and Size

For silicon nanostructures predicted to exhibit visible light emission according to quantum confinement considerations (1-3 nm or 50-1000 atoms), atomic structure is a very strong function of particle size. These structural differences will radically affect the electronic properties of the material. Theoretical molecular orbital calculations have predicted non-diamond cubic structures for silicon clusters up to 10 atoms.[86] Raman spectroscopy of clusters up to 7 atoms has confirmed these structures. For example, Si_7 has been shown to exhibit a pentagonal bipyramid structure.[87] Some studies have indicated that small silicon clusters have close packed high coordination number structures, approaching the β-tin structure.[88] Models have been constructed to demonstrate potential structures of clusters as large as 61 atoms, but much disagreement still exists among these studies.[89,90] Gas phase

absorption studies of small silicon clusters have suggested structural similarities between clusters of 18-41 atoms, but dissimilarity to bulk diamond cubic behavior.[91] The minimum stable size for the bulk structure has been predicted to be ~4200 atoms, using a tight-binding density-functional technique.[92]

Direct microscopic and x-ray diffraction evidence for the size of the emitting nanostructures in porous and nanocrystalline silicon is not complete. Crystallites above ~2 nm (~500 atoms) in diameter have been shown to exhibit the diamond cubic lattice structure of bulk silicon systems, by both TEM and Raman spectroscopy.[48,93] As the size gets smaller, direct examination of the structures is impossible using current experimental techniques. Experimental evidence has shown that the oxidized silicon nanocrystals emitting at 680 nm are approximately 2.5 nm in diameter by direct TEM measurement, with an estimated silicon core of only 1.1 nm (~80 atoms) in diameter.[60] This size has been derived through NEXAFS measurements of the silicon and silicon oxide volume fractions, and using the information to determine inner core and oxide shell thickness. Time-dependent tight binding calculations of electronic structure at this size range have been done to support these conclusions.[94]

The detailed crystalline structure of these small materials has not been clearly characterized. In fact, evidence exists that amorphous silicon emits visible light whose emission energy varies according to quantum confinement considerations,[95] that EXAFS and XPS characterization of porous silicon shows significant bond disorder and amorphicity,[43,96] and that amorphous silicon materials contain 1.4 nm crystallites that are not diamond cubic in structure.[97] In general, silicon regions on the order of 1-2 nm are found to exhibit tetrahedral coordination and have fairly well defined values of second and third nearest neighbor distance, similar but not identical to bulk diamond cubic silicon. This work suggests the possibility of the existence of phase which lies in between what is commonly referred to as crystalline or amorphous.

At these small sizes, surface effects will strongly influence atomic structure. Due to their high surface to volume ratios, nanocrystalline systems will show lattice distortion all along their surfaces and interfaces.[98,99] The lattice parameter of porous silicon has been measured by x-ray diffraction to be larger than bulk silicon ($\Delta a = \sim 10^{-4}$ nm), and increases with increasing porosity.[100] Capillary forces generated by particle's surfaces can produce

internal pressures which can alter atomic structure. Surface adsorbed species have also been shown to affect the lattice constant in nanoscale silicon systems.[101] In a dynamic sense, one might question whether surface structure (or structure at all) exists in nanosystems. High vibrational amplitudes of poorly constrained surface atoms might lead to "drum head" and diffusive collective modes, resulting in a structure which is constantly in a state of flux.[5]

The issue of the crystal structure of silicon of size smaller than 3 nm will become critical in the final determination of the nanocrystallite band structure. Also to be considered is that nanocrystalline silicon is built up into a structure from single atoms, while porous silicon is broken down from the bulk silicon lattice. These differences should play an important role in the observed behaviors of the materials. Better characterization of the sizes and structures and correlating them to emission behavior will shed considerable light on emission model debates.

1.7.4 Light Emitting Devices

A number of groups have begun to fabricate electroluminescent devices using silicon nanostructures as the active material. A wide variety of approaches have been used to develop practical silicon nanocrystallite based light emitting devices. For example, visible room temperature electroluminescence, with emission peaks of various wavelengths, was first observed from porous silicon based diodes formed by evaporating a semitransparent metal contact onto a porous silicon layer.[102] However, these devices reported very low quantum efficiencies (~10^{-6} to 10^{-7}). The emission intensity has been improved by incorporating a p-n homojunction or heterojunction into the device architecture and thus increasing carrier injection efficiency into the emitting region.[103] It has also been suggested that the comparatively low efficiency and poor stability of the porous silicon devices is due to localized carrier injection and electric field concentration resulting from the spotty porous silicon/electrode interface. Efforts to develop electrical contacts which permeate the porous silicon film, providing increased surface coverage and more uniform carrier injection, such as conducting polymer layers, have also led to improved device performance.[104]

This work has shown that device performance in these materials is strongly a function of carrier transport and injection efficiencies into and among the many layers of these systems.

In addition, the important problems of size distribution, interfacial properties, and of course the luminescence mechanism still play an important role in defining the characteristics of these devices.

1.8 Recombination Mechanisms

Electrons which are excited into the conduction band of a material can lose their energy in two manners. The electron can either recombine radiatively with its corresponding hole in the valence band and give off photons of energy equivalent to the energy of the recombination transition, or nonradiatively, where the energy is dissipated in the system without a photon emission event. The recombination implies that the system is already in a nonequilibrium state. The path that the excited electron uses to relax back down to its ground state is a function of the band structure of the material and therefore is dependent on the structure, defect concentration, surface properties, and carrier concentrations in the system.

1.8.1 Radiative Recombination

All materials emit light. If this emission is the result of an optical excitation, it is called photoluminescence. If the emission is due to electrical excitation, it is known as electroluminescence. Other forms of luminescence include cathodoluminescence from excitation by an electron beam or triboluminescence due to mechanical excitation. The types of radiative recombination can be differentiated by the location and origin of the initial and final transition levels for the emission event. Examples of these mechanisms are shown in Figure 1-17.

Light emission in semiconductors is typically characterized by photoluminescence (PL). This technique will be described in detail elsewhere. In it, photoexcited carriers give back energy in the form of emitted photons. This emission is typically characterized by its energy or wavelength, intensity as a function of wavelength, spectral width, and lifetime or duration of emission. These characterizations give insight into the nature of the emitting species and the recombination mechanism.

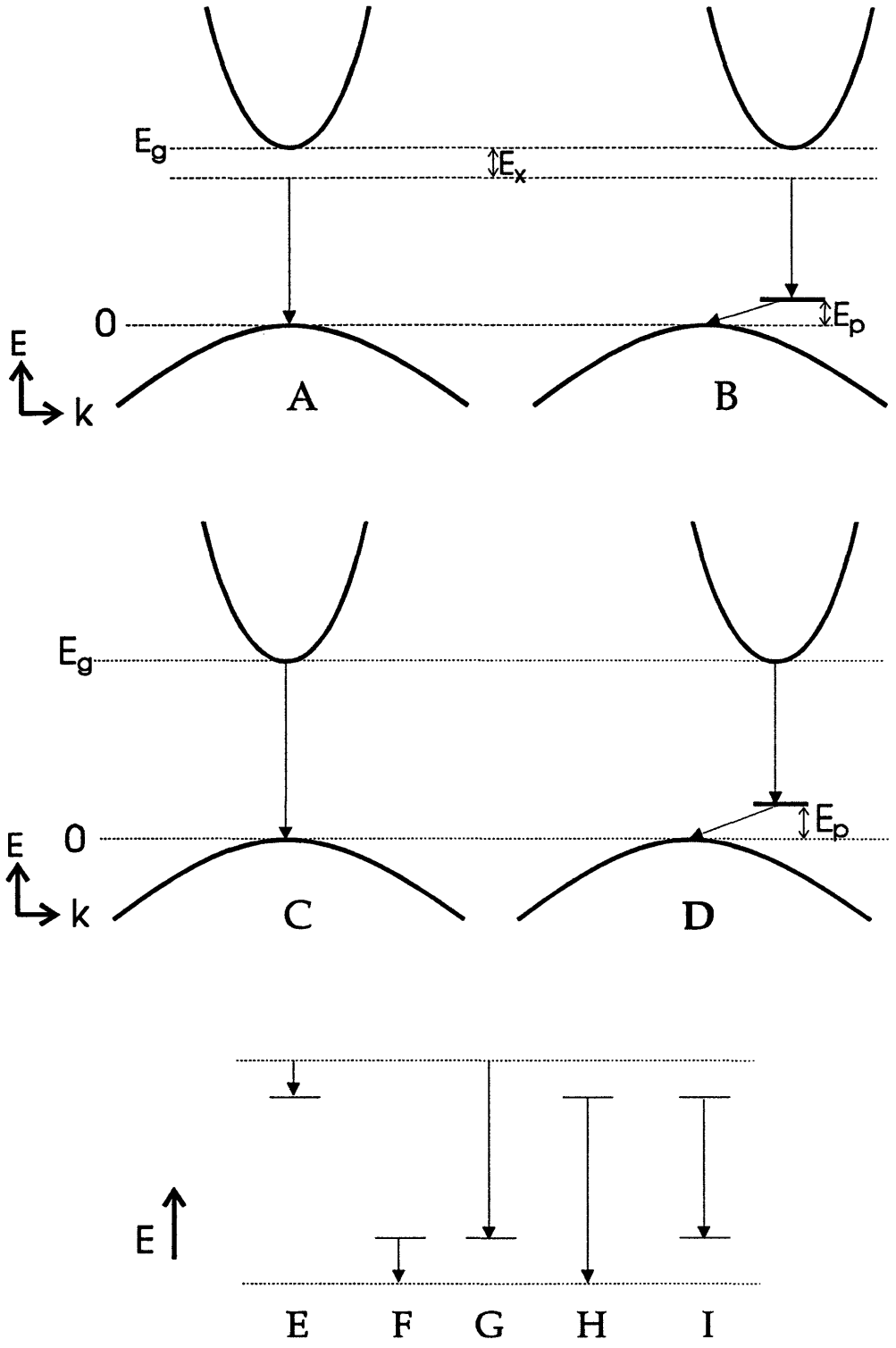

Figure 1-17 Schematic of radiative recombination mechanisms in semiconductors. Pictured are: Excitonic recombination in direct (A) and indirect (B) gap materials; band-to-band recombination in direct (C) and indirect (D) materials; shallow transition to donor (E) and acceptor (F) states; deep transitions to acceptor (G) and from donor (H) states; and donor-acceptor (I) transition.

1.8.1.1 *Excitonic Recombination*

A free hole and a free electron in a system can feel a Coulombic attraction. Thus, the electron can be thought of as orbiting around the hole. This pairing is called an exciton, and has a radius as was described in section 1.5. The electron and hole can be thought of as wandering as a pair throughout the crystal, a free exciton, or as being localized near an impurity or defect in the system, a bound exciton.

When a free exciton recombines in a direct gap system, the energy of the transition is given by,

$$\Delta E = E_g - E_x$$

where E_g is the energy gap of the material and E_x is the ionization or binding energy of the exciton. This ionization energy is a measure of the Coulombic attraction between the charged particles. This energy is given by,

$$E_x = \frac{-m_r e^4}{2h^2 \varepsilon^2}$$

Thus the energy emitted by the exciton is slightly lower than that from a strict band to band recombination event. In an indirect gap material, the presence of the momentum conserving phonon changes the transition energy of the exciton to

$$\Delta E = E_g - E_x - E_p$$

where E_p is the phonon energy. Excitons may also be bound to an impurity in the lattice. The ionization energy for a bound exciton is given by

$$E_i = E_x + E_b$$

where E_b is the additional energy binding the free exciton to the impurity center.

The luminescence emission from an exciton is very narrow spectrally, and shows up as a sharp, intense line in an emission spectrum. Figure 1-18 shows the low temperature emission from Si, and clearly shows a number of exciton related luminescence peaks.[105] The separation of these peaks correlates to the energy of phonons active in the process of emission.

Excitons represent the lowest energy state for electron-hole pairs, however excitonic effects are only seen in the purest materials, and at very low temperatures. Excitons tend to break up in the presence of electric fields caused by defects in the lattice, and thermalize when

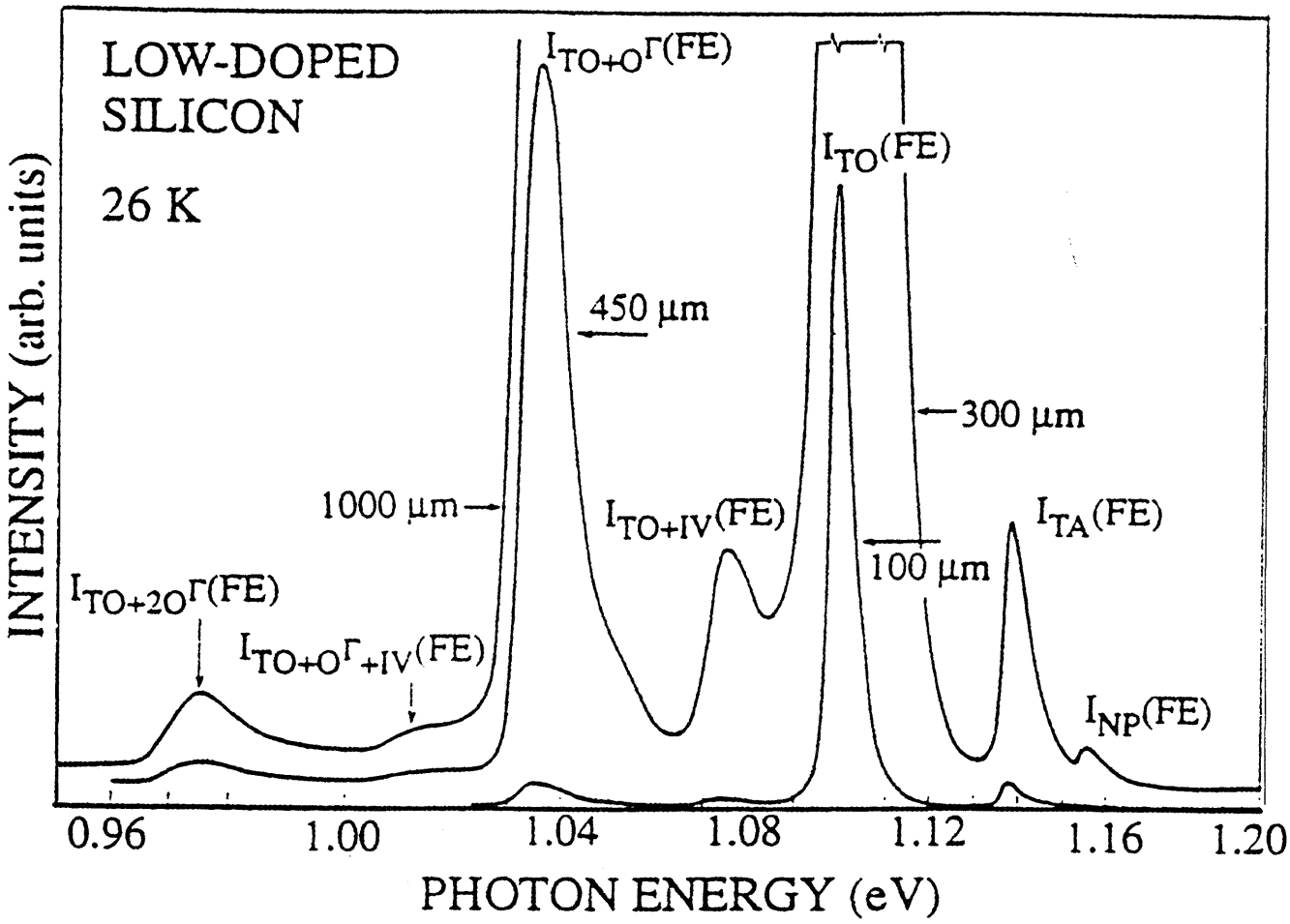

Figure 1-18 Low temperature luminescence from n-type bulk silicon showing excitonic luminescence and a number of phonon related peaks. (From Ref. 105)

the thermal energy is greater than the exciton's binding energy,

$$kT > E_x$$

where k is Boltzmann's constant and T is the system temperature. In nanocrystalline materials, the exciton binding energy has been predicted to be greater than in bulk systems.[22] Roughly, as nanostructure size decreases, localization increases the energy gap and reduces the dielectric constant, leading to an increase in binding energy. This means that for a given semiconductor, excitons can survive thermalization longer in a quantum confined system than in its bulk counterpart. This opens up the possibility for nonlinear optical effects, such as the saturable absorption described in section 1.5. These intense, narrow bandwidth nonlinearities may also be exploitable in the development of photonic applications.[106]

1.8.1.2 *Band to Band Transitions*

Although most electrons and holes will remain in excitons before recombination, a number are thermalized into the conduction and valence bands and can undergo band to band recombination. Direct gap band to band recombination results in the emission of energy equivalent to the band gap of the material. In an indirect transition, this is modified by the energy of the momentum conserving phonon absorption or emission event. For a direct gap material this recombination occurs very quickly, resulting in a nanosecond luminescence lifetime. In an indirect gap material this lifetime can be longer, extending into the microsecond or millisecond regimes. In these band to band type events, the density of states of the material will control the lineshape of the luminescence, through the control of how many carriers can be at specific energies, and where those energies lie with respect to each other. Therefore, in a monodisperse nanocrystalline semiconductor system, like chemically synthesized CdSe, one would expect to see narrow emission linewidths reflecting recombination from discrete energy levels.[20]

1.8.1.3 *Impurity Level Transitions*

Radiative transitions can also occur through energy states created within the band gap of a material by the presence of impurities, defects, or surfaces. Electrons or holes can become trapped within these defects and recombine radiatively with their oppositely charged

counterparts in bands or at other midgap states. For example, it is possible to get emission through shallow donor or acceptor states, involving low energy transitions to a nearby band. These radiative transitions have been found to be much less likely to occur than carrier relaxation to the band through a number of very small energy, nonradiative, phonon events. Deep transitions involve larger energy relaxations between donor levels and the valence band, or acceptor levels and the conduction band. Recombination can also occur between impurity or defect states that lie at different levels in the band gap. These transitions can also be relatively sharp, as the levels are fixed in energy. The transition energy is a measure of the Coulombic attraction of the impurity centers and so is strongly dependent on their spatial separation. The lifetime of the emission is a function of this energy, where higher energy transitions represent impurities in close proximity and therefore shorter lifetimes, while lower energy transitions represent spatially distant impurities and result in longer lifetimes. In general, radiative transitions that are coupled through a defect state are slower than band to band or excitonic recombination, because of the extra time required for a carrier to move into the impurity level, for example by tunneling processes.

1.8.1.4 *Intraband Transitions*

Intraband recombination is another type of transition present in semiconductor materials. Here a carrier relaxes to another level within its own band and this results in the emission of a photon. This transition is much more common in the reverse direction, intraband absorption, but has been observed in emission on occasion.[107] It is more likely that an excited carrier deep within a band relaxes via a thermalization process accompanied by the absorption or emission of phonons.

1.8.2 Nonradiative Recombination

An electron and hole can also recombine nonradiatively, giving off their excess energy in forms other than the emission of light. In many systems, this is the dominant form of recombination and so results in very poor emission efficiencies. For example, in germanium the radiative lifetime is predicted to be on the order of one second, however, the minority carrier lifetime in these systems is measured to be in the millisecond range. This means that

many carriers are losing their energy quickly to nonradiative transitions that are much faster and more probable than typical radiative emission.

In general, nonradiative transitions between two energy levels will occur if the energy difference between the excited state and the adjacent level is small, that is on the order of phonon emission. Once the difference becomes larger, it becomes more likely that a radiative recombination event will occur, and a photon of equivalent energy will be emitted. The presence of specific defects in a material creates a continuum of closely spaced states which act as a complete nonradiative bridge between the excited and ground levels.

There are a number of physical phenomenon which do not result in photon emission, but serve as relaxation pathways for excited carriers. These nonradiative recombination processes include: phonon emission, Auger recombination, and surface or defect recombination. These processes are often difficult to study since they only manifest themselves as a decrease in radiative emission, and there is often no clear way to isolate the specific mechanism of nonradiative recombination in a system.

1.8.2.1 *Phonon Emission*

Electrons excited into the conduction band can give back their energy through the emission of phonons or lattice vibrations. The typical energy for an individual phonon is on the order of millielectronvolts (meV) and so a number of these transitions must occur for the carrier to return to its ground state. These phonon emission events are similar in effect to the thermalization process that carriers excited deep into a band undergo while they relax back down to the band edge.

1.8.2.2 *Auger Recombination*

The Auger effect results when the emitted radiation from a carrier recombination event is used to excite another excited carrier, which then dissipates the energy nonradiatively. This dissipation typically occurs through a cascade emission of phonons. Since the effect requires carrier interaction, the effect becomes more intense with larger carrier concentrations. This has been seen in luminescence excitation studies, where the emission intensity scales with the excitation intensity until a point where the excitation process creates too many carriers and

induces Auger nonradiative recombination. It has also been shown that porous silicon luminescence can be quenched through an application of voltage, due an injection of extra carriers into the system.[41] Auger recombination also results in processes that utilize the energetic or "hot" carrier created during the event. These carriers can recombine radiatively to emit a high energy photon, or even have enough energy to be ejected from the semiconductor entirely.

1.8.2.3 *Surface and Defect Recombination*

The presence of perturbations, such as structural defects or surfaces, can disrupt the periodicity of the crystalline lattice and cause disturbances in the energy band structure of the material. These can act as sites for the nonradiative relaxation of excited carriers. Figure 1-19 is a model of a defect's effect on the density of states of a semiconductor. At the defect or surface, a continuum of localized states is created, linking the conduction band to the valence band. An excited carrier that is spatially within a diffusion length of the defect will be drawn to it and lose its energy nonradiatively through the continuum of states. For example, this effect has been observed in light emitting device structures that lose efficiency due to the presence of dislocations.[108]

In the case of surface states, the continuum of nonradiative transition states in the gap is thought to be the result of unsatisfied dangling bonds on the semiconductor surface. These missing bonds trap carriers and prevent them from recombining radiatively, thereby reducing the emission efficiency in the system. In nanocrystalline systems, it is expected that even one dangling bond will be enough to trap carriers and prevent photon emission.[109] In addition, the fast relaxation caused by these trap sites and continuum of states prevents a buildup of excess carriers in the energy levels of the quantum dot material. This prevents the development of any nonlinear optical effects in the semiconductor nanocrystallite. Therefore, it becomes vitally important to remove these nonradiative centers from the system in order to promote novel optical behaviors.

The nonradiative recombination centers present due to dangling bonds on the semiconductor surface can be eliminated by chemically passivating the bonds. Experimental work has shown that aging a bulk silicon surface in air and thereby oxidizing it reduces the

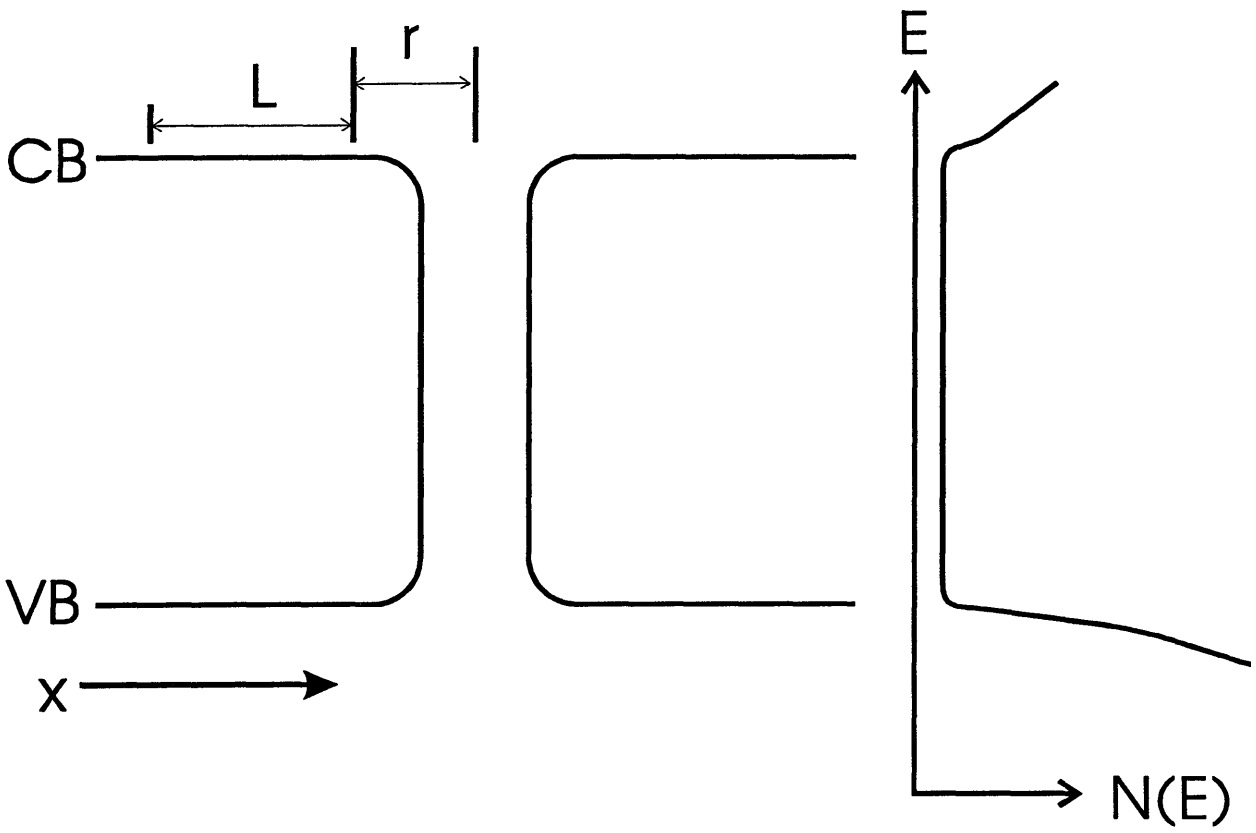

Figure 1-19 Model for effect of defect state on energy band and density of states of semiconductor. Defects create a continuum of states in gap which act as a nonradiative pathway for the relaxation of excited carriers. *L* represents the carrier diffusion length and *r* the defect radius. (From Ref. 107)

number of surface states from ~10^{15} cm^{-2} to ~10^{11} cm^{-2}.[110] Theoretical work has shown that passivation of the silicon surface by hydrogen moves surface states out of the band gap and into the conduction band.[76,111] This correlates well with work in amorphous silicon, where hydrogenation eliminates many nonradiative defect states and enables light emission. Silicon surfaces have also been efficiently passivated using halogen species.[112] This surface control of emission efficiency behavior is also key in nanocrystalline and porous silicon. The role of surface is determining the emission behavior from silicon nanocrystallites will be described in section 1.10.

1.9 Silicon Processing Basics

1.9.1 Oxidation of Silicon

Over time the surface of bulk silicon exposed to air becomes covered with a surface oxide layer. This layer quickly grows of a few monolayers of oxide, but then growth rate slows so that the layer reaches a stable thickness of ~3 nm.[113] This oxide has been one of the biggest advantages for working with silicon based microelectronics, since the layer serves both as a passivation and insulation layer. A defect free, stoichiometric oxide (SiO_2) can be grown using well controlled thermal or chemical oxidation techniques. As has been discussed above, the presence of defects in this oxide or along the silicon crystallite and oxide interface can create electronic traps and has also been cited as a possible origin of the observed visible luminescence from silicon nanostructures.

In bulk silicon systems, the growth of this oxide has been modeled extensively for a variety of oxidation techniques. The mechanisms for the formation of the oxide are based on the fact that the oxidizing species must diffuse through the oxide layer to react with silicon at the semiconductor surface. The reactions for the formation of the oxide depend on the oxidizing species. For "dry" oxidation by oxygen gas (O_2), oxygen ions (O^{2-}) diffuse through the oxide layer to react with silicon, giving an overall reaction,

$$Si + O_2 \rightarrow SiO_2$$

Oxidation of silicon by water vapor or "wet" oxidation has been modeled by the reaction,

$$Si + 2H_2O \rightarrow SiO_2 + 2H_2$$

Here the oxidizing species that diffuses through the oxide layer are hydroxyl ions (OH^-). In both of these cases some of the crystalline silicon material is consumed by the reaction. In the case of planar bulk silicon, the growth of an oxide film of thickness r_O consumes a layer of silicon $0.45r_O$ thick. In spherical nanocrystalline materials, this size reduction coupled would increase carrier quantum confinement and could change the emission wavelength of the material.

Silicon processing commonly uses hydrofluoric acid etches of bulk silicon oxide to produce a hydrogen passivated surface. When exposed to air, it is gradually replaced by oxygen in the formation of a native oxide layer. The initiation of this process has been studied by infrared spectroscopy to understand the chemistry of the oxidation.[114] After the initial hydrogen layer is removed, the oxidation proceeds as described above.

The kinetics of the oxidation process can be modeled based on three phases of the motion of the oxidizing species towards the silicon surface. First, it must be transported from the bulk of the gas to the surface of the oxide layer. In most oxidation systems, this step is extremely fast and therefore not the rate limiting process. It can be assumed that the concentration of the oxidizing species is its solid solubility in the oxide layer. The charged oxidizing species is transported through the oxide layer by diffusion to the silicon interface. Here a reaction between the oxidizing species and the silicon must occur.

The rate of growth of the oxide then becomes a function of the rate limiting step in this process. During the initial stages of growth, the interfacial reaction limits the process, and the growth rate is given by,

$$\frac{dx}{dt} = \frac{N_0 k}{n}$$

where x is the oxide layer thickness, t is the time of oxidation, N_0 is the concentration of the oxidizing species at the outer surface of the oxide layer, k is the interfacial reaction rate constant, and n is the number of molecules of the oxidizing species per volume of oxide. At later stages, when the oxide thickness has increased, ionic diffusion is the limiting step, leading to a rate of

$$\frac{dx}{dt} = \frac{1}{2}\sqrt{\frac{2DN_0}{nt}}$$

where D is the diffusion coefficient of the oxidizing species in the oxide. In practice these simple models only roughly describe the oxidation process in silicon. Effects such as crystallographic orientation, defect levels, and geometry play important roles in determining the oxidation rate.

The reactivity of small clusters of silicon cannot be assumed to follow the same patterns as that of planar bulk silicon. Structural characterization of silicon nanocrystallites has shown oxide shells ranging from 0.5 to 1 nm in thickness, on particles ranging from ~2 to 10 nm in total diameter.[60] In the case of small semiconductor systems, the spherical nature of the nanocrystallite surface must be taken into account to model the oxide growth process.[115] A number of groups have begun studying the effects of shape and size on the oxidation process in silicon nanostructures.[54,116] Some theoretical work has predicted that curvature of the oxide layer creates strain effects which can slow the ionic diffusion process.[117] It can be assumed that prolonged oxidation of these nanocrystalline silicon systems will eventually result in the conversion of the silicon cores entirely into silicon oxides and a corresponding drastic change in electrical and optical properties.

The electronic properties of the oxide layer will have strong effects on the nanocrystallite properties. This is also the case for planar bulk silicon, where trapped oxide charges and unsaturated bonds result in midgap states that reduce device performance. In the same way, the silicon oxide interface has been predicted to play a strong role in the emission properties of nanocrystalline silicon.[118] Emission models based on interfacial recombination and on nonstoichiometric oxides are based on the fact that the oxide passivation for complex nanocrystalline silicon surfaces is far from perfect. In these models, the emission characteristics of the nanostructures are shown to have a correlation to the chemistry and stoichiometry of the oxide layer. The properties of the surface layer will be discussed further in section 1.10.

In the microelectronics industry, thermal oxidation of silicon is typically accomplished through high temperature furnace treatments under precisely controlled oxygen flows. Both the temperature and flow rates are carefully controlled to insure the growth of defect free, stoichiometric oxides when device performance requires it. In addition, it possible to include other elements in the gas flow, such as halogens, to further reduce the density of oxide related

defect states and further improve device performance. Oxidation of silicon can also be accomplished through wet chemical techniques. One typical chemical oxidizer used in the microelectronics industry is nitric acid (HNO_3). Nitric acid promotes silicon oxidation through a complex series of reactions whereby holes are formed by the reaction of nitric acid with trace amounts of nitrous acid (HNO_2) present in solution. These holes then react with hydroxide ions present in the solution from the dissociation of water and with the silicon surface to produce silicon dioxide. In practice, nitric acid is combined with an oxide etchant, hydrofluoric acid (HF), to create a system that simultaneously oxidizes silicon and etches the newly grown oxide. This mixture is therefore a powerful etchant for crystalline silicon.

1.9.2 Etching of Silicon and Oxides

The silicon microelectronics industry is also dependent on the ability to remove the native oxide layer from silicon and even some of the crystalline layers themselves through etch steps. These steps can be used selectively to shape the oxide and crystalline layers on wafers in order to create complex device architectures. Hydrofluoric acid is typically used to remove oxide layers, and is used in combination with nitric acid to etch away crystalline silicon.

The etching reaction of hydrofluoric acid on silicon dioxide is written as

$$SiO_2 + 6HF \rightarrow H_2SiF_6 + 2H_2O$$

In industry, a mixture of HF and NH_4F, called a buffered HF etch, is typically used to remove oxide layers consistently without damaging photoresist layers. The kinetics of the process is strongly dependent on the concentration of HF and HF_2^- in solution. The etch rate for thermal oxides in 100:1 H_2O:HF is 100 nm per minute.[119] In addition, there are enhancements of the etch rate caused by higher polymeric species, such as $H_3F_4^-$, which are present as well. Etch rates for oxides are also strongly dependent on the quality of the oxide itself. It has been shown that thermal oxides etch slower than other oxides. This relates to structure, porosity, and stoichiometry of the films. In general, films of higher porosity and with a larger defect concentration will etch faster than more perfect films, but recently some porous silicon work suggests that nonstoichiometric oxides etch more slowly than SiO_2.[120]

After removing the oxide layer, the HF can begin to etch the underlying crystalline silicon. This rate has been measured as .03 nm per minute.[121] The HF reaction with silicon

was described earlier in the context of porous silicon passivation. After oxide removal by HF, the silicon surface is fluorine terminated. As shown in Figure 1-20, the Si-F bond is strongly ionic and so polarizes the Si-Si back bond by drawing negative charge towards the surface F, and leaving the Si charged positively and allowing for the insertion of the H^+ ion into the Si-Si bond. The upper Si gains another fluorine bond, while the lower silicon becomes bonded to the hydrogen. In this way, the HF leaves the silicon surface hydrogen terminated, and results in the removal of silicon in a soluble H_2SiF_6 complex. These surfaces have experimentally measured low surface defect densities.[122] The specific termination of the surface seems to be dependent on the crystallographic orientation and total hydrogen content, as monohydride, dihydride, and trihydride terminations have all been observed, depending on specific conditions.[123,124]

There are a large number of other etching techniques used for the removal of both silicon and silicon dioxide from surfaces in standard microelectronics processing. One dry etching technique is plasma etching of semiconductors by reaction with gas phase etchants and ion bombardment. Ion milling and sputter etching also involve the bombardment of the surface by energetic ions in order to physically dislodge atoms. Finally, there is a whole spectrum of concentration and component variations in wet chemical etching, each of which has been designed for use as fast or slow or crystallographically controllable etches.[125]

1.9.2.1 *Stain Etched Porous Silicon*

A common etchant for planar bulk silicon is a mixture of HF, HNO_3, and H_2O. This combines the oxidation properties of nitric acid with oxide removal by hydrofluoric acid to remove crystalline silicon. The overall reaction for the etching process then becomes,

$$Si + HNO_3 + 6HF \rightarrow H_2SiF_6 + HNO_2 + H_2O + H_2$$

A large amount of research has been done to characterize this etching system and the rates are well understood as a function of solution concentration.[126] HNO_3 attacks the silicon surface at the local cathode and donates holes. If these holes react with Si, SiO_2 is formed and the site now acts as an anode site. This oxide is subsequently etched by HF, producing H^+ which aids in further attacks by HNO_3. The cycling of one site between cathodic and anodic behavior results in a polishing etch. It has been found that systems with low HNO_3 and high HF

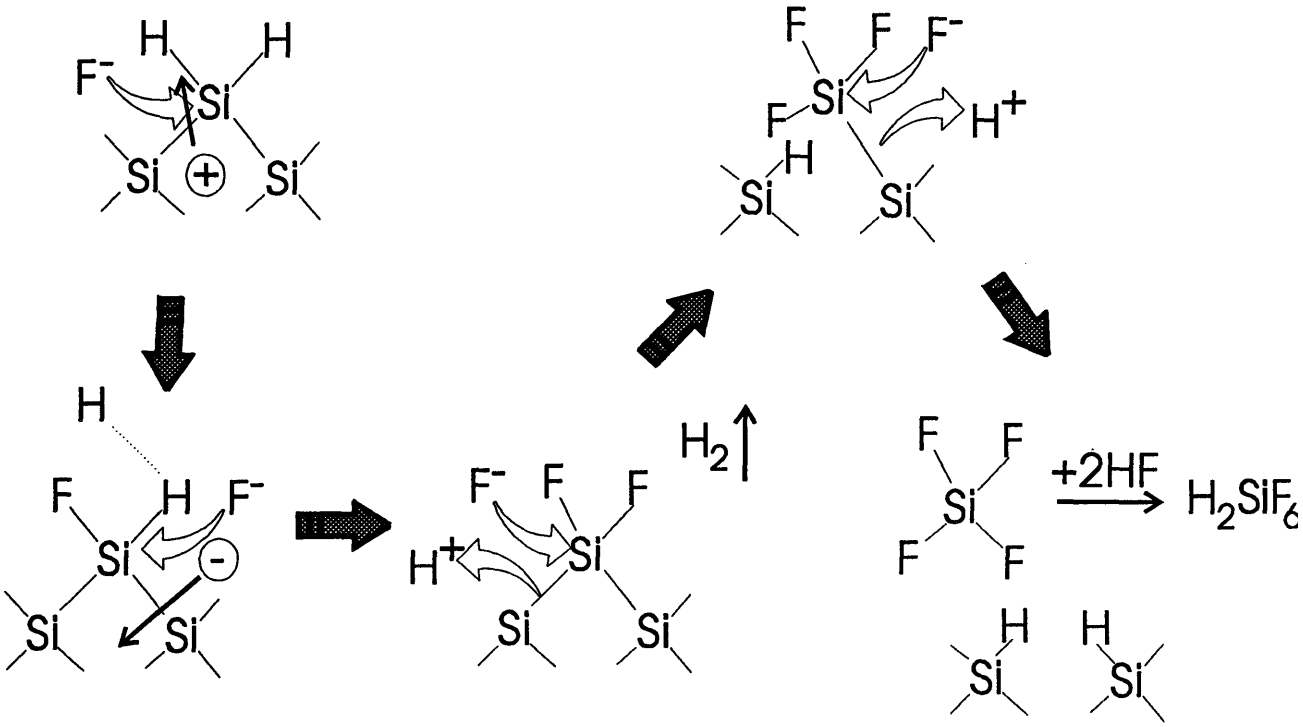

Figure 1-20 Proposed mechanism for etching of silicon by hydrofluoric acid. Silicon is removed in H_2SiF_6 complexes, leaving the surface hydrogen terminated. (From Ref. 46)

concentrations are limited by the rate of silicon oxidation, while systems with lower HF concentrations are limited by the oxide etch rate. The oxidation limited systems produce films which are hydrogen passivated, but eventually they are replaced by a layer of oxide through natural oxidation processes. The etch limited systems are produced with an oxide passivating layer covering the surface. In either case, one important factor is the continual stirring of the solution above the semiconductor surface, to maintain a constant source of the ions necessary for the reactions to run.

The $HF/HNO_3/H_2O$ system has been used recently in the fabrication of light emitting porous silicon layers.[127] Here, the holes created at the anode diffuse to other sites on the silicon surface before they react with silicon, so there is no cycling of individual sites between anodic and cathodic behavior. In the same way that initial pore formation leads to a preferential transport of holes to pore tips in anodically etched porous silicon, stain etched films oxidize and etch more efficiently in different specific areas of the crystalline substrate, leading to the formation of a porous microstructure. These films are produced without the necessity of an external source for holes in the silicon system, since they are provided by the nitric acid oxidation step.

The $HF/HNO_3/H_2O$ system results in the dissolution of crystalline silicon material. This again provides a method for reducing the size of silicon nanostructures, while maintaining a hydride or oxide passivating layer. These alterations in surface and size should be critical to light emission properties of the materials.

1.10 Surfaces

1.10.1 Nanocrystalline Silicon Surfaces

When considering the properties of nanostructured materials, it is critical to understand the role of the surfaces of the systems. In these small systems, the surface to volume ratio is much larger than in bulk systems. In a diamond cubic system, the ratio of surface atoms to total atoms for a cube of n unit cells truncated on the (100) surfaces is,[128]

$$\%Surface = \frac{6n^2 + 2(n+1)^2 + 2(n^2-1) + 2(n-1)^2}{(n+1)^3 + 3n^2(n+1) + 4n^3}$$

For example, if one assumes a quantum dot of diamond cubic structure consisting of 27 unit cells, then of the 280 total atoms in the system, 110 of them lie on the surface of the dot. In silicon, this means that a cubic dot with ~1.63 nm edges is 39% surface, dictating a strong surface control over materials performance. The passivation, chemistry, and cleanliness of the surface will all play roles in determining the energy band structure and therefore recombination physics of the nanocrystallites. When considering the development of nanocrystallite based optoelectronic or photonic applications, it is clear that the active optical semiconductor materials must be incorporated into carefully designed host matrices. Possible semiconductor nanoheterostructure materials could include Si nanocrystallites embedded within polycrystalline bulk silicon, conducting polymers, oxides, or in the case of the photonic switch, a waveguiding material.[129] The interfaces between the nanocrystallites and these hosts will be a strong factor in controlling device characteristics and performance.

In the specific case of nanocrystalline or porous silicon, the role of the surface in determining optical properties has already come in serious debate. The intricate morphologies of nanostructured silicon materials provide room for adsorbates which can alter the band structures of the underlying material, and in some cases emit visible light on their own, as is predicted by polysilane and siloxene emission models. As mentioned above, the presence of defects and dangling surface bonds will strongly limit the efficiency of band to band radiative recombination. Oxide defect models of porous silicon emission are based on interfacial defects that control the luminescence of the system. The smart quantum confinement model of emission relies on the presence of states created in the energy gap of silicon by the bonding of the surface silicon with hydrogen or oxygen, and the resulting recombination through these levels. In all cases, the surface properties of the particles are predicted to play an important role in the optical properties.

1.10.2 Surface Structure

The surface of a crystal is more than just the line that ends the periodic lattice structure. More importantly, the surface atoms are not tetrahedrally coordinated, as are atoms within the mass of the crystal, and as such they have higher energy and are less firmly bonded than the internal atoms. Thus surfaces will have different structures and properties than the

cores of the crystal. In spherical nanocrystallites, these problems are compounded by issues of shape and the high surface to volume ratios in the systems.

An ideal surface is one that retains the structure of an internal plane of the system, with no atomic adjustments for surface effects, resulting in a perfect crystal terminated at a plane. This is not seen in practice. A real surface undergoes some degree of relaxation, where bonding changes on the surface allow the outer atoms to relax away from the core of the crystal, resulting in a slightly larger lattice spacing near the surface. This relaxation effect reduces as one moves into the heart of the crystallite. Surfaces will also have counterparts to all of the defects seen in the cores of crystals. Impurity atoms, interstitials, vacancies, terraces, and steps will all be present to some degree, and will play a major role in passivation and adsorption processes.

In silicon nanocrystallite systems, the most important surface process is the passivation of unsatisfied surface bonds. The silicon surface atoms do not have their normal tetrahedral coordination, and as such the extra unsatisfied bonds are considered "dangling". In nanocrystalline silicon, these bonds are often terminated with hydrogen or oxygen. Hydrogen termination results in a monolayer of a combination of silicon monohydride (SiH), dihydride (SiH_2), and trihydride (SiH_3) complexes. These have all been detected on the surfaces of nanocrystalline silicon using infrared spectroscopy. Oxygen passivation of the surface results from the growth of a thin layer of silicon oxide, usually SiO_2, a number of monolayers deep into the crystalline core. The stoichiometry and defect content of this oxide varies in the samples, as does its thickness. In addition to hydrogen and oxygen, it has also been possible to terminate silicon surfaces using halogens. It is also conceivable to create silicon based polymers and organic molecules on the surfaces of nanocrystalline or porous silicon, given the complex surface morphology and the presence of reactive hydrogen and oxygen. In all cases, these layers are critical in the determining the extent of surface passivation and the creation of midgap defect centers.

1.10.3 Electronic Properties

The electronic structure of the surface layer in nanocrystallites can control most of its optical behavior. As discussed earlier, the creation of states in the gap through the presence

of impurities, structural defects, or dangling bonds can alter or eliminate both visible light emission and nonlinear optical response. Since the nanostructures of interest are smaller than the diffusion length of carriers in silicon, it can be expected that all the carriers generated in the system will feel the effects of changes in electronic structure caused by the surface. This means it may be impossible to separate the surface and bulk properties in such small systems.

1.10.3.1 *Dangling Bonds*

Dangling bonds on the surface of the material present one kind of state which is detrimental to visible light emission. These create nonradiative pathways which quench emission. A simple dangling bond normally is a broken covalent bond, and thus contains one electron. It is considered amphoteric, able to donate or accept an electron, and thus can lie anywhere in the energy gap of the material. The dangling bonds can act as traps for electrons and holes both in the gap and in the bands, localizing carriers at physical sites. It has been shown that in nanocrystalline semiconductors that by passivating these bonds it is possible to enable visible light emission.[130] These results have been matched by theoretical predictions that hydrogen or oxygen passivation of silicon dangling surface bonds moves them out of the gap and into the bands.[109]

1.10.3.2 *Surface Defect States*

The surface structures of nanocrystalline materials can create a number of different types of states in the energy gap of the semiconductor which can prevent the radiative relaxation of carriers. Intrinsic surface states result from a pure surface and its bonding. These states are a property of the semiconductor itself, through the merger of core and surface properties, and as such their position should track the expansion of the energy gap that occurs when the material is quantum confined.[94] Typically, the state will lie inside the energy gap of the material and as such will result in a lower energy transition than band to band recombination. Theoretical models show that this position can depend on the specific chemical bonding occurring at the surface, for example the states created by hydride passivated and oxide passivated surfaces may be different.[131] In a nanocrystallite system, if

such lower energy states exist, they are likely to be easily coupled to excited carriers due to spatial confinement, and thus control the luminescence behavior.

Extrinsic surface defects are those caused by defects in a surface layer, for example, oxygen hole centers in SiO_x. These defects can create states in the band gap of the material as above and act as nonradiative transition centers. These defects can also create special states within the band structure which can act as a radiative recombination centers for excited carriers.[71] These centers would not be a function of the semiconductor material, but only of the specific defect under consideration. This implies that the defect levels will not track the motion of the band edges as determined by quantum confinement. In many cases, these levels can be shifted through modification of the defects themselves, such as increasing hydrogen content of NBOHCs.[132]

The role of a silicon oxide surface layer is important in the development of the electronic properties of a nanocrystallite. The oxide layer contains interface trapped charge which results in the development of states within the band gap of the silicon. These oxide interface states will have a faster recombination lifetime than transitions from the band edges. They can also be removed through passivation, as has been demonstrated by wet hydrogen treatments of silicon oxide surfaces. There are also a number of slower states that can be created at the silicon oxide interface which can have either positive or negative charge. These states have been show to change the mobility of carriers in the surface region of the semiconductor and thus alter electronic device performance. The oxide layer can also contain mobile oxygen ion vacancies whose charge can alter the band structure of the material in the surface region. Though in bulk semiconductors these problems are considered interface or surface issues, in a nanocrystallite these effects will be felt throughout the entire system.

1.10.3.3 *Adsorbed Materials*

Materials which adsorb onto the surfaces of the silicon structures can also act to modify the emission behavior. Siloxene like structures on the surfaces of porous silicon can act as independent visible emission agents, regardless of the nanocrystallinity or band structure of the underlying material. Polar molecules sitting on the surface of nanostructures can induce local electric fields that will change the position of energy levels, especially surface states

within the material.[133] This can lead to the favoring of nonradiative pathways which would quench the luminescence behavior, as has been observed with methanol quenching of porous silicon luminescence.[134, 135]

1.11 Objectives and Outline

1.11.1 Questions

Having described the opportunities in optoelectronics and photonics available for silicon based materials and looking at the current state of research into the optical properties of nanostructured silicon, it becomes clear that there are a number of questions which still need to be answered and clarified before useful devices are developed in this materials system. The work described in this thesis helps to better define many of the questions and provide preliminary answers to some of them. It is clear that the optical properties of silicon nanostructures are a very complex problem and that the debate over theories of physical behavior and claims of useful devices will last for a number of years before there is ever a well developed technology in place. At this point it is only possible to provide a broad overview of behaviors, and hopefully clarify directions for possible further exploration.

1.11.1.1 *Can optically active silicon nanostructures be synthesized using pulsed laser ablation supersonic expansion?*

An important goal of this work will be the demonstration that pulsed laser ablation supersonic expansion can be used to create thin films of silicon nanocrystallites that can be used for visible light emission and nonlinear optical response. The system has often been used to study smaller gas phase clusters, but not to develop thin films for extensive post deposition characterization or device fabrication. Along with this, some facility with the controllable parameters of the deposition process should be achieved, allowing the reproducible synthesis of silicon nanocrystallites with tunable and useful optical properties.

Alongside the optimization of the synthesis of optically active silicon nanocrystallites will come the basic description of the characteristics of these new artificial materials. Comparisons of thin films of silicon nanocrystallites with other silicon nanostructures will be

made through considerations of the observed properties. As a result of the characterization of the material's properties, the overall value of the system as a potential optoelectronic or photonic material will be tested.

1.11.1.2 *What role does nanostructure size play in controlling optical behavior?*

Theory has predicted that nanocrystalline semiconductors should act drastically differently than their bulk counterparts. This work hopes to demonstrate these new effects in light emission and nonlinear optical response and garner some insight into the physical processes that are involved in these new characteristics. The determination of the ability of size to control the manifestation of these properties will be examined, as well as the requirements for optimization of this parameter for future device considerations.

A large part of this question revolves around the role that quantum confinement is playing in the emission and nonlinear response of the nanocrystallites. Experiments will be done to test the role of quantum confinement in these behaviors. This will help point out what the actual emission mechanism may be in the system.

1.11.1.3 *What role does nanostructure surface play in defining optical behavior?*

Due to the importance of surface properties in determining all of the properties of a nanocrystalline system, a large portion of this work must concentrate on the effects of the surface in defining the optical behaviors. These question will become vitally important during the development of heterostructure applications, since the nanocrystallites will have to embedded in matrices in most imaginable device architectures.

The role of surface passivation in defining or enabling the emission behavior and nonlinear optical response of the systems is the central question here. The determination of surface control of emission energy and intensity will provide some insight into the role that surface chemistry, defects, and adsorbed species play in the optical behaviors. Through modification and characterization of the surfaces and correlation to optical behavior, it may be possible to define the role of surface in these systems.

1.11.2 Proposed Work

This work revolves around the synthesis and characterization of thin films of silicon nanocrystallites and their optical properties. Films are produced by pulsed laser ablation supersonic expansion on a variety of substrates. The deposition system will examined and optimized to reproducibly create optically active silicon films.

The films will then be characterized for their visible emission and nonlinear optical response. The role of size in these behaviors will be examined through control of nanocrystallite diameter via post deposition processing regimens and correlation to optical response. The role of surface in the optical response will be studied through characterization of the film properties in a variety of passivating environments as produced by processing steps. The surface properties of the films will then be correlated to the optical response. These results will then be used to draw some conclusions as to the origin of novel optical behaviors in nanocrystalline silicon and its viability as a useful photonic and optoelectronic material.

Chapter One References

[1] B.E.A. Saleh and M.C. Teich, *Fundamentals of Photonics*, p.835 (1991)
[2] R.W. Keyes, *The Physics of VLSI Systems*, p. 184 (1987)
[3] H.S. Hinton, SPIE Vol. 1215 *Digital Optical Computing II*, p. 132 (1990)
[4] L.A. Chiu, M.S. Thesis, Massachusetts Institute of Technology (1993)
[5] L.C. Kimerling, K.D. Kolenbrander, J. Michel, and J. Palm, Sol. St. Phys., in press.
[6] J. Weber, W. Schmid, and R. Sauer, Phys. Rev. B 21(6), 2401 (1980)
[7] B. Zheng, J. Michel, F.Y.G. Ren, L.C. Kimerling, D.C. Jacobson, and J.M. Poate, Appl. Phys. Lett. 64, 2842 (1994)
[8] S. Oguz, W. Paul, T.F. Deutsch, B.-Y. Tsaur, and D.V. Murphy, Appl. Phys. Lett. 43(9), 849 (1983)
[9] L.C. Lenchyshyn, M.L.W. Thewalt, J.C. Sturm, P.V. Schwartz, N.L. Rowell, J.-P. Noël, and D.C. Houghton, J. Electron. Mater. 22, 233 (1993)
[10] R.A. Street, Adv. Phys. 30(5), 593 (1981)
[11] J.I. Pankove and D.E. Carlson, Appl. Phys. Lett. 31(7), 450 (1977)
[12] H. Matsumura and S. Furukawa in *Amorphous Semiconductor Technologies and Devices 1982*, Y. Hamakawa, ed., p. 88 (1982)
[13] B. Abeles and T. Tiedje, Phys. Rev. Lett. 51(21), 2003 (1983)
[14] D.J. Lockwood, Z.H. Lu, and J.-M. Baribeau, Phys. Rev. Lett. 76(3), 539 (1996)
[15] S.M. Prokes, J. Appl. Phys. 73(1), 407 (1993)
[16] A.P. Alivisatos, Science 271, 933 (1996)
[17] G. Burns, Solid State Physics, p. 208 (1985)
[18] S. Schmitt-Rink, D.A.B. Miller, and D.S. Chemla, Phys. Rev. B 35(15), 8113 (1987)
[19] C.B. Murray, D.J. Norris, and M.G. Bawendi, J. Am. Chem. Soc. 115, 8706 (1993)
[20] L.E. Brus, J. Chem. Phys. 80(9), 4403 (1984)
[21] J.P. Proot, C. Delerue, and G. Allan, Appl. Phys. Lett. 61(16), 1948 (1992)
[22] T. Takagahara and K. Takeda, Phys. Rev. B 46(23), 15578 (1992)
[23] A.D. Yoffe, Adv. Phys. 42(2), 173 (1993)
[24] M. Danek, K.F. Jensen, C.B. Murray, and M.G. Bawendi, Appl. Phys. Lett. 65(22), 2795 (1994)
[25] M.A. Hines and P. Guyot-Sionnest, J. Phys. Chem. 100(2), 468 (1996)
[26] S.-T. Ngiam, K.F. Jensen, and K.D. Kolenbrander, J. Appl. Phys 76(12), 8201 (1994)
[27] K.V. Shcheglov, C.M. Yang, K.J. Vahala, and H.A. Atwater, Appl. Phys. Lett. 66 (6), 745 (1995)
[28] F. Vega, R. Serna, C.N. Afonso, D. Berrnejo, G. Tejeda, J. Appl. Phys. 75(11), 7287 (1994)
[29] S. Sato, S. Nozaki, H. Morisaki , M. Iwase, Appl. Phys. Lett. 66(23), 3176 (1995)
[30] J.R. Heath, J.J. Shiang, and A.P. Alivisatos, J. Chem. Phys. 101(2), 1607 (1994)
[31] Y. Kanemitsu, H. Uto, Y. Masumoto, and Y. Maeda, Appl. Phys. Lett. 61(18), 2187 (1992)
[32] S. Hayashi, Y. Kanzawa, M. Kataoka, T. Nagareda, and K. Yamamoto, Z. Phys. D 26, 144 (1993)
[33] Y. Maeda, N. Tsukamoto, Y. Yazawa, Y. Kanemitsu and Y. Masumoto , Appl. Phys. Lett. 59(24), 3168 (1991)

[34] W.A. Saunders, P.C. Sercel, H.A. Atwater, K.J. Vahala, Appl. Phys. Lett. 60(8), 950 (1992)
[35] O.I. Micic, J.R. Sprague, C.J. Curtis, K.M. Jones, J.L. Machol, A.J. Nozik, H. Giessen, B. Fluegel, G. Mohs, and N. Peyghambarian, J. Am. Chem. Soc. 99(19), 7754 (1995)
[36] Y.S. Tang, C.M. Sotomayor Torres, R.M. Kubiak, T.E. Whall, E.H.C. Parker, H. Presting, and H. Kibbel, J. Electron. Mater. 24(2), 99 (1995)
[37] A. Nakamura, Y.L. Lee, T. Kataoka, and T. Tokizaki, J. Lum 60&61, 376 (1994)
[38] B. Hamilton, Semicon. Sci. Tech. 10(9), 1187 (1995)
[39] L. Canham, MRS Bulletin, July, 22 (1993)
[40] A. Uhlir, Bell Syst. Tech. J. 35, 333 (1956)
[41] G. Bomchil, A. Halimaoui, I. Sagnes, P.A. Badoz, I. Berbezier, P. Perret, B. Lambert, G. Vincent, L. Garchery, and J.L. Regolini, Appl. Surf. Sci. 65/66, 394 (1993)
[42] V. Petrova-Koch, T. Muschik, A. Kux, B.K. Meyer, F. Koch, and V. Lehmann, Appl. Phys. Lett. 61(8), 943 (1992)
[43] S.C. Bayliss, D.A. Hutt, Q. Zhang, P. Harris, N.J. Phillips, and A. Smith, Thin Solid Films 255, 128 (1995)
[44] L. Tsybeskov, Ju. V. Vandyshev, and P.M. Fauchet, Phys. Rev. B 49(11), 7821 (1994)
[45] M.I.J. Beale, J.D. Benjamin, M.J. Uren , N.G. Chew, A.G. Cullis, J. Cryst. Growth 75, 408 (1986)
[46] V. Lehmann and U. Gösele, Appl. Phys. Lett 48(8), 381, (1991)
[47] M.I.J. Beale, N.G. Chew, M.J. Uren, A.G. Cullis, J.D. Benjamin, Appl. Phys. Lett. 46(1), 86 (1985)
[48] A.G. Cullis, L.T. Canham, G.M. Williams, P.W. Smith, and O.D. Dosser, J. Appl. Phys. 75(1), 493 (1994)
[49] J.M. Perez, J. Villalobos, P. McNeill, J. Prasad, R. Cheek, J. Kelber, J.P. Estrera, P.D. Stevens, and R. Glosser, Appl. Phys. Lett. 61(5), 563 (1992)
[50] E. Takasuka and K. Kamei, Appl. Phys. Lett. 65(4), 484 (1994)
[51] W.L. Wilson, P.F. Szajowski, and L.E. Brus, Science 262, 1242 (1993)
[52] W.A. Saunders, P.C. Sercel, R.B. Lee, H.A. Atwater, K.J. Vahala, R.C. Flagan, E.J. Escorcia-Aparcio, Appl. Phys. Lett. 63(11), 1549 (1993)
[53] J.R. Heath, Science 258, 1131 (1992)
[54] R. Okada and S. Iijima, Appl. Phys. Lett. 58(15), 1662 (1991)
[55] J.M. Jasinski and F.K. LeGoues, Chem. Mater. 3, 989 (1991)
[56] L.T. Canham, Appl. Phys. Lett. 57(10), 1046 (1990)
[57] S.M. Prokes, J. Mater. Res. 11(2), 305 (1996)
[58] M. Kondo and H. Yokomichi, J. Phys. Soc. Jpn. 63B, 145 (1994)
[59] E. Bustarret, M. Ligeon, I. Mihalescu, and J. Oswald, Thin Solid Films 255, 234 (1995)
[60] S. Schuppler, S.L. Friedman, M.A. Marcus, D.L. Adler, Y.-H. Xie, F.M. Ross, Y.J. Chabal, T.D. Harris, L.E. Brus, W.L. Brown, E.E. Chaban, P.F. Szajowski, S.B. Christman, and P.H. Citrin, Phys. Rev. B 52, 4910 (1995)
[61] V.A. Joshkin, M.N. Naidenkov, V.N. Pavlenko, A.V. Kvit, S.R. Oktyabrsky, Phys. Rev. B 52(16), 12102 (1995)
[62] P. Deák, M. Rosenbauer, M. Stutzman, J. Weber, M.S. Brandt, Phys. Rev. Lett. 69(17), 2531 (1992)

[63] M. Stutzmann, M.S. Brandt, M. Rosenbauer, J. Weber, and H.D. Fuchs, Phys. Rev. B, 47(8), 4806 (1993)
[64] S.L. Friedman, M.A. Marcus, D.L. Adler, Y.-H. Xie, T.D. Harris, and P.H. Citrin, Appl. Phys. Lett. 62(16), 1934 (1993)
[65] J. Lin, L.Z. Zhang, B.R. Zhang, B.Q. Zong, and G.G. Qin, J. Phys.: Condens. Matter 6, 565 (1994)
[66] J.H. Stathis and M.A. Kastner, Phys. Rev. B 35, 2972 (1987)
[67] A. Loni, A.J. Simons, P.D.J. Calcott, and L.T. Canham, J. Appl. Phys. 77(7), 3557 (1995)
[68] Y. Kanemitsu, Phys. Rev. B 49(23), 16845 (1994)
[69] K. Takeda and K. Shiraishi, Sol. St. Comm. 85(4), 301 (1993)
[70] Y.-H. Xie, W.L. Wilson, F.M. Ross, J.A. Mucha, E.A. Fitzgerald, J.M. Macaulay, and T.D. Harris, J. Appl. Phys. 71(5), 2403 (1992)
[71] S.M. Prokes and W.E. Carlos, J. Appl. Phys. 78(4), 2671 (1995)
[72] S. Munekuni, T. Yamanaka, Y. Shimogaichi, R. Tohmon, Y. Ohki, K. Nagasawa, and Y. Hana, J. Appl. Phys. 68(3), 1212 (1990)
[73] P.D.J. Calcott, K.J. Nash, L.T. Canham, M.J. Kane, and D. Brumhead, J. Lum. 57, 257 (1993)
[74] L.E. Brus, P.F. Szajowski, W.L. Wilson, T.D. Harris, S. Schuppler, and P.H. Citrin, J. Am. Chem. Soc. 117, 2915 (1995)
[75] F. Koch, V. Petrova-Koch, and T. Muschik, J. Lum. 57, 271 (1993)
[76] V.I. Gavrilenko and F. Koch, J. Appl. Phys. 77(7), 3288 (1995)
[77] M.B. Robinson, A.C. Dillon, D.R. Haynes, and S.M. George, Appl. Phys. Lett. 61(12), 1414 (1992)
[78] J.M. Lauerhaas and M.J. Sailor, Science 261, 1567 (1993)
[79] L. Tsybeskov and P.M. Fauchet, Appl. Phys. Lett. 64(15), 1983 (1994)
[80] Y.H. Xie, M.S. Hybertsen, W.L. Wilson, S.A. Ipri, G.E. Carver, W.L. Brown, E. Dons, B.E. Weir, A.R. Kortan, G.P. Watson, A.J. Liddle, Phys. Rev. B 49 (8), 5386 (1994)
[81] J. Lin, L.Z. Zhang, B.R. Zhang, B.Q. Zong, and G.G. Qin, J. Phys.: Condens. Matter 6, 565 (1994)
[82] K.A. Littau, P.J. Szajowski, A.J. Muller, A.R. Kortan, and L.E. Brus, J. Phys. Chem. 97, 1225 (1993)
[83] A. Nakajima, T. Itakura, S. Watanabe, and N. Nakayama, Appl. Phys. Lett. 61(1), 46 (1992)
[84] I. Sagnes, A. Halimaoui, G. Vincent, and P.A. Badoz, Appl. Phys. Lett. 62(10), 1155 (1993)
[85] M. Rosenbauer, M. Stutzmann, H.D. Fuchs, S. Finkbeiner, and J. Weber, J. Lum 57, 153 (1993)
[86] K. Raghavachari and V. Logovinsky, Phys. Rev. Lett. 55(26), 2853 (1985)
[87] E.C. Honea, A. Ogura, C.A. Murray, K. Raghavachari, W.O. Sprenger, M.F. Jarrold, and W.L. Brown, Nature 366, 42 (1993)
[88] K. Raghavachari, Phase Trans. 24-26, 61 (1990)
[89] E. Kaxiras, Phys. Rev. Lett. 64(5), 551 (1990)
[90] K. Jug and M. Krack, Chem. Phys. 173, 439 (1993)
[91] M.L. Mandich and K.D. Rinnen, Z. Phys. D 26, 147 (1993)

[92] D. Tomanek and M.A. Schluter, Phys. Rev. B 36(2), 1208 (1987)
[93] I. Gregora, B. Champagnon, and A. Halimaoui, J. Appl. Phys 75(6), 3034 (1994)
[94] N.A. Hill and K.B. Whaley, J. Electron. Mater. 25(2), 269 (1996)
[95] Z.H. Lu, D.J. Lockwood, and J.-M. Baribeau, Nature 378, 258 (1995)
[96] R.P. Vasquez, R.W. Fathauer, T. George, A. Ksendzov, and T.L. Lin, Appl. Phys. Lett. 60(8), 1004 (1992)
[97] M.L. Rudee and A. Howie, Phil. Mag. 25(4), 1001 (1972)
[98] H. Sugiyama and O. Nittono, J. Cryst. Growth 103, 156 (1990)
[99] Y. Sun and T. Miyasato, Jpn. J. Appl. Phys. 34 Pt. 2 No. 10A, L1248 (1995)
[100] K. Barla, R. Herino, G. Bomchil, and J.C. Pfister, J. Cryst. Gr. 68, 727 (1984)
[101] T. Ito, H. Kiyama, T. Yasumata, H. Watabe, and A. Hiraki, Phys. B 170, 535 (1991)
[102] N. Koshida and H. Koyama, Appl. Phys. Lett 60, 347 (1992)
[103] A. Loni, A.J. Simons, T.I. Cox, P.D.J. Calcott, and L.T. Canham, Electron. Lett. 31, 1288 (1995)
[104] T.A. Burr, A.A. Seraphin, and K.D. Kolenbrander, "International Symposium on Advanced Luminescent Materials", Proc. of the Electrochem. Soc. (1995)
[105] P.J. Dean, J.R. Haynes, and W.F. Flood, Phys. Rev. 161, 711 (1967)
[106] D.S. Chemla, Physics Today, May, 57 (1985)
[107] J.I. Pankove, *Optical Processes in Semiconductors*, p. 154 (1975)
[108] R. Gupta, M.S. Thesis, Massachusetts Institute of Technology (1995)
[109] C. Delerue, G. Allan, and M. Lannoo, Phys. Rev. B 48(15), 11024 (1993)
[110] A.S. Grove, *Physics and Technology of Semiconductor Devices*, p.144 (1967)
[111] B. Delley and E.F. Steigmeier, Phys. Rev. B 47(3), 1397 (1993)
[112] H. M'Saad, J. Michel, J.J. Lappe, and L.C. Kimerling, J. Electron. Mater. 23, 487 (1994)
[113] R.J. Archer, J. Electrochem. Soc. 104(10), 619 (1957)
[114] M. Niwano, J.-I. Kageyama, K. Kurita, K. Kinashi, I. Takahashi, and N. Miyamoto, J. Appl. Phys. 76(4), 2157 (1994)
[115] S.-T. Ngiam, Ph.D. Thesis, Massachusetts Institute of Technology (1996)
[116] J. E. Bower and M.F. Jarrold, J. Chem. Phys. 97(11), 8312 (1992)
[117] H.I. Liu, B.K. Biegelsen, F.A. Ponce, N.M. Johnson, R.F.W. Pease, Appl. Phys. Lett. 64 (11), 1383 (1994)
[118] W.E. Carlos and S.M. Prokes, J. Vac. Sci. Tech. B 13(4), 1653 (1995)
[119] S.M. Sze, *VLSI Technology*, p. 259 (1988)
[120] H. Aoyagi, A. Motohashi, A. Kinoshita, T. Aono, and A. Satou, Jpn. J. Appl. Phys. 32, L1 (1993)
[121] S.M. Hu and D.R. Kerr, J. Electrochem. Soc. 114(5), 414 (1967)
[122] E. Yablonovitch, D.L. Allara, C.C. Chang, T. Gmitter, T.B. Bright, Phys. Rev. Lett. 57(2), 249 (1986)
[123] P. Gupta, V.L. Colvin, and S.M. George, Phys. Rev. B 37(14), 8234 (1988)
[124] Y.J. Chabal, G.S. Higashi, K. Raghavachari, and V.A. Burrows, J. Vac. Sci. Tech. A 7, 2104 (1989)
[125] S.K. Ghandhi, *VLSI Fabrication Principles*, 2nd ed., p.587 (1994)
[126] R.J. Archer, J. Phys. Chem. Solids 14, 104 (1960)

[127] R.W. Fathauer, T. George, A. Ksendzov, and R.P. Vasquez, Appl. Phys. Lett. 60(8), 995 (1992)
[128] D.A. Blom, private communication.
[129] J.S. Foresi, M.R. Black, A.M. Agrawal, and L.C. Kimerling, Appl. Phys. Lett. 68(15), 2052 (1996)
[130] L. Brus, Isr. J. Chem. 33, 9 (1993)
[131] F.J. Himpsel, Surf. Sci. 299-300, 525 (1994)
[132] S. Munekuni, T. Yamanaka, Y. Shimogaichi, R. Tohmon, Y. Ohki, K. Nagasawa, and Y. Hana, J. Appl. Phys. 68(3), 1212 (1990)
[133] L. Brus, Phys. Rev. B 53(8), 4649 (1996)
[134] J.M. Rehm, G.L. McLendon, L. Tsybeskov, and P.M. Fauchet, Appl. Phys. Lett. 66(26), 3669 (1995)
[135] I. Schechter, M. Ben-Chorin, and A. Kux, Anal. Chem. 67, 3727 (1995)

2. Experimental Procedure

2.1 Nanocrystalline Film Synthesis

Thin films of agglomerated silicon nanocrystallites embedded within a native oxide matrix were synthesized using a pulsed laser ablation supersonic expansion source. Nanostructures ranging in size from atomic silicon to micron sized particles are deposited in films onto a variety of substrates, including Teflon, transmission electron microscopy (TEM) grids, and silicon wafers. Modifications of the deposition system allowed for experimentation with gas phase passivation of the silicon nanoclusters, as well as gas phase photoluminescence spectroscopy on unpassivated nanocrystallites.

2.1.1 Pulsed Laser Ablation Supersonic Expansion Source

The silicon nanocrystallites in this work were produced using a pulsed laser ablation supersonic expansion source.[1] This source was developed for the synthesis of metal clusters,[2] but it has also been used in the production and spectroscopy of semiconductor clusters.[3] A rotating 0.25 inch diameter, 3 inch long, 99.9999% pure, polycrystalline silicon target rod is placed inside a stainless steel source block, as shown in Figure 2-1. A pulsed, frequency doubled Neodymium doped Yttrium Aluminum Garnet (2xNd:YAG) laser (Continuum Model NY60) is focused to a 1 mm diameter spot at the surface of the target rod. The laser is pulsed at 20 Hz with a wavelength of 532 nm, and has a 7 nanosecond pulse duration. The ablation laser delivers a power of 3-10 milliJoules per pulse (mJ/pulse) to the target rod, which corresponds to a power density of 15-50 W/cm^2.

The target rod and stainless steel block are kept inside a vacuum chamber attached to a diffusion pump and a backing mechanical pump. The chamber is held at a background pressure of 10^{-7} torr. The laser vaporizes the surface of the target rod, generating a silicon plasma. The target rod is positioned adjacent to a high speed pulsed solenoid valve which

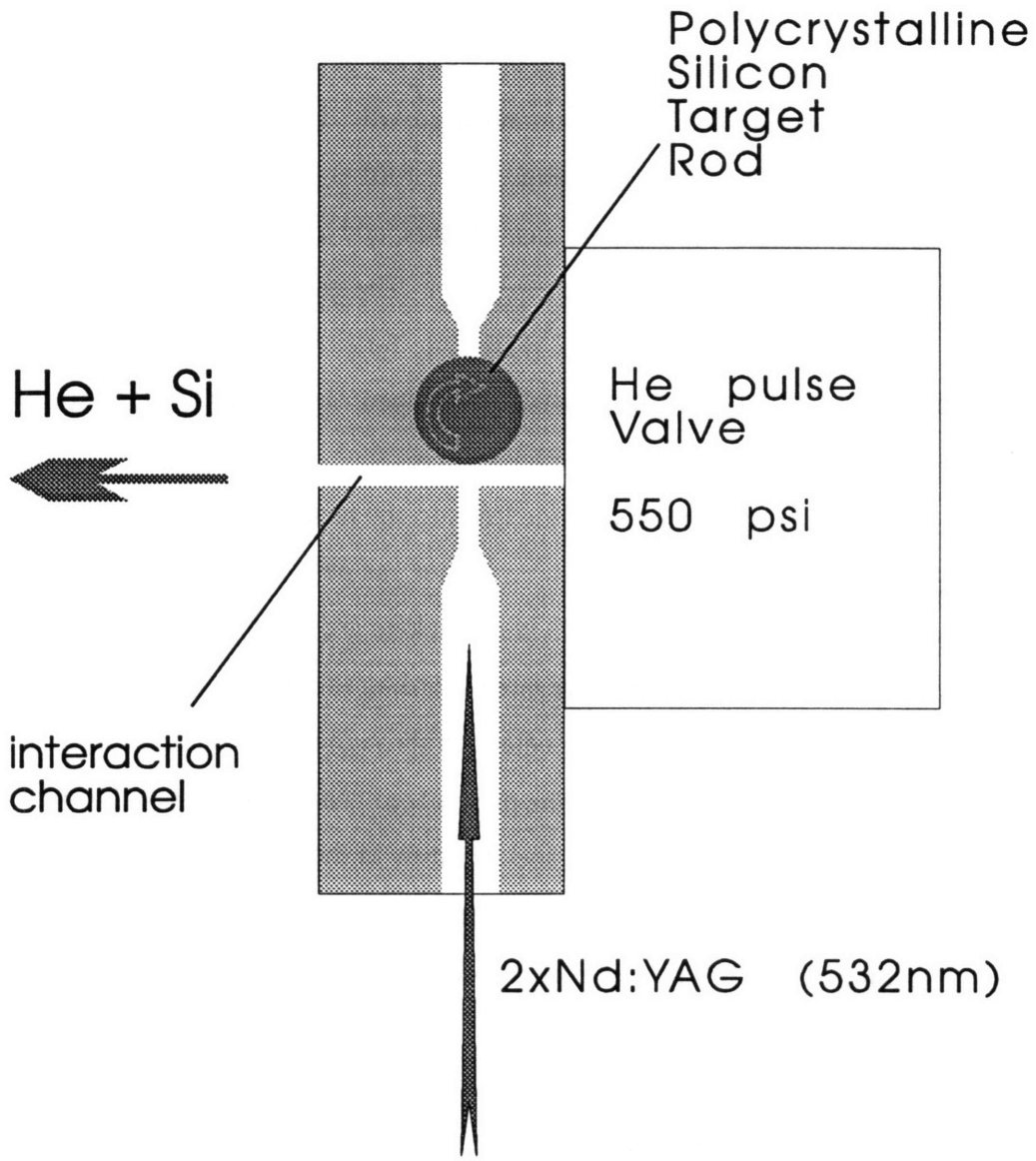

Figure 2-1 Schematic of stainless steel block used in pulsed laser ablation supersonic expansion system.

opens at a fixed time synchronized to the ablation laser pulse. The valve gates the flow of pressurized helium (He) gas (99.999% pure). The helium gas line pressure is ~550 psi and so the gas expands rapidly into the evacuated chamber. The helium gas entrains the silicon plasma and carries the atoms into a 1 mm diameter, 8 mm long interaction channel. The helium carrier gas collides with the silicon atoms in the plasma and cools them, making them thermodynamically favorable sites for continued growth. In the channel, the cooled silicon atoms act as heterogeneous nucleation sites where further collisions with silicon atoms lead to the building up of clusters. The carrier gas, clusters, and unreacted silicon atoms then expand into the vacuum system in a supersonic expansion. The gas expansion raises the chamber pressure to ~10^{-4} torr. At this pressure, there is no further interaction between the clusters and carrier gas and the particle sizes remain unchanged. In the gas phase, the clusters are still very hot, with temperatures expected to be ~500 K.[4]

The pulsed nature of the technique leads to the production of twenty individual gas phase packets of silicon clusters and helium carrier gas per second. These are separated in time by 50 milliseconds, so that the individual packets are completely independent of each other. In the packets, the clusters segregate according to size due to a phenomenon known as velocity slip.[5] Since the particles are accelerated through the vacuum system through momentum conserving collisions with the pressurized helium carrier gas, the smallest, least massive particles will attain the largest speed and fly in the front of the cluster packet, while the larger particles will remain in the rear. The packet's time of flight has been measured using a fast ion gauge (FIG) placed in an attached secondary vacuum chamber, as shown in Figure 2-2. The FIG is a fast version of the familiar Bayard-Alpert ionization gauge, that measures pressure fluctuations caused by the presence of gas clusters, with microsecond resolution. By knowing the distance between the stainless steel source block and the FIG, as well as the relative timings of the ablation laser pulse and the fast ion gauge signal, the cluster velocity distribution can be studied. The fastest clusters within an individual packet travel at 2120 m/s, while the slowest ones travel at 1620 m/s.[6]

The source grows clusters through collisions involving single silicon atoms. These collisions occur for a very short time, on the order of tens of microseconds, in a chaotic, nonequilibrium system. As a result, clusters of many different sizes are nucleated,

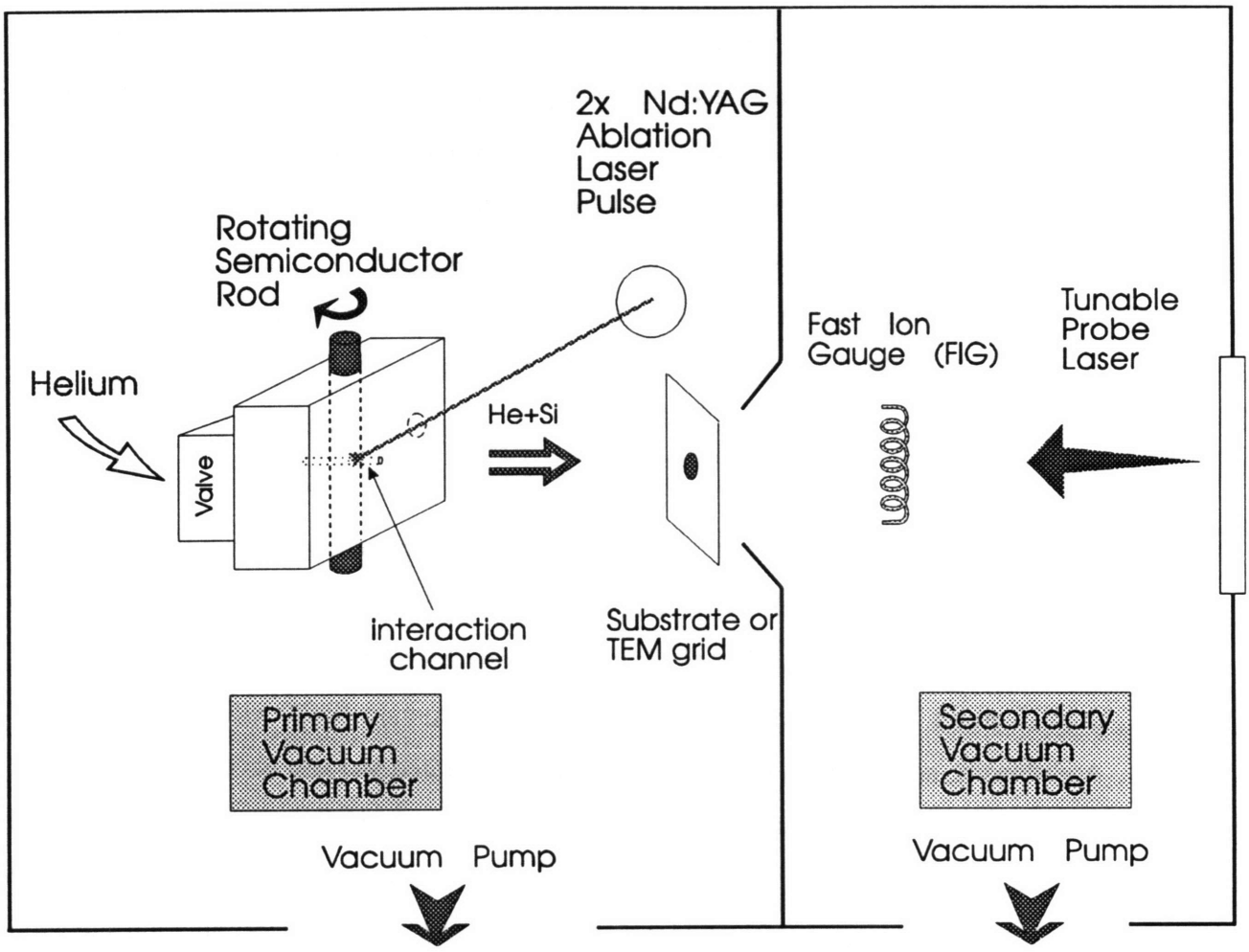

Figure 2-2 Top view schematic of pulsed laser ablation supersonic expansion system. (From Ref. 1)

ranging from atomic silicon up to clusters microns in diameter. These larger particles might be the result of micron sized pieces of the target rod being ablated as single entities during the initial ablation process.[7] In similar sources, particles falling within this wide size range have been confirmed through gas phase techniques, such as mass spectroscopy,[8] and thin film characterization techniques, such as electron microscopy.[9]

Laser ablation sources have been predicted to produce a lognormal size distribution of clusters.[10] This distribution is given by the function,

$$F(x) = \frac{1}{x}\frac{1}{\sqrt{2\pi\sigma^2}}\exp\left(-\frac{(\ln x - \mu)^2}{2\sigma^2}\right)$$

where x is number of particles at a given size, σ is the statistical median, and μ is the standard deviation of the distribution. This distribution has an exponential tail of particles at larger sizes. Pulsed laser vaporization of silicon has shown maxima in the size distribution at less than 30 atoms.[11] Visibly emitting clusters (50-1000 atoms) will fall within the exponential tail. Additionally, some cluster sizes are coordinately saturated and will have a low probability of further growth. These "magic number" sizes then occur more frequently and appear as sharp peaks in the size distribution. In general, little work has been done to characterize the size distribution of the larger (50+ atoms) clusters produced by pulsed laser ablation supersonic expansion sources.

It has been possible to control some of this large size distribution by modifying deposition parameters. The clusters are nucleated through cooling collisions with the helium carrier gas. By increasing the amount of helium available for interaction by opening the helium valve earlier with respect to the ablation pulse, it is possible to enhance this nucleation and subsequent cluster growth and increase the mean particle size. Increasing the length of the interaction channel should result in a similar enhancement of the helium carrier gas and silicon plasma interaction and produce a larger mean cluster size. It is also possible to use a mechanical velocity selector synchronized to ablation laser pulses to chop out a single portion of the cluster packet and control which particles are deposited onto substrates. The effects of these deposition parameters on nanocluster size has been correlated with time of flight analysis and photoluminescence characterization.[6,12]

The building of clusters from single atoms also plays a critical role in determining the final structure of the particles. Transmission electron microscopy (TEM) and glancing angle x-ray diffraction (GAXRD) analysis of deposited thin films of agglomerated clusters has shown that particles of > 3 nm in diameter (~1000 atoms) can be clearly identified as showing the bulk silicon diamond cubic lattice structure.[1] Microscopy has also shown deposits that amorphous in nature. Previous work with these systems has shown that smaller clusters, on the order of 1 - 41 atoms, have structures which have optical properties different than the bulk silicon diamond cubic structure.[13] There is no reason to believe that these different structures will be modified during the film deposition process. The pulsed laser ablation supersonic expansion source can be altered in many ways in order to control the synthesis and characterization of the nanostructured materials. The target rod can be changed to nearly any material that can be easily ablated; thus far, work has been done in silicon, erbium, carbon, germanium, silver, and indium phosphide. The expansion can be changed to attempt gas phase passivation of the clusters using a seeded beam, for example using a mixture of oxygen and helium as the carrier gas. The clusters could also be passivated by directing a crossbeam of a reacting species to interact with the particles for gas phase chemical reactions. In addition to the FIG time of flight measurements and size selection through deposition parameter adjustments, it is also possible to examine the gas phase clusters in the supersonic expansion using a counterpropagating, co-axial spectroscopy laser beam to measure elastic light scattering or photoluminescence as seen in Figure 2-2. Finally, it is also possible to deposit the nanocrystallites into a variety of host matrices that can be simultaneously grown in the chamber during the synthesis process. Clusters have been deposited into organic hosts produced by simple thermal evaporation and condensation onto cold fingers, semiconductor hosts produced by chemical vapor deposition[14] or using a secondary ablation target rod,[15] and polymer matrices[16] deposited on a substrate and placed in the path of the supersonic expansion. These matrices have been used to create nanoheterostructure systems that have been examined to determine the nature of the dot and host interface and its effect on the electrical, optical, and structural properties of the material.

2.1.1.1 *Deposition Rate*

The pulsed laser ablation supersonic expansion system deposits thin films of silicon nanocrystallites at an approximate rate of 10 nm per hour. This is based on measurements by Ngiam using a quartz crystal monitor placed 24 cm away from the source block in the center line of the expansion.[17] He calculated a deposition rate of 250 nanograms/cm^2 hr with a laser power of 5 mJ/pulse. Using the bulk silicon density of 2.33 grams/cm^3 and assuming deposition rate falls off as the square of source-to-substrate distance, we can calculate a rate of 10 nm per hour. This estimate is a lower bound, as the density of the nanocrystallite thin film should be less than that of a bulk silicon, given the likely porous nature of the film structure. Ngiam also measured the rate 6.3 cm above the center line and found it to be 200 ng/cm^2 hr. He concluded that the angular distribution of clusters in the deposition is not described by either a cosine law or a spherical distribution. The angular distribution of clusters is more forward peaked than a cosine distribution and falls off rapidly with displacement from the center line.

2.2 Materials

2.2.1 Target Rods

The target rods for the pulsed laser ablation supersonic expansion system are 0.25 inches in diameter and 3 inches long. For this work, they are composed of 99.9999% pure polycrystalline silicon, but the system has been used with other semiconductor and metallic rods. Since the ablation process removes material from the target, it is necessary to rotate the rod to prevent it form being quickly destroyed. To this end, the rod is attached to a rotating threaded screw so that the laser spot effectively moves around the surface of the target. This results in a threading pattern being ablated into the source rod. The direction of travel of the rod is controlled by mechanical switches.

2.2.2 Substrates

The substrate materials used for thin film deposition were chosen according to their suitability for characterization techniques. The majority of this work involved wet chemical

processing and photoluminescence emission spectroscopy of the thin films, so the films were deposited onto 0.060" thick Teflon substrates. The Teflon was resistant to the acidic etches and showed very little luminescence behavior in the wavelength ranges of interest. Teflon substrates were also used for x-ray photoelectron spectroscopy experiments.

Films were also deposited on silicon wafer substrates for infrared spectroscopy and oxidation furnace treatments. These substrates were also resistant to the processing techniques used, and showed very little luminescence behavior in the wavelength range of interest. Samples deposited onto silicon wafers tended to show less luminescence efficiency than those deposited on Teflon. This may reflect the cluster's ability to better stick to the rougher surface of the Teflon.

A number of other substrates were used for characterization techniques mentioned in this work. TEM grids were used to create samples for microscopic analysis. Niobium substrates were used to deposit samples for use in GAXRD studies. Poly(vinyl carbonate) substrates were used to deposit films for use in degenerate four wave mixing spectroscopy (DFWM) and absorption measurements. This substrate showed no nonlinear optical response as measured by DFWM, was transparent to the visible wavelengths used in these techniques, and was resistant to the etching processing steps.

The samples were placed at a distance of 9 cm from the stainless steel source block, directly in the path of the supersonic expansion. The substrates used were of a variety of sizes and shapes, ranging from individual pieces of 1 cm^2 Niobium to entire 4" silicon wafers. A typical deposition on Teflon was performed onto a 2" x 2" square sheet of material. This films was then cut up into individual samples, typically ~1 cm^2 each. Similarly, the other substrates could be broken up so that samples from the same deposition could be processed and characterized individually.

2.3 Processing

The samples were processed using a variety of techniques to change the surface passivation or control the sizes of the nanocrystallites. Oxidation of the particles was performed through aging the samples in normal room atmosphere, heat treating them in air or

under oxygen flow, and treating them with nitric acid. The oxide layer could be etched using hydrofluoric acid, leaving the system hydride passivated. The films were also treated with boiling water, iodine:methanol solutions, and methanol to study the role of surface and size in the visible emission behavior.

2.3.1 Aging

The simplest way to oxidize the samples was to allow them to age in the normal room air. This was done without controlling for humidity or impurities that might be present in the aging environment. For comparison, samples were also aged in a vacuum cryostat under a vacuum of 10^{-3} torr for a period of days.

2.3.2 Wet Chemical Treatments

2.3.2.1 *Hydrofluoric Acid Dip*

In order to etch the surface oxide layer on the silicon crystallites and provide a hydride passivation layer, films on Teflon, silicon, and poly(vinyl carbonate) were dipped in 48 $^{w}/o$ Hydrofluoric acid (HF). The films were etched for different lengths of time. Typically, a standard film was etched for 60 seconds, and stirred in the solution during the dip and then blown dry with nitrogen gas. This type of solution was used in the HF/HNO_3 cycles experiments. Repeated or extended HF dips often damaged the films and reduced their luminescence efficiency.

2.3.2.2 *Nitric Acid Dip*

In order to chemically oxidize the surfaces of the silicon crystallites, films on Teflon, silicon, and poly(vinyl carbonate) were dipped in nitric acid (HNO_3). The solution was made using 10 ml of 70 $^{w}/o$ reagent grade HNO_3 in 40 ml of distilled water. Samples were typically dipped into the nitric acid solution for ten minutes, and then blown dry in nitrogen gas. This type of solution was used in the HF/HNO_3 cycles experiments.

2.3.2.3 *Boiling Water Treatment*

The films on Teflon substrates were also oxidized by placing them in distilled water that was boiling on a hot plate, and then blown dry with nitrogen gas. This treatment typically lasted for twenty minutes. The boiling was a very violent process and resulted in some damage to the films.

2.3.2.4 *$HF/HNO_3/H_2O$ Treatments*

Samples deposited on Teflon were etched in $HF/HNO_3/H_2O$ solutions for extended periods of time in order to reduce the silicon nanostructure sizes and change the emission wavelength. The solution was made with 6 ml of reagent grade 48 $^{w}/o$ HF, 100 ml reagent grade 70 $^{w}/o$ HNO_3, and 40 ml distilled H_2O. The samples were stirred in the solution, and then blown dry with nitrogen gas. Extended dips into this solution degraded the film.

2.3.2.5 *Methanol and Iodine:Methanol Dips*

Films on Teflon substrates were treated with methanol to see its effect on hydride and oxide passivated silicon nanocrystallite surfaces. The dips were performed for 60 seconds in HPLC grade methanol. Hydride and oxide passivated films on Teflon substrates were also treated with iodine dissolved in methanol in order to attempt to passivate their surfaces with a halogen species. The samples were dipped in 16 gm of I_2 dissolved in 90 ml of HPLC grade methanol for ten minutes.

2.3.3 Oxidation Furnace Treatments

Films deposited on silicon substrates were oxidized using annealing treatments in a tube furnace. Both hydride and oxide passivated surfaces were treated in the furnace. The films were heated to a temperature of between 200 °C and 450 °C and under oxygen gas flow or air with no flow. The time of heat treatment ranged from 30 minutes to ten hours. Samples deposited on Teflon were not used in the furnace as Teflon degrades under the heat treatment.

2.4 Photoluminescence Emission Spectroscopy

Samples were characterized for light emission using photoluminescence emission spectroscopy. This was done as a function of nanostructure size and surface passivation, both in thin films and in the gas phase. The emission was also characterized as a function of sample temperature and excitation pump intensity. This data provided insight into the role that size and surface play in the emission and into the recombination mechanism in the silicon nanostructures.

2.4.1 Basics

Photoluminescence emission spectroscopy measures the emission of materials after photoexcitation. In general, an ultraviolet lamp or laser is used to excite carriers within a material. The carriers eventually relax back down to their ground state and emit photons. These emissions are collected and the intensity of the signal is measured as a function of emitted photon energy. The luminescence emissions are typically characterized according to their emission energy and intensity, which provide evidence as to the energy and efficiency of the radiative transitions in the material. The emission can also be monitored while adjusting sample temperature and by adjusting the power of the excitation source to gain insight into the system's radiative and nonradiative recombination processes.

2.4.2 Experimental Setup

2.4.2.1 *Lasers and Optics*

Room temperature photoluminescence spectroscopy was performed using a pulsed Continuum model NY61 Nd:YAG laser. The laser was frequency tripled to 355 nm and used at a power of 1 mJ/pulse. Typical luminescence spectra were taken for a period of three minutes, meaning that the samples were excited by 3600 laser pulses. The laser had a 7 nanosecond pulse duration and a ~1 cm^2 spot area. A schematic of the luminescence optical line is shown in Figure 2-3. The beam was first passed through a filter which cut out the residual 532 nm and 1064 nm light produced by the laser. After reflecting off a mirror, the beam was passed through a diverging lens to increase the spot size, and directed at the sample

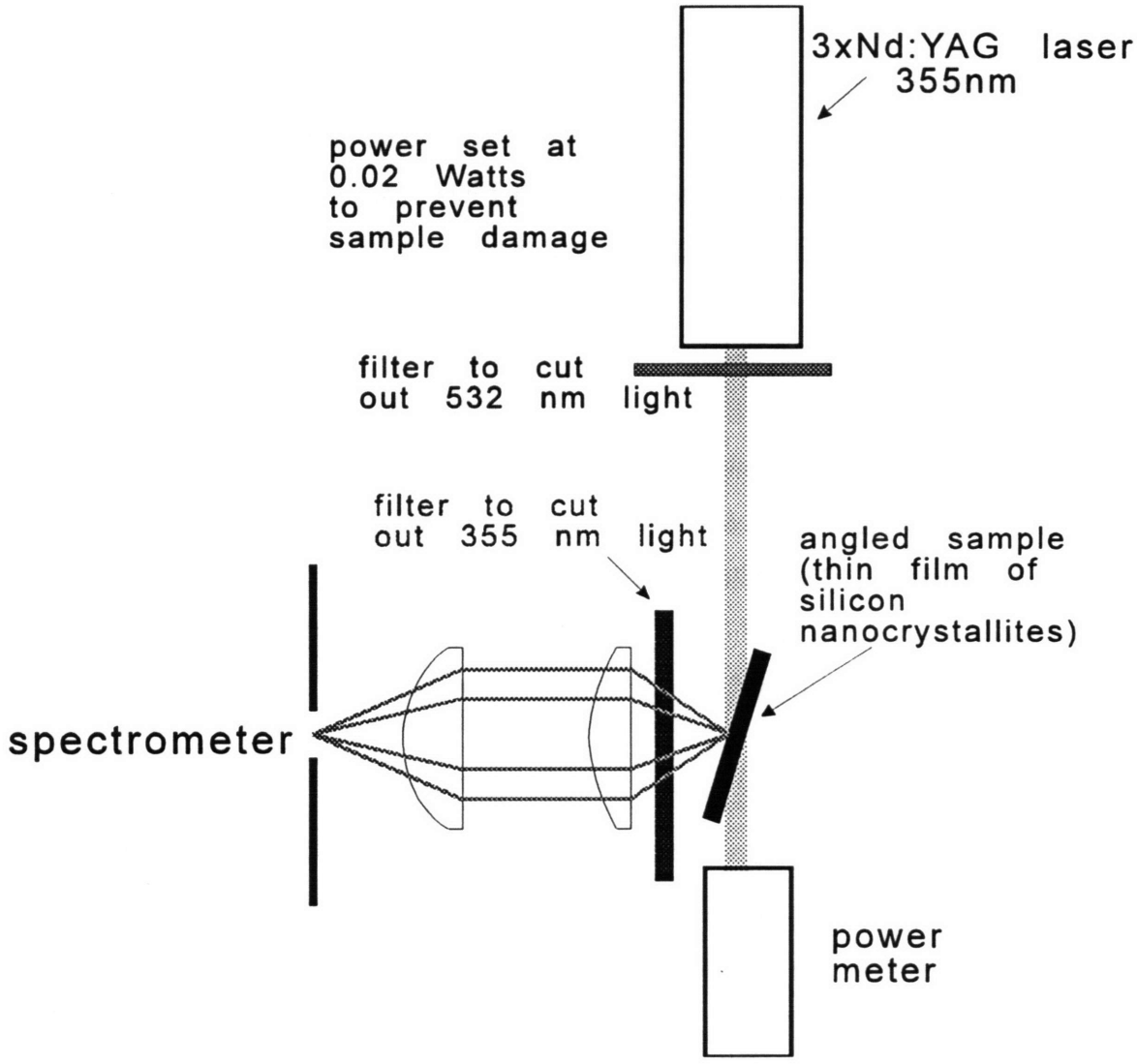

Figure 2-3 Schematic of photoluminescence experimental setup.

surface. A power meter could be placed at this point in the optical line in order to monitor the excitation power, as was required during excitation intensity photoluminescence studies. The sample was clamped into a sample holder such that the pump beam struck the film surface at approximately 85° to the surface normal. The length of time for collection of emission signal was kept as short as possible, because it was found that the ultraviolet laser pulses degraded the films over time.

A baffle with a small aperture was used to keep the amount of reflected ultraviolet entering the collection optics to a minimum. The collection optics consisted of a 418 nm long pass filter which served to eliminate any stray ultraviolet light, a 62.9 mm focal length, 2 inch diameter collecting lens, and a 62.9 mm focal length, 2 inch diameter focusing lens with an antireflection coating. The collected and focused emission light was finally passed through a 4 mm aperture placed 15 mm in front of the 75 micron entrance slit to the monochromator, in order to match the f-number of the detection system optics.

2.4.2.2 *Detector*

The luminescence emission is focused into an EG&G PARC Model 1235 Digital Triple-Grating Spectrograph. This is a 0.28 m focal length spectrograph attached to an EG&G PARC Model 1453A 1024 element silicon photodiode array detector. The detector is sensitive over a wavelength range of 200 to 1100 nm. It is cooled to -20 °C with water and a thermoelectric cooler in order to reduce dark counts. The spectrograph and detector have a significant nonlinearity in their spectral response in the wavelength range of interest. This was corrected for by calibrating the detector to the known emission of an Oriel Model 6333 quartz tungsten halogen white light source. This provided correction for the spectral response of the detection system, but not absolute measurements of emission signal power or quantum efficiency. Spectra were also automatically corrected for the presence of background light emissions.

2.4.2.3 *Data Collection and Processing*

The silicon array detector was connected to a Model 1471A Detector Interface. This in turn was networked to a computer via an IEEE-488 General Purpose Instrument Bus

(GPIB). The computer ran OMA Vision optical multichannel analyzer data acquisition and analysis software to setup the spectral correction functions, set sample detection times, and collect and process the spectral data. The software was also used to convert files into ASCII format for export to data analysis and graphing software.

The ASCII data files were imported into Genplot version 1.01, a scientific plotting program. The spectra were usually processed using a 16 point averaging scheme to smooth them. Integrated intensities were calculated by performing a simple integration over the wavelength ranges of interest. Since the photoluminescence spectra were rarely symmetrical, the peak emission wavelengths were most easily found by simple observation of the peak structures.

2.4.2.4 *Absolute Intensities and Wavelengths*

The experimental setup made it difficult to measure absolute emission intensities or wavelengths. The intensities of samples were difficult to compare for a number of reasons. Film depositions were very uneven, as indicated in section 2.1.1.1, so great care had to be taken in using samples that appeared to be of the same approximate thickness. The sample thickness would control the number of possible luminescent centers in the film, and therefore affect the emission intensity. In a given set of experiments, it was possible to control the laser power and positioning of the films and optics carefully so comparisons could be made more easily. This is the case for the work described in methanol treatments and halogen passivation of samples. Other intensity comparisons are made between samples who show little or no intensity at all and significantly more efficient samples, so that the distinction is clear. In the work on the effect of hydrofluoric acid dip time on the luminescence efficiency, comparisons are made between samples whose processing would tend to reduce its efficiency, but where passivation has overcome this effect to significantly increase intensities. In this case, the problem of sample thickness affecting emission intensity does not seem to come into play, as the observed trend is opposite to the expected effect.

Sample emission wavelengths are also approximate measurements. Samples being compared for shifts in emission energy were measured with the same optical setup, so these comparisons are valid within the experimental error of the system. The wavelength accuracy

of the system is expected to be on the order of 1 channel, or ± 0.2 nm, according to manufacturer's specifications. This inaccuracy could be compounded by poor optical alignment or improper wavelength calibration using known sources. Wavelength accuracy was checked periodically using a HeNe laser or a Neon lamp.

2.4.2.5 *Temperature Control of Films*

The temperature dependence of the film's luminescence behavior was measured between 300 and 4 K. Samples deposited on Teflon or silicon were placed in an Oxford Instruments Model CF1204 continuous flow cryostat. Both liquid nitrogen and liquid helium were used as the cryogen. The samples were kept under a helium environment in order to prevent condensation on their surfaces at low temperatures. The cryostat was equipped with windows for easy optical access to the samples. The samples were mounted on a specimen holder whose position could be controlled to allow for retention of an optical alignment during a set of experiments. The cryostat was also used to vacuum age samples for a period of days at 10^{-3} torr.

2.4.2.6 *Gas Phase Photoluminescence*

The photoluminescence response of the silicon clusters in the gas phase was measured by directing the 355 nm output of the frequency tripled Nd:YAG (3xNd:YAG) laser counterpropagating and coaxial to the supersonic expansion. The power of the spectroscopy laser was varied up to 50 mJ/cm^2 while looking for the visible luminescence. Emission was detected using a 25.4 mm focal length collection lens and a focusing lens along with the spectrograph and optical multichannel analyzer described earlier. The deposition parameters used to control particle size were also varied during this experiment to produce different packets for excitation.[12] The timing of the excitation laser was varied so that different portions of the cluster packet, and therefore different particle sizes, could be monitored for emission. This was the same experimental setup that was used to examine the elastic scattering of visible wavelengths by the silicon nanoclusters in the gas phase.[18]

2.5 Degenerate Four Wave Mixing Spectroscopy

The third order nonlinear optical susceptibility of the silicon nanocrystallite thin films was measured using degenerate four wave mixing spectroscopy (DFWM). This work was done at the US Army Natick Research, Development and Engineering Center in Natick, MA. Thin films on poly(vinyl carbonate) substrates were processed and then examined for their nonlinear response. These results were correlated to the luminescence properties to gain insight into the role of surface passivation on these properties in the silicon nanostructures.

2.5.1 Experimental Setup

A schematic of the DFWM setup is shown in Figure 2-4. The output of a pulsed 2xNd:YAG laser (λ_{ex}= 532 nm) with a 30 picosecond pulse width and an average energy of 3 mJ/pulse was split into three beams, two pump beams and a probe beam, which are directed at the sample film. The electric fields of the three beams interact in the nonlinear medium and produce an intensity dependent nonlinear polarization. This in turn creates a fourth beam which is the phase conjugate of the probe beam. The intensity of the phase conjugate signal beam is measured using a Si photodetector. This intensity is proportional to the square of $\chi^{(3)}$ in the sample material, as shown by the relation,

$$I_4(\omega) \propto \left|\chi^{(3)}\right|^2 d^2 I_1(\omega) I_2(\omega) I_3(\omega)$$

where d is the interaction length, ω is the frequency of the optical radiation, and I_1, I_2, and I_3 are the intensities of the forward pump, backward pump and probe beam, respectively.[19]

The relationship between the intensity of the signal beam and $\chi^{(3)}$ is obtained from a comparison of the intensities of the beams produced in the unknown sample to that produced in a known nonlinear optical material such as CS_2. Then $\chi^{(3)}$ for the unknown sample can be calculated from:

$$\chi^{(3)}_{sample} = \chi^{(3)}_{CS_2}\left(\frac{n_{Sample}}{n_{CS_2}}\right)^2\left(\frac{-\ln(T)}{1-T}\right)\left(\frac{1}{\sqrt{T}}\right)\left(\frac{d_{CS_2}}{d_{sample}}\right)\sqrt{\frac{I_{sample}}{I_{CS_2}}}$$

where n is refractive index, T is the transmission of the sample at 532 nm, d is film thickness, and I is phase conjugate beam intensity. It is assumed that the third order nonlinear optical

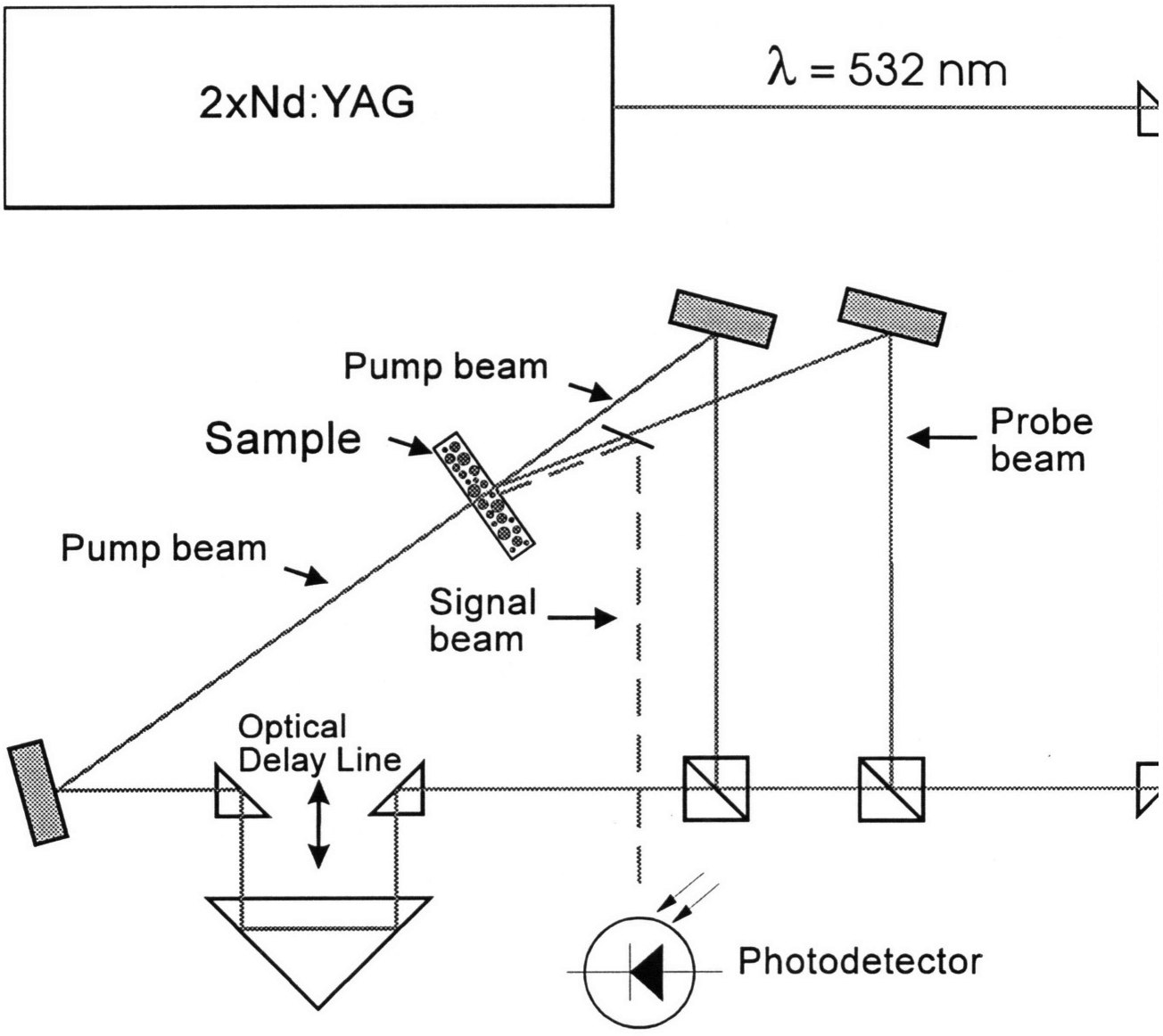

Figure 2-4 Schematic of degenerate four wave mixing spectroscopy (DFWM) experimental setup.

susceptibility of CS_2 is 6.8 x 10^{-8} esu.[20] Transmission spectra of the samples were taken using a quartz tungsten halogen white light source and the silicon photodiode array detector used in the photoluminescence measurements. The signal was analyzed using a computerized optical multichannel analyzer system. A detailed description of the characterization technique and a derivation of the $\chi^{(3)}$ expression have been shown elsewhere.[21]

The DFWM setup was also used to determine the temporal response of the optical nonlinearity in the samples. The optical delay line was used to control the timing of the backward pump beam and determine the strength of the nonlinearity as a function of time after the interaction of the forward pump and probe beam. The length of this delay line was compared to the reduction in signal beam intensity measured by the photodetector to understand the system's response as a function of time.

2.6 Other Characterization Techniques

2.6.1 X-ray Photoelectron Spectroscopy

X-ray photoelectron spectroscopy (XPS) was used to characterize the chemical bonding of the surface silicon atoms of the nanostructures. XPS was performed using the Perkin-Elmer 5100 system in the MIT Center for Materials Science and Engineering. The data and analysis was a collaborative effort with S.-T. Ngiam.[22]

2.6.1.1 *XPS Basics*

XPS involves the absorption of energy from an x-ray source by a solid with the subsequent ejection of a photoelectron whose kinetic energy is a measure of the binding energy of an electron in the target atom.[23] The emitted electron's kinetic energy is given by,

$$E_K = E_P - E_B$$

where E_p is the energy of the incident x-ray photon, and E_B is the binding energy of the ejected electron. This is the energy required to remove an electron to infinity with no kinetic energy, basically an ionization energy. The ejected photoelectrons are collected and sorted by energy using an electron spectrometer. XPS is primarily a surface technique, sampling to a depth of 1-2 nm, because photoelectrons ejected from deeper in the film lose most of their

energy in escaping from the film or fail to escape at all. An XPS spectrum will then reveal information about the binding energy of electrons in the surface atoms in the film.

The electron spectra for most elements have been catalogued at this time. Thus it is known that the binding energy corresponding to Si 2p electrons is 99.15 eV for silicon atoms in the Si^0 oxidation state, while that for silicon atoms in the Si^{4+} oxidation state sits at 102.5 eV. The 4^+ state is indicative of silicon in SiO_2. This shift is due to the shift in binding energy that electrons feel when the chemical environment of an atom is altered, for example by changes in chemical bonding. The changes in bonding lead to a redistribution of the atom's valence electrons which alters the attractive force on the core electrons and therefore the binding energy of the those electrons.

2.6.1.2 *Experimental Details*

For this study, the incident source was a 300 W, Mg K_α (1253.6 eV) non-monochromatized x-ray beam. The take-off angle measured between the surface and the detector was 45°. The XPS system was held at a base pressure of less than 5×10^{-9} torr. Spectra were acquired in multiplex mode, typically looking at the Si 2p, C 1s, and I $3d_{5/2}$ peaks. Sample acquisition time was 7.07 minutes. Since the films studied were deposited on Teflon, an insulator, there is a buildup of charge on the film as the sample loses photoelectrons. The positively charged surface leads to a change in the measured binding energy of the ejected photoelectrons. This correction varies along with the charge buildup and therefore may change over the course of the experiment and the surface of the sample. Since this correction will effect all the ejected photoelectrons equally, it is possible to correct for this effect by normalizing the XPS spectra to the adventitious carbon peak at 284.6 eV.[24] This peak is present on all the samples and is believed to be due to carbon that adsorbs on the film surfaces during the deposition or sample transfer process.

In this work, it was possible to examine the relative position of the binding energy peaks in the spectra. In an individual spectrum, it was also possible to compare the relative intensities of peaks, for example the Si^0 and Si^{4+} peaks to watch for the oxidation of silicon due to processing. However, it was not possible to compare the intensities of spectra between samples due to differences in sample positioning. All comparisons between samples are

limited to the comparisons of ratios of peaks within individual spectra or the positions or presence of individual peaks.

2.6.2 Fourier Transform Infrared Spectroscopy

Fourier Transform Infrared Spectroscopy (FTIR) was also used to characterize the surfaces of the thin films of silicon nanocrystallites. The spectra were taken on a Nicolet 510P spectrometer equipped with a liquid nitrogen cooled MCT-B detector. The spectra were taken from 400-4000 cm^{-1}. The wavelength resolution was 4 cm^{-1} and a total of 512 scans were run per spectrum. The samples were deposited on silicon wafer substrates.

2.7 Films

2.7.1 Structure

The pulsed laser ablation supersonic expansion source deposits thin films on substrates placed in the path of the expansion. Typical film thickness is on the order of 100 nanometers. This reflects an average deposition rate of 10 nm per hour[7] and a typical deposition time of ten hours. After ten hours, the interaction channel has clogged with silicon particles enough to severely reduce the deposition rate. On a given 2" x 2" substrate surface, the deposited film is by no means of uniform thickness, in fact it tends to be peaked towards the point of the substrate that is best aligned with the interaction channel, and therefore in the direct path of the most intense part of the expansion. The films appear golden brown under normal room light when deposited on Teflon. On silicon wafers, they can begin brown in color, but gain an iridescence after oxidation in air, reflecting interference fringes due to thickness variation.

The films appear to consist of a polydisperse collection of silicon nanocrystallites embedded within a native oxide matrix that connects the particles into a continuous film.. By placing etchable substrates, such as glass slides, into an HF bath, it is possible to lift off the film in agglomerated pieces. A schematic of the proposed film structure is shown in Figure 2-5.[25]

Glancing angle x-ray diffraction (GAXRD) analysis of films deposited on niobium substrates confirmed a significant amount of material within the films that matched the

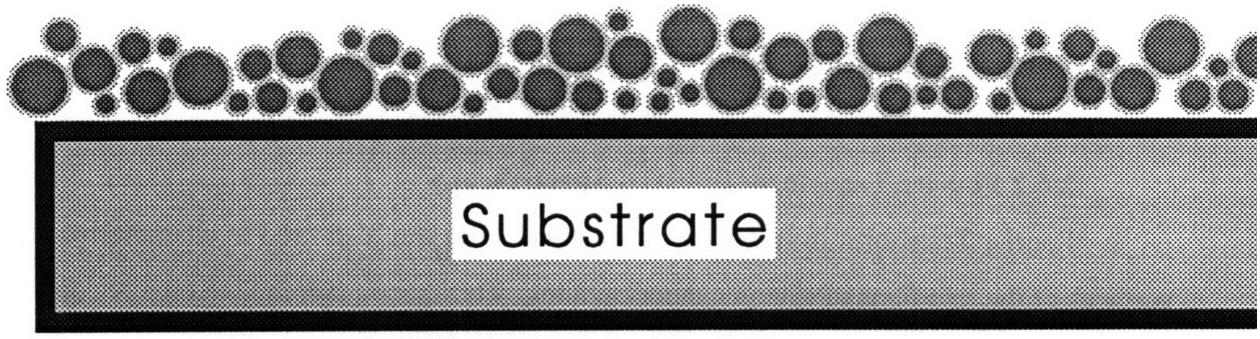

Substrates:
Teflon
Silicon wafer
Poly(vinyl carbonate)

Figure 2-5 Schematic of thin film of silicon nanocrystallites embedded in native oxide matrix on substrate material. Deposition is drawn to highlight size distribution present in all films. (From Ref. 25)

patterns expected from bulk silicon.[1] However, the diffraction patterns also showed extremely narrow linewidths, indicating the presence of some very large, possibly micron scale, crystalline particles within the film. TEM analysis of the deposited films has also confirmed the presence of larger sized crystallites. Some of these particles are seen to be flattened out, with a thickness on the order of 10 nm, and having diameters of hundreds of nanometers.[9] Some of these larger particles appear amorphous and several show indications of structural defects within them.

TEM analysis has shown the films to consist of a distribution of particle sizes, ranging from micron scale structures down to 2-3 nm particles. Since similar deposition sources are known to generate atomic scale clusters, this lower bound only reflects the smallest size which has been clearly resolved thus far. High resolution electron microscopy (HREM) analysis has identified crystalline silicon particles on the order of 2-5 nm present in the films.[1] One such particle is shown in Figure 2-6. These nanostructures are in the size range where quantum confinement effects can be expected from silicon. HREM analysis of larger particles has allowed observation of the surface layer of the crystallites. This work has imaged a ~30 nm diameter particle, which shows a crystalline interior and an amorphous surface layer, as shown in Figure 2-7. This surface layer is approximately 1 nm thick, and is believed to be the oxide layer that grows on the particles as they age in normal room air. It is important to note that there is no reason to suspect that smaller particles do not oxidize as well.

2.7.1.1 *Nanocrystallite structure*

The individual silicon nanostructures have their crystal structures determined during the initial stages of the pulsed laser ablation process. Clusters are believed to be formed through the sequential collisions of atomic silicon, implying that the final structure results from the buildup of individual silicon atoms. In this case, it is not obvious that smaller clusters will take on the diamond cubic lattice structure of bulk silicon. Raman spectroscopy has shown that small silicon clusters have very different atomic structure than bulk silicon.[26]

The clusters are also believed to be very hot during the entire deposition process, at approximately 500 K.[4] It is believed that the particles still have enough energy to reorganize themselves into equilibrium structures, possibly the diamond cubic structure. This was shown

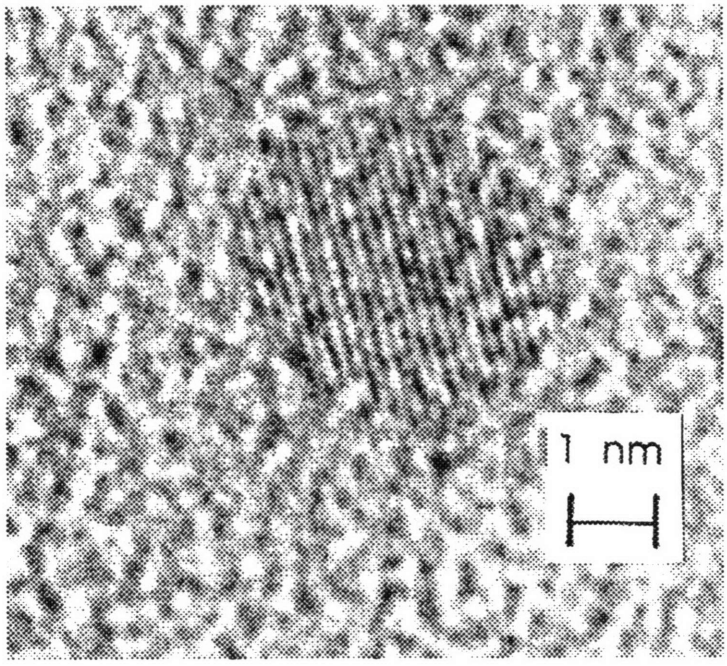

Figure 2-6 High resolution electron micrograph of a silicon nanocrystallite deposited on an amorphous carbon substrate. (From Ref. 1)

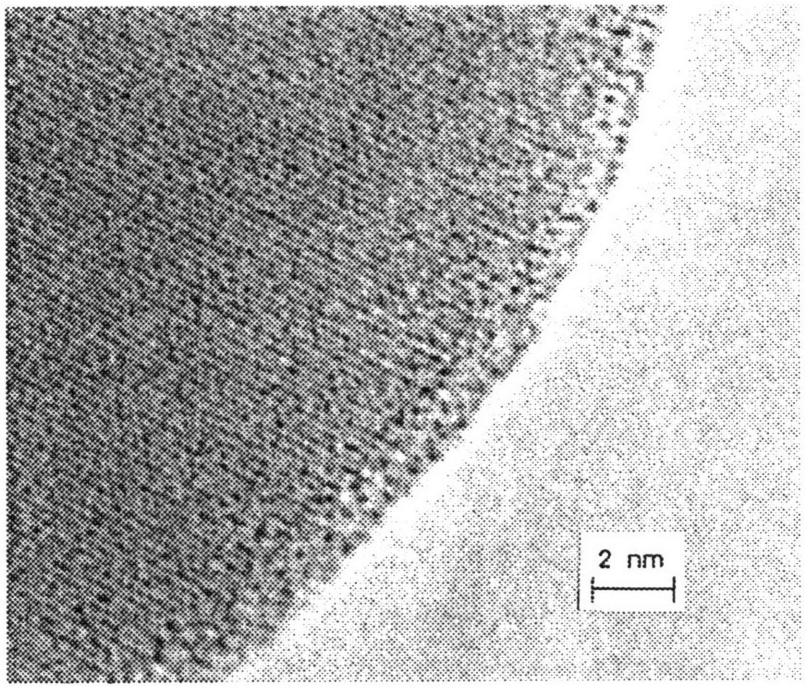

Figure 2-7 High resolution electron micrograph of a silicon nanocrystallite with an amorphous surface layer.

in the carbon system where the same source produced 60 atom carbon fullerenes by building them up from atomic carbon.[2] However, the high cluster temperature may also imply that some of their final structure is formed as they cool after impinging on the substrate. Finally, there is only a very limited time for clusters to nucleate and grow in the interaction channel. This will strongly determine the final structure of the silicon clusters.

Another possibility for cluster formation is through the ablation of pieces of polycrystalline silicon from the target, which then undergo the growth process in the interaction channel. These particles will initially have the diamond cubic lattice structure. This structure may be modified by the vaporization and collision processes, as well as the deposition step onto the substrate material. It is not clear what temperature these larger clusters are, or in fact whether they are an entirely liquid phase.

The formation process of the nanostructures during the nonequilibrium laser ablation process is critical to determining the final structure of the particles. This information will be useful for correlations with the emission behavior to confirm the nature of the recombination process in the material. However, the lack of this knowledge does not diminish the insights that can be gained through optical characterization of the films. In fact, information on electronic structure gained through optical studies can play an important role in directing future structural characterization of the individual nanoparticles.

2.7.2 Properties

The film properties themselves will have some effect on the experimental processing and characterization of the system. This is unfortunate since the focus of this work is not the structural properties of the film or crystallites, but rather their optical properties. The thickness of the film will mean that some crystallites will be buried deep within the layer, and may not be affected by etching or oxidation steps. During some wet chemical etch steps, the oxide matrix holding the particles together may completely dissolve, breaking pieces off from the film. Also, some films are very thin and cannot survive the handling and dipping that is entailed in repeated processing steps.

The optical properties of the films were also affected by the microstructure. The films were very thin, leading to poor emission intensities and difficulty in collecting luminescence

signal. The large size distribution implied that many particles which are not expected to emit light from quantum size considerations were still present in the films under examination. The films tended to ablate during some photoluminescence measurements, preventing repeated measurements from a single film. Because the films were so thin, it is likely that the entire film could be irradiated by the excitation beams during photoluminescence experiments, and that very little signal would be lost to absorption in the films themselves. Finally, the rough surfaces of the samples made it difficult to measure some of the transmission characteristics, especially after films had been processed.

2.7.3 Comparison with Porous Silicon

The film structure of pulsed laser ablation deposited nanocrystallite films has some similarities to porous silicon. They both consist of crystalline silicon particles, which can be passivated by an oxide or hydrogen passivated. The films are both extremely rough and have a complex surface morphology, opening the possibility that adsorbed species could play a role in the optical properties. There are also a number of differences between the two materials. Porous silicon does not consist of isolated nanocrystallites, but rather interconnecting wire like structures, whose undulations and constrictions shrink it down to a nanoscale regime. In general, porous silicon films are approximately ten times thicker than silicon nanocrystallite films, thereby making more characterization techniques possible. Porous silicon substrates are usually p-type, and therefore a small fraction of the crystallites would be doped after the etching process, and as such would be expected to show very different behavior. Porous silicon is nanostructured silicon broken down from bulk diamond cubic silicon, while nanocrystalline silicon is built up from atomic silicon. It is possible that even at the same sizes, their atomic structures will be different. Finally, the porous silicon films are directly connected to their bulk silicon substrate, unless they are lifted off chemically or mechanically scraped away. All of these differences must be kept in mind when considering the properties of the two material systems.

Chapter Two References

[1] E. Werwa, A.A. Seraphin, L.A. Chiu, C. Zhou, and K.D. Kolenbrander, Appl. Phys. Lett. 64(14), 1821 (1994)
[2] D.E. Powers, S.G. Hansen, M.E. Geusic, A.C. Pulu, J.B. Hopkins, T.G. Dietz, M.A. Duncan, P.R.R. Langridge-Smith, and R.E. Smalley, J. Phys. Chem. 86, 2556 (1982)
[3] M.L. Mandich and K.D. Rinnen, Z. Phys. D 26, 147 (1993)
[4] K.D. Kolenbrander and M.L. Mandich, J. Chem. Phys. 92(8), 4759 (1990)
[5] K. Tanaka, T. Kato, I. Koyano, N. Takahashi, T. Moriya, and K. Teshima, Proc. 14th Int. Symp. on Rarefied Gas Dyn. 2, 751 (1984)
[6] E. Werwa and K.D. Kolenbrander, Mat. Res. Soc. Symp. Proc. Vol. 397, in press.
[7] S.-T. Ngiam, private communication.
[8] B.K. Rao, S.N. Khanna, and P. Jena, Phase Trans. 24-26, 35 (1990)
[9] C. Zhou, unpublished result.
[10] C-R. Wang, R.-B. Huang, Z.-Y. Liu, and L.-S. Zheng, Chem. Phys. Lett. 227, 103 (1994)
[11] K. Raghavachari, Phase Trans. 24-26, 61 (1990)
[12] L.A. Chiu, A.A. Seraphin, and K.D. Kolenbrander, J. Electron. Mater. 23(3), 347 (1994)
[13] K.-D. Rinnen and M.L. Mandich, Phys. Rev. Lett. 69(12), 1823 (1992)
[14] S.-T. Ngiam, K.F. Jensen, and K.D. Kolenbrander, J. Appl. Phys. 76(12), 8201 (1994)
[15] A. Thilderkvist, J. Michel, S.-T. Ngiam, L.C. Kimerling, and K.D. Kolenbrander, Mat. Res. Symp. Proc. Vol. 405, in press.
[16] T.A. Burr, A.A. Seraphin, and K.D. Kolenbrander, "International Symposium on Advanced Luminescent Materials", Proc. of the Electrochem. Soc. (1995)
[17] S.-T. Ngiam, Ph.D. Thesis, Massachusetts Institute of Technology (1996)
[18] J.D. MacKenzie, B.S. Thesis, Massachusetts Institute of Technology (1993)
[19] B.E.A. Saleh and M.C. Teich, *Fundamentals of Photonics*, p.756 (1991)
[20] N.P. Xuan, J.L. Ferrier, J. Gaxengel, and G. Rivoire, Opt. Comm. 51, 433 (1989)
[21] D.V.G.L.N. Rao, F.J. Aranda, J.F. Roach, and D.E. Remy, Appl. Phys. Lett. 58(12), 1241 (1991)
[22] A.A. Seraphin, S.-T. Ngiam, and K.D. Kolenbrander, Mat. Res. Soc. Symp. Proc. Vol. 405, in press.
[23] L.C. Feldman and J.W. Mayer, *Fundamentals of Surface and Thin Film Analysis*, p.213 (1986)
[24] D. Briggs and M.P. Seah, *Practical Surface Analysis*, p.437 (1983)
[25] T.A. Burr, private communication.
[26] E.C. Honea, A. Ogura, C.A. Murray, K. Raghavachari, W.O. Sprenger, M.F. Jarrold, and W.L. Brown, Nature 366, 42 (1993)

3. Results and Discussion

3.1 Photoluminescence

Figure 3-1 shows a typical photoluminescence spectrum from a silicon nanocrystallite thin film deposited on a Teflon substrate and aged in normal air. The spectrum is peaked at ~650 nm or 1.9 eV and has a broad emission peak, with a full width at half maximum of ~0.5 eV. A film such as this emits orange light under photoexcitation from a 3xNd:YAG or Ar^+ laser or a handheld ultraviolet lamp. The orange color is bright enough to be visible under normal room lighting conditions, though it still requires photoexcitation. These emissions are not present when examining bare substrates. This orange emission appears to be stable indefinitely; samples which were deposited four years ago show no change in luminescence color or appearance over long periods of time, beyond what will be described as being the result of processing steps.

A few broad conclusions can be drawn from this observed spectral behavior. The very existence of visible luminescence from these films is evidence of novel optical properties in a silicon based material. The films are emitting visible light, which implies that the active material is not traditional bulk silicon. The films are also emitting light that has some intensity, therefore it is not likely that the radiative transitions are bulk indirect gap recombination events. The fact that the luminescence is similar to that seen in porous silicon also points out that it is likely that the emission mechanism between the two systems may be the same. The stability of the emission over time and its reproducibility strongly argues against it being a result of any accidental deposits which arise on the film due to the deposition procedure.

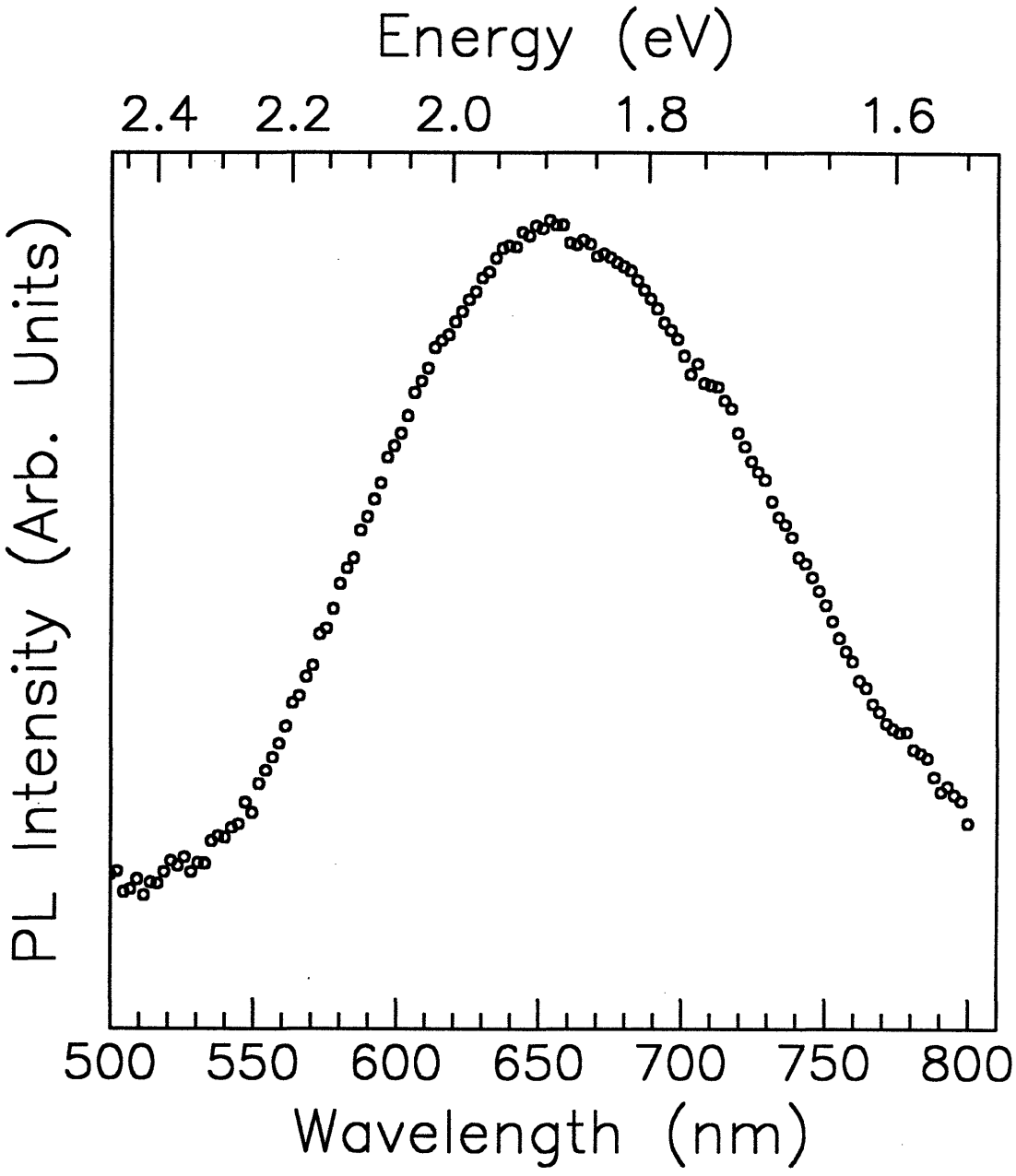

Figure 3-1 Typical photoluminescence spectrum for a thin film of silicon nanocrystallites on a Teflon substrate. Spectrum was taken at 300 K using a 3xNd:YAG (λ_{ex}= 355 nm) laser as the excitation source.

3.1.1 Size Distribution of Nanocrystallites

The photoluminescence emission spectrum can be used to calculate a crude size distribution of emitting crystallites in the film. This calculated distribution does not include crystallites too large to contribute to the emission behavior, nor does it include crystallites whose unpassivated surfaces or defect content prohibit efficient emission. The calculation is based on the model proposed by Khurgin which assumes quantum confinement of carriers in the silicon nanostructures.[1] The energy gap of the particles is given as a function of the dimensions of the particle, d_1, d_2, and d_3, but for simplicity here it is assumed that the nanocrystallites are cubes with edge length r. The crystallite energy gap is given as,

$$E_g = E_{g,0} + \frac{h^2}{2}\left[\frac{m_l^{-1} + m_{hp}^{-1}}{d_1^2} + \frac{m_l^{-1} + m_{hp}^{-1}}{d_2^2} + \frac{m_l^{-1} + m_{hp}^{-1}}{d_3^2}\right]$$

where $E_{g,0}$, m_l, m_h, and m_{hp} represent the band gap, longitudinal effective mass, heavy hole effective mass, and heavy hole mass in the direction normal to confinement in bulk silicon, respectively. This leads to a parabolic relationship between size and energy, as has been proposed in other models.[2] The model also postulates that smaller particles have a larger oscillator strength than larger particles, and so will play a larger role in determining luminescence properties. This assumption is physically sensible, because smaller particles would tend to have more wavefunction overlap. The oscillator strength of the transition is given by the relation,

$$f \propto r^{-6}$$

Applying this simple model to a typical luminescence spectrum gives a size distribution of emitting crystallites as shown in Figure 3-2. The larger end of the size spectrum is undefined, as particles that are too large will not have the oscillator strength necessary to give any emission, and at some point will behave as bulk materials. Preliminary TEM results indicate that the larger end of the size distribution is a long tail stretching out to include micron sized particles.[3] The smaller end of the size distribution is equally undefined, as the source is known to produce many clusters smaller than 3 nm in diameter, which this model predicts play no role in the emission behavior at all.

The sizes predicted to emit visibly for silicon crystallites are large when compared to the Bohr exciton radius in silicon and to some experimental results,[4] including HREM studies

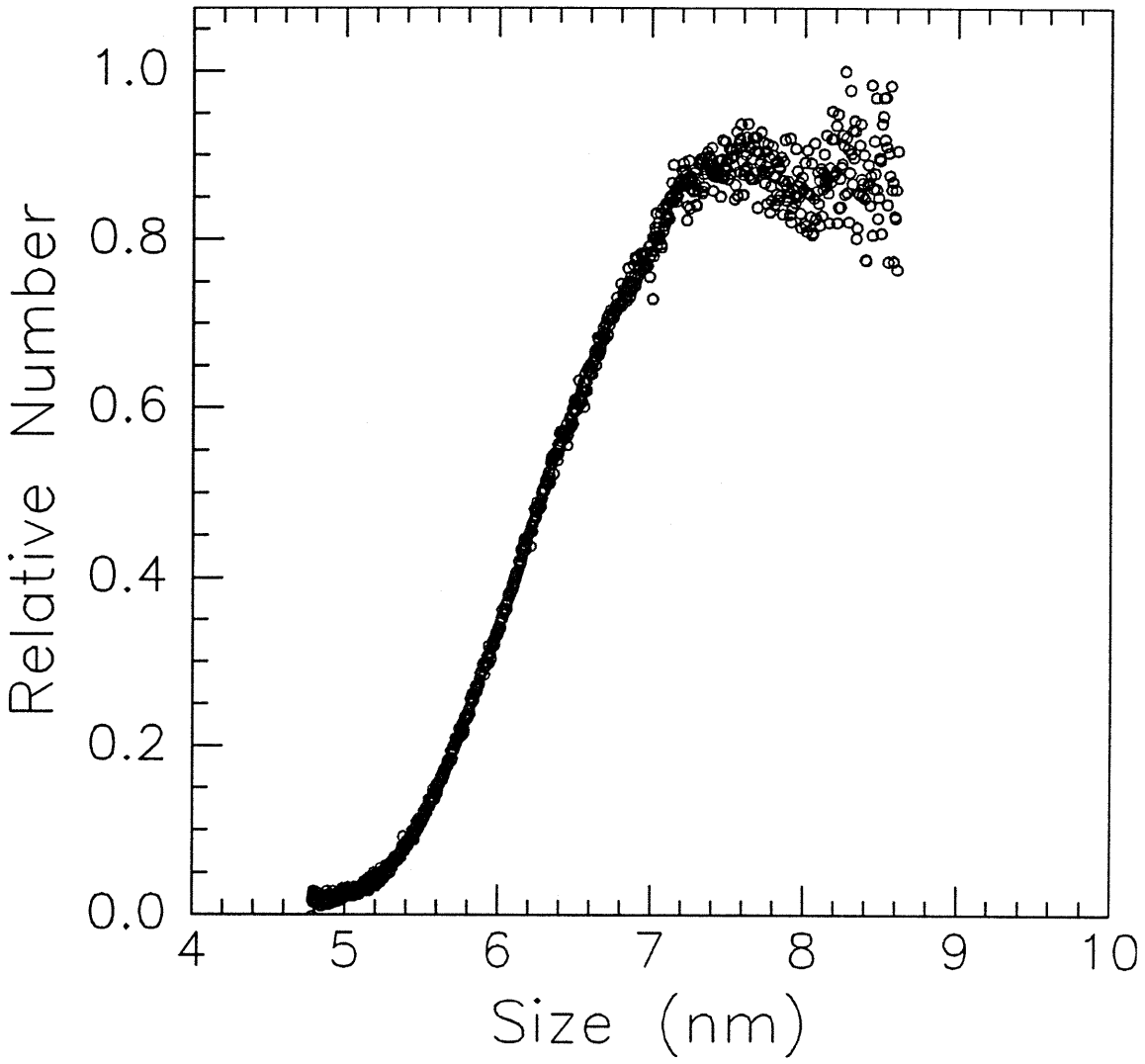

Figure 3-2 Size distribution calculated from PL spectrum in Figure 3-1 using Khurgin model.

of the nanocrystallite thin films.[5] At this time, this size discrepancy is a common feature of most theoretical models.[6,7] A closer match in predicted size with measured sizes can be achieved by assuming that $E_{g,0}$ has a larger value than 1.12 eV, for example, the 1.6 eV gap found in amorphous silicon. This correction reflects a physical reality in the relative disorder of nanocrystalline silicon structure with respect to that of the bulk.

The Khurgin model also does not consider the important role that luminescence from the oxide in the films plays. Oxide luminescence from defects is expected to occur at shorter wavelengths, starting at about 550 nm. A spectrum from a typical defect ridden oxide, a glass slide, is shown in Figure 3-3. This luminescence makes assigning emission wavelengths at the small end of the size scale more difficult. The model does not allow for nonradiative recombination due to defects in the particles, which may scale with particle size. In addition, the assumption that the effective masses of carriers in the nanocrystalline material will be the same as the bulk is questionable, since there is no doubt a change in band structure and shape due to quantum confinement.

The attempted calculation of a size distribution using this simple model points out the difficulty in identifying the dimensions of the optically active species in the films. While the quantum confinement of carriers described in the Khurgin model will be shown to play a determining role in the emission properties of the nanocrystallites, the specific size ranges predicted by the model are very likely to be incorrect. In fact, this model predicts emitting particles will be larger than the Bohr exciton radius of bulk silicon, violating one of the basic premises of quantum confinement, as discussed in section 1.5.

Currently, there is no one universally accepted theoretical model which can accurately reflect all the observed behaviors in porous and nanocrystalline silicon. There is in fact still disagreement in experimental data concerning the size and structure of the emitting species. These problems make any description of a size distribution based on optical properties very unreliable. However, information on the electronic structure of the films of polydisperse nanostructures derived from optical characterization can provide significant insight into the emission mechanism in the material, and can be correlated to future characterizations of the sizes and structures in the system.

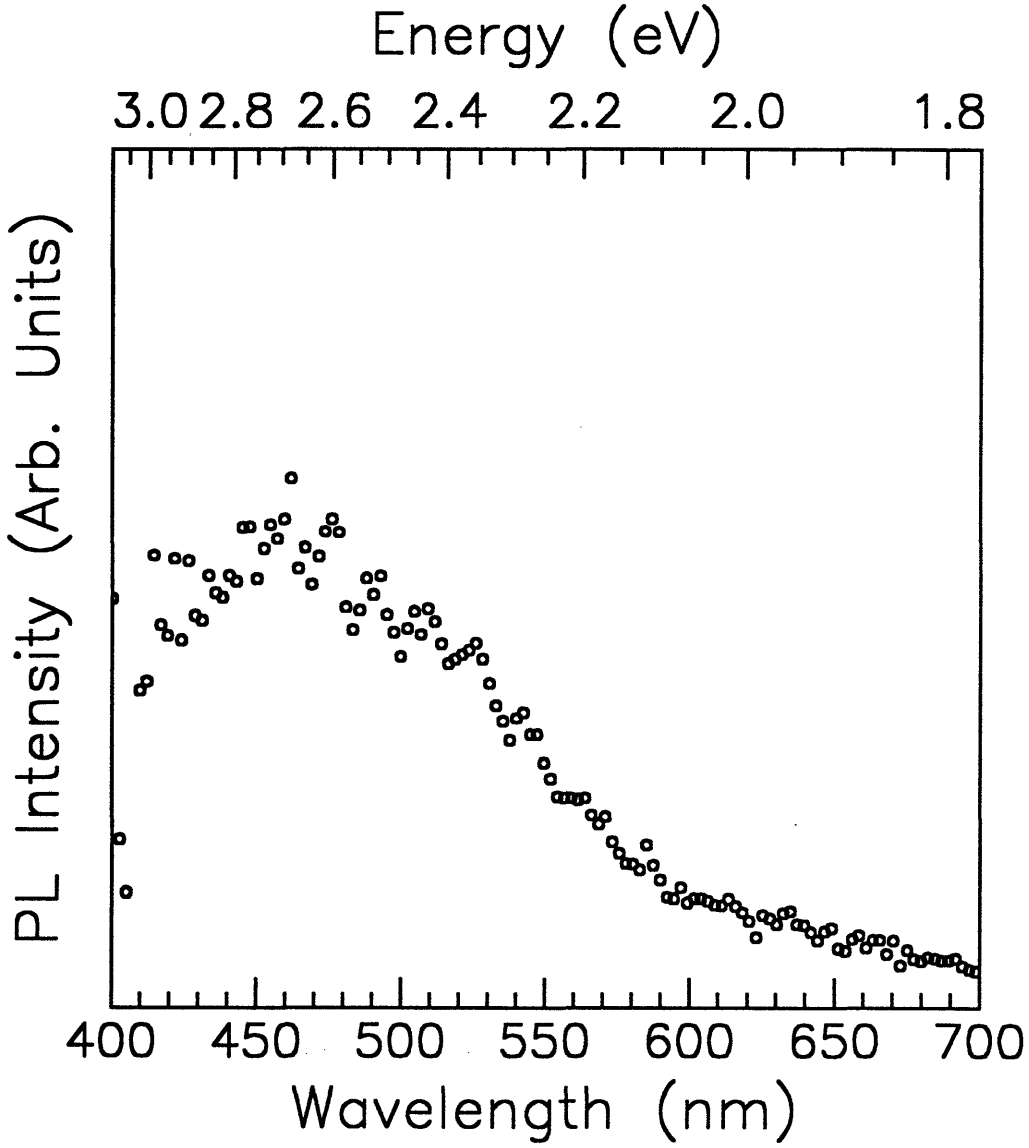

Figure 3-3 PL spectrum from a defect ridden oxide (glass slide) at 300 K showing significant sub-550 nm spectral structure.

Assuming that nanocrystallite size controls emission energy implies that each wavelength corresponds to one crystallite size. The FWHM of the spectrum then reflects the broad size distribution in the particles. As described in section 3.1, the FWHM in the thin films of silicon nanocrystallites is ~0.5 eV. In 3.85 nm chemically size selected CdSe quantum dots with a size distribution of ±4.5%, the luminescence FWHM is ~0.2 eV at 300 K, reflecting a much smaller size range of emitting particles.[8] For a single GaAs/AlGaAs quantum dot, the FWHM has been reported as 0.9 meV at 15 K.[9]

3.2 Processing Effects on Luminescence Behavior

A number of experiments were performed to alter the sizes and surfaces of the silicon nanocrystallites and to correlate these changes with differences in the photoluminescence behavior. The processing of the samples to reduce their size would create a corresponding shortening of the emission wavelength, if quantum size effects played a role in the emission process. By altering the type of surface passivation on the samples, it would be possible to gain insight into the role of the surface species in determining the characteristics of the emission behavior.

3.2.1 Size Effects

The size of the nanocrystallites was altered using the silicon processing techniques described earlier. In each case, the goal was to reduce the crystalline core size in order to increase the confinement of carriers in the particle. Here, converting a portion of the silicon cores into oxide will shrink its size. By using hydrofluoric acid (HF) to remove this oxide and then growing a new one, it became possible to gradually shift the size distribution to smaller particles.

3.2.1.1 *Aged Films*

A set of photoluminescence spectra of a film as it ages in normal room air is shown in Figure 3-4. These films show a clear blueshift in the emission wavelength as aging time increases. This is indicative of a gradual reduction in particle size by extended oxidation of

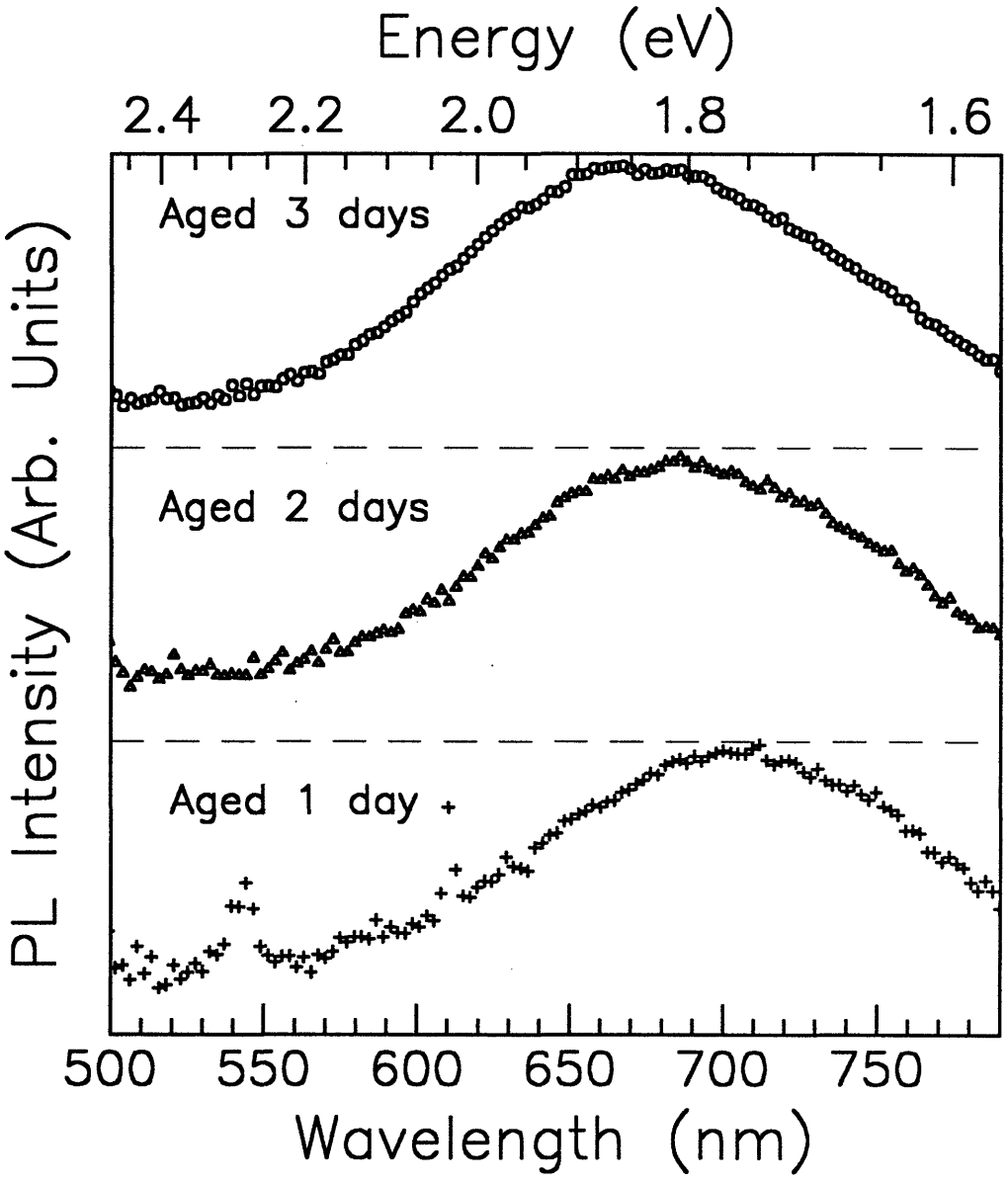

Figure 3-4 Effect of aging in atmosphere on PL spectrum of silicon nanocrystallite thin films. PL wavelength blueshifts with increased aging, consistent with crystallite size reduction due to extended oxidation.

the crystallites. This size reduction is expected as crystalline silicon material is used up during the oxidation reaction. The luminescence intensity also increases from the as deposited film to the three day aged film, indicating an enhancement of the surface passivation in the samples. The luminescence peak stops shifting after this point and remains basically fixed indefinitely in both emission energy and intensity.

By converting the photoluminescence spectra to size distributions, it is possible to get a rough idea of the size reduction necessary to see this magnitude of shift in the photoluminescence behavior. A correlation of size to emission energy can be developed by modifying a model developed by Delerue, based on a calculation of the electronic structure of nanocrystallites using a linear combination of atomic orbitals (LCAO) technique.[10] This predicts a weaker dependence of energy gap on than effective mass models, with energy gap going as $d^{-1.39}$, where d is particle diameter. Fitting this proportionality to the experimental results of Schuppler correlating particle size to peak emission energy,[4] gives a relationship between energy gap and size of,

$$E = E_0 + 0.93d^{-1.39}$$

where E_0 is the bulk energy gap at 0 K (1.17 eV).

Using this relationship and the size dependent oscillator strength described in section 3.1.1, the second 24 hours of aging are calculated to have an oxidation rate of ~.065 nm per day, while the third 24 hours show a rate of ~.035 nm per day. It is important to note that first 24 hours of aging also contribute to the oxide thickness, so the total layer thickness can also be approximated as being over ~0.1 nm thick. This initial aging cannot be modeled using this method, since there is no as-deposited film photoluminescence spectrum to convert into a size distribution. This gradual growth of the native oxide has also been observed for bulk silicon systems.[11,12] The bulk oxidation rate is ~0.9 nm per day, and also slows with increasing oxidation. The slower rate measured in the nanocrystalline system supports models of self-limiting oxidation of nanostructured systems.[13]

This correlation of size to peak wavelength strongly supports models of emission based on quantum size effects, since core size reductions lead to blueshifts in the luminescence behavior. However, it is possible that the hydrogen content of the films may be increasing with time and lead to a blueshifting of the emission, so models based on oxygen defects, such

as non bridging oxygen hole centers, or based on hydrogenated amorphous silicon are equally feasible. It is also possible that as time passes there are more surface species adsorbing to the film and increasing the luminescence emission, however this is not likely to result in such a consistent shift in the emission wavelength.

3.2.1.2 *HF/HNO_3 Cycles*

Photoluminescence spectra of a film used in etch and oxide regrowth cycles is shown in Figure 3-5. The spectra show a clear blueshift of peak emission wavelength that correlates with the expected reduction of particle size. Each step in the process is expected to reduce the size of the crystalline cores due to the oxidation of silicon by nitric acid or the etching of crystalline silicon by hydrofluoric acid. At the same time there is a gradual distortion of the luminescence peak shape towards higher energy, shorter wavelength emissions. This indicates that a large portion of the crystallites are being converted completely to oxide and show the oxide related short wavelength emission behavior. This cycling to reduce particle size and emission wavelength correlates well with cycles of samples repeatedly aged in air and then stripped of their oxide with HF,[14] as well as similar work in porous silicon.[15]

Extended cycling of the etch and oxide steps resulted in the destruction of the films due to handling and removal of material. After a few cycles, there was not enough material left to emit sufficient light for signal collection. Regardless, this tunability of the emission wavelength is strong support for models of emission that are based on quantum size effects. However, it is important to point out that after an HF dip the samples are expected to be hydrogen passivated, and after a nitric acid etch or aging in air, they should by oxygen passivated. The presence of the two types of passivation does not appear to alter the overall trend with respect to particle size. It is not clear that more hydrogen would be expected to be incorporated into the films as the cycling continued so models based on non-bridging oxygen hole centers or amorphous silicon cannot easily explain these results. In addition, the clear blueshift with reducing particle size makes a surface species explanation unlikely.

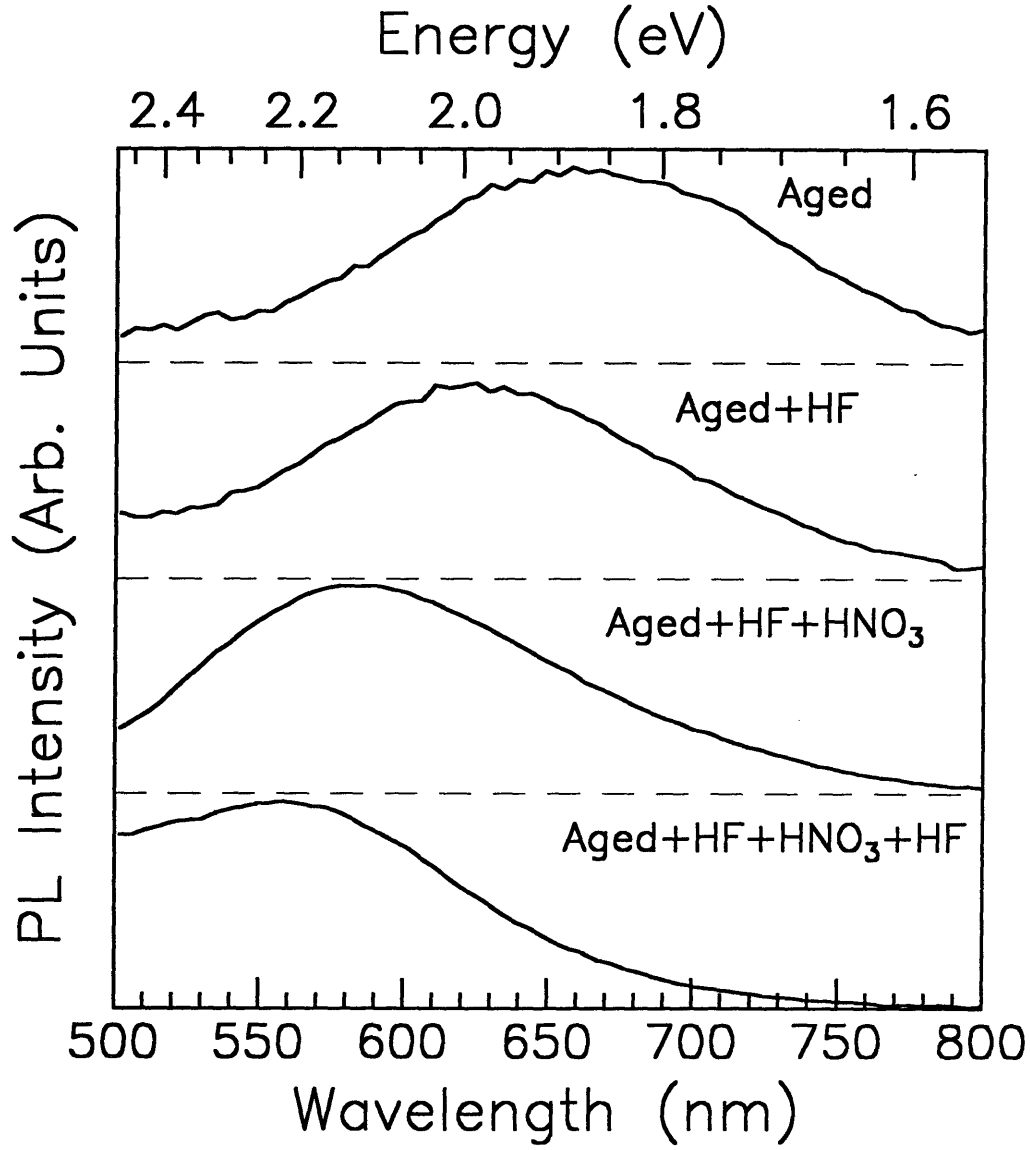

Figure 3-5 Effect of HF/HNO_3 cycles on PL emission. As etch/oxide regrowth cycles reduce the size of the silicon nanocrystallites, a blueshift in the emission is observed.

3.2.1.3 *$HF/HNO_3/H_2O$ Dip Time*

The photoluminescence spectra for a group of films used in a series of etches for gradually longer dip times is shown in Figure 3-6. As the etch time increases, the etching of the silicon nanocrystallites should progress further, resulting in smaller particle sizes. The luminescence peak shifts with the expected reduction in particle size. This indicates some control of particle size over the emission wavelength. The intensity of the emissions from the films decreased with increasing etching time. This reflects the destruction or oxidizing of crystalline luminescence centers in the film during the processing.

The samples once again showed an increase in the relative amount of short wavelength oxide behavior as the etch time increases. This can be explained as the increasing relative intensity of the oxide luminescence with respect to the nanocrystallite luminescence. A simple model of luminescence based on quantum size effects is enough to explain this data as well. The reduction in particle leads to an expansion of the energy gap and a blueshifted luminescence wavelength. Models of emission based on amorphous silicon or oxide defects cannot be easily used to explain these results.

3.2.1.4 *Deposition Parameter Control of Size*

The pulsed laser ablation supersonic expansion system can be modified to change the size distribution of particles in the film, as described in section 2.1.1. Work has been done to change particle sizes by adjusting the relative timing of the ablation laser and carrier gas valve, and also by extending the length of the interaction channel. Adjustments of deposition parameters which should have resulted in smaller nanocrystallites being produced, resulted in a shifting of the luminescence peak wavelength to the blue.[14] This once again shows the importance of quantum size effects in controlling the emission wavelength of the nanostructures.

3.2.1.5 *Oxidation Furnace Treatments*

A number of samples on silicon substrates were treated in oxidation furnaces under oxygen gas flow or in air with no flow. Here the intent was to examine the shift in the luminescence emission as a result of the reductions in crystalline core sizes that would be

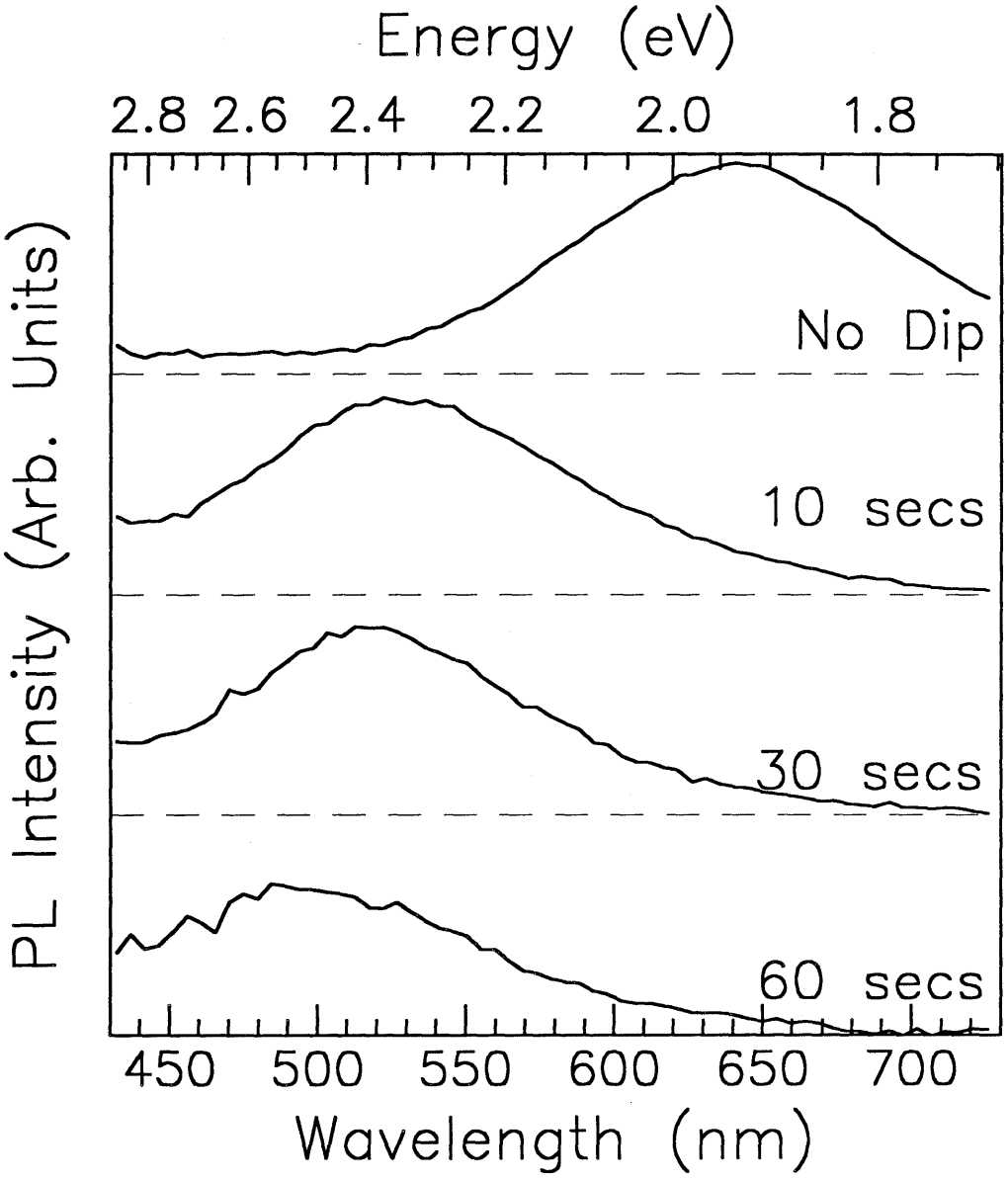

Figure 3-6 Effect of increasing dip time in $HF/HNO_3/H_2O$ solution. As dip time increases and silicon nanocrystallite size is reduced, a blueshift in emission is observed.

expected from oxidation steps. Figure 3-7 shows a typical result from the oxidation of a film deposited on a silicon wafer. This sample was heated for 30 minutes at 450 °C under O_2 flow. Before the heat treatment, the film showed orange emission, but after the oxidation step this orange signal was lost. However, there was never any gradual blueshift of the peak wavelength detected in any of the samples that were furnace treated. Instead, there was an increase in the amount of sub-500 nm emission signal. The disappearance of the longer wavelength behavior indicates that there was a complete oxidation of the crystalline silicon material in the samples. This resulted in the increase in the amount of oxide present, and so an increase in the blue or yellow signal expected from oxides under ultraviolet excitation.

These results point out that the blue band behavior seen in silicon nanocrystallites and porous silicon can be correlated to the appearance of oxide in the films. This defect ridden oxide is expected to emit at these short wavelengths.[16] If one tries to attribute the orange luminescence in other samples to defects in the oxide or blue luminescence to recombination of quantum confined carriers in the silicon cores, then these results are difficult to explain. First, it is unlikely that the oxidation step removed the defects in the oxide layer, as is indicated by the quenching of the orange emission, according to the oxide defect emission model. Second, the increase in blue emission intensity is correlated with an expected reduction in the number of silicon crystallites in the film, which should reduce the number of core recombination events. However, it is possible to argue that these results are an example of converting the size distribution of particles over to small sizes that emit in the blue region of the spectrum. Explanations for silicon visible emission based on polysilanes, siloxene, or hydrogenated amorphous silicon may also hold here, since none of these materials would be expected to survive the heat treatment, and this would correlate with the loss of orange luminescence.

3.2.1.6 *Summary*

In each of these experiments, the sizes of the nanocrystallites were altered to change the photoluminescence emission energy. There is a clear correlation between the size of the particles and the emission wavelength. Reducing the particle sizes through processing parameters succeeded in reducing the emission wavelength, as is predicted by models of light

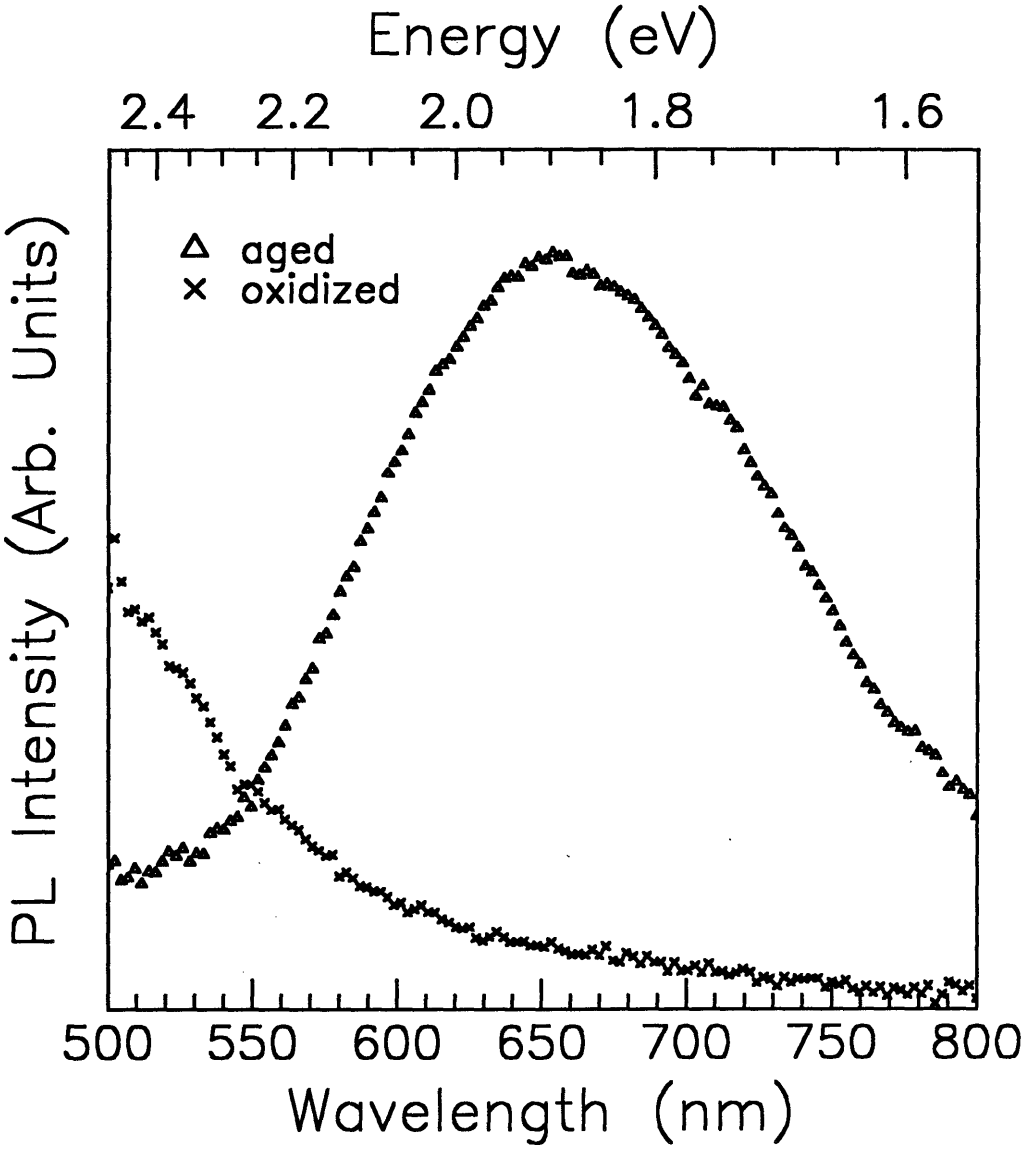

Figure 3-7 Comparison of PL spectra for aged and oxidation furnace treated samples. The furnace treated sample has lost its red band behavior and shows the blue signal indicative of oxide emission.

emission based on quantum confinement. It was also shown that the intensity increases in the high energy, short wavelength emission correlated well with expected increases as the amount of oxide in the film due to processing steps. In no case did any evidence contradict emission models based on quantum size effects.

3.2.2 Surface Effects

The surfaces of the nanocrystallites were altered using the silicon processing techniques described earlier. In each case, the goal was to change the passivating environment of the crystallites, and correlate the changes to the observed photoluminescence behavior. Two major effects were studied with these series of experiments, first the role of surface passivation in determining the emission intensity of the films, and second the role that the chemical nature of the passivating species plays in determining the emission energy or wavelength.

3.2.2.1 *Gas Phase Photoluminescence*

In an effort to study the emission of nanocrystallites in the simplest passivating environment, photoluminescence was performed on clusters in the expanding molecular beam while still in the vacuum deposition system. These nanocrystallites would be completely isolated, with no passivating surface layer at all. In addition, at the time of ultraviolet excitation, it is believed that the clusters are fully formed and isolated, existing in a collision-free environment. A number of different timings were tried so that different portions of the traveling cluster packet were photoexcited. The investigation of the gas phase silicon nanocrystallites revealed no observable luminescence emission. Varying deposition parameters to change particle sizes also produced no visible emission.

Direct comparison of the results of this emission study on isolated Si nanocrystallites with previous results on thin film materials is limited by several differences. Most significant is the difference in temperature of the Si nanocrystallites in the thin films and in the gas phase. Although the nanocrystallites were produced through condensation resulting from the tremendous cooling of the helium carrier gas in the supersonic expansion, they remain quite hot, with temperatures expected to be approximately 500K.[17] A second difference relates to

the time available for detection of emission. Time of flight measurements on the clusters has determined that the fastest clusters travel at 2120 meters per second, while the slowest clusters have a velocity of 1620 m/s.[18] This high velocity implies that the nanocrystallites are only available for observation for several hundreds of microseconds. If the luminescence decay lifetime is too long, hundreds of milliseconds or more, very little emission will be observed during the relatively short time available for the gas phase measurements. However, most models of silicon nanocrystallite emission predict lifetimes on a much shorter timescale,[19] and experiments have measured these faster emissions, ranging from picoseconds to milliseconds.[20,21,22] Finally, the density of isolated nanocrystallites is likely to be significantly less than that of agglomerated thin films, limiting the available intensity. However, the density is large enough to produce easily detectable elastically scattered light when the pump laser is tuned to visible wavelengths.[23]

It is not surprising that unpassivated silicon nanocrystallites do not appear to emit the visible light that is readily observed in the passivated thin films composed of the same material. The surfaces of the particles are covered with dangling bonds, which create a multitude of states in the energy gaps of the crystallites, as described in section 1.10. These states will act as rapid nonradiative recombination centers for any photoexcited carriers present in the system. The capture time for these traps is expected to be on the order of microseconds at room temperature, and is likely faster at higher temperatures.[10] Therefore, it is probable that no carriers will have sufficient time to undergo radiative recombination. It is clear that the inability to see luminescence from the isolated silicon particles points to the necessary, enabling role of surface passivation in the kinetic activation of the radiative pathway manifested in the visible emission behavior of silicon nanocrystallites.

The lack of luminescence from unpassivated clusters brings about the question of the emission properties of passivated nanocrystallites in the gas phase. The pulsed laser ablation supersonic expansion system provides a number of ways to attempt *in situ* passivation of gas phase clusters, as described in section 2.1.1. However, attempts to seed the carrier gas line with oxygen in order to passivate the crystallites during the nucleation step in the interaction channel were not successful. These deposition runs quickly clogged the narrow interaction channel with material such that no deposition was possible. The presence of oxygen in the

interaction channel with the highly reactive silicon surfaces would likely result in the rapid formation of silicon oxide (SiO_x) structures that would clog the channel. It might be possible to achieve gas phase passivation of the clusters using a crossbeam experiment or by passing the clusters through a reaction chamber filled with oxygen.[24] In these two experiments, the crystalline core of the clusters would have already formed, leaving the oxygen to react with and passivate the particles' surfaces.

3.2.2.2 *Atmospheric Aging: Oxide Passivation*

In the same way that unpassivated gas phase clusters show no visible photoluminescence, unpassivated as deposited films initially show no luminescence signal either. Figure 3-8 compares the photoluminescence behavior of as deposited, vacuum aged, and air aged films deposited on Teflon substrates. The as deposited film shows no luminescence behavior, as can be expected with the poor surface passivation of these films. Films that were aged in vacuum will also show no luminescence behavior, since they also cannot oxidize the crystallite surfaces. Films aged in normal room air do eventually develop the typical orange emission as they are passivated by a growing oxide (SiO_x) layer.

The length of time required for this passivation to occur has varied greatly between samples. It is possible that this time depends strongly on the surfaces of the films and the humidity of the oxidizing atmosphere. In each case, the intensity of the luminescence reaches a stable value, from which it does not change for a time period of years. This indicates that the kinetics of the oxidation process have slowed down on the crystallite and the oxide layer hits a stable thickness, just as would be expected on bulk silicon surfaces.

3.2.2.3 *Chemical Treatments*

A series of chemical treatments was performed on the films to try to vary the passivating environments of the nanocrystallites and alter the luminescence behavior. Newly deposited films were treated with hydrofluoric acid (HF), nitric acid (HNO_3), and boiling water (H_2O). As shown in Figure 3-9, each of these treatments results in the development of visible luminescence that appears orange to the eye.

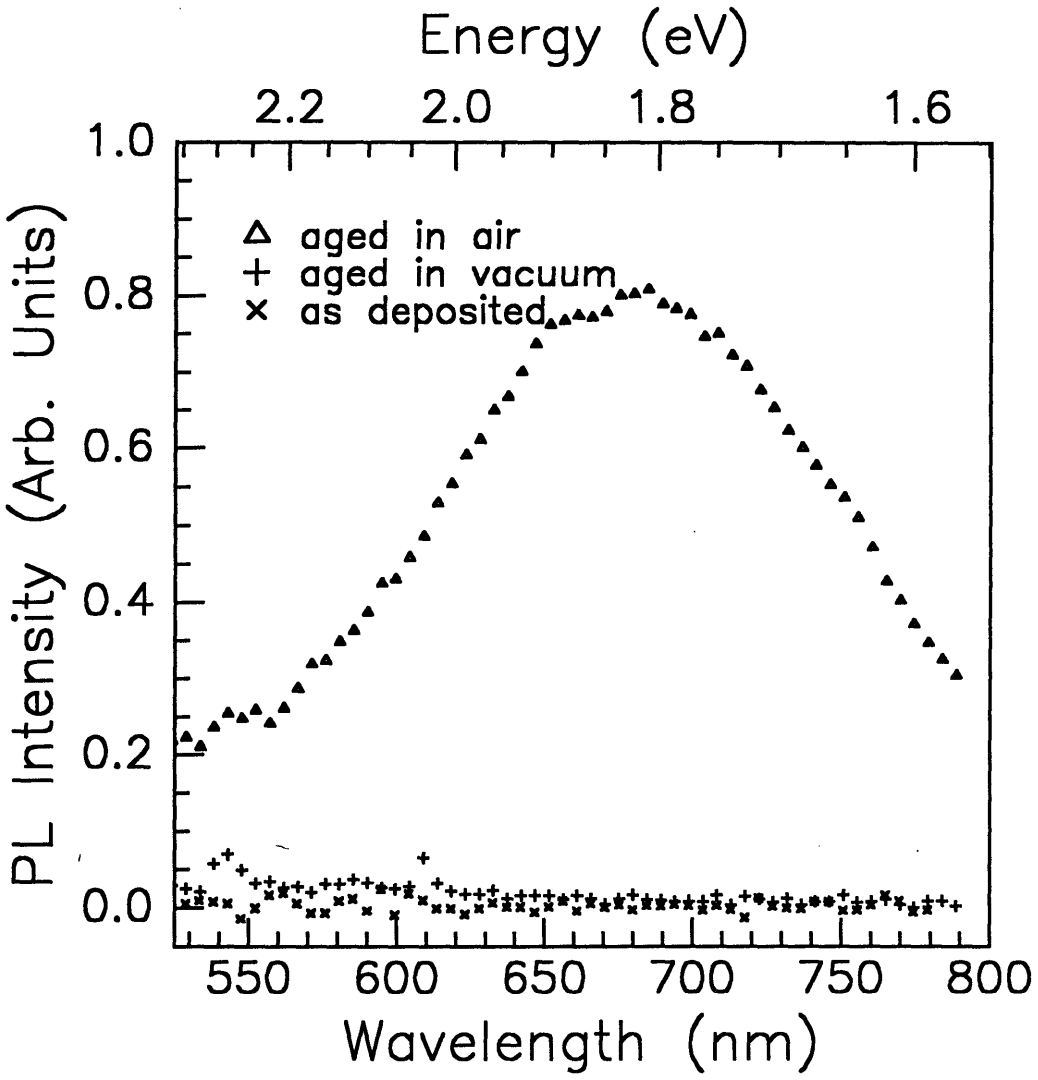

Figure 3-8 Comparison of PL spectra of atmospherically aged, vacuum aged, and as deposited films. Only the surface passivated, air-aged sample shows any emission intensity.

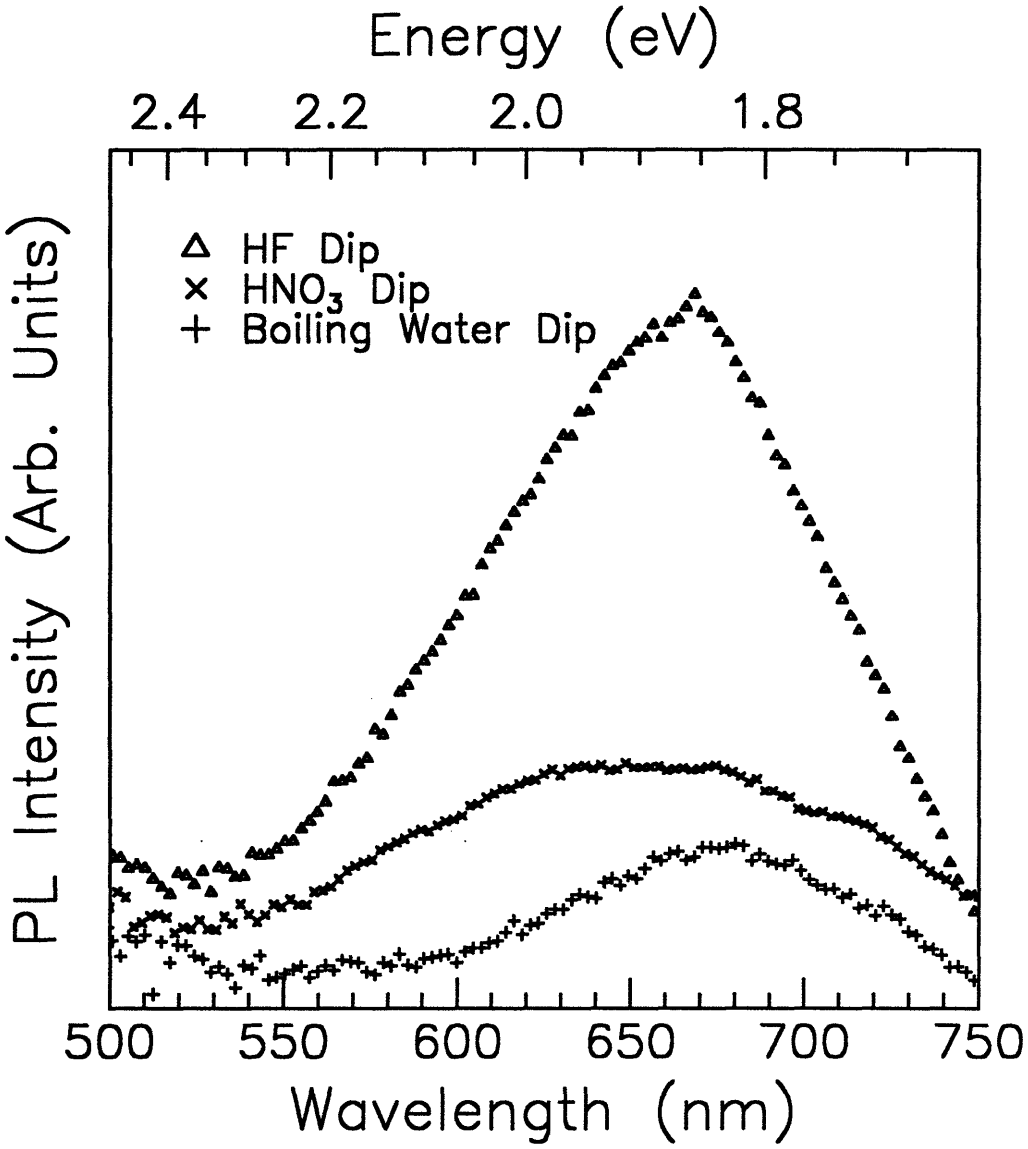

Figure 3-9 Comparison of samples treated in HF, HNO_3, and boiling water. All three show luminescence behavior indicating passivation of the nanocrystallite surfaces.

The appearance of luminescence in all of these samples reflects the ability of a number of chemical species to passivate the silicon surfaces. The samples are expected to have different passivating species as a result of the treatments as described in section 1.9, yet each appears to enable the luminescence. It has been shown that HF leaves a silicon surface hydride passivated,[25] while H_2O leaves the surface hydroxyl passivated,[26] and HNO_3 results in an oxygen passivated surface.[27] Each of these passivating environments appears to be sufficient to move dangling bond induced surface states out of the energy gap and enable radiative recombination.[28,29] The relative intensity differences of each would suggest that the hydride passivation is more efficient in eliminating surface defects than the hydroxide or oxygen passivation. This behavior has been seen in measurements of the electronic passivation of silicon surfaces by various passivating media.[25] However, differences in sample thickness and placement make comparisons of emission intensity between films difficult.

The relative emission energies of each of the peaks can be interpreted in a number of ways. It is possible that the peak shifts reflect the relative ability of each of the processing steps to oxidize or etch the silicon and shrink the crystalline core sizes. However, it is also very possible to interpret these results as implying that the luminescence is a function of the development of different types of surface states in the samples. Each of these states would result in radiative transitions of different energies, and a different peak wavelength.[30] It is also possible to conclude that the processing has resulted in the deposition of polysilanes or siloxene on the surfaces of the samples and is responsible for the luminescence behavior. Due to the complex nature of these molecules and their emission, it can be argued that the broad spectra and slightly different peak wavelengths are not unexpected. It is difficult to argue that oxide defects are responsible for this behavior, as the HF dipped sample would have the smallest amount of oxide present on it, yet still shows the greatest intensity.

The films show their greatest intensity when they are illuminated by a handheld ultraviolet lamp while still in the HF solution. Here it is very unlikely that there are a high concentration of nonstoichiometric oxides present to give luminescence as described by NBOHC theory. Attempts to collect spectra from samples during etching were unsuccessful. It is interesting to note that when a sample was immersed in a polystyrene container filled with HF and illuminated with an ultraviolet laser, the emission spectrum changed visibly with time

and quickly disappeared. This is indicative of photoexcitation creating holes in the nanostructures which enhance the etching rate of the silicon.

These results do not strongly support any one emission mechanism, however they also do not contradict arguments based on quantum size effects. In fact, they do clearly show that a number of different passivating species can be used to enable the luminescence behavior in the material. They also point out that many of the lessons learned from the processing of bulk silicon materials can be directly brought over to these nanocrystalline systems -- an inherent advantage of working in silicon.

3.2.2.4 *Effect of Dip Time on Luminescence Intensity*

Figure 3-10, shows the photoluminescence spectra from as series of silicon nanocrystallite films deposited on Teflon substrates aged in air and then dipped in hydrofluoric acid for different lengths of time. The luminescence intensity of the films increases as the length of the dip time increases, indicating the role that surface passivation plays in improving the emission intensity of the films.

As described earlier, the HF serves to strip away the native oxide layer on the particles and etch the silicon as well, resulting in a hydride passivation of the surface. This hydride passivation provides a more complete surface coverage than the defect filled native oxide that grows on the particles. Therefore, increasing the dip time should allow for enhanced surface coverage and promote the tying up of dangling bonds. The removal of these dangling bonds will increase the probability for radiative recombination and therefore emission efficiency.

The spectra also show a slight blueshift in peak wavelength with increasing dip time. The shift in wavelength from the aged to dipped samples is explained as shrinkage in crystallite size. After removing the oxide, it is likely that the HF continues to etch the crystalline silicon core and reduces crystallite size further as the dip time increases. This correlation between size and emission wavelength is once again supportive of models of emission based on quantum size effects. In bulk systems, the etch rate of HF on silicon has been measured as 0.03 nm per minute.[31] By calculating the size distributions of emitting particles from the photoluminescence spectra as in section 3.2.1.1 and correlating them to size shifts, the etch rate for the silicon nanocrystallite thin films can be roughly estimated. In these

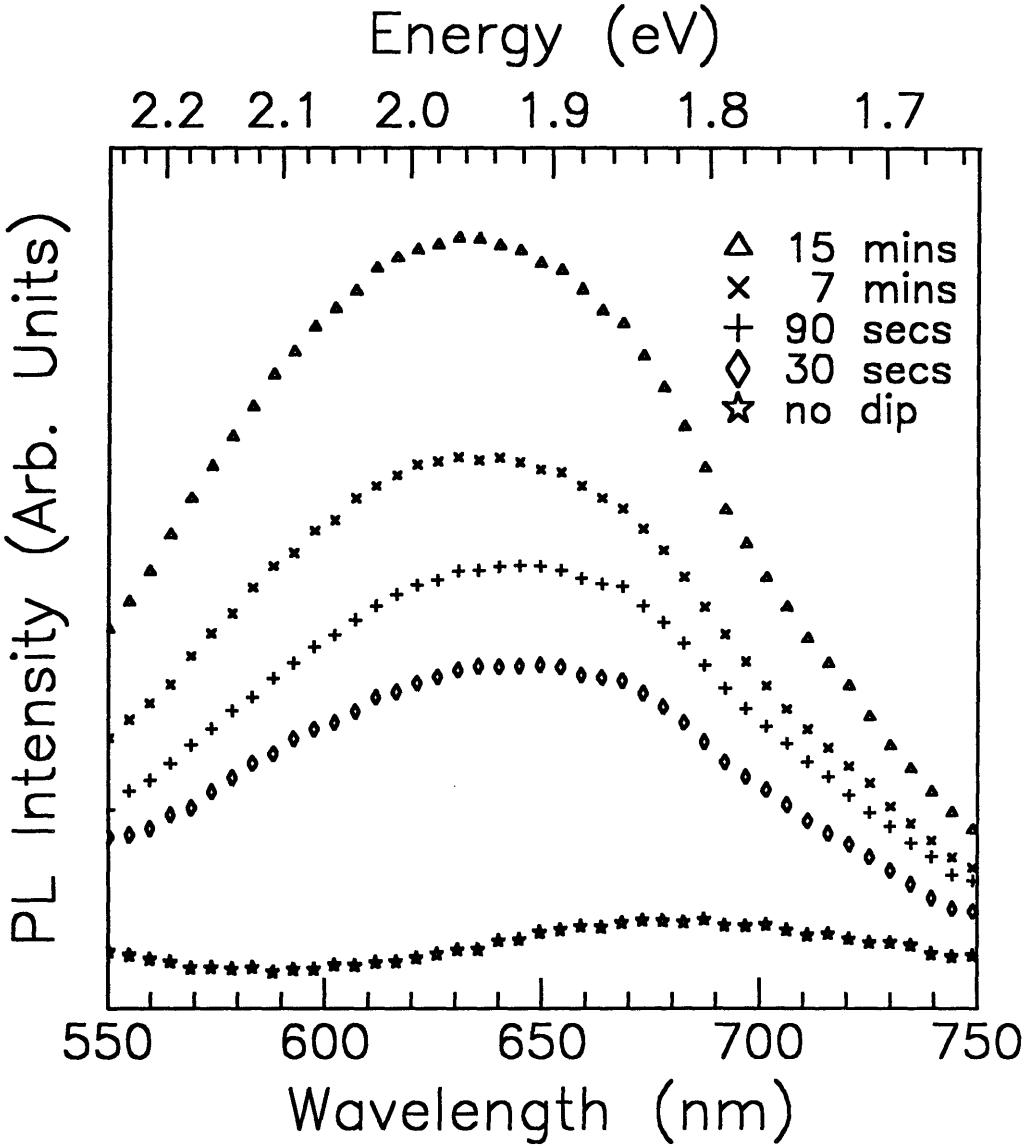

Figure 3-10 Effect of increasing HF dip time on PL spectra of silicon nanocrystallite thin films. With increasing dip time and enhanced surface passivation, emission efficiency improves.

small systems, the rate is slightly slower, ranging from ~0.01 to ~0.001 nm per minute, and slows down as the peak wavelength sits at higher energies, and therefore smaller particle sizes.

It is also possible to explain the blueshift as being due to increasing hydrogen content on the silicon surface, as is expected in amorphous silicon. However, the surface state models expect emission from oxygen passivated samples to be at higher energies than hydrogen passivated samples, and so cannot explain the observed behavior.[32] Although this experiment does not strongly support a single emission mechanism, it still does not contradict the quantum confinement emission model. The experiment does provide further evidence that surface passivation of dangling surface bonds is very important for removing trap states and enabling efficient visible light emission behavior.

3.2.2.5 *Methanol Quenching of Luminescence*

Samples were also dipped in methanol to further study the role of chemical treatments in nanocrystallite luminescence. Two sets of samples were used, hydrogen passivated crystallites and oxygen passivated crystallites. As shown in Figure 3-11, the intensity of the photoluminescence emission from the hydride passivated sample was reduced after the methanol dip. However, when the oxide passivated sample was treated with methanol, there was no quenching of the luminescence behavior, as shown in Figure 3-12. In both cases, x-ray photoelectron spectroscopy (XPS) of the samples has indicated no shift in the oxidation state of the surface silicon, indicating that the surfaces are chemically resistant to methanol attack. This will be discussed in detail in section 3.4.2.2.

The methanol quenching of the hydride passivated nanocrystallite luminescence is likely due to a kinetic favoring of nonradiative relaxation pathways.[33,34] This effect has also been postulated for dyes and other organic species in contact with a silicon surface.[35] It is believed that large polar molecules on the silicon surface create electric fields within the crystallites that alter their band structure.[36] Charge may be stabilized in near surface regions where nonradiative processes dominate.[37] Some groups have reported that the alteration of these pathways has resulted in an ability to shift the luminescence wavelength of porous silicon through surface treatments.[38]

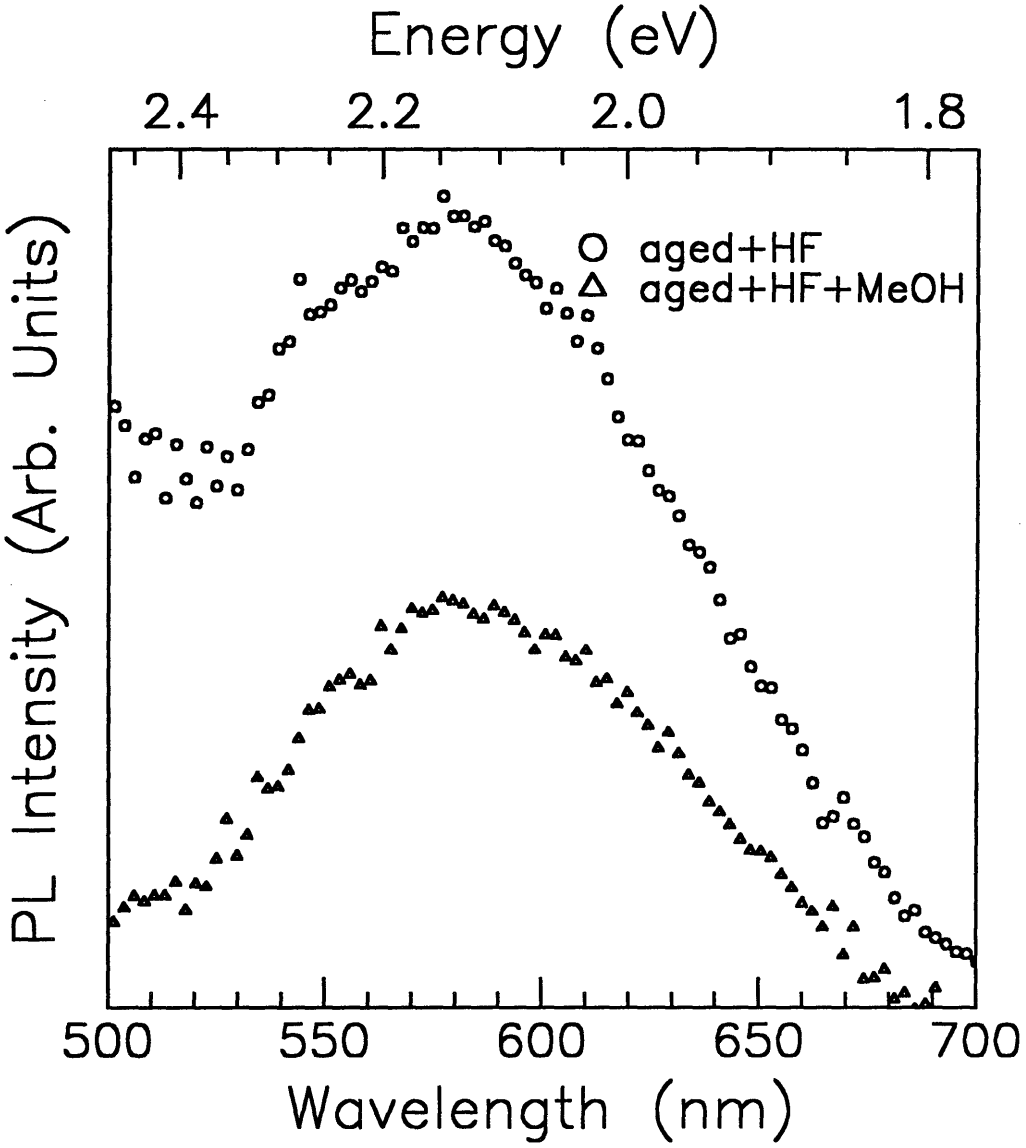

Figure 3-11 PL spectra of HF dipped film before and after methanol treatment. Methanol significantly reduces the luminescence intensity of the H-passivated sample.

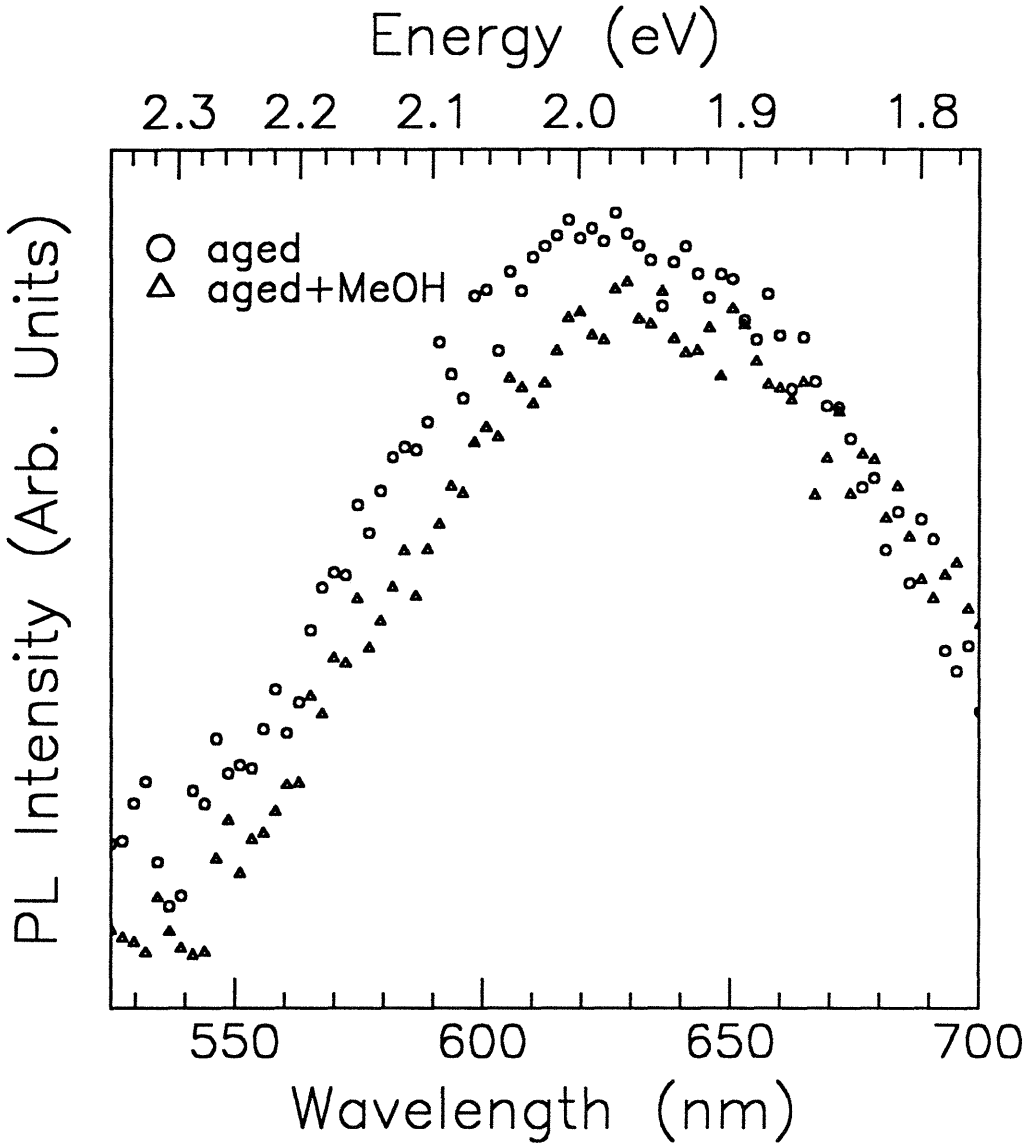

Figure 3-12 PL spectra of an aged (oxide passivated) sample before and after a methanol dip.

The insensitivity of the oxide passivated nanocrystallites to methanol quenching is a result of the insulation provided by the oxide layer itself. Here, the methanol induced electric fields are too weak to strongly affect the band structure of the silicon nanocrystallites, and electron injection across the wide band gap of the oxide layer is largely improbable.

The methanol quenching of the luminescence behavior points out a number of important factors in nanocrystalline silicon luminescence and its applications. First, once again these results do not contradict emission mechanisms based on quantum size effects, since there has been no clear shifts in emission energy due to the surface changes. However, they do point out the importance of controlling the surfaces of the particles in enabling the radiative emission pathways defined by the quantum confined band structure. Quenching of the luminescence by the presence of adsorbed species creates the possibility that the system could find use as sensor materials for large polar molecules, which would alter the carrier concentration, and therefore the electrical and optical properties.

3.2.2.6 *Halogen Passivation*

There has been recent interest in terminating silicon surfaces using halogens because of safety and environmental concerns and theoretically predicted passivation improvements. Halogen passivation has been demonstrated on bulk silicon surfaces.[39] In this vein, samples were treated with iodine in order to try to passivate the nanocrystallite surface and enable visible luminescence. Figure 3-13 shows the luminescence behavior of an oxide passivated nanocrystallite film treated with an iodine:methanol solution. Here, there is little or no change in the luminescence behavior seen. XPS studies of the surface indicate that the oxide layer has protected the surface from iodine attack, as will be described in section 3.4.2.3. Iodine was also used to treat a hydride passivated silicon nanocrystallite film. Here, XPS showed an increase in the oxidation state of the surface silicon, consistent with a change in bonding from Si-H to Si-I. These results will also be described in section 3.4.2.3. The photoluminescence emission from these particles did not completely quench with the surface chemistry change, as seen in Figure 3-14.

The ability to change the passivating species on the nanocrystallite surfaces from oxygen to hydrogen to iodine without affecting the luminescence energy, is strong evidence

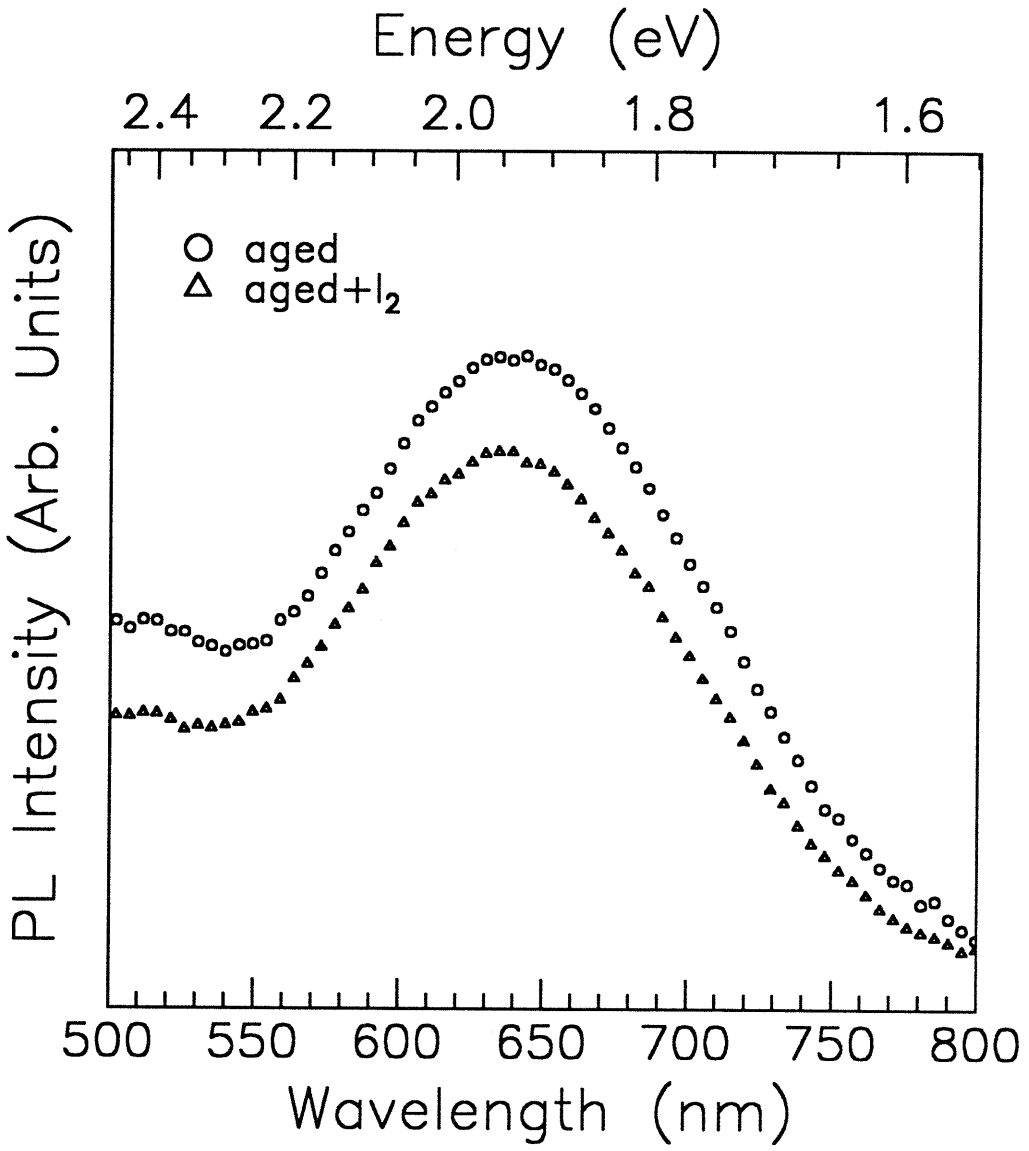

Figure 3-13 Comparison of the PL spectra of an aged (oxide passivated) film before and after I_2 treatment.

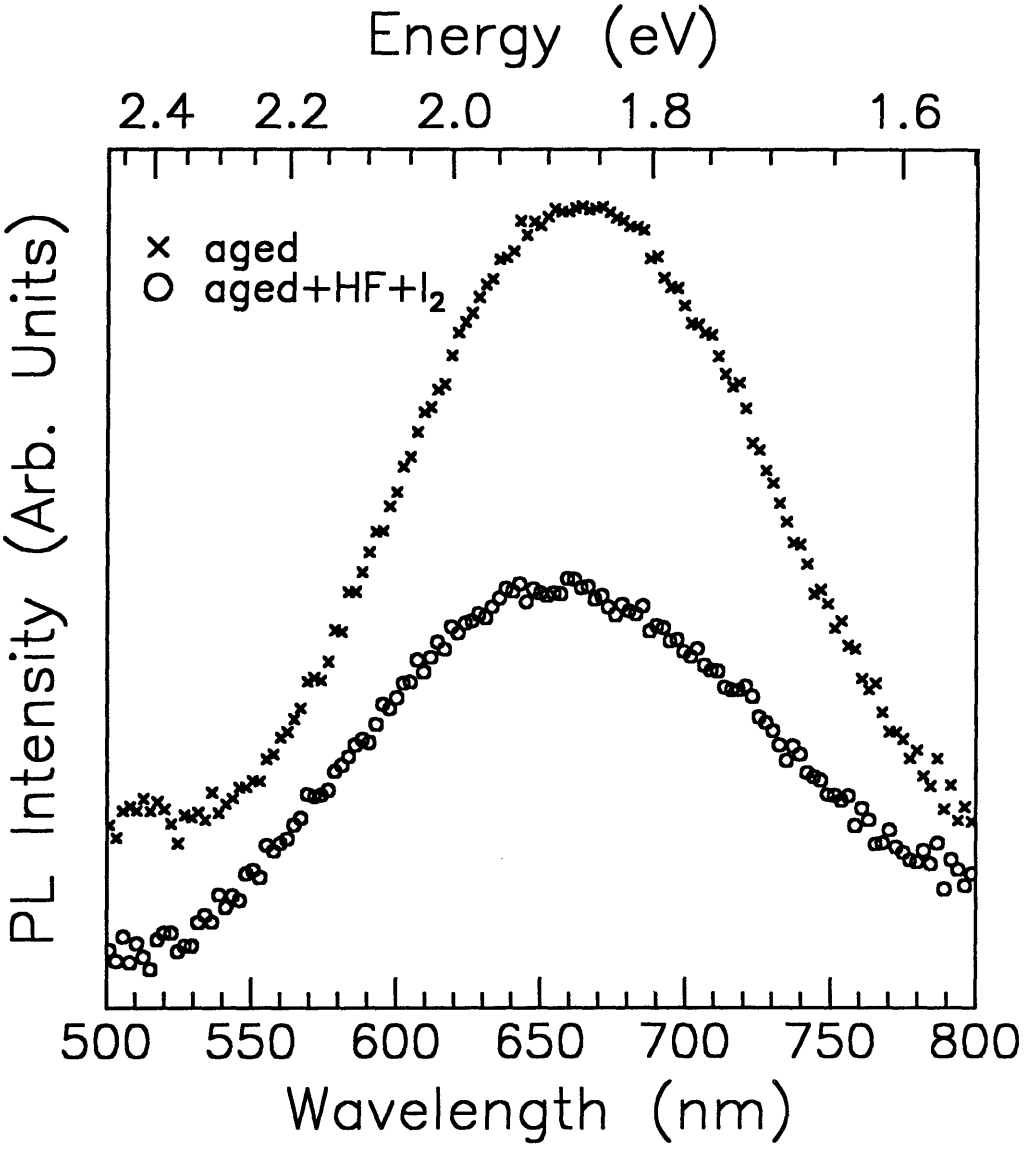

Figure 3-14 PL spectra of an aged (oxide passivated) sample and an HF dipped (H-passivated) sample treated with I_2.

for the simple quantum confinement emission model. Changes in surface chemistry should have created different intrinsic surface states in the material, and altered any transitions that were coupled to those states. These results indicate that the chemical nature of the passivating species does not affect the emission energy of the samples. Although there is some quenching of the luminescence in the iodine passivated sample, this can be attributed to the effect of methanol. Once again, the oxide layer on the surface of atmospherically aged films protects the silicon from the iodine and methanol, so no effect was observed on the emission behavior.

3.2.2.7 *Summary*

This set of experiments investigated the role that surface passivation and surface species played in determining the luminescence behavior of the silicon nanocrystallites. It has been shown that surface passivation of the nanocrystallites is a necessary condition to achieve any luminescence at all. The passivation is believed to serve in removing midgap nonradiative traps that result from dangling surface bonds. The species passivating the silicon surfaces was changed between hydrogen, oxygen, iodine, and hydroxide. In each case, the emission energy could still be explained using simple quantum confinement arguments. The chemical nature of the passivating species appears to be irrelevant to the actual emission process. However, it was also demonstrated that adsorbed species on the surface of the molecules can act to quench the luminescence emission by activating nonradiative recombination mechanisms. In every case, all the results can be explained using the requirements of surface passivation to enable emission as defined by the size of the nanocrystallites. This supports models of emission based on quantum confinement.

3.3 Temperature Dependence of Photoluminescence Emission

The temperature dependence of the photoluminescence behavior of the thin silicon nanocrystallite films can reveal a great deal about the recombination mechanisms in the nanostructures. Aged samples on Teflon substrates were examined for luminescence emission at a range of temperatures. The behavior of the emission energy and intensity provides strong

evidence for the role of quantum size effects in determining the luminescence behavior from the films.

3.3.1 Temperature Dependence in Light Emitting Silicon

A great deal of work has been done in characterizing the luminescence behavior of porous silicon as a function of temperature. The literature is filled with many contradictory results, and no clear description of the temperature dependence of the photoluminescence from the material has emerged. Both increasing[40] and decreasing[41] emission intensities have been reported over a temperature range from 300 K to 0 K. Other groups report behavior that is neither monotonically increasing nor decreasing,[42,43] or show temperature dependences that vary by wavelength.[44] Groups have also reported both blueshifts[45] and redshifts[46] with decreasing temperature. As a result, no clear consensus has emerged as to the temperature dependence of the material.

Figure 3-15 shows the emission energy temperature dependence of bulk silicon.[47] Emission which originates from band to band recombination would be expected to follow this type of dependence. Exciton emission will also be very similar, since exciton binding energies are very small and will only show a weak temperature dependence. Porous silicon emission models based on intrinsic surface defects will also show similar dependence on emission energy, since the states tend to track the levels of the band edges, however redshifts in emission with decreasing temperature have also been ascribed to surface state recombination.[48] Luminescence attributed to oxide defects such as nonbridging oxygen hole centers is likely to show little to no change in emission energy with temperature, as are emissions from polysilane or siloxene adsorbed on the silicon surfaces. In amorphous material, the emission energy has been seen to increase in energy at lower temperatures due to localization of carriers at the deepest parts of the band tails. In these systems, the recombination between carriers at the tops of the band tails produce the highest energy emission but are also thermalized at the lowest temperature, so that at higher temperatures only the more localized, lower energy carriers are involved in emission.

The emission intensity in the nanocrystallites is also expected to be a function of temperature. In bulk semiconductor systems, the band to band emission intensity tends to

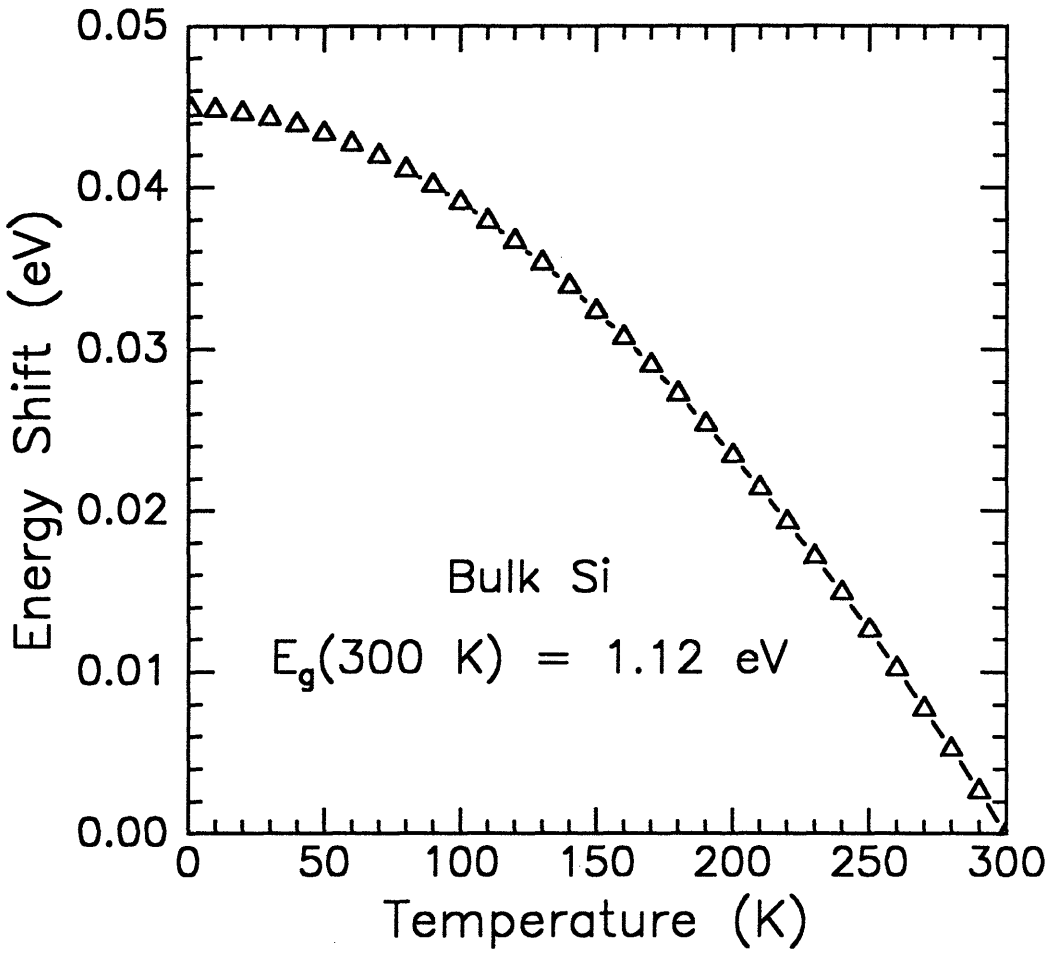

Figure 3-15 Energy gap of bulk silicon as a function of temperature (From Ref. 50).

increase with decreasing temperature due to the reduction of nonradiative pathways, such as phonon emission events. In silicon, bound excitonic emission increases in intensity as temperature is raised from 0 K to ~30 K, as carriers are released from shallow sites and trapped at deep centers. Above this temperature, thermalization of the exciton reduces the luminescence intensity.[49] For emission from defect levels in the gap of the material, reducing the temperature would result in a decrease in emission intensity, as carriers would have less ability to tunnel and nonradiatively decay into the surface state transition levels. This reduction of intensity is therefore also expected in extrinsic or oxide defect based models. In polysilane or siloxene based systems, a general increase in intensity with decreasing temperature has been observed,[50] as is the case for hydrogenated amorphous silicon materials.[51] In both of these cases, a saturation of the intensity enhancement is often observed for temperatures below ~60 K.

3.3.2 Temperature Dependence in Silicon Nanocrystallites

In order to get further insight into the emission mechanism in the silicon nanocrystallite thin films, the temperature dependence of the photoluminescence behavior was studied. As shown in Figure 3-16, the peak wavelength of the luminescence signal is a strong function of sample temperature. With decreasing temperature, the luminescence blueshifts or goes to higher energies. The temperature-emission energy relationship has two distinct regimes of behavior. It appears to be linear with temperature at high temperatures and nonlinear at lower temperatures. This is the same type of behavior that has been commonly observed in many bulk semiconductor systems, including Si.[52,53] The energy gap expansion in nanocrystalline samples over the temperature range 300 K - 4 K is 2-4 times larger in than the change seen in bulk Si (~50 meV).[54] This difference is to be expected when one considers the properties of nanocrystalline materials relative to bulk systems.

In semiconductors, the gap change with temperature has been described with the expression,

$$\left(\frac{\partial E_g}{\partial T}\right) = \left(\frac{\partial E}{\partial T}\right)_{ph.} + \left(\frac{\partial E}{\partial T}\right)_{id.}$$

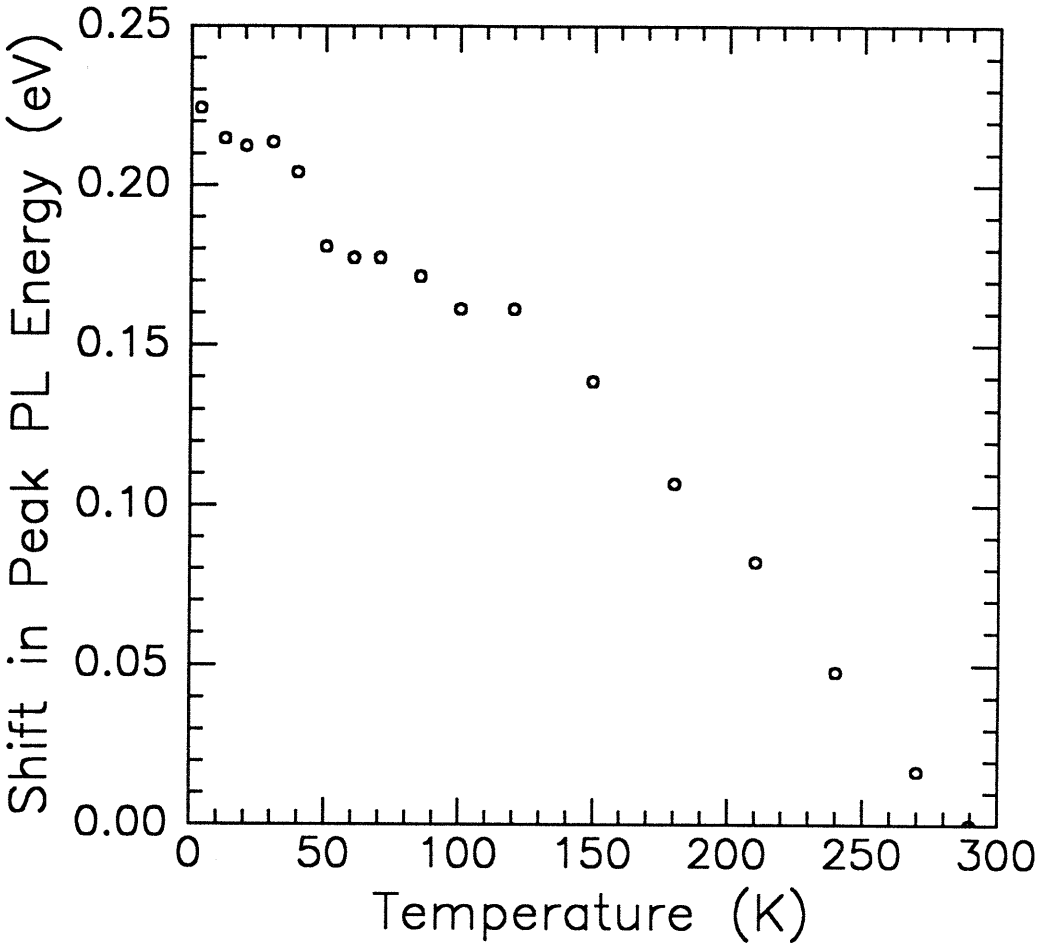

Figure 3-16 Shift in peak PL energy of thin film of silicon nanocrystallites as temperature is reduced from 300 K.

where the first term represents shifts due to electron-phonon interactions and the second term represents the effects of lattice dilation.[55] The lattice dilation effect on the energy gap can be given as,

$$\left(\frac{\partial E}{\partial T}\right)_{ld.} = \left(\frac{\partial E}{\partial P}\right)_{V}\left(\frac{\partial \Delta}{\partial T}\right)\left(\frac{\partial P}{\partial \Delta}\right)$$

where Δ is the volume dilation. The three terms represents the pressure coefficient of the gap, the thermal expansion coefficient of the material, and the bulk modulus of the material, respectively. Typical literature values for bulk and nanocrystalline silicon for each of these terms are listed below.

	Bulk Silicon	Nanocrystalline Silicon
Pressure Coefficient[56]	-15 meV/GPa	-18 meV/GPa
Thermal Expansion Coefficient[57]	7.5×10^{-6} K^{-1}	?
Bulk Modulus[58]	100 GPa	86 GPa

Since the thermal expansion coefficient of amorphous silicon is within 1% of the bulk silicon coefficient,[59] the nanocrystalline silicon value can be approximated as being equal to the bulk value. Using these values gives an overall contribution of lattice dilation to the temperature dependent energy shift of 0.01 meV/K for the bulk and 0.02 meV/K for nanocrystallites. Given an overall shift of 16 meV/K for bulk silicon and 75 meV/K for nanocrystallites, then the lattice dilation plays a very small role in the energy gap shift in the materials. In bulk silicon, it is ~6% of the shift, while in the nanocrystallites it is ~2.5%. In bulk GaAs, it has been estimated to be ~13% of the total energy gap shift.[60]

This result implies that the majority of the temperature dependent energy gap shift is due to electron-phonon coupling. The coupling strength of electrons to phonons varies inversely with crystallite volume, and so will be larger in nanocrystallites than in bulk systems.[19,61] It has also been shown to increase with structural disorder in amorphous semiconductors.[62] This explains the enhanced shifting of energy gap of nanocrystallites over bulk material over the same temperature range.

The emission energy temperature dependence has strong similarity to that of bulk silicon, and semiconductor materials in general. This correlation provides more evidence that the active light emitter in these materials is a recombination of carriers in the nanostructured silicon cores. It is also possible that this result could also reflect an emission from surface states that are controlled by the size dependent positions of the band edges. Amorphous silicon materials have been shown to produce a much larger change in luminescence energy with decreasing temperatures than bulk silicon.[63] This is due to the fact that emission is controlled by carriers in the Urbach tails that lie within the band gap, rather than the band edges themselves. As described in section 1.4.3, these states have different temperature dependences according to their degree of localization.

The full width at half maximum (FWHM) of the luminescence spectra from the samples is also temperature dependent. At 300 K, the luminescence FWHM was ~490 meV. This broad emission represents the distribution of nanocrystallite sizes found within a thin film. As the films are cooled the FWHM broadens, as seen in Figure 3-17. This broadening is manifested in a pronounced shift to higher emission energies by the blue edge of the emission band and a smaller shift to higher energies of the red edge, as shown in Figure 3-18. This reflects the enhanced energy gap expansion at lower temperatures that is seen as particle size decreases. A similar effect has been observed in porous silicon.[45]

As shown in Figure 3-19, the peak emission intensity is a weak function of temperature. There is a gradual increase in the quantum efficiency of the thin films of silicon nanocrystallites with decreasing temperature. This behavior has been observed in both bulk semiconductors[64] and porous silicon.[65] As the temperature of the nanostructure is reduced, lattice vibrations are diminished. These vibrations normally act as nonradiative recombination pathways via phonon emission events. At low temperatures these vibrations are suppressed and radiative transitions are favored, resulting in increased luminescence intensity. This process appears to be relatively independent of crystallite size, as all emission wavelengths increase in intensity with reducing temperature. The very weak temperature dependence is evidence of the enhanced exciton binding energy predicted in quantum confined systems.[7] This binding energy has been predicted to be ~200 meV in ~2 nm silicon particles, well above room temperature thermal energy, therefore excitons which in the bulk would rapidly

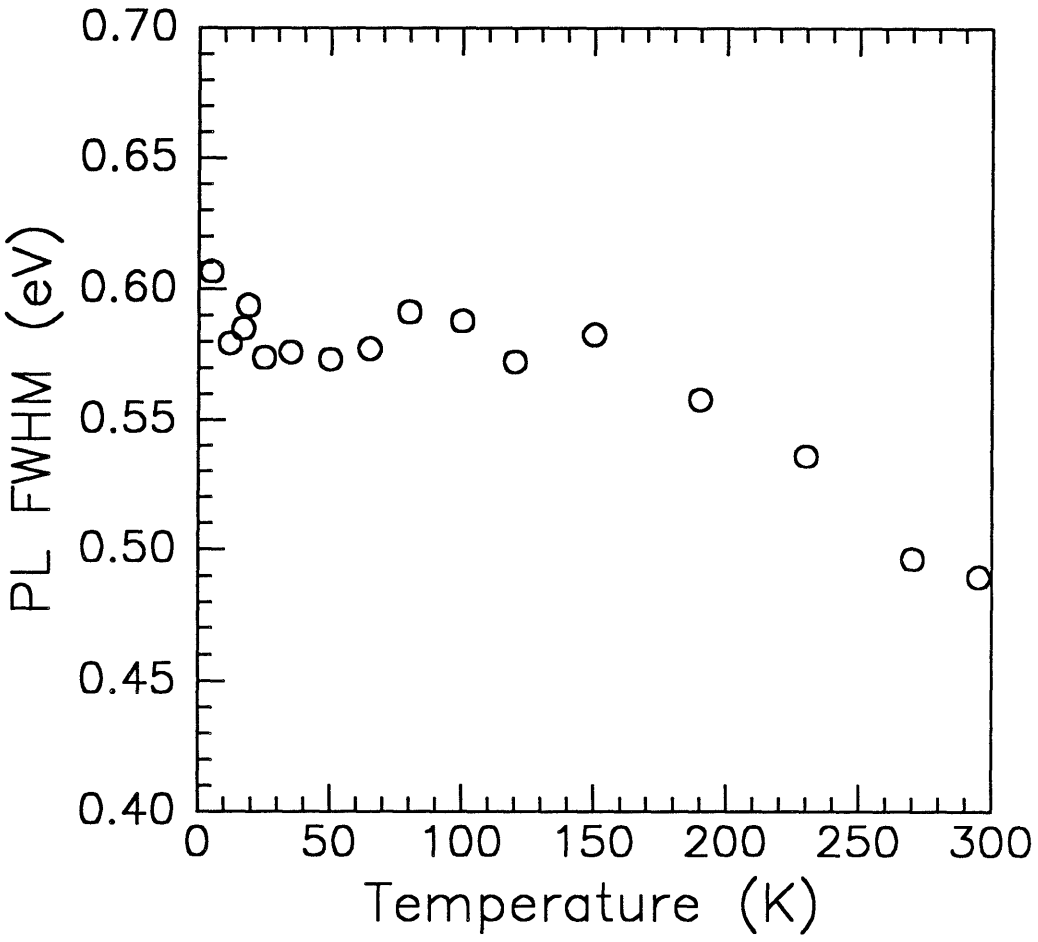

Figure 3-17 Full width at half maximum (FWHM) of the PL spectrum of a thin film of silicon nanocrystallites as a function of temperature.

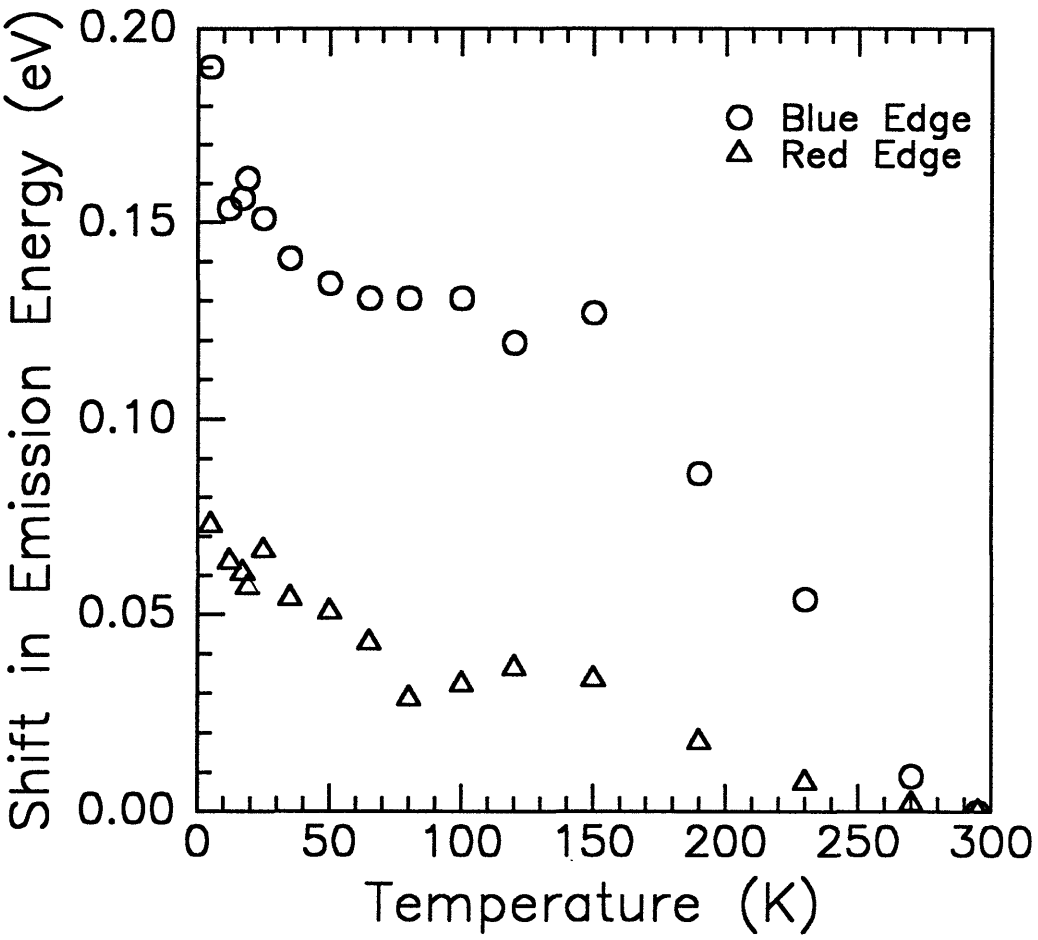

Figure 3-18 Relative shift in blue and red edge of PL emission spectrum of a thin film of silicon nanocrystallites as temperature is reduced from 300 K. The blue edge shows a larger shift to higher energies as temperature is reduced.

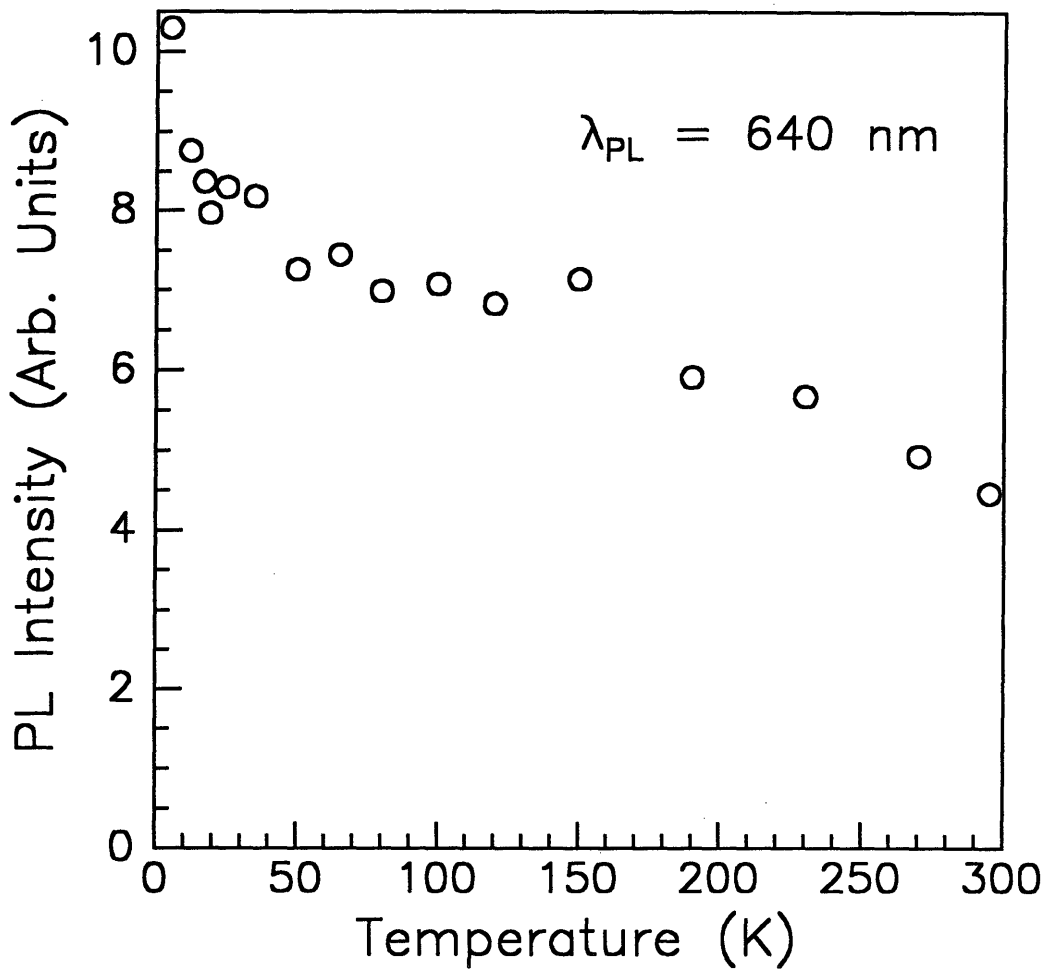

Figure 3-19 Temperature dependence of the intensity of PL emission at 640 nm for a thin film of silicon nanocrystallites.

thermalize could exist to much higher temperatures in nanocrystalline systems. This weak temperature dependence has been observed in other quantum confined semiconductors, including CdSe nanocrystals,[66] and $Si_{1-x}Ge_x$ quantum wells.[67]

The correlation between emission intensity and temperature is another similarity between the behavior of nanocrystalline silicon and bulk semiconductors. Emission mechanisms based on intrinsic or extrinsic defects would tend to have decreasing emission intensities as temperature decreased, as there would be a smaller probability of carriers tunneling to the defect levels.[44] An increase of emission intensity with decreasing temperature is also characteristic of siloxene and hydrogenated amorphous silicon, however these materials show a strong saturation of emission efficiency below ~60 K,[50] which was not observed in the nanocrystalline silicon films.

3.4 Surface Characterization of Silicon Nanocrystallites

Correlations between surface species and luminescence properties required some characterization of the silicon surfaces after processing steps. In many cases, the processing steps are understood well enough that the presence of a specific passivation could be assumed. In other instances, infrared absorption spectroscopy and x-ray photoelectron spectroscopy (XPS) were used to characterize the surfaces. These results confirmed the presence of the anticipated surface species on the silicon nanocrystallites, and confirmed that the chemical nature of the passivating species does not directly control the emission behavior.

3.4.1 Passivating Species by Infrared Spectroscopy

Fourier transform infrared spectroscopy was used to determine the passivating species on the samples after different sample preparation techniques. As shown in Figure 3-20, aged samples had a strong absorption at ~1100 cm^{-1} reflecting the presence of a Si-O-Si asymmetric stretch mode, while after a dip in hydrofluoric acid, this peak was reduced in intensity. Figure 3-21 compares the absorption spectrum for an HF dipped sample to an aged sample, showing the development of a $Si-H_2$ scissor mode at ~900 cm^{-1}. These spectra indicate that aged samples are strongly oxide passivated, but that the HF treatment removes this oxide and

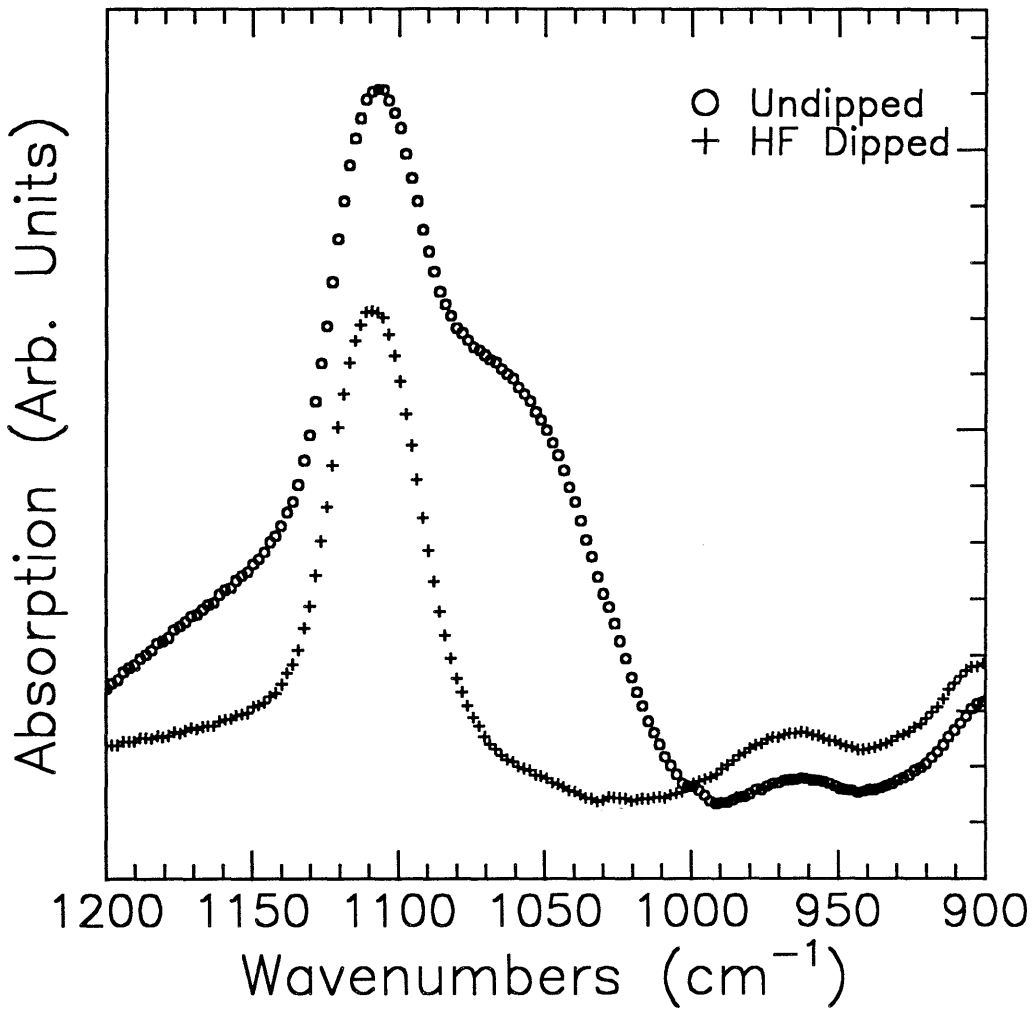

Figure 3-20 FTIR spectra of a silicon nanocrystallite thin film showing the reduction in the ~1100 cm^{-1} oxide stretch mode after a dip in hydrofluoric acid.

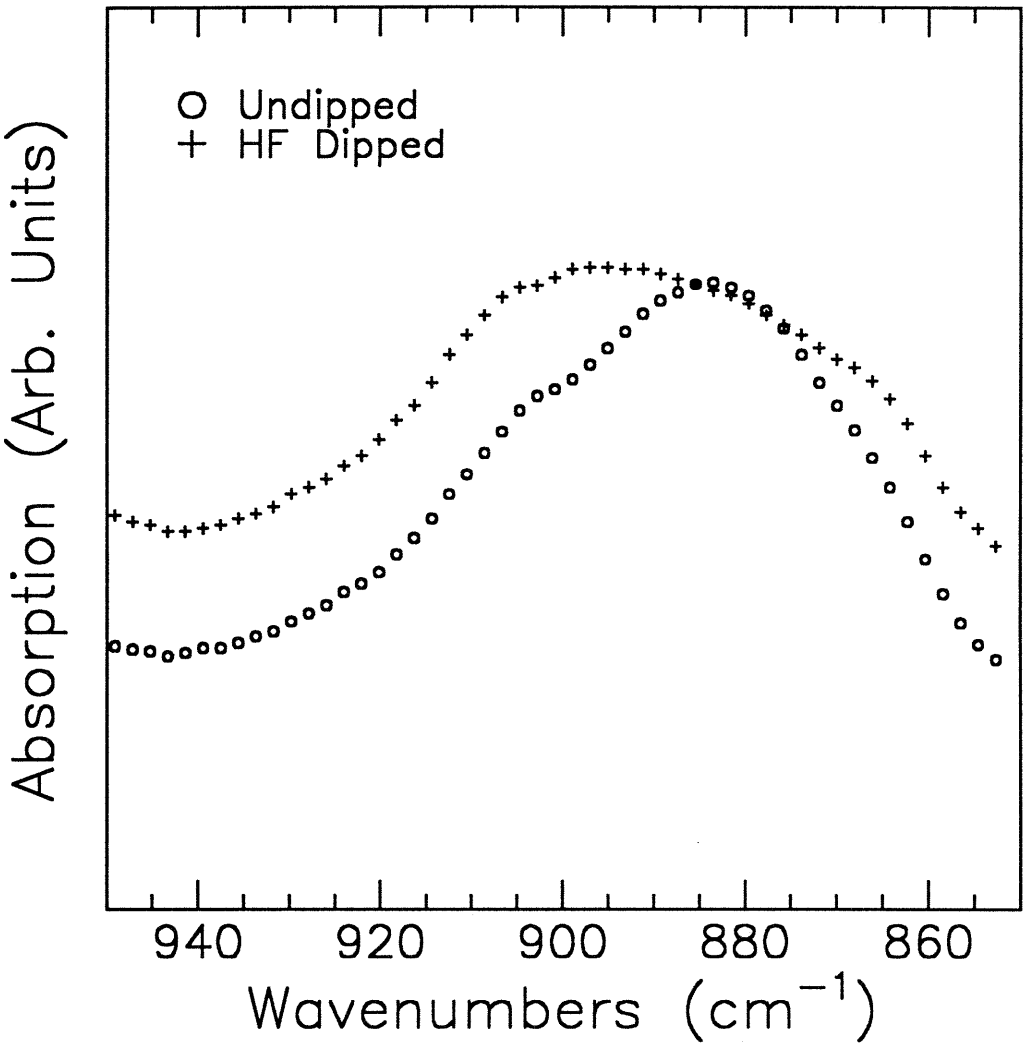

Figure 3-21 Comparison of the FTIR spectra of HF dipped and undipped silicon nanocrystallite thin films. There is an increase in the Si-H_2 scissor mode at ~900 cm^{-1} after the HF treatment.

leaves the surface hydride passivated. This is completely expected from the fundamentals of bulk silicon processing.[68]

Correlating the presence of surface oxides and hydrides to the emission energy revealed that the energy of emission always tracked the expected crystalline core size reductions due to processing, as discussed earlier. The luminescence never seems to be defined by the presence of the hydride or oxide, rather only is enabled by the presence of either of them. This indicates the importance of surface passivation in eliminating nonradiative recombination pathways, and the unimportance of the chemical nature of the surface species.

3.4.2 Surface Species by X-ray Photoelectron Spectroscopy

X-ray photoelectron spectroscopy was also used to characterize the surface environment of the silicon nanocrystallites. By monitoring shifts in the Si 2p binding energy, it is possible to determine if the surface silicon atoms are being oxidized or whether they retain bulk like character. Previous XPS research has determined that hydrogen passivated silicon will retain the bulk Si 2p binding energy at ~99.1 eV, while silicon dioxide shifts this peak to ~103 eV.[69] XPS was also used to indicate the presence of iodine during the halogen passivation experiments, and the chemical changes in the silicon surface under the presence of methanol. As described in section 2.6, charging of the Teflon substrate made measurements of exact binding energies very difficult, so only approximate values can be reported.

3.4.2.1 *Hydride and Oxide Passivation of Silicon*

Figure 3-22 depicts the evolution of the Si 2p binding energy peak for a film of silicon nanocrystallites on Teflon as a function of processing steps. The aged, oxygen passivated film shows a peak at ~99 eV, as well as a stronger peak at ~103 eV. Samples which are aged and then etched in hydrofluoric acid show a reduction of the intensity of this second peak. The intensities of each of these peaks is difficult to compare between samples in this type of characterization, but the ratio of the primary and secondary peaks are important in determining the dominant form of surface passivation on the crystallites.

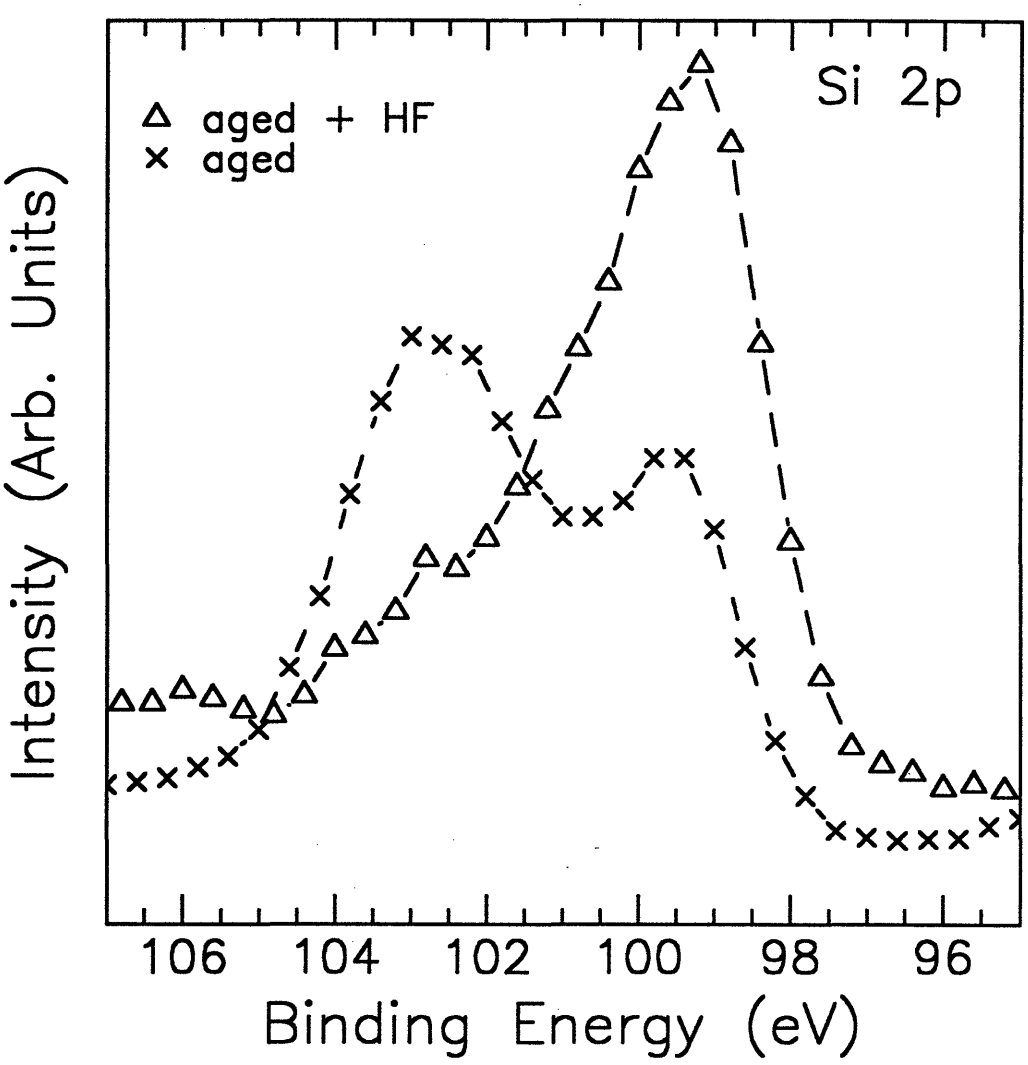

Figure 3-22 Comparison of Si 2p XPS spectra for HF treated and aged silicon nanocrystallite thin films. Aged film shows development of Si^{4+} behavior at ~103 eV.

The binding energy of an electron in an atom will depend strongly on the chemical environment of the atom. The core electrons in a system have their energy determined by a number of factors, including Coulombic interactions with valence electrons. As the chemical environment of an atom changes, the valence electron charges will be redistributed resulting in an alteration of this Coulombic interaction. This affects the binding energies of the core electrons that are measured by XPS. In silicon systems, the 2p peak will sit at 99 eV for elemental silicon. This is where the peak would be expected to lie for an unpassivated silicon surface. Changing the oxidation state of silicon from 0^+, as it is in elemental or bulk silicon, to 4^+, as it is in SiO_2, shifts the 2p binding energy from 99 eV to 103 eV. Here the large electronegativity of the oxygen atoms strongly displaces the Si valence electrons and increases the core electron's binding energy. This effect is shown for bulk silicon in Figure 3-23. Between these two peaks are the intermediate oxidation states of Si, which have been correlated to the presence of Si-H, $Si-H_2$,[70] nonstoichiometric oxides (SiO_x),[71] and dangling bonds[72] on the silicon surface.

The aged sample shows a significant degree of Si in the 4^+ state, as well as the presence of intermediate oxidation states. This is evidence for the significant oxidation of the surface by atmospheric aging, and indicates the presence of both SiO_2 and nonstoichiometric oxides. The sample which was aged and then etched in hydrofluoric acid shows a significant reduction in the intensity of higher oxidation state signal relative to the elemental peak. This indicates that the surface oxide has been largely removed, resulting in passivation by hydride species by the acid. In all these peaks, it is important to note that the intensities are difficult to compare between films because of problems of surface roughness and sample positioning.

The XPS data shows that the processing the nanocrystallite films can change the surface species that is passivating the nanostructure's surfaces. Aging the sample leads to an oxidized surface, while hydrofluoric acid leads to a hydride passivated surface. It is not clear that the passivating species is completely homogenous across the film. The aged films show both stoichiometric and nonstoichiometric oxides, while the hydride passivated films show evidence of Si-H, $Si-H_2$, and $Si-H_3$. The etched sample's XPS signal may also be due to the presence of residual oxide on the silicon surfaces or from the matrix material. In general,

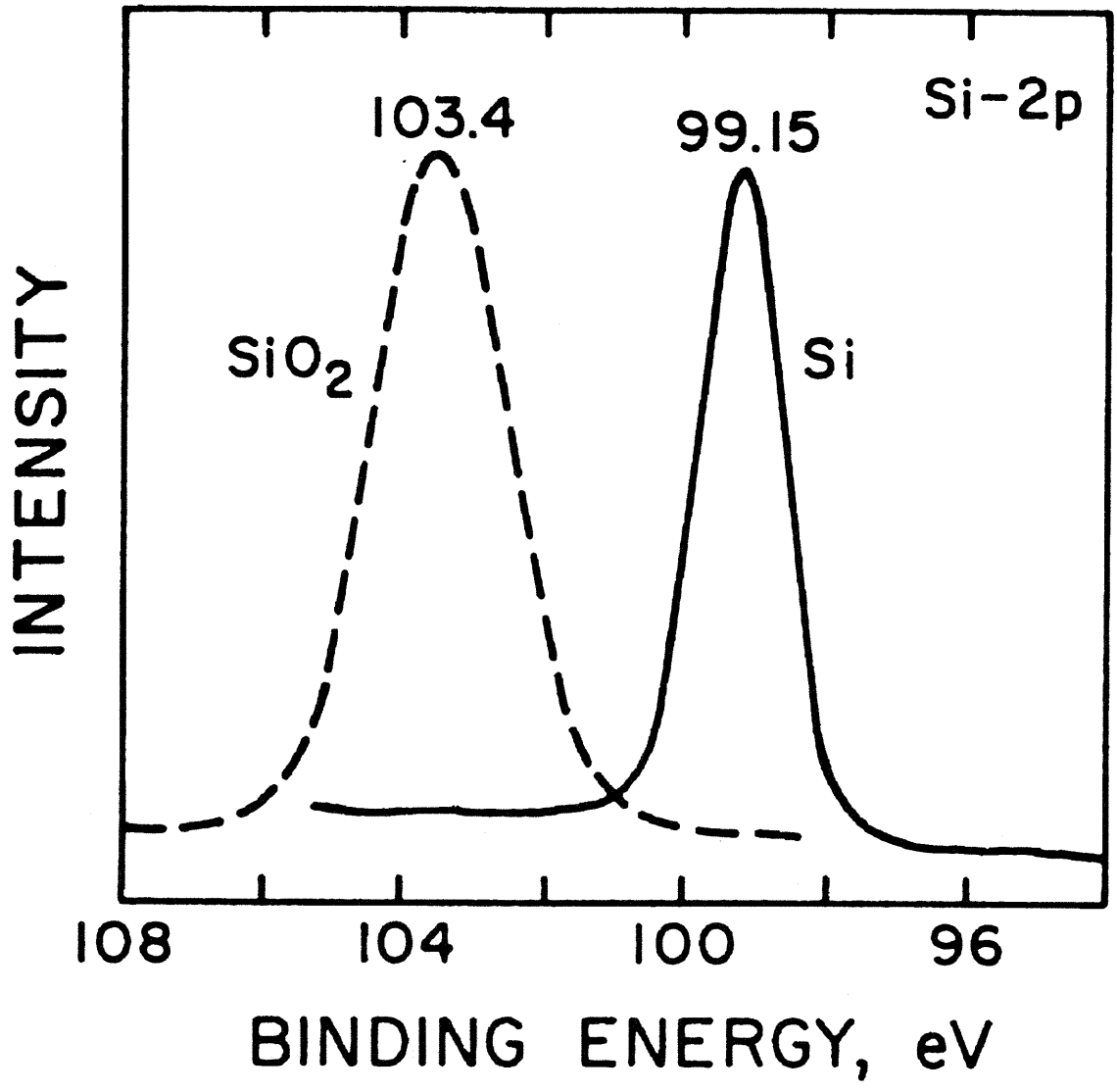

Figure 3-23 The chemical shift in binding energy of the Si 2p XPS line for elemental Si and SiO_2. (From Ref. 69).

these results are expected from the understanding that has developed of bulk silicon surfaces and processing.

3.4.2.2 *Effect of Methanol Dip*

Figure 3-24 shows the XPS spectrum of an aged sample before and after a methanol dip. The two peaked spectrum indicative of an oxidized silicon surface is present in both cases. This indicates that the chemical bonding of the silicon surface has not changed during the processing. It is not possible to interpret the absolute intensities of the peaks as these are dependent on many other factors. The similarity in the spectra shows that the oxide layer that has grown on the aged sample has protected the surface from attack from the methanol.[34] This correlates well with the photoluminescence behavior of the samples that was described in section 3.2.2.5. The oxide layer has chemically protected the surface, and it has also excluded the electric fields that would be induced by the presence of adsorbed methanol. This is evidence of the important role that silicon dioxide plays in making silicon a dominant electronic and potentially interesting optoelectronic materials platform.

Figure 3-25 show the XPS spectra for a sample dipped in hydrofluoric and then dipped into methanol. Once again, we see no change in the behavior of the hydride passivated surface. This indicates that the hydride passivated surface is chemically resistant to methanol attack, as has been reported in porous silicon.[73] In this case, although the surface was chemically resistant to methanol attack, the proximity of the polar molecule's electric field to the nanocrystallite induced a slight quenching of the luminescence, as shown in Figure 3-11.

3.4.2.3 *Halogen Passivation*

XPS was also used to provide evidence for the iodine passivation of samples. Figure 3-26 shows the Si 2p signal from an aged sample that was treated with an iodine:methanol solution. There is no clear change in the ratio of oxidized to unoxidized silicon signal. The actual intensities of these peaks cannot be compared due to changes in sample position and surface. However, the spectra indicate that the iodine treatment does not appear to have added more or less signal to either the oxidized or unoxidized signal at the expense of the other. Therefore, it can concluded that the silicon surface has not been chemically altered by

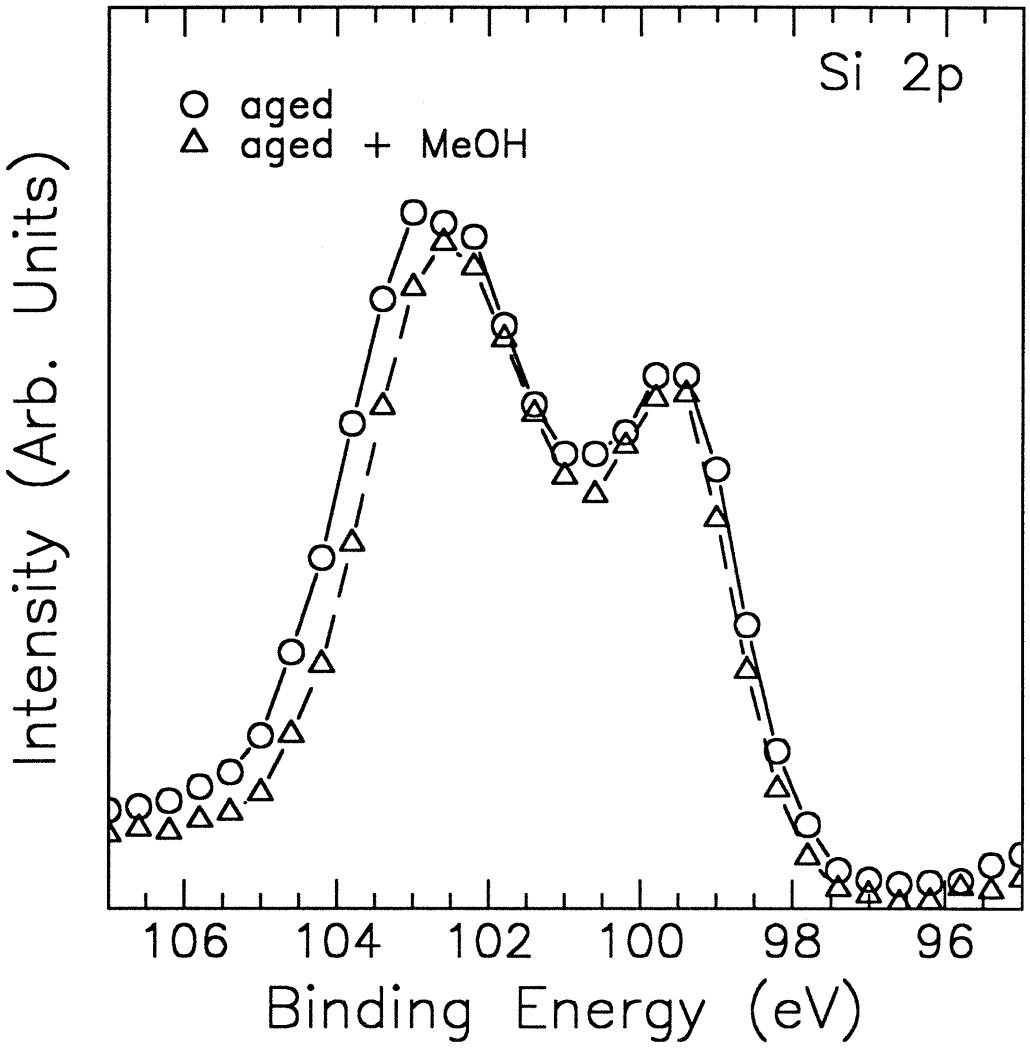

Figure 3-24 Comparison of Si 2p XPS spectra for an aged (O-passivated) thin film of silicon nanocrystallites before and after a methanol dip. There is no change in the ratio of oxidized to unoxidized silicon as a result of the treatment.

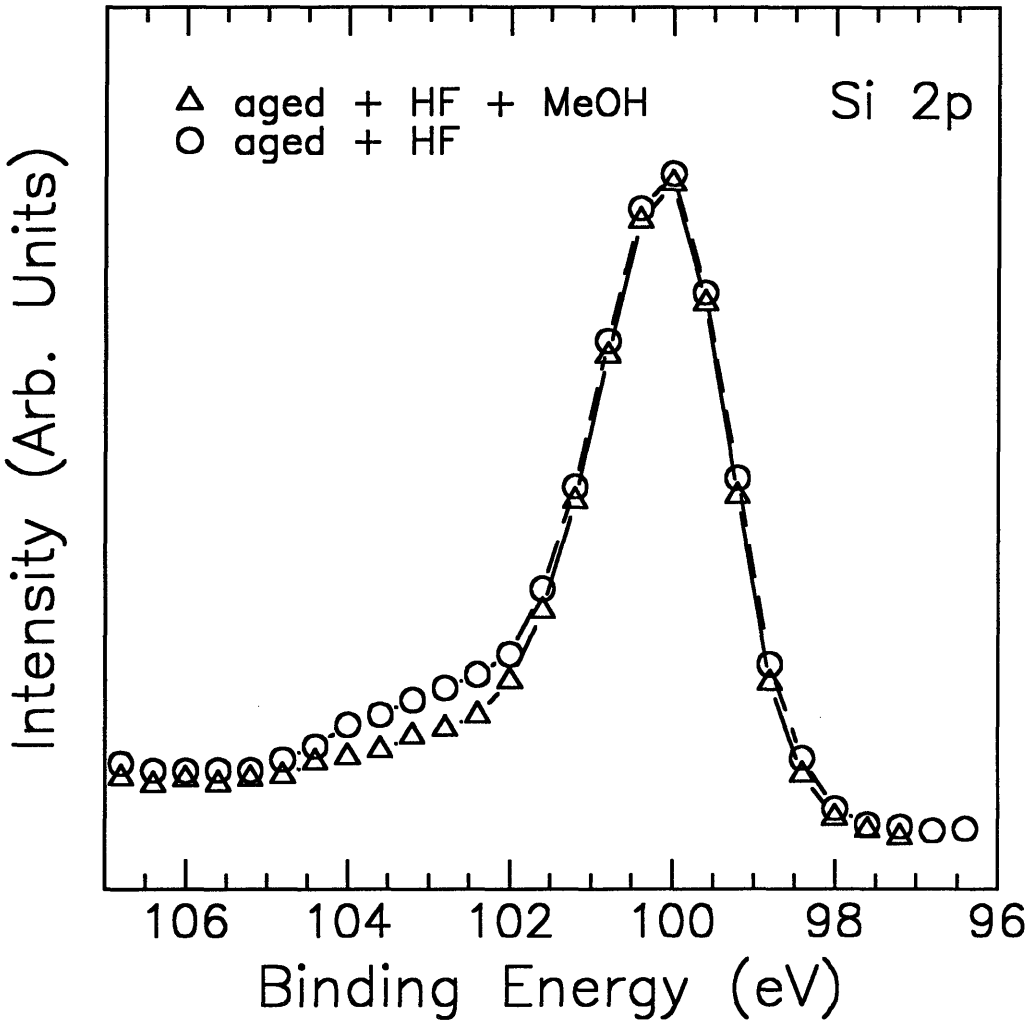

Figure 3-25 Effect of methanol treatment on Si 2p XPS signal of an H-passivated thin film of silicon nanocrystallites.

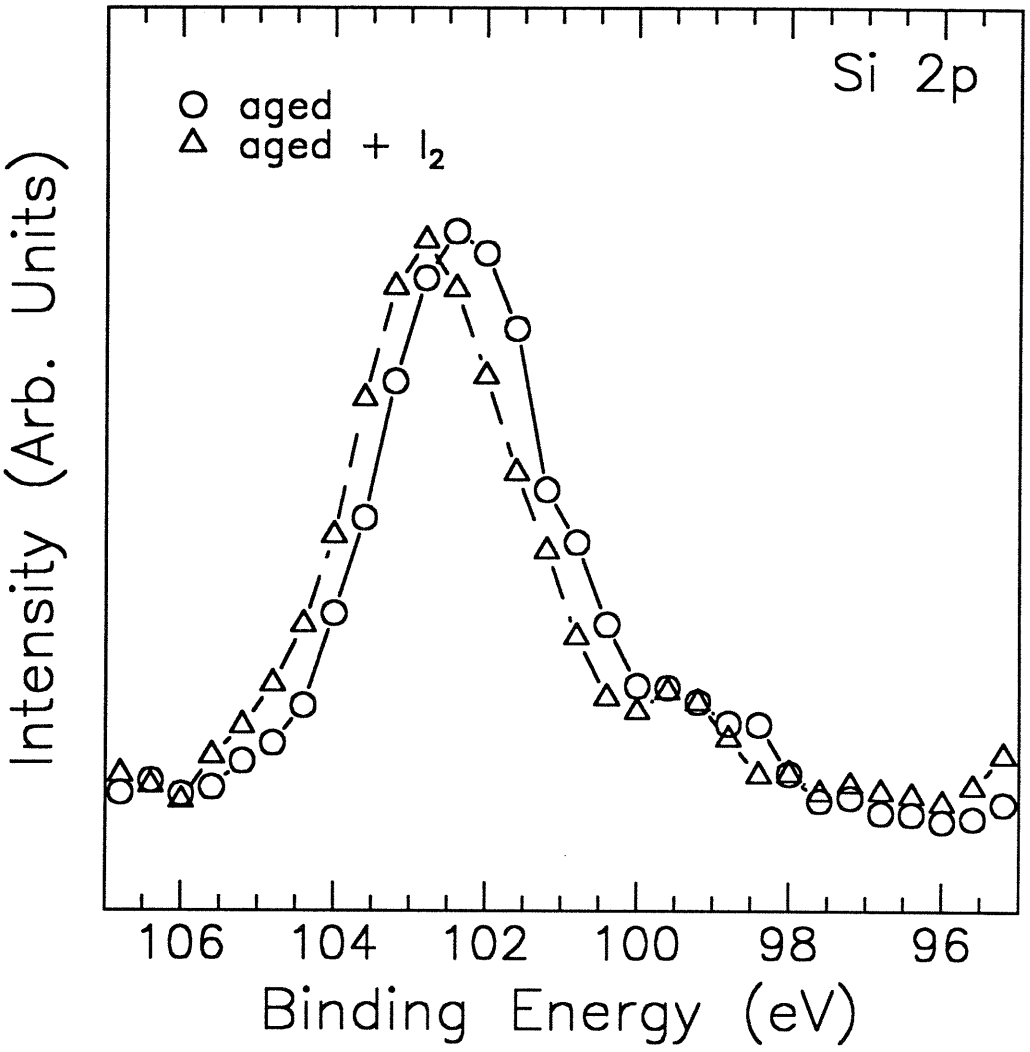

Figure 3-26 Effect of iodine treatment on Si 2p XPS spectrum of O-passivated silicon nanocrystallite thin film.

the iodine. Once again, the oxide layer has chemically protected the silicon nanocrystallite surface. This chemical resistance resulted in no change in the photoluminescence behavior, as shown in Figure 3-13.

However, treating a hydride passivated surface with the iodine:methanol solution resulted in a change in the XPS behavior of the film. In Figure 3-27, the evolution of the Si 2p XPS signal from a sample aged then etched in hydrofluoric acid and finally treated with iodine:methanol is shown. The spectra show changes similar to the effects that were described above, as the oxide passivation on the aged sample is replaced by a hydride passivation in the etched sample. After this hydride passivated sample is treated with iodine, the XPS spectrum changes once again. The ratio of oxidized silicon signal to unoxidized silicon signal increases after the treatment. This is consistent with iodine bonding with the silicon surface, as its large electronegativity would shift the binding energies of the surface silicon's core electrons. Iodine passivation of silicon has been demonstrated in bulk systems as well.[39] The presence of iodine was confirmed by looking at the I $3d_{5/2}$ XPS signal from the film, as shown in Figure 3-28.

The XPS spectra indicates that there is evidence of iodine passivation of silicon. This surface change did not result in any shift in the emission energy of the photoluminescence, as shown in Figure 3-14. This indicates that the chemical nature of the passivating species does not seem to determine the emission energy. It is very probable that the silicon surface is passivated by a combination of hydrogen, oxygen, and iodine, since it is difficult to separate out the individual peaks of the hydrides, nonstoichiometric oxides, and iodine. However, this combination of passivating species has not shifted the luminescence peak to any significant degree.

The halogen passivation of the silicon surface is further evidence that the emission mechanism is independent of the chemical nature of the passivating species. Silicon nanocrystallites have been passivated with hydrides, oxides, halogens, and hydroxides, and in no case has the emission behavior conflicted with the predictions of a simple quantum confinement model. In every case, the emission energy has been determined by the expected changes in particle radius as expected from quantum size effects. The surface of the system is key to controlling the emission intensity, but does not control the emission wavelength.

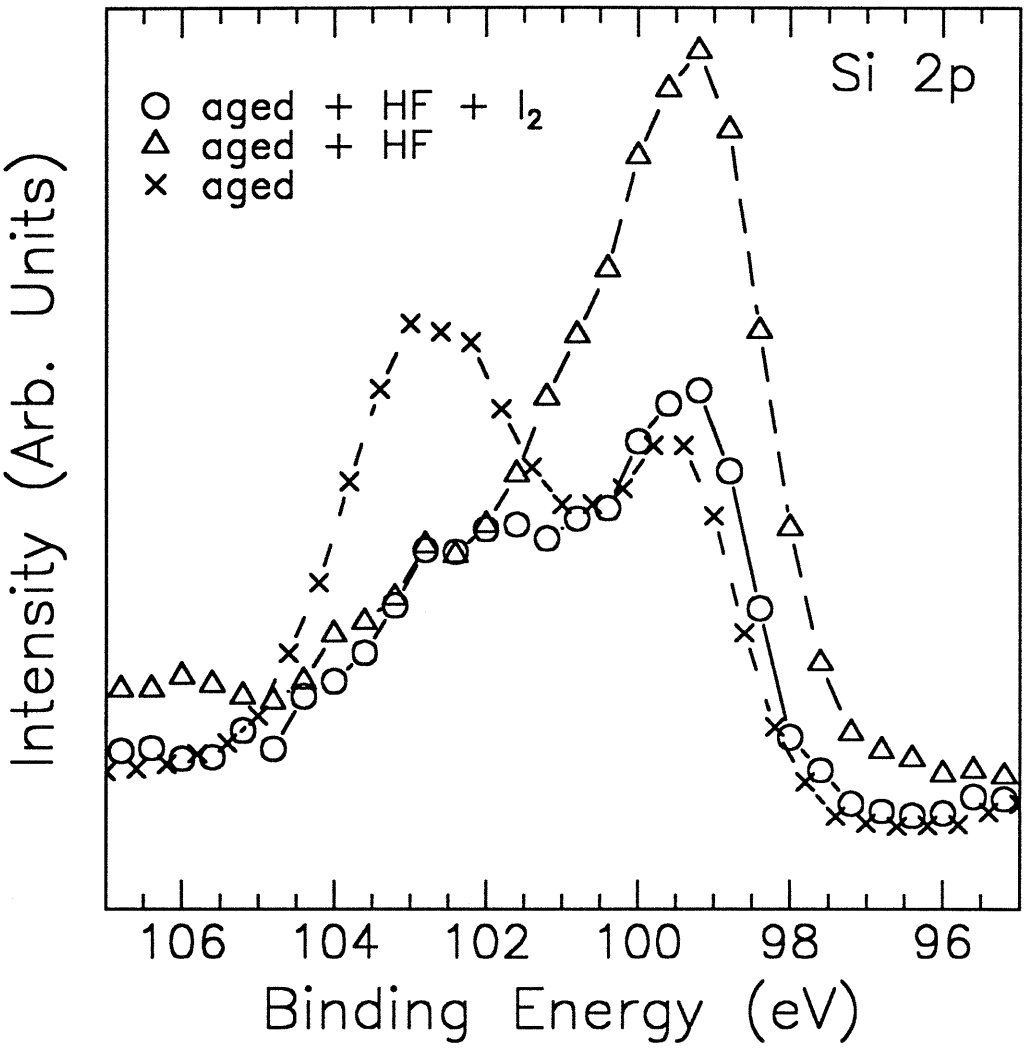

Figure 3-27 Si 2p XPS spectra of aged, HF dipped, and I_2 treated silicon nanocrystallite thin films. The change in ratio of oxidized to unoxidized silicon in the I_2 sample, as compared to the HF treated sample, indicates that I is bonding to the surface and changing its oxidation state.

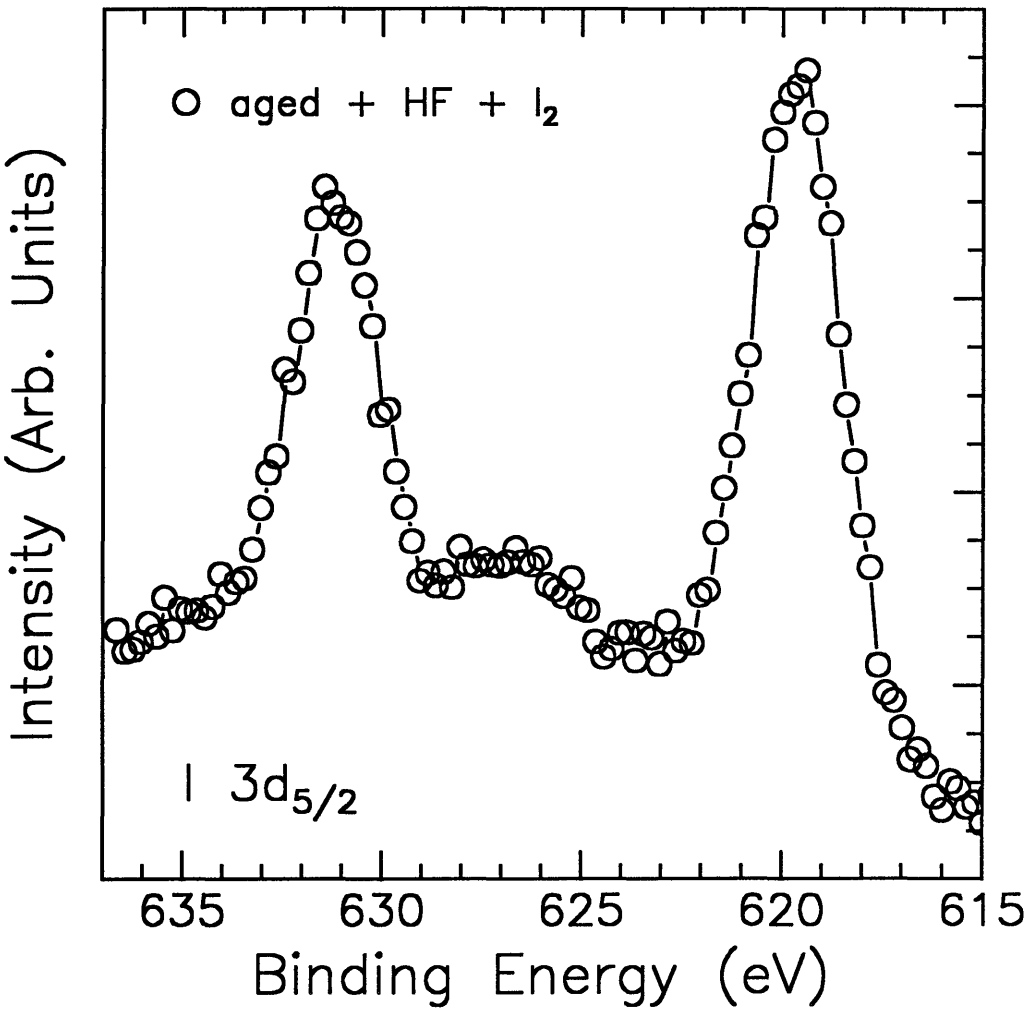

Figure 3-28 I $3d_{5/2}$ XPS spectrum of H-passivated silicon nanocrystallite thin film treated with iodine.

3.5 Nonlinear Optical Response

Research in nanostructured silicon has centered on the visible light emitting properties of nanocrystalline and porous silicon. Though potential applications of silicon visible light emitters are of considerable interest, another major advantage of this system is its ability to be relatively easily integrated into existing silicon based microelectronics technology for photonic applications. For example, the production of Si based photonic switches would provide for considerable advantages over other materials systems, when one takes into account the vast database of knowledge that already exists in silicon synthesis and processing techniques. Useful photonic devices will require that the systems being used show strong optical nonlinearities, since they will be based on the interaction of light beams with an active material. To this end, we have examined the nonlinear optical properties of the thin films of visible light emitting silicon nanostructures.

In particular, the $\chi^{(3)}$ response of the thin films of silicon nanocrystallites was studied. All-optical switches are being developed in systems whose nonlinearity results from the third order nonlinear optical susceptibility.[74] In these systems, though the materials are usually transparent, it is possible to induce a change in their refractive index as a function of the intensity of the incident light. In ultrafast switching devices, this should be a nonresonant interaction. Nonresonant nonlinearities are the intensity dependent changes in refractive index and absorption measured at photon energies away from band edge absorption, usually below the energy of the band gap. The reduced oscillator strength of the system at these photon energies means that these responses are usually very weak and require intense laser pumping. The advantage for optical switching is twofold: first, the nonlinearity tends to be very fast, in some systems around 10^{-14} seconds,[75] and second, the limited absorption away from the band edge leads to the possibility of very high device throughputs.

In order to avoid excessively large laser intensities or interaction lengths, it would be preferable to design devices using a material with a large $\chi^{(3)}$. To date, no third order nonlinear materials applications are practical because observed nonlinearities are orders of magnitude lower than what will be required for use with reasonable laser powers.[76] Ideally, a

photonic switch would be based on an integrable silicon materials platform that shows strong, fast optical nonlinearities at the wavelengths of technological interest.

As was described in section 2.5, degenerate four wave mixing spectroscopy (DFWM) was used to determine the third order nonlinear optical susceptibility. This measurement is dependent on the intensity of the phase conjugate beam produced as a result of the nonlinearity and the transmission of the sample at the experimental wavelength, in this case 532 nm. The relationship between the intensity of the signal beam and $\chi^{(3)}$ is obtained from a comparison of the intensities of the beams produced in the unknown sample to that produced in a known nonlinear optical material such as carbon disulfide, CS_2. Then $\chi^{(3)}$ for the unknown sample can be calculated from:

$$\chi^{(3)}_{sample} = \chi^{(3)}_{CS_2}\left(\frac{n_{Sample}}{n_{CS_2}}\right)^2\left(\frac{-\ln(T)}{1-T}\right)\left(\frac{1}{\sqrt{T}}\right)\left(\frac{d_{CS_2}}{d_{sample}}\right)\sqrt{\frac{I_{sample}}{I_{CS_2}}}$$

where n is refractive index, T is the transmission of the sample at 532 nm, d is film thickness, and I is phase conjugate beam intensity.[77]

As shown in Figure 3-29, the DFWM results show a strong dependence on the surface passivation of the samples. Typical silicon nanocrystallite thin films treated with hydrofluoric acid had $\chi^{(3)}$ values on the order of ~3 x 10^{-9} esu. The $\chi^{(3)}$ values of untreated films were measured at ~4 x 10^{-10} esu. This represents nearly an order of magnitude increase in the nonlinear response of the passivated films over the unpassivated films. These values are also larger than those expected from bulk Si; this enhancement has also been observed in porous silicon.[78] Neither treated nor untreated poly(vinyl carbonate) substrates showed any measurable $\chi^{(3)}$ signal. The measured silicon nanocrystallite response is still much smaller than the 10^{-7} esu that has been reported in polymer materials that are considered to have strong potential for photonic applications.[76]

A typical absorption spectrum for a film of silicon nanocrystallites is shown in Figure 3-30. Since the films do show some absorption at 532 nm and emit light strongly at longer wavelengths, it is likely that the nonlinear response represents a resonant behavior for the light emitting nanocrystallites.

Degenerate Four-Wave Mixing Results

$\chi^{(3)}$ at 532 nm :

Bulk Polycrystalline Silicon: ~ 4×10^{-10} esu

Unpassivated Nanocrystalline Silicon: ~ 4×10^{-10} esu

Passivated Nanocrystalline Silicon: ~ 3×10^{-9} esu

Figure 3-29 Third order nonlinear optical susceptibility $\chi^{(3)}$ at 532 nm for passivated nanocrystallites, unpassivated nanocrystallites, and bulk polycrystalline silicon as measured by degenerate four wave mixing spectroscopy (DFWM).

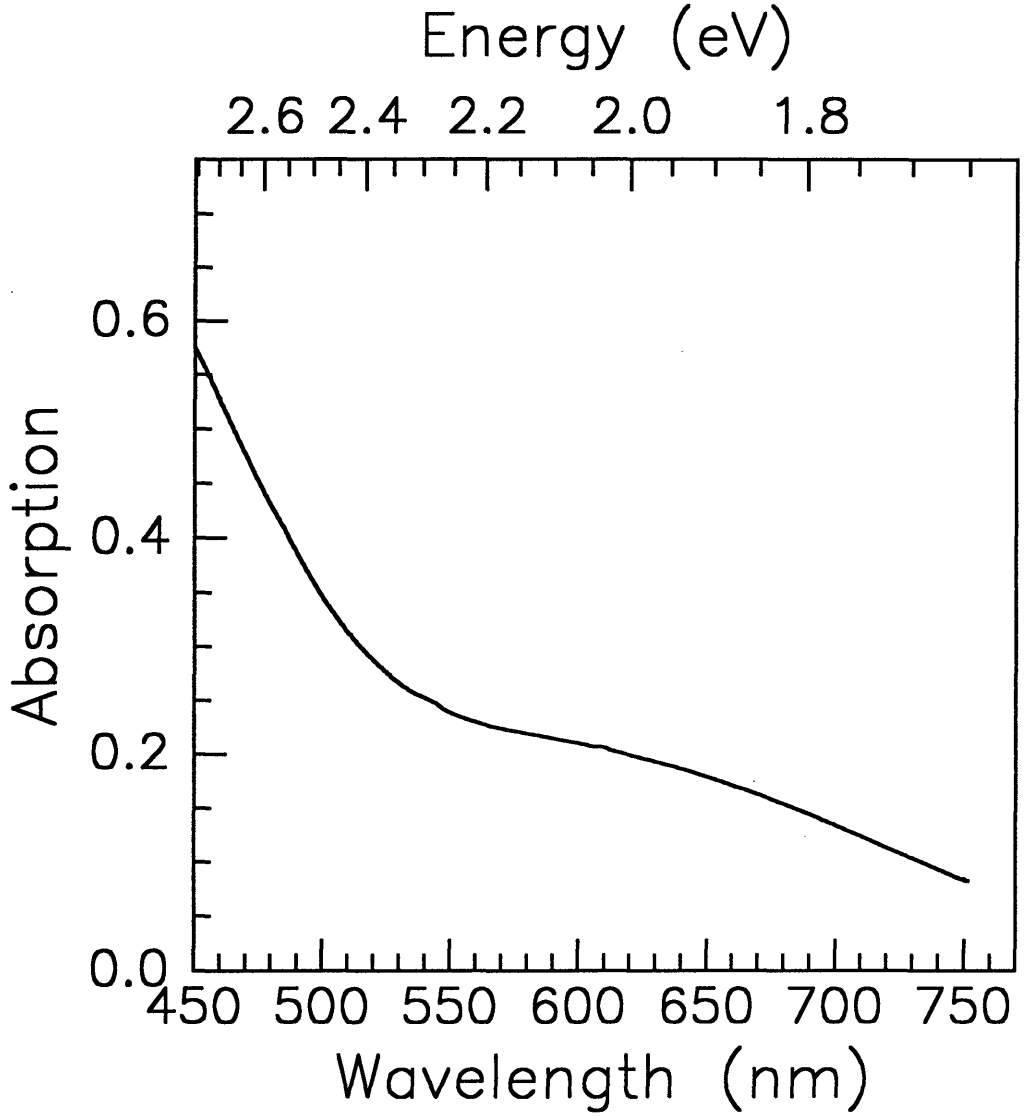

Figure 3-30 Absorption spectrum of HF treated thin film of silicon nanocrystallites on poly(vinyl carbonate) substrate.

The induced third order nonlinear optical susceptibility is manifested in the intensity dependent refractive index that develops in the samples. This change in refractive index is due to a change in the occupancy of levels in the conduction band of the material by excited carriers. The change in index of refraction (Δn) is proportional to the change in the number of empty states in the saturating level (ΔN),

$$\Delta n = \frac{-4\pi}{n_0}(\Delta N)\frac{|er_{ba}|^2}{E_{ba}}\frac{E_{ba}}{(E_{ba}-E_p)}$$

where n_0 is the index of refraction, $/er_{ba}/$ is the strength of transition between levels a and b, E_{ba} is the energy of the transition, and E_p is the incident photon energy.[79] From this relation, as the final transition state fills, ΔN increases, and the index of refraction experiences a large negative change. The third order nonlinear optical susceptibility is proportional to this index change, and thus can be used as a figure of merit for the behavior.

Both bulk and nanocrystalline silicon will show nonlinear effects as their energy levels fill with charge carriers under high photoexcitation. However, in nanocrystalline materials this nonlinearity should be easier to achieve due to the effects of quantum confinement on the system's band structure. First, the enhanced oscillator strength at small sizes[10] increases $/er_{ba}/$ and enhances the index change. Also, in these nanostructures, energy levels in bands begin to separate and take on a more discrete nature. These effects will reduce the probability of intraband transitions that would depopulate the states. This allows electronic levels to fill more quickly under excitation, increasing ΔN. At the same time, the system's size leads to a finite number of states that encourages saturation. This state filling then becomes the source of the nonlinearity, since the material can no longer respond to photoexcitation in the same manner. This effect leads to the saturable absorption that could exploited in photonic switches, as was discussed in section 1.2.

The intensity of the nonlinear response of the samples is a strong function of surface passivation. Time-resolved measurements for both passivated and unpassivated nanocrystallites have indicated that the nonlinearity has a lifetime on the order of hundreds of microseconds. This is evidence for a resonant process which involves the excitation of free carriers.[80] The presence of the unpassivated surface bonds creates an extremely fast relaxation

pathway for the excited carriers, and disrupts the state filling process which induces the optical nonlinearity. These dangling surface bonds also act as nonradiative recombination centers, which quench the visible luminescence behavior. Nonradiative recombination also leads to the release of energy to the lattice in the form of heat via phonons. This temperature increase leads to a reduction of the energy gap of the material, but also an increase in the index of refraction. This effect has been demonstrated in many semiconductors, including ZnSe.[81] This positive change in index is opposite in sign to the nonlinearity that is caused by state filling as described above. Passivating the surface using hydrofluoric acid (HF) leads to hydride species satisfying the silicon surface bonds and eliminates the nonradiative recombination pathways and associated thermal effects. In this case, excited carriers can remain in the conduction band long enough for saturation processes to occur and a nonlinear response to develop. Therefore, passivated samples show a significantly larger $\chi^{(3)}$ response than unpassivated samples.

It is important to note that as our samples age in air their properties change. The samples which were not treated with HF began to show increased visible luminescence intensity and an enhanced third order nonlinear optical response. The chemically treated samples show no significant change in either their luminescence or DFWM response over time. Atmospheric aging of samples leads to oxidation of the nanocrystallites and passivation of the dangling silicon bonds. This in turn results in an enhancement of the luminescence intensity and $\chi^{(3)}$ response in the same way as hydride passivation. This similarity indicates that it is not the chemical nature of the passivation that determines the optical properties of the nanocrystallites. Passivation seems to only enable the visible light emission and nonlinear optical response by reducing the probability of fast nonradiative recombination and reducing thermal effects in the system.

The thin films of silicon nanocrystallites showed a nonlinear optical response that was enhanced over polycrystalline bulk values when passivated by a hydride or oxide layer. However, the response was still very weak, over three orders of magnitude below materials that are considered to have viable commercial application.[76] In addition, the effect seen at 532 nm was resonant in nature, implying that it would be too slow for high speed optical switching applications. It is possible to improve the nonlinear optical response of the films by improving

both the size distribution and surface passivation of the materials. This would lead to larger index changes and remove any possibility of excited carriers tunneling from smaller to larger crystallites and then recombining nonradiatively. It is also possible that faster, nonresonant nonlinearities exist at energies below the energy gap of the clusters. These responses might be exploitable in high speed photonic switching devices working at infrared wavelengths of technological interest, such as the 1.54 micron dispersion minimum of silica optical fiber.

3.6 Excitation Intensity

Further evidence for the role of quantum confinement plays in the luminescence behavior of the silicon nanocrystallite thin films was seen in the excitation energy dependence of the photoluminescence emission. As shown in Figure 3-31, the luminescence emission intensity increases with increasing pump excitation power. However, at large excitation intensities there is a saturation of the transition at the specific wavelength. Looking at the entire spectrum as a function of pump power in Figure 3-32 there is a clear blueshift in the peak emission wavelength with increasing pump power, an interesting nonlinear optical response. This shift appears to result from an increase in the amount of short wavelength behavior as compared to the longer wavelength response, rather than a complete shifting of the entire spectrum.

The response of the nanocrystallites under increased photoexcitation provides some insights into the recombination mechanism in the films. First, the response has some variation between the individual wavelengths. In particular, the sub-500 nm wavelengths have a different functionality than the longer wavelengths. This is evidence that they represent a different type of emission. The short wavelength behavior at the blue end of the spectrum is attributed to the presence of the surface and matrix oxide, while the longer wavelength behavior is from emission of the nanocrystallites themselves.

Second, the emission behavior saturates at large excitation intensities. This saturation can be seen as the result of enhanced Auger nonradiative recombination caused by the density of carriers excited into the material's conduction band. However, it is more likely that the saturation of the longer wavelengths is coupled to the blueshift of the spectrum as a whole. At higher excitation intensities, enough carriers are excited to fill the lowest conduction levels,

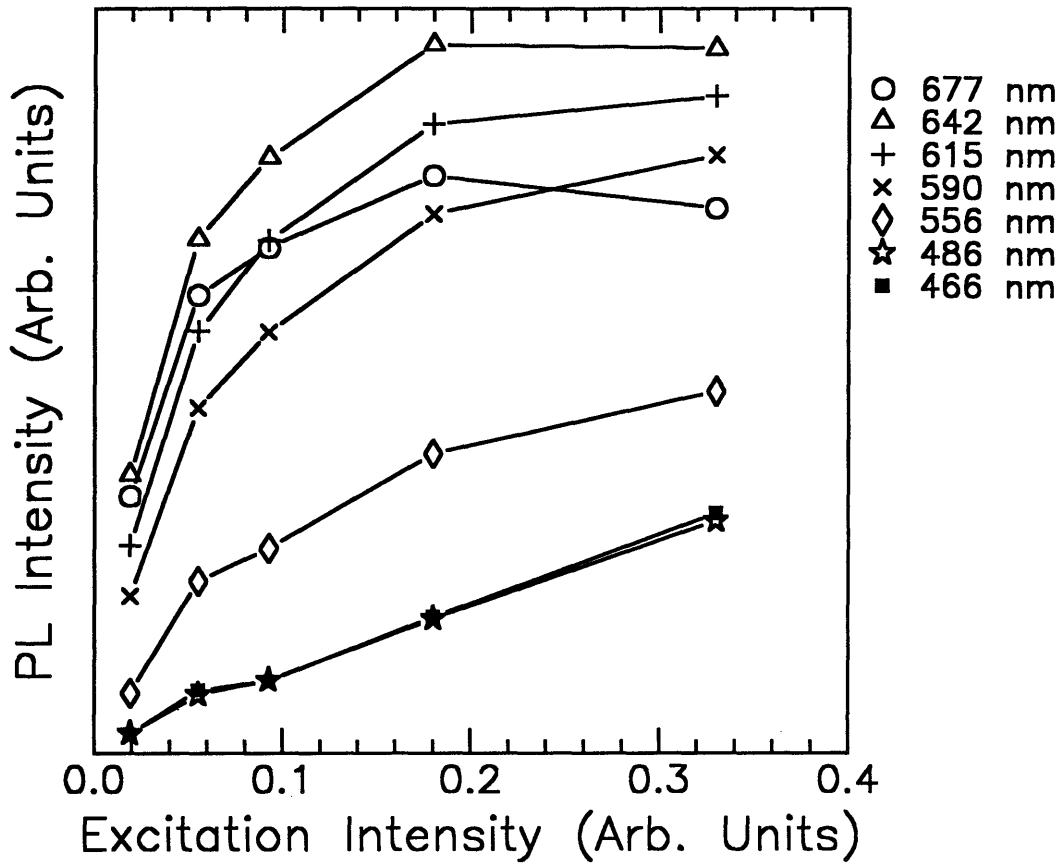

Figure 3-31 PL intensity dependence on excitation intensity. Different wavelengths are plotted to highlight difference in red-orange emission behavior and blue emission behavior.

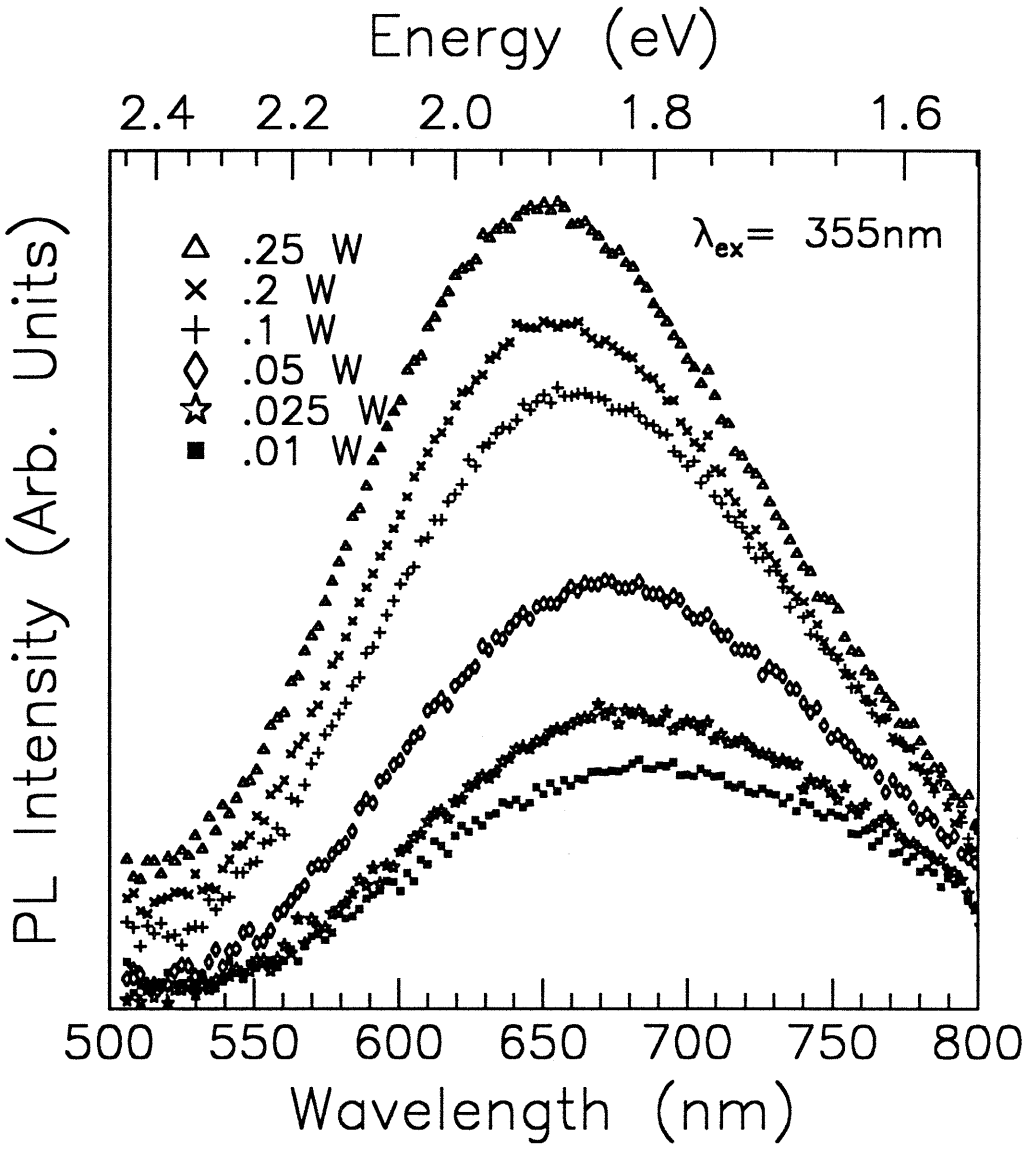

Figure 3-32 PL spectra from a thin film of silicon nanocrystallites at increasing excitation intensities. A pulsed 3xNd:YAG laser was used as the excitation source. As excitation intensity increases, PL emission intensity increases and shifts to higher energies.

so that excess carriers have to sit at higher energy levels. This leads to radiative recombination at higher energies than what is observed at lower intensities and a blueshift in emission. Using a simple model for energy levels in a cubic quantum dot,

$$E_n = \frac{n^2 \hbar^2 \pi^2}{2md^2}$$

where d is cube edge length, it is possible to get an idea of the shift in transition energy after the lowest energy transitions are saturated. In this system, the transitions between the n=1 levels would be seen at lower excitation intensity and transitions involving higher levels would be seen at higher excitation intensities. A dot with edge length 2-3 nm has an energy spacing between the n=1 and n=2 conduction levels of 100-250 meV, consistent with the magnitude of the shift seen in the nanocrystallite films under higher excitation. This calculation assumes a bulk effective electron mass ($1.2m_0$), as well as a stronger dependence of energy on size than what is observed experimentally, as discussed in section 3.2.1.1, but still shows that the excitation intensity behavior correlates well with models of emission based on quantum size effects. In contrast, emission due to fixed surface states in the band gap of the material would have shown a spectrally constant intensity dependence and a saturation of emission across the spectrum, since there is no band of emission states present into which excess carriers can migrate. Once again, these results can best be explained by an emission model based on the quantum confinement of carriers in a nanostructured system.

3.7 Summary

In order to study the role of particle size and surface in the visible photoluminescence behavior of silicon nanostructures, thin films of Si nanocrystallites were deposited using a novel pulsed laser ablation supersonic expansion source. The films efficiently emit visible light under ultraviolet photoexcitation. The films have been treated using a number of post-deposition processing steps, including hydrofluoric acid and nitric acid etches and oxidation furnace treatments, in order to control the sizes and surfaces of the Si particles. The films have been characterized using photoluminescence emission spectroscopy, FTIR, and XPS to correlate the sizes and surface properties to the luminescence behavior. Additionally, the non-

linear optical response of the films were studied using degenerate four-wave mixing spectroscopy.

Particle size determines the energy of the orange emission of the films through the quantum confinement of photoexcited carriers. The size of the nanostructures has been controlled through the use of acid etch/oxide regrowth cycles. This has resulted in a consistent increase of the emission energy, as is predicted by theories of quantum confinement in semiconductor nanostructures. Both the photoluminescence temperature and pump power dependence of the orange photoluminescence are consistent with emission due to a recombination of excited carriers in a quantum confined system. The blue band of emission has been correlated to the extended oxidation of crystalline silicon material and growth of SiO_x. Therefore, it is concluded that the orange band emission behavior is controlled by the recombination of carriers within the nanostructures, while the blue photoluminescence is related to oxide defect emission.

Optical properties are also strongly influenced by the extent of surface passivation. Surface passivation controls the density of nonradiative recombination centers in the nanocrystallites. Unpassivated, gas phase nanoparticles show no visible luminescence behavior, as do as-deposited, unpassivated thin films. Conversely, films processed through atmospheric aging, nitric acid, or hydrofluoric acid dips to passivate their surfaces show efficient visible emission. The third order nonlinear optical susceptibility of the films also improves by an order of magnitude with surface passivation.

While the emission intensity scales with the extent of surface passivation, the emission energy is independent of the exact chemical nature of the passivating species. The surfaces of the particles have been controlled by passivating the nanocrystallites with hydrogen, oxygen, and iodine, as confirmed by XPS and FTIR. In each case, the observed emission can be attributed to recombination of excited carriers within quantum confining surface passivated nanostructures, and shows no anomalous behavior due to the changes in passivating species.

Chapter Three References

[1] J.B. Khurgin, E.W. Forsythe, S.I. Kim, B.S. Swye, B.A. Khan, and G.S. Tompa, Mat. Res. Symp. Proc. Vol. 358, 193 (1994)
[2] L.E. Brus, J. Chem. Phys. 80(9), 4403 (1984)
[3] D.S. Russell, unpublished result.
[4] S. Schuppler, S.L. Friedman, M.A. Marcus, D.L. Adler, Y.-H. Xie, Y.J. Chabal, T.D. Harris, L.E. Brus, W.L. Brown, E.E. Chaban, P.F. Szajowski, S.B. Christman, and P.H. Citrin, Phys. Rev. B 52(7), 4910 (1995)
[5] E. Werwa, A.A. Seraphin, L.A. Chiu, C. Zhou, and K.D. Kolenbrander, Appl. Phys. Lett. 64(14), 1821 (1994)
[6] C. Delerue, M. Lannoo, and G. Allan, J. Lum 57, 249 (1993)
[7] T. Takagahara and K. Takeda, Phys. Rev. B 46(23), 15578 (1992)
[8] C.R. Kagan, C.B. Murray, M. Nirmal, and M.G. Bawendi, Phys. Rev. Lett. 76(9), 1517 (1996)
[9] Y. Nagamune, H. Watabe, M. Nishioka, and Y. Arakawa, Appl. Phys. Lett. 67(22), 3257 (1995)
[10] C. Delerue, G. Allan, and M. Lannoo, Phys. Rev. B 48(15), 11024 (1993)
[11] R.J. Archer, J. Electrochem. Soc. 104(10), 619 (1957)
[12] F. Lukes, Surf. Sci. 30, 91 (1972)
[13] H.I. Liu, B.K. Biegelsen, F.A. Ponce, N.M. Johnson, R.F.W. Pease, Appl. Phys. Lett. 64(11), 1383 (1994)
[14] L.A. Chiu, A.A. Seraphin, and K.D. Kolenbrander, J. Electron. Mater. 23(3), 347 (1994)
[15] A. Nakajima, T. Itakura, S. Watanabe, and N. Nakayama, Appl. Phys. Lett. 61(1), 46 (1992)
[16] J.H. Stathis and M.A. Kastner, Phys. Rev. B 35, 2972 (1987)
[17] K.D. Kolenbrander and M.L. Mandich, J. Chem. Phys. 92, 4759 (1990)
[18] E. Werwa and K.D. Kolenbrander, Mat. Res. Soc. Symp. Proc. Vol. 397, in press.
[19] M.S. Hybertsen, Phys. Rev. Lett. 72(10), 1514 (1994)
[20] T. Matsumoto, H. Mimura, and Y. Kanemitsu, J. Phys. Soc. Jpn. 63B, 182 (1994)
[21] M. Kondo and H. Yokomichi, J. Phys. Soc. Jpn. 63 Suppl. B, 145 (1994)
[22] L.E. Brus, P.F. Szajowski, W.L. Wilson, T.D. Harris, S. Schuppler, and P.H. Citrin, J. Am. Chem. Soc. 117, 2915 (1995)
[23] J.D. MacKenzie, B.S. Thesis, Massachusetts Institute of Technology (1993)
[24] J.C. Polanyi and J.-X. Wang, J. Phys. Chem. 99(37), 13691 (1995)
[25] E. Yablonovitch, D.L. Allara, C.C. Chang, T. Gmitter, and T.B. Bright, Phys. Rev. Lett. 57(2), 249 (1986)
[26] M. Rüchschloss, Th. Wirschem, H. Tamura, G. Ruhl, J. Oswald, and S. Veprek, J. Lum. 63, 279 (1995)
[27] R. Czaputa, R. Fritzl, and A. Popitsch, Thin Solid Films 255, 212 (1995)
[28] N.A. Hill and K.B. Whaley, J. Electron. Mater. 25(2), 269 (1996)
[29] S.Y. Ren and J.D. Dow, Phys. Rev. B 45(12), 6492 (1992)
[30] L. Tsybeskov, Ju. V. Vandyshev, and P.M. Fauchet, Phys. Rev. B 49(11), 7821 (1994)
[31] S.M. Hu and D.R. Kerr, J. Electrochem. Soc. 114(4), 414 (1967)
[32] L. Tsybeskov and P.M. Fauchet, Appl. Phys. Lett. 64(15), 1983 (1994)

[33] L. Brus, Phys. Rev. B 53(8), 4649 (1996)
[34] J.M. Rehm, G.L. McLendon, L. Tsybeskov, and P.M. Fauchet, Appl. Phys. Lett. 66(26), 3669 (1995)
[35] O. Gorbounova, A. Mejiritski, and A. Torres-Filho, J. Appl. Phys. 77(9), 4643 (1995)
[36] I. Schechter, M. Ben-Chorin, and A. Kux, Anal. Chem. 67, 3727 (1995)
[37] J.M. Lauerhaas, G.M. Credo, J.L. Heinrich, and M.J. Sailor, J. Am. Chem. Soc. 114, 1911 (1992)
[38] J.M. Lauerhaas and M.J. Sailor, Science 261, 1567 (1993)
[39] H. M'Saad, J. Michel, A. Reddy, and L.C. Kimerling, J. Electrochem. Soc. 142(8), 2833 (1995)
[40] D.J. Lockwood, G.C. Aers, L.B. Allard, B. Bryskiewicz, S. Charbonneau, D.C. Houghton, J.P. McCaffrey, and A. Wang, Can. J. Phys. 70, 1184 (1992)
[41] Y.A.R.R. Kessener, G.L.J.A. Rikken, and A.H.J. Venhuizen, J. Lum. 57, 77 (1993)
[42] C. H. Perry, F. Lu, F. Namavar, N.M. Kalkhoran, R.A. Soref, Appl. Phys. Lett. 60(25), 3117 (1992)
[43] Y. Kanemitsu, H. Uto, Y. Matsumoto, T. Matsumoto, T. Futagi, and H. Mimura, Phys. Rev. B 48(4), 2827 (1993)
[44] J. Oswald, J. Pastrñák, A. Hospodková, and J. Pangrác, Sol. St. Comm. 89(3), 297 (1994)
[45] A.A. Lebedev, A.D. Remenyuk, and Y.V. Rud', Semiconductors 27, 1017 (1993)
[46] K.L. Narasimhan, S. Banerjee, A.K. Srivastava, and A. Sardesai, Appl. Phys. Lett. 62(4), 331 (1993)
[47] Y.P. Varshni, Physica 34, 149 (1967)
[48] J.B. Xia and K.W. Cheah, Appl. Phys. A 59, 227 (1994)
[49] L.C. Kimerling, K.D. Kolenbrander, J. Michel, and J. Palm, Sol. St. Phys., in press.
[50] M. Rosenbauer, M. Stutzmann, H.D. Fuchs, S. Finkbeiner, and J. Weber, J. Lum 57, 153 (1993)
[51] R.W. Collins, M.A. Paesler, and W. Paul, Sol. St. Comm. 34, 833 (1980)
[52] M.B. Panish and H.C. Casey, J. Appl. Phys. 40(1), 163 (1969)
[53] C.D. Clark, P.J. Dean, and P.V. Harris, Proc. Roy. Soc. A 277, 312 (1964)
[54] W. Bludau, A. Onton, and W. Heinke, J. Appl. Phys. 45, 1846 (1974)
[55] M.L. Cohen and D.J. Chadi, in *Handbook on Semiconductors: Vol. 2 Optical Properties of Solids*, M. Balkanski, ed. p. 155 (1980)
[56] N. Kuroda, Y. Matsuda, S. Nakajima, I. Taketsu, and N. Ookubo, J. Appl. Phys. 78(5), 3520 (1995)
[57] Y. Okada and Y. Tokumaru, J. Appl. Phys. 56(2), 314 (1984)
[58] J.A. Lupo and M.J. Sabochick, Nanostr. Mater. 1, 131 (1992)
[59] A. Witvrouw and F. Spaepen, J. Appl. Phys. 74(12), 7154 (1993)
[60] J.P. Walter, R.L. Zucca, M.L. Cohen, and Y.R. Shen, Phys. Rev. Lett. 24, 102 (1970)
[61] S. Schmitt-Rink, D.A.B. Miller, and D.S. Chemla, Phys. Rev. B 35(15), 8113 (1987)
[62] R.A. Street, Adv. Phys. 25(4), 397 (1976)
[63] R.A. Street, Adv. Phys. 30(5), 593 (1981)
[64] J.I. Pankove, *Optical Processes in Semiconductors*, p. 165 (1975)
[65] X. Chen, D. Uttamchandani, C. Trager-Kowan, and K.P. O'Donnell, Semicon. Sci. and Tech. 8(9), 92 (1992)

[66] M. Nirmal, private communication.
[67] S. Fukatsu, J. Cryst. Gr. 157, 1 (1995)
[68] S.K. Ghandhi, *VLSI Fabrication Principles* (1994)
[69] L.C. Feldman and J.W. Mayer, *Fundamentals of Surface and Thin Film Analysis*, p.224 (1986)
[70] C.H. Bjorkman, J.L. Alay, H. Nishimura, M. Fukuda, T. Yamazaki, and M. Hirose, Appl. Phys. Lett. 67(14), 2049 (1995)
[71] S. Hayashi, S. Tanimoto, and K. Yamamoto, J. Appl. Phys. 68(10), 5300 (1990)
[72] D. Rioux, F. Stepniak, R.J. Pechman, and J.H. Weaver, Phys. Rev. B 51(16), 10981 (1995)
[73] J.A. Glass, E.A. Wovchko, and J.T. Yates, Surf. Sci. 338, 125 (1995)
[74] M.N. Islam, Physics Today 47, 34 (1994)
[75] R.W. Munn and C.N. Ironside, *Principles and Applications of Nonlinear Optical Materials*, p.46 (1993)
[76] D.F. Eaton, Science 253, 281 (1991)
[77] D.V.G.L.N. Rao, F.J. Aranda, J.F. Roach, and D.E. Remy, Appl. Phys. Lett. 58, 1241 (1991)
[78] T. Matsumoto, N. Hasegawa, T. Tamaki, K. Ueda, T. Futagi, H. Mimura, and Y. Kanemitsu, Jpn. J. Appl . Phys. 33, L35 (1994)
[79] H. Haug, *Optical Nonlinearities and Instabilities in Semiconductors*, p.250 (1988)
[80] R.W. Munn and C.N. Ironside, *Principles and Applications of Nonlinear Optical Materials*, p.52 (1993)
[81] H. Haug, *Optical Nonlinearities and Instabilities in Semiconductors*, p.265 (1988)

4. Conclusions

4.1 Review

A pulsed laser ablation supersonic expansion source was used to synthesize silicon nanostructures. The particles were examined in the gas phase and in thin film form in order to characterize their light emission properties and nonlinear optical response. The films were processed using standard semiconductor etch and oxidation steps to alter their sizes and surfaces, and to determine the role that each plays in controlling the novel optical behaviors. Light emission was characterized using photoluminescence emission spectroscopy, including temperature and pump power dependence studies. Surface properties were examined with infrared spectroscopy, gas phase luminescence measurements, and x-ray photoelectron spectroscopy. The nonlinear optical response of the thin films was determined by degenerate four wave mixing spectroscopy. These results were used to better understand the mechanism of luminescence in the silicon nanostructures, and the role that size and surface plays in the process.

4.2 Conclusions

This work on the optical properties of silicon nanostructures produced by pulsed laser ablation supersonic expansion and the existing work in light emitting silicon nanostructure materials leads to the following conclusions.

4.2.1 Synthesis

Pulsed laser ablation supersonic expansion can be used to deposit thin films of silicon nanostructures which emit visible light and can demonstrate nonlinear optical effects. Thin films were deposited on a variety of substrates and can be routinely processed to enable visible luminescence, through acid etches or oxidation steps. The production of the nanostructures

has been optimized to the point that process parameters can be used to roughly control the size distribution of the deposited film. In addition, the versatility of the synthesis technique has been exploited through the gas phase characterization of the clusters, the ability to switch carrier gases and attempt *in situ* passivation of the clusters, deposition of nanocrystallites from a number of target materials, and codeposition of nanostructures into semiconductor host matrices. This versatility has also enabled deposition on nontraditional substrates, such as Teflon or TEM grids, which were necessary for film characterization. These advantages have given the technique an ability to help answer questions about the role of the matrix or heterostructure environment in determining optical properties, as particles can be examined without surface capping and with caps of increasing complexity.

It is becoming increasing clear that the interesting nanostructures in silicon light emission are on the order of 50-500 atoms. As such, they are too small to be easily handled by traditional film growth and characterization techniques. In fact they are best suited to be studied by traditional gas phase chemical techniques, including laser ablation supersonic expansion. Since the atomic structures of the light emitting particles should bear as strong a resemblance to very small silicon clusters as they do to bulk silicon materials, it is sensible to try to approach the problem both by building up from the gas phase or small side as well as breaking down from the wafer scale or large side.

While the source has proven valuable as an experimental tool, it does have a number of drawbacks. The technique seems best suited for work with elemental semiconductors, as the creation of compound materials while maintaining stoichiometry will present difficulties. The laser ablation technique produces small quantities of materials at a very slow rate; it will be difficult to scale up for commercial applications or even for use with some characterization techniques. Most porous silicon workers have microns worth of film to characterize, making a number of techniques, such as infrared absorption, easier to use. The source also produces a large size distribution of particles, so that separating out the characteristics of individual nanocrystallites is very difficult. It will be critical to control this size distribution in order to better characterize the material and produce usable devices.

4.2.2 Nanostructured Silicon Materials

The silicon nanostructures being produced using the pulsed laser ablation supersonic expansion technique show very different optical properties than bulk silicon. This is evidence that the nanostructures are structurally different than traditional diamond cubic silicon; that other materials exist on the films that exhibit the novel optical properties; or that the quantum confinement of carriers within the nanostructures alters the optical properties. This novel visible light emission and nonlinear optical response should open the door for further research and eventual development of commercial silicon-based applications.

The films have been shown to emit visible light on a variety of substrates when under photoexcitation. The emission is very stable and lasts indefinitely, and is efficient enough to be seen in normal room light when under ultraviolet excitation. The emission intensity and energy can be shifted by controlling the surfaces and sizes of the particles through variation of processing and deposition techniques. This ability has made it possible to characterize the sample luminescence as a function of size and surface, and gain some insight into emission mechanisms in the silicon nanostructures.

The fact that silicon has been demonstrated to reproducibly give visible light using standard deposition and processing techniques is not one that should be taken lightly. The material has until now been interesting and commercially successful because of its electronic properties and processing advantages. The development of novel optoelectronic behaviors in this system, while not theoretically inconceivable, has always presented practical difficulties. The first few years of light emitting silicon nanostructure research, while not answering all the questions in the field, have seen significant advances in the characterization of the properties and potential of this new technology. It is important to remember that at the core, this is an indirect gap semiconductor system which should not show the optical properties that are currently being debated. This very fact, coupled with the seemingly limitless possibilities of silicon photonics and optoelectronics, should fund and fuel the scientific debate for years to come.

4.2.3 Surface Control of Optical Properties

Nanostructured materials have a very large surface area to volume ratio, implying that the surface properties will be very important in determining their light emission and nonlinear optical behavior. The development of useful applications from these materials will strongly depend on controlling the interfaces of the heterostructure systems on which the devices will be based. Surfaces and interfaces create modifications to the electronic structures of these materials, such as oxide defects and dangling bonds introducing nonradiative and radiative states into the energy gaps of the silicon nanostructures. Finally, porous and nanocrystalline silicon surfaces have been characterized as being complex in morphology, and this opens the possibility that materials can grow or adsorb during the synthesis process. Some of these materials, such as polysilanes, have been shown to emit visible light in the same wavelength range as nanostructured silicon. All of these factors make the silicon surfaces critical in controlling the emission behavior.

Through the study of the luminescence properties of the clusters in a variety of passivating environments, it has become clear that surface passivation is a necessity to enable both the visible light emission and enhance the nonlinear optical response of the silicon nanocrystallites. Gas phase photoluminescence experiments have shown that no visible emission is possible in the unpassivated systems, but that when thin films are deposited and passivated by a surface layer they show efficient visible photoluminescence. This is due to the removal of states from the energy gap of the material through the passivation of dangling silicon surface bonds. These dangling bonds have been shown, both theoretically and experimentally, to be sites of efficient, fast nonradiative recombination which quench visible emission. Therefore, in gas phase clusters or unpassivated, as-deposited thin films, excited carriers quickly recombine through a continuum of nonradiative transitions rather than through photon emission. Similarly, the nonradiative recombination centers present on unpassivated films act to reduce the nonlinear optical response of the films by inhibiting the saturation of excited carrier energy levels needed to induce the nonlinearity. Passivating the surfaces improved the third order nonlinear optical susceptibility response by an order of magnitude, as measured by degenerate four wave mixing spectroscopy, over unpassivated nanocrystallites and bulk polycrystalline silicon.

Though the passivation of the nanocrystallite surfaces is necessary for the novel optical properties to be expressed, the chemical nature of the surface species does not define the emission behavior. Passivation can be accomplished by many different species, as has been demonstrated by visible light emission observed from thin films of nanocrystallites passivated by hydrogen, oxygen, and iodine, and correlation with surface characterization by infrared spectroscopy and x-ray photoelectron spectroscopy. Each of these capping species served to eliminate the nonradiative surface traps from the energy gap of the nanocrystallites and enabled the visible light emission that is defined by quantum size effects in the nanostructures. By processing the films in order to reduce the particles sizes, it was possible to gradually shift the emission to higher energies, as would be expected from models of emission based purely on quantum confinement. The presence of different surface species on the nanostructures during these steps did not alter the trends.

4.2.4 Size Control of Emission Behavior

Processing the samples using standard silicon etching and oxidation techniques has demonstrated that the sizes of the particles can be adjusted to shift the emission behavior. By cyclically etching and regrowing an oxide layer on the nanostructures, it is possible to shrink particle size and increase the quantum confinement of carriers within the silicon cores. This shrinkage has resulted in a consistent blueshift of the emission energy, as is predicted by models of emission based on the simple quantum confinement of carriers in silicon nanocrystallites. This correlation between size and emission energy has been demonstrated using nitric acid and hydrofluoric acid cycles, as well as in other work adjusting deposition parameters to control particle sizes.

Though the lower energy, orange emission can be gradually shifted from ~750 nm to ~550 nm, it gradually becomes mixed with higher energy blue emission that sits below ~550 nm. This emission is due to the defects in the oxide layer that exists around the oxygen passivated particles and in the matrix material of the film. This emission has been shown to increase when the films are expected to be converted over to an oxide-rich material, that is, after oxidation furnace treatments or repeated etch and oxide regrowth cycling. This emission also shows a different excitation intensity dependence than the longer wavelength light,

implying that it has a different mechanism and origin. The conversion of small nanocrystallites into oxide material may represent a limitation on the shortest wavelength of emission possible from nanocrystalline silicon.

4.2.5 Emission Model

All of the work described here can be explained using a model of visible light emission based on quantum confinement of carriers in silicon nanostructures.[1] The low energy, orange emission represents recombination of carriers in systems whose energy gaps are controlled by particle diameter and quantum size effects. As the particle sizes are reduced through processing steps the carrier confinement increases and results in an expansion of the gap. The ability to consistently blueshift the emission wavelength by reducing particle size is strong evidence for quantum confinement effects controlling the energy of luminescence. In addition, the similarity of the temperature dependence of the luminescence behavior to bulk systems, and the blueshift of emission wavelength at increasing excitation intensities, provide further evidence for a bulk like recombination of carriers.

The role of surface passivation in these materials is to remove defect states from the gap of the material. These states have been shown to act as nonradiative recombination centers, by allowing excited carriers to relax down to the valence band through a continuum of levels, rather than a larger energy transition that is coupled to light emission. Passivation by a variety of species has been used to eliminate these traps and improve the emission intensity, as well as showing that the chemical nature of the surface species does not control the energy levels of the radiative transition. This disagrees with surface state controlled models of emission. These traps are very important in nanocrystalline systems, since even one of them on a nanocrystallite will be enough to capture excited carriers and quench the visible luminescence behavior. This effect has also been seen in silicon nanoheterostructure systems, where poor surface passivation has eliminated any visible luminescence behavior.

The blue or higher energy emission from the samples is due to recombination of carriers within the oxide matrix that exists in the film or exists at the surfaces of oxide passivated samples. This higher energy emission behavior has been seen in many oxide materials and probably represents recombination coupled to defects states in the band gap of

the nonstoichiometric oxide in the thin films. This emission increases in intensity as the films are oxidized to a large extent, and shows different excitation energy dependence than the longer wavelength, orange behavior. At these short wavelengths (~500 nm), any emission from very small nanocrystallites is lost in the oxide emission, so it is impossible to tell if there is any bulk like recombination of carriers in the crystallite cores that is occurring at high energies, or what is the shortest emission wavelength than can be ascribed to the nanocrystallites themselves.

The data from these experiments cannot be easily, consistently explained using other models of silicon nanostructure emission. Emission from siloxene[2] or related materials would not be expected to blueshift with particle size or show bulk like emission energy temperature dependences. Emission from oxide defects[3,4] would also not show these temperature dependences, nor the blueshifting due to size reduction or increasing excitation pump power. The fact that there is intense orange emission from films immersed in hydrofluoric acid and that it decreases as the crystallites are converted to oxide is further evidence that the orange behavior is not due to the oxide layer. The ability to change the passivating species on the nanocrystallites without producing anomalous shifts in emission energy or altering the consistent blueshifting of emission with size are evidence that the radiative transitions are not controlled by surface states in the gap, as would be expected from a surface controlled smart quantum confinement model.[5,6] The evidence presented here can all be explained most easily and simply through a model based on the recombination of carriers within a confined semiconductor nanostructure.

Taking this work in the context of porous and nanocrystalline silicon research as a whole further clarifies the origin of the visible light emission. There is evidence of structural disorder in the material, as can be seen in the temperature dependence behavior and in structural characterization.[7] This may indicate that the structures that show interesting optical properties are surface passivated, but not diamond cubic in structure. They can be < 3 nm diameter nanostructures with some order embedded within amorphous matrices of oxide or silicon. These systems can be thought of as lying structurally between bulk crystalline materials and amorphous silicon. This idea is supported by gas phase work,[8] observations and theoretical understanding of disorder at nanostructure interfaces,[9,10] reports of similar emission

behavior in amorphous material,[11] and demonstrations of the size range needed for visible emission in silicon nanostructures.[12] The small sizes of the particles will control the energy gap of the material through quantum confinement effects, but will also drastically effect its physical structure. This does not imply that the emission can be explained as being due to hydrogenated amorphous silicon, as hydrogen passivation is not necessary for visible emission, only that the systems are of a new structure that cannot be thought of as wholly crystalline nor wholly amorphous in nature.

Evidence that the radiative transitions are phonon assisted[13] and that the luminescence lifetime shows a multiexponential decay behavior[14] also leads one to believe that the light emitting structures lie between indirect gap bulk crystalline silicon and traditional hydrogenated amorphous silicon. Models of emission based on surface states, amorphous silicon, and quantum confinement would converge with a non-diamond cubic structure that was small enough to confine carrier wavefunctions. A quantum confined amorphous-like silicon structure that was still similar to crystalline silicon would have energy states analogous to band tails extending into an expanded energy gap. Carrier localization within these tail states would increase moving away from the band edge into the gap, meaning that as temperature increased, a redshifting of the photoluminescence behavior is expected. These tail states would be extensions of the bands, and would explain many of the similarities in nanocrystalline silicon to band edge recombination. The tails would result in multiexponential luminescence decays and explain the blueshifts seen with particle size shrinkage through normal quantum confinement principles. Surface passivation would still be required to remove defect states from the gap between band tail states, but would not define the emission transition levels. In this case, the light emitting species is a surface passivated, indirect gap, non-diamond cubic, silicon nanostructure.

4.2.6 Porous and Nanocrystalline Silicon Research

The porous and nanocrystalline literature is muddled because of a combination of poorly defined materials and difficulty in using standard characterization techniques to describe the properties of the nanostructures. Nearly every research group uses a different starting material and a different synthesis technique to produce their samples, yet each is

compared as if it were the same material.[15] Porous silicon films are created through dissolution of bulk silicon, while nanocrystalline silicon is built up from atomic silicon, and this difference should lead to discrepancies in the structural and optical properties. Every synthesis technique produces large size distributions of crystalline material, and significant amounts of amorphous material, both of which serve to confuse characterization techniques. Attempts at controlling the size distributions, along the lines of work in compound semiconductor nanostructures, are still very crude and largely unsuccessful. The materials are also being produced with traces of many different types of visibly emitting silicon structures on them, including amorphous silicon and polysilanes, making isolating of the luminescing center difficult.

The silicon nanostructure system also suffers from difficulty in characterizing the structural aspects of light emitting centers that are at very small sizes, have large size distributions, and are neither clearly crystalline nor amorphous. There has been no direct evidence for any particular size of particle leading to a specific wavelength of emission, though there is much indirect evidence pointing to a wide variety of sizes and structures as being its origin. Thin film analysis of light emitting silicon has concluded that the active species are on the size scales normally associated with gas phase analysis, and which have been shown to have structures that are not diamond cubic when clusters are built up from atomic silicon. Direct microscopic structural characterization of structures below 2 nm in size has been difficult to obtain and verify.

The field has also been confused by the lack of terminology in describing the properties of systems between the bulk and molecular levels. For example, there may be no need to discuss issues of bulk lattice or band structure, crystallinity versus amorphicity, or direct versus indirect energy gap in these materials, as they are more molecular than solid in many ways. At these sizes, the very idea of a surface comes into question, both electronically, as bulk and surface states mix, and structurally, as surface atomic motion could lead to continuous instability at all interfaces.[16] Attempting to force the frameworks of traditional solid state analysis to this new type of material will cause some initial difficulties.

Finally, the field is currently confused by the sheer volume of material being produced that is seemingly contradictory. There are now five major models explaining the visible light

emission in silicon nanostructures. Each of these can be supported and refuted using a significant amount of published work from respected scientific journals. The field of theories is slowly clearing as the optical and structural characterization of the materials begins to improve, however, it will definitely take a significant amount of time before any single, widely accepted model is developed.

4.2.7 Applications

Demonstrations of light emission and nonlinear optical response show some promise for the development of usable silicon photonics and optoelectronics. It is clear now that silicon nanostructures can be used to reproducibly create light emitters across the visible spectrum. While it is not clear what the specific emission mechanism is at this time, it is not essential that this must be determined before useful devices are produced. Many groups are already producing crude light emitting devices, sensors, and photodetectors, and with continued improvements these may see some commercial application. While the knowledge of the emission mechanism may not be critical to working on devices, the actual mechanism may prove crucial. For example, it is unlikely that a large scale commercial technology can be developed for systems whose emission properties depend on the creation of oxide defects or adsorbed surface polymers.

From this work and other published results it is clear that the performance of silicon nanostructure materials, both in emission and nonlinear optical response, must significantly improve before commercial technologies based on them become viable. In some cases, intrinsic system constraints may control the development of applications. The observed indirect gap nature of the nanostructure systems may making them too slow for some high speed optoelectronic and photonic switching applications. The structural differences between the nanostructures and traditional bulk silicon will severely complicate issues of epitaxy and heterostructure growth. Emission efficiencies and broad spectral behaviors need to be controlled through better defect and surface control and a tightening of the size distribution. The measured nonlinear optical responses are still orders of magnitude away from the levels expected from commercial optical switch technologies. It is also clear that more knowledge

of the effects of heterostructures in creating defects and strain in the system needs to be developed before significant progress can be made.

Despite these difficulties, the materials have shown enough promise to warrant further research and development. The eventual advantages of producing optoelectronic integrated circuits from silicon far outweigh the costs and difficulties encountered in the technology's development. In the past five years, a solid foundation of theoretical and experimental work has been laid that will be exploited during the development of the silicon based optical technology of the future.

4.3 Future Work

4.3.1 Luminescence Lifetime Measurements

By measuring the rate of decay of the luminescence signal it may be possible to further examine the recombination mechanism in the nanostructures. This should be done as a function of wavelength and temperature. For emission that results from a excitonic recombination of carriers, the lifetime should be in the millisecond range for indirect transitions and in the nanosecond range for direct transitions. The functionality of the decay will be important as well, for example, the multiexponential decay in porous silicon has been explained as being the result of surface states, siloxene, and amorphous materials. The wavelength dependence of the lifetime will help determine which emission can be ascribed to oxide defects and which parts of the emission are the result of recombination in the nanostructures themselves. The temperature dependence of the lifetime can provide insight into the nature of the competing nonradiative processes that exist in the system, such as thermalization of excited carriers into traps in the oxide layers or in neighboring large crystallites.

4.3.2 Photoluminescence Excitation Spectroscopy

The absorption mechanism in the nanocrystallites can be examined using photoluminescence excitation spectroscopy. This spectrum can be compared to the behavior of bulk silicon and other silicon based emitters; similarities would indicate a common origin of

emission. The functionality of this spectrum will also provide evidence of the direct or indirect nature of the transitions in the material. The excitation spectrum will also show evidence of Stokes shifts or relaxation of carriers between absorption and luminescence behavior.

4.3.3 Gas Phase Passivation

The full potential of the pulsed laser ablation supersonic expansion technique can be exploited if the system is used to provide gas phase passivation of the clusters in order to enable their luminescence behavior. This can be done by seeding the carrier gas beam using trace amounts of oxygen or hydrogen or by performing a crossbeam experiment in which the clusters are passivated by another flow of gas that interacts with the expansion in a reaction chamber. The gas phase clusters should then show the luminescence that would be expected from thin films of passivated nanocrystallites. This would eliminate the possibility of siloxene or oxide defects being the cause of the emission behavior. It may also be possible to ionize the clusters and use gas phase mass spectroscopic techniques to get an idea of the particle size distribution produced by the source, to understand the size range of particles needed to show luminescence.

4.3.4 Nonresonant Nonlinear Optical Effects

The previous work in examining the optical nonlinearities in the thin films of silicon nanostructures was performed at 532 nm. This created a slow, resonant nonlinearity in the material that was measured using degenerate four wave mixing spectroscopy (DFWM). Actual implementation of these materials as optical switches would require faster response times, as are expected from nonresonant interactions. By performing DFWM at 1064 nm or other infrared wavelengths it would be possible to look at transitions that are lower in energy than the energy gap of the nanocrystallites, as defined by their emission properties. These studies should also be done at wavelengths of technological interest, such as 1.54 microns, and measure the temporal response and temperature dependence of the nonlinearity.

4.3.5 Size Selection Of Silicon Nanocrystallites

In order to narrow the broad emission spectra from the thin films it will be necessary to control the size distribution of the deposited particles. Currently, this can be done very roughly by adjusting deposition parameters. This only shifts the mean particle size produced by the source and does not narrow the distribution at all. Currently, work is being done to develop a mechanical velocity selection apparatus placed in the path of a supersonic expansion.[17] This system exploits the velocity slip present in the supersonic expansion in order to permit deposition of only one part of the packet and therefore one size of particle.

By selecting out one size of particle for deposition it may be possible to better determine how crystallite size controls emission wavelength and the linewidth of the emission spectra. Size selected crystallite films may also show the same type of narrow resonances in absorption and emission that are common in monodisperse compound semiconductor systems. The ability to narrow and tune the emission wavelength is likely to be critical in many device applications.

4.3.6 Structural Characterization of Light Emitting Species

There is extensive experimental and theoretical evidence that the light emission from nanostructured silicon is due to quantum confined carriers in silicon clusters in the size range of 1-2 nm.[12,18] However, at these small sizes, on the order of 70-500 atoms per nanocrystallite, it is not clear that the structure will have the diamond cubic lattice of bulk silicon. This material will then appear amorphous to most standard structural characterization techniques.[10] Further evidence for "disorder" in the light emitting nanostructures comes from the multiexponential lifetimes,[19] the similarity to amorphous silicon in temperature dependence[20] and photoluminescence excitation spectra,[21] and the similar behavior that has been observed in nonhydrogenated amorphous silicon quantum wells[22] and microcrystallites in hydrogenated amorphous silicon.[23]

In order to probe structures at these small sizes that would give rise to this behavior, it is not possible to use standard film characterization techniques. However, it may be possible to examine this size range by using the structural and optical characterization techniques available in gas phase spectroscopy.[24,25] The pulsed laser ablation supersonic expansion

system can be used both to characterize the optical absorption and Raman spectra of the 70-500 atom silicon clusters, as well as to grow thin films of the same structures. Passivation of the species can be performed in both the gas and solid phase so that the photoluminescence behavior can be compared. These results can be compared to amorphous, crystalline, porous, and other types of solid phase nanoscale silicon.

In addition, a concerted effort must be made to model the expected structural and optical properties of nanoparticles in the size range of interest. Particular attention must be paid to the formation of band structure in these small particles, especially with regards to oscillator strength and the necessity for phonon assisted optical emission transitions.[26] Efforts should also be made at further structural characterization of very small particles in thin film form, to see at what sizes this type of characterization is no longer useful, and where ideas of crystallinity lose their meaning.

By approaching the light emitting structures from both the small side, in the gas phase, and the large side, in thin film form, it may be possible to answer some of the pressing questions about the origin of the nanostructure luminescence. Resolving the problem of structural disorder in the emitting species would clarify the differences between models of emission based on quantum confinement,[27] surface states,[5] and amorphous silicon.[11]

4.3.7 Device And Heterostructure Fabrication

Alongside the work to further characterize the emission properties of the individual nanocrystallites and tighten the distribution of particle size produced by the source, attempts should be made to develop heterostructure systems based on semiconductor nanocrystallites. This can involve silicon nanocrystallites in semiconductor, glass, or polymer matrices, or even other semiconductor systems embedded within single crystal silicon matrices simultaneously grown in the deposition system. These materials should be characterized for their optical properties and interfacial structure, to better learn how the heterostructure environment affects the nanocrystalline structure and properties.

This heterostructure work will then be an important step towards the development of usable light emitting devices based on semiconductor nanocrystallites. Significant progress has already been made in characterizing the electrical transport and emission properties of

multilayer devices using silicon nanocrystallites as the emitting active layer. This should be extended to develop new structures using size selected crystallites and the knowledge of nanoheterostructures developed from work with the deposition system.

The pulsed laser ablation supersonic expansion technique has demonstrated its unique ability to synthesize nanocrystallites in a range of semiconductor systems and into a variety of host systems. Silicon nanocrystallites have already shown significant promise as tunable, visible light emitters. In addition, there is evidence that nonlinearities in the optical response of the nanostructures hold promise for the development of photonic materials. Efficient emission is being demonstrated both in photoluminescence and in light emitting devices, and improvements in tunability and performance are being made continuously. Alongside this, the base of knowledge of gas phase and bulk silicon systems processing and device fabrication is being modified and extended into nanocrystalline systems. These advances can provide significant insights into the important effects of quantum confinement, surfaces, and heterostructure interfaces and their relationship to device performance in nanocrystalline semiconductor systems.

The field of silicon photonics and optoelectronics is at a similar stage of development as the silicon microelectronics industry was nearly fifty years ago. The basic physics and device concepts for fantastic new applications have been worked out, but what is still required is the development of materials that can meet the processing and performance demands of this new technology. After a few years of intensive research, semiconductor nanocrystallites in general, and silicon nanocrystallites in particular, have shown that they can meet the requirements of these new systems. However, in the same way as it took twenty five years of research and development for the silicon transistor to become a staple of modern society, it is likely to take a significant amount of time, debate, failure, and controversy to clear up the detailed issues of device properties and performance in these new systems. This work and the parallel research that is going on around the world are an important step in that long developmental process, and a necessary prelude to the production of the silicon based optoelectronics and photonics which will be the basis of the telecommunications and computing technologies of the future.

Chapter Four References

[1] L.T. Canham, Appl. Phys. Lett. 57(10), 1046 (1990)
[2] S.M. Prokes, J. Appl. Phys. 73(1), 407 (1993)
[3] S.M. Prokes and W.E. Carlos, J. Appl. Phys. 78(4), 2671 (1995)
[4] Y. Kanemitsu, Phys. Rev. B 49(23), 16845 (1994)
[5] F. Koch, V. Petrova-Koch, and T. Muschik, J. Lum. 57, 271 (1993)
[6] P.M. Fauchet, E. Ettedgui, A. Raisanen, L.J. Brillson, F. Seiferth, S.K. Kurinec, Y. Gao, C. Peng, and L. Tsybeskov, Mat. Res. Soc. Symp. Proc. Vol. 298, 271 (1993)
[7] S.C. Bayliss, D.A. Hutt, Q. Zhang, P. Harris, N.J. Phillips, and A. Smith, Thin Solid Films 255, 128 (1995)
[8] M.L. Mandich and K.D. Rinnen, Z. Phys. D 26, 147 (1993)
[9] S.R. Phillpot, D. Wolf, and J.F. Lutsko, J. Appl. Phys. 67(11), 6747 (1990)
[10] H. Sugiyama and O. Nittono, J. Cryst. Growth 103, 156 (1990)
[11] Z.H. Lu, D.J. Lockwood, and J.-M. Baribeau, Nature 378, 258 (1995)
[12] S. Schuppler, S.L. Friedman, M.A. Marcus, D.L. Adler, Y.-H. Xie, F.M. Ross, Y.J. Chabal, T.D. Harris, L.E. Brus, W.L. Brown, E.E. Chaban, P.F. Szajowski, S.B. Christman, and P.H. Citrin, Phys. Rev. B 52(7), 4910 (1995)
[13] P.D.J. Calcott, K.J. Nash, L.T. Canham, M.J. Kane, and D. Brumhead, J. Phys: Condens. Matter 5, L91 (1993)
[14] Y. Kanemitsu, Phys. Rev. B 48(16), 12357 (1993)
[15] Overheard at the Muddy (1996)
[16] L.C. Kimerling, K.D. Kolenbrander, J. Michel, and J. Palm, Sol. St. Phys., in press.
[17] E. Werwa and K.D. Kolenbrander, Mat. Res. Soc. Symp. Proc. Vol. 397, in press.
[18] N.A. Hill and K.B. Whaley, J. Electron. Mater. 25(2), 269 (1996)
[19] Y.-H. Xie, W.L. Wilson, F.M. Ross, J.A. Mucha, E.A. Fitzgerald, J.M. Macaulay, and T.D. Harris, J. Appl. Phys. 71(5), 2403 (1992)
[20] X. Chen, D. Uttamchandani, C. Trager-Cowan, and K.P. O'Donnell, Semicon. Sci. Tech. 8(9), 92 (1992)
[21] E. Bustarret, M. Ligeon, I. Mihalescu, and J. Oswald, Thin Solid Films 255, 234 (1995)
[22] D.J. Lockwood, Z.H. Lu, and J.-M. Baribeau, Phys. Rev. Lett. 76(3), 539 (1996)
[23] S. Furukawa and T. Miyasato, Phys. Rev. B 38(8), 5726 (1988)
[24] E.C. Honea, A. Ogura, C.A. Murray, K. Raghavachari, W.O. Sprenger, M.F. Jarrold, and W.L. Brown, Nature 366, 42 (1993)
[25] K.D. Kolenbrander and M.L. Mandich, J. Chem. Phys. 92(8), 4759 (1990)
[26] L.E. Brus, P.F. Szajowski, W.L. Wilson, T.D. Harris, S. Schuppler, and P.H. Citrin, J. Am. Chem. Soc 117, 2915 (1995)
[27] A.G. Cullis, L.T. Canham, G.M. Williams, P.W. Smith, and O.D. Dosser, J. Appl. Phys. 75(1), 493 (1994)

7637-18